Monitoring the Molecular Dynamics of Acquired Chemoresistance in Ovarian Carcinoma by Noninvasive Molecular Imaging

By

SNEHAL M. GAIKWAD

[LIFE09200904007]

TATA MEMORIAL CENTRE

A thesis submitted to the Board of Studies in Life Sciences

In partial fulfilment of the requirements for the Degree of

DOCTOR OF PHILOSOPHY

Of

HOMI BHABHA NATIONAL INSTITUTE

SEPTEMBER, 2015

Homi Bhabha National Institute
Recommendations of the Viva Voce Board

As members of the Viva Voce Board, we recommend that the dissertation prepared by Ms. Snehal M. Gaikwad titled 'Monitoring the molecular dynamics of acquired chemoresistance in ovarian carcinoma by non-invasive molecular imaging' be accepted as fulfilling the requirements for the Degree of Doctor of Philosophy.

S. Chiplunkar ----------Date: 16.9.15
Chairperson: S.V. Chiplunkar, Ph.D., ACTREC

Pritha Ray ----------Date: 16.9.15
Convener: Pritha Ray, Ph.D., ACTREC

Shirsat ----------Date: 16-9-2015
Member 1: Neelam Shirsat, Ph.D., ACTREC

TR Teni ----------Date: 16.9.2015
Member 2: Tanuja Teni, Ph.D., ACTREC

Sabapat ----------Date: 16.9.2015
Advisor: Sharmila Bapat, Ph.D., NCCS, Pune

Maheshwari ----------Date: 16.9.15
Member: Dr. Amita Maheshwari, TMH

Padma Shastry ----------Date: 16.9.2015
External Examiner: Dr. Padma Shastry, NCCS, Pune

The final approval and acceptance of this dissertation is contingent upon the candidate's submission of the final copies of the dissertation to HBNI. I hereby certify that I have read this dissertation prepared under my direction and recommend that it may be accepted as fulfilling the dissertation requirement.

Date: 16.09.15

Pritha Ray.

Place: Kharghar, Navi Mumbai. Guide: Pritha Ray, Ph.D.

Statement by Author

This dissertation has been submitted in partial fulfilment of requirements for an advanced degree at Homi Bhabha National Institute (HBNI) and is deposited in the library to be made available to borrowers under rules of the HBNI. Brief quotations from this dissertation are allowable without special permission, provided that accurate acknowledgement of source is made. Requests for permission for extended quotation from or reproduction of this manuscript in whole or in part may be granted by the competent authority of HBNI when in his or her judgment the proposed use of the material is in the interests of scholarship. In all other instances, however, permission must be obtained from the author.

Gaikwad

Snehal M. Gaikwad

Declaration

I declare that the thesis titled 'Monitoring the molecular dynamics of acquired chemoresistance in ovarian carcinoma by non-invasive molecular imaging' is a record of the work carried out by me during the period of September 2009 to September 2014 under the supervision of Dr. Pritha Ray. This work is original and it has not been submitted earlier as a whole or in part for a degree, diploma, associateship or fellowship at this or any other institute or university.

January 2015

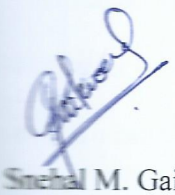

Snehal M. Gaikwad

Navi Mumbai

List of Publication Arising From Thesis

Research Articles

- **Gaikwad, S. M.**, L. Gunjal, A. R. Junutula, A. Astanehe, S. S. Gambhir, and P. Ray **(2013)** Non-invasive imaging of phosphoinositide-3-kinase-catalytic-subunit-alpha (PIK3CA) promoter modulation in small animal models. *PLOS ONE* 8:e55971. doi:10.1371/journal.pone.0055971

- Singh R. K., **Gaikwad S. M.**, Chaudhury S., Jinager A., Maheshwari A., Ray P. **(2014)** IGF-1R inhibition potentiates cytotoxic effects of chemotherapeutic agents in early stages of chemoresistant ovarian cancer cells, *Cancer Letters*. doi: 10.1016/j.canlet.2014.08.

- **Gaikwad S. M.,** Thakur B., Sakpal A., Ray P. **(2015)** Differential activation of NF-κB signaling is associated with Platinum and Taxane resistance in MyD88 deficient epithelial ovarian cancer cells, *International Journal of Biochemistry and Cell Biology,* 1C:90-102. doi: 10.1016/j.biocel.2015.02.001.

Review Article

- **Gaikwad, S.M.,** Ray P. **(2012)** Non-invasive Imaging of PI3K/AKT/mTOR signalling in Cancer', *Am J Nucl Med Mol Imaging* 2(4):418-431

Book Chapter

- Ram K Singh, **Snehal M Gaikwad**, Subhoshree Chatterjee and Pritha Ray (2014). 'Stem cell: The Holy Grail of Regenerative Medicine', 19- 70, Engineering in Translational Medicine ISBN 978-1-4471-4371-0 ISBN 978-1-4471-4372-7 (eBook) DOI 10.1007/9781-4471-4372-7 Springer London Heidelberg New York Dordrecht Springer Publications, London

Conference Abstracts

- **Snehal M. Gaikwad**, Bhushan Thakur, Asmita Sakpal and Pritha Ray, Non-invasive imaging of NF-κB activation upon cisplatin resistance in epithelial ovarian carcinoma tumor xenograft mice. World Molecular Imaging Congress, 2014, Seoul, Korea.
- **Snehal M. Gaikwad**, Asmita Sakpal and Pritha Ray, 2013, Differential activation of NFκB in cisplatin and paclitaxel resistance in ovarian cancer cells. XXXVII All India Cell Biology Conference, In Stem, JN Tata Auditorium, IISC, Bangalore, India.
- **Snehal M. Gaikwad** and Pritha Ray, 2012, 'Non- invasive imaging of PIK3CA promoter modulation during acquired chemoresistance in ovarian cancer,' Indian Association of Cancer Research Conference (IACR), ACTREC, Mumbai, India.
- **Snehal M. Gaikwad** and Pritha Ray, 2012, 'Monitoring the modulation of PIK3CA in germ cell ovarian cancer tumors by non-invasive molecular imaging' in Conference of the Asia Oceania research organisation on Genital Infections and Neoplasia- India (AOGIN India), Mumbai, India.
- **Snehal M. Gaikwad**, Lata Gunjal and Pritha Ray, 2010, 'Monitoring the role of PIK3CA in the dynamics of acquired chemo-resistance in germ cell ovarian cancer tumors', XXXIV All India Cell Biology Conference, Bose Institute, Kolkata, West Bengal, India.

Dedicated to my father...

ACKNOWLEDGEMENT

At the end of my Ph.D. tenure, I wish to express my sincerest gratitude to my mentor Dr. Pritha Ray for introducing someone as naive as myself to the wonderful discipline of molecular imaging and cancer biology. Her support, encouragement, patience, guidance, and constant efforts to mould me into a good scientist has helped me throughout these years.

I thank Dr. Shubhada Chiplunkar (Director, ACTREC), Dr. Rajiv Sarin (ex-Director, ACTREC) and Dr. Surekha Zingde (ex-Dy. Director, ACTREC) for providing me with an excellent research atmosphere and infrastructure. I am thankful to Dr. Rita Mulherkar, Dr. Neelam Shirsat, Dr. Tanuja Teni, Dr. Sharmila Bapat and Dr. Amita Maheshwari, my doctoral committee members, for their timely and valuable suggestions for improving my doctoral research. I am grateful to Dr. Abhijit De for his expert comments and critical analysis of my work during lab meetings. I also thank Dr. B. N. Pande (BARC) for his guided support with the ICP-MS facility at BARC. The Council of Scientific and Industrial Research (CSIR, Gov. of India) is also sincerely acknowledged for providing fellowship support.

I extend my gratitude to the staff at the Common Instrument Facility, Animal House Facility, ACTREC Digital Imaging Facility, Flow Cytometry Facility, Library and administration for their constant help and support. The establishment of the Molecular Imaging Facility was a bliss to my endeavour.

The long scientific and technical discussions generated during the lab meetings by the members of both Ray and De lab have been a compilation towards the improvement of my scientific attitude. I thank all my labmates: Asmita Sakpal, Ram Kumar Singh, Subhoshree

Chatterjee, Smrita Chaudhary, Ankit Jinager, Bhushan Thakur, Ajit Dhadve, Deepak Chavan, and Amol Samant for their indispensable support. I would specially mention Lata, Ram, Thakur, Smrita and Amir for meaningless/meaningful talks and fights, short tea breaks and uncountable dinners we had together. These wonderful memories will be always cherished. I also feel blessed to have wonderful batchmates (Rubina, Srikanta, Kedar, Shafqat and Tanmoy) who kept the batch 2009 atmosphere lively. I will always cherish my hostel days spent with my roommates Madhura, Rupa, Pooja, Sushmita, Monica, and Abira.

I would also like to thank my seniors Dr. Ajit Kumar Sharma, Dr. Amit Kumar Singh Gautam, and Dr. Gaurav Arora who were amongst the major source of expert technical guidance during my Ph.D. days. I am grateful to all the Ph.D. research scholars who have made each day at ACTREC a new experience for me.

Saying 'thank you' will belittle the love and moral support given to me by Srikanta.

Finally, I genuinely express my thanks towards my mother, my sister 'Mint', and my all family members for their love and endless support which made my journey to this apex possible.

Thank you all!

Snehal

Contents

Publications

Synopsis

A SYNOPSIS OF THE THESIS TO BE SUBMITTED

TO

HOMI BHABHA NATIONAL INSTITUTE

FOR THE DEGREE OF

DOCTOR OF PHILOSOPHY
IN
LIFE SCIENCES

1. **Title of Thesis:** Monitoring the Molecular Dynamics of Acquired Chemoresistance in Ovarian Carcinoma by Non-invasive Molecular Imaging
2. **Name of the Student:** Ms. Snehal M. Gaikwad
3. **Name and Designation of Guide:** Dr. Pritha Ray
   Principal Investigator & S.O. 'F'
   ACTREC, Tata Memorial Centre, Kharghar, Navi Mumbai – 410210

4. **Place of Research:** Advance Centre for Treatment, Research and Education in Cancer, Tata Memorial Centre, Kharghar, Navi Mumbai - 410210
5. **Number and Date of Registration:** LIFE09200904007; 1st September 2009

6. **Date of submission of Synopsis:** **17.**11.2014

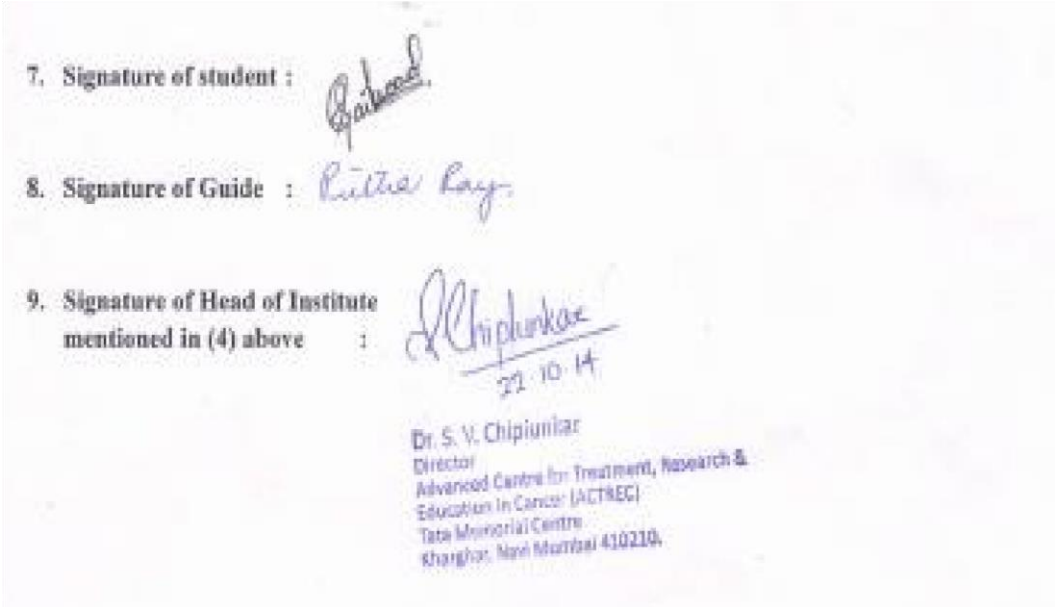

Homi Bhabha National Institute

Ph. D. PROGRAMME

1. Name of the Student:	Snehal M. Gaikwad
2. Name of the Constituent Institution:	Tata Memorial Centre**,** Advanced Treatment Research and Education in Cancer Centre
3. Enrolment No. :	LIFE09200904007
4. Title of the Thesis:	Monitoring the Molecular Dynamics of Acquired Chemoresistance in Ovarian Carcinoma by Non-invasive molecular imaging.
5. Board of study:	Life Science

SYNOPSIS

1. Introduction

Ovarian cancer (OC is the fifth most common of all gynecological malignancies and accounts for large number of deaths worldwide [1]. Among the three subtypes of OC arising from different cells types present in ovary (stromal cells, germ cells and epithelial cells), epithelial ovarian cancer (EOC) accounts for 90-95% occurrence and comprises of four major histologically and genetically distinct subtypes [2]. The conventional treatment strategy for EOC includes cytoreductive surgery followed by cisplatin/carboplatin and paclitaxel based combination adjuvant therapy however, neoadjuvant therapy which involves chemotherapy treatment of patients prior to surgery is also practiced [3]. Despite of promising therapeutic response at initial stages, majority of the patients show recurrence due to development of chemoresistance. Overall survival (OS) for patients is thus short (5 year OS: 30-40% for all stages) and has remained stable for last two decades [3]. Therefore, late detection and development of drug resistance are the two major clinically observed obstacles for effective treatment of EOC. Chemoresistance is a multifaceted problem and several pathways like apoptosis, drug transportation, and detoxification of the drugs, DNA-repair and reinforcement of survival signals could be involved [4]. A major hurdle to suppress or reverse chemoresistance lies in its multifactorial nature and thus intervention at early stages during resistance development could be more effective. Such interventions require repetitive and non-invasive monitoring to understand true reversal/suppression of chemoresistance. In recent days, molecular imaging techniques have become essential tools for non-invasive measuring of the cellular and molecular alterations in small animals as well as in humans [3, 5].

Among various survival pathways, the PI3K/AKT/mTOR signaling pathway, a key player in mediating apoptosis, metabolism, cell proliferation, cell growth, is frequently

dysregulated in cancers. Several components of this signaling pathway, including proteins like PTEN, PIK3CA, AKT and mTOR are deregulated by the gain- or loss- of function mutations in various malignancies [6]. According to the cancer genome atlas network study, amplification (18%) rather than mutations (<1%) in Phosphoinositide Kinase Catalytic subunit-α (PIK3CA) gene, a component of Phosphoinositide Kinase (PI3K) signaling pathway, is more prevalent in high grade EOC [7]. Similarly, another study revealed that 16-24% of EOCs harbour PIK3CA amplification irrespective of histological subtypes and is negatively associated with platinum sensitivity [8]. PI3K/AKT/mTOR signaling also plays an important role in the development of cisplatin and paclitaxel resistance in OC [9, 10]. However, the consequence of the amplification in PIK3CA gene has hardly been studied. Another important cell survival regulatory factor, often activated by the PI3K signaling pathway is NF-κB (nuclear factor kappa light chain enhancer of activated B cells). NF-κB activation facilitates cell death in sensitive OC cells, but has shown to switch to an antiapoptotic 'oncogenic' pathway in chemoresistant isogenic variants [11]. Studies in the last few years have unravelled that multiple mechanisms that enable NF-κB to support carcinogenesis and drug resistance [12-14]. NF-κB pathway is also activated by the Toll-like receptor (TLR) family which plays a central role in initiation of innate immunity via myeloid differentiation factor 88 (MyD88) dependent or independent pathways [15-17]. Studies revealed that EOC cells possess an active TLR-4 signaling and presence of MyD88 mediated NF-κB signaling may lead to intrinsic paclitaxel resistance and poor survival [18]. However, the role of NF-κB in governing resistance and survival in MyD88 deficient EOC patients is not yet understood.

Rationale

As described in earlier section, amplification in PIK3CA gene is a more common phenomenon than mutation in EOC which requires attention for therapeutic intervention.

Gene amplification at chromosomal level may lead to increased transcript level as well as increased promoter modulation. PIK3CA promoter was first isolated from normal human ovarian surface epithelium (OSE) by Astanehe et al, (2008) who showed that PIK3CA promoter bears four p53 binding response elements and undergoes p53 mediated repression after activation of p53 [19]. Both cisplatin and paclitaxel are known to induce cell death through p53 activation. However, the effect of these drugs on PIK3CA promoter in ovarian cancer cells is yet to be understood. Similarly, PIK3CA promoter activity during acquirement of chemoresistance still remains to be investigated.

Understanding the action of NF-κB, one of the downstream components of PI3K signaling axis during acquired resistance is another question of the study. As mentioned in the introduction, active TLR-4/MyD88 signaling is present in EOCs and presence of MyD88 not TLR-4 determines the sensitivity of EOC cells to paclitaxel [18]. However, a significant percentage of EOC patients (~60%) were shown to be $MyD88^{negative}$, out of which around 40% cases exhibited disease recurrence [18]. The status and role of NF-κB signaling in these chemoresistant $MyD88^{negative}$ populations is unclear and certainly requires further investigation for devising new therapeutic strategies.

2. Hypothesis

Both cisplatin and paclitaxel, two very different types of cytotoxic drugs may induce modulation of PIK3CA promoter in EOC cells. This drug induced modulation may alter with development of resistance and can be measured in real time by non-invasive molecular imaging. Development of drug resistance would also affect the downstream molecules of PIK3CA signaling.

3. <u>Objectives:</u> To address the hypothesis the following objectives were designed.

Objective 1. Construction of a PIK3CA sensor consisting of a reporter system and to study the effects of drugs in the ovarian cancer cell lines and in vivo tumor xenografts stably expressing this sensor: A 900bp PIK3CA promoter obtained from Dr. Astanehe [19], was PCR amplified and cloned in a *CMV-fluc2-tdt* bifusion (CMV promoter driven firefly luciferase, *fluc2* and fluorescence gene tandem dimer tomato, *tdt*) plasmid by replacing the CMV promoter. This unique PIK3CA sensor was stably expressed in PA1, A2780 and SKOV3 ovarian cancer cells to understand the PIK3CA promoter modulation upon drug treatments. PA1 and A2780 cells with wild-type p53 background demonstrated a dose dependent attenuation of PIK3CA promoter activity upon cisplatin and paclitaxel treatment for 24h as measured by luciferase reporter assay. On contrary, SKOV3, a p53 deficient ovarian cancer cell showed no change in the promoter activity upon cisplatin and paclitaxel treatment. Drug induced p53 activation and nuclear localization were evident in PA1 and A2780 cells without any obvious change in endogenous PIK3CA expression. The kinetics of PIK3CA promoter modulation was studied non-invasively in living subjects using bioluminescence imaging. In both PA1 and A2780 tumor xenografts cisplatin treatment attenuated the PIK3CA promoter activity. However, no such attenuation was observed in SKOV3 tumor xenografts after cisplatin treatment. The above results suggest that p53 could be the major regulator of PIK3CA promoter. In fact, sequential mutations in the p53 binding sites showed increased promoter activity and decreased effect of cisplatin treatment. A2780 cells stably expressing a construct with mutations at Site 1, 3 and 4 (A2780-MPFT-3), showed less repression of promoter activity upon cisplatin and paclitaxel treatment. Non-invasive imaging of A2780-MPFT-3 tumor xenografts also demonstrated reduced effect of cisplatin and no change in promoter activity corroborating with the *in-vitro* study.

Objective 2. Development of cellular chemo-resistant models expressing the PIK3CA sensor and monitor the modulation of PIK3CA promoter activity in effect of chemotherapeutic drugs: In order to understand the behaviour of PIK3CA promoter during resistance development, A2780 cells stably expressing the PIK3CA sensor was treated with repeated and increasing concentration of either cisplatin or paclitaxel for a period of 6 months. Both cisplatin (A2780-Cis^{LR}) and paclitaxel (A2780-Pac^{LR}) resistant cells show approximately 90% viability as measured by MTT assay at IC_{50} concentration of the sensitive cells. Resistance Index (RI) value calculated was 8 and 5 fold higher in cisplatin and paclitaxel resistant cells respectively. Cisplatin/paclitaxel induced attenuation in PIK3CA promoter activity observed in A2780 cells was abolished in these A2780-Cis^{LR} and A2780-Pac^{LR} cells. However, unlike cisplatin resistant cells the early paclitaxel resistant cells showed a two-fold increase in PIK3CA promoter activity which later decreased at late stages of resistance. The endogenous PIK3CA transcript levels decreased in late cisplatin and paclitaxel resistance which matched with the PIK3CA promoter activity. Both these cisplatin and paclitaxel resistant cells showed slower proliferation and higher clonogenic potential (at higher drug concentration) in comparison to the sensitive cells. They also exhibited elongation in G0-G1 phase and occurrence of aneuploidy. The cisplatin resistant cells demonstrated high ROS generation and less γH2AX foci formation upon cisplatin treatment. The cisplatin resistant cells also showed less uptake of cisplatin as measured by Inductively Coupled Plasmon Mass Spectrometry (ICPMS) analysis. Interestingly, evaluation of the membrane transporters like hCTR1 (cisplatin influx protein), ATP7A and ATP7B and ABCB 1 (cisplatin efflux proteins) by quantitative real time PCR showed no change in the expression levels between sensitive and cisplatin resistant cells. In contrast, the paclitaxel resistant cells showed significant increase ($p<0.002$) in ABCB1 expression. This was further confirmed when verapamil, an inhibitor of ABCB1, treatment sensitized

these resistant cells to paclitaxel. Thus, acquirement of cisplatin and paclitaxel resistance leads to alteration in PIK3CA promoter activity in EOC cells.

Objective 3. Non-invasive optical imaging of the development of an in-vivo chemoresistant models and monitoring dynamics of chemo-resistance in the tumors formed by the stable cells expressing the PIK3CA sensor. To check the tumorigenic property of the cisplatin resistant cells, A2780-Cis-LR were implanted in mice and tumor growth was monitored by real time imaging. As compared to the sensitive A2780 tumor xenografts, the cisplatin resistant cells showed delay in tumor formation of about 20 days corroborating with our *in-vitro* data which suggests slower proliferation of cisplatin resistant cells. These cells when directly cultured from the tumors showed 80% viability at IC_{50} concentration of cisplatin sensitive cells. The PIK3CA promoter activity was monitored in the A2780-Cis-LR tumors in nude mice upon treatment with cisplatin (8 mg/kg) using bioluminescence imaging. It was observed that the promoter activity of these A2780-Cis^{LR} tumor xenografts did not decrease after first treatment rather slightly increased and remained constant even after the second dose of cisplatin. Tumor volume of the treated A2780-Cis^{LR} tumors remained stable whereas the untreated tumor xenografts exhibited gradual increase. Thus, corroborating with our *in vitro* results, the cisplatin resistant tumor xenografts retained the resistant characteristics in *in vivo* conditions. ***Objective 4. Characterize the chemo-resistant models by monitoring genetic alterations in the PI3K-AKT signaling, NF-κB pathway and antiapoptotic genes:*** Both the resistant cellular models showed gradual activation of AKT with acquirement of resistance without any significant change in total AKT level. The activation of AKT seemed to occur at much earlier stages for cisplatin resistance than paclitaxel resistance. Use of PI3K inhibitor like wortmannin, was found to have a more cytotoxic effect on A2780-Cis^{LR} cells, as compared to the parental A2780 cells. However, no effect of wortmannin was observed on the paclitaxel resistant cells.

Rapamycin, an inhibitor of mTOR, a downstream effector of the PI3K/AKT pathway, was found to have no effect on viability of both the cisplatin and paclitaxel resistant cells. As mentioned earlier, another pathway downstream to AKT and a key player in chemoresistance development is the NF-κB pathway. A NF-κB sensor

(NF-κB response element followed by minimal TA promoter driving Renilla luciferase, hRL, and green fluorescence protein, eGFP developed in the laboratory was used to induce stable expression in MyD88^{negative} A2780, A2780-Cis^{LR} and A2780-Pac^{LR} cells which mimics the clinical scenario of MyD88 negativity in EOCs patients. While the sensitive cells exhibited an attenuated luciferase activity after cisplatin treatment, their resistant counterpart showed an augmentation in NF-κB sensor activity. These luciferase results corroborated with immunoblotting and immunofluorescence data which demonstrated activation and nuclear localization of NF-κB in resistant cells after drug treatment. On contrary, the paclitaxel resistant cells demonstrated a significant decrease in NF-κB activity after paclitaxel treatment. In contrast to A2780 sensitive cells, where paclitaxel could induce nuclear localization, the paclitaxel resistant cells did not exhibit nuclear localization of NF-κB after paclitaxel treatment. Western blot analysis showed decreased nuclear NF-κB after paclitaxel treatment. For understanding the molecular alteration in the downstream targets of NF-κB, expression levels of anti-apoptotic proteins Bcl-2 and XIAP were studied. Enhanced Bcl-2 expression was found in cisplatin resistant cells but not in paclitaxel resistant cells. On contrary, antiapoptotic protein XIAP transcripts did not show any change after drug treatments in A2780-Cis-LR and A2780-Pac-LR cells. To noninvasively monitor NF-κB activation, subcutaneous tumor xenografts of cisplatin resistant cells stably expressing the NF-κB-RL were developed in nude mice and sequential bioluminescence imaging for firefly and renilla luciferase were performed. As expected firefly luciferase activity of cisplatin tumor xenografts showed no change after cisplatin treatment in

comparison to the vehicle treated tumor xenografts. However, a 14 fold increase in NF-κB-RL activity was found after cisplatin treatment as compared to the vehicle treated tumor xenografts. To the best of our knowledge this is a unique report in which NF-κB reporter activity was studied non-invasively in effect of cisplatin treatment in cisplatin resistant tumor xenografts.

4. Conclusions and Future Prospects:

The PIK3CA signaling pathway is a crucial player in the acquirement of chemoresistance in ovarian cancer. Using a reporter based system and non-invasive imaging approach we showed that the PIK3CA promoter exhibited attenuated activity in response to cisplatin and paclitaxel treatments in EOC cells. This attenuated promoter activity however, was not evident when the cells acquired resistance towards the drugs. Development of this unique PIK3CA sensor thus can be used as a screening tool for potential drugs targeting the PI3K/AKT signaling pathway. This has also given an opportunity to further work upon the potential regulators of PIK3CA promoter like p53. Further, our study showed that NFκB is activated upon cisplatin treatment in MyD88 deficient EOC cells resistant to cisplatin, however, no changes were observed with isogenic taxol resistant cells upon treatment. Thus, our study signifies that presence or absence of MyD88 in the EOC patients can determine the success of treatment regime and NF-κB pathway can serve as a therapeutic target in treatment of cisplatin resistant ovarian cancer.

5. References

1. Tomao, F., et al., *Investigating molecular profiles of ovarian cancer: an update on cancer stem cells.* J Cancer, 2014. **5**(5): p. 301-10.
2. Bast, R.C., Jr., B. Hennessy, and G.B. Mills, *The biology of ovarian cancer: new opportunities for translation.* Nat Rev Cancer, 2009. **9**(6): p. 415-28.
3. Chaudhury S , Maheshwari .A., Ray P, *Ovarian Cancer: An ever challenging malady.*

Biomedical Research Journal, 2014 **1**(1): p. 34-55.

4. Gaikwad, S.M. and P. Ray, *Non-invasive imaging of PI3K/Akt/mTOR signalling in cancer.* Am J Nucl Med Mol Imaging, 2012. **2**(4): p. 418-31.
5. Blasberg, R.G., *In vivo molecular-genetic imaging: multi-modality nuclear and optical combinations.* Nucl Med Biol, 2003. **30**(8): p. 879-88.
6. Karakas, B., K.E. Bachman, and B.H. Park, *Mutation of the PIK3CA oncogene in human cancers.* Br J Cancer, 2006. **94**(4): p. 455-9.
7. Network, T.C.G.A., *Integrated genomic analyses of ovarian carcinoma.* Nature, 2011. **474**(7353): p. 609-15.
8. Kolasa, I.K., et al., *PIK3CA amplification associates with resistance to chemotherapy in ovarian cancer patients.* Cancer Biol Ther, 2009. **8**(1): p. 21-6.
9. Orr, G.A., et al., *Mechanisms of Taxol resistance related to microtubules.* Oncogene, 2003. **22**(47): p. 7280-95.
10. Peng, D.J., et al., *Role of the Akt/mTOR survival pathway in cisplatin resistance in ovarian cancer cells.* Biochem Biophys Res Commun, 2010. **394**(3): p. 600-5.
11. Yang, G., et al., *The biphasic role of NF-kappaB in progression and chemoresistance of ovarian cancer.* Clin Cancer Res, 2011. **17**(8): p. 2181-94.
12. Alvero, A.B., *Recent insights into the role of NF-kappaB in ovarian carcinogenesis.* Genome Med, 2010. **2**(8): p. 56.
13. Annunziata, C.M., et al., *Nuclear factor kappaB transcription factors are coexpressed and convey a poor outcome in ovarian cancer.* Cancer, 2010. **116**(13): p. 3276-84.
14. Karin, M., *NF-kappaB as a critical link between inflammation and cancer.* Cold Spring Harb Perspect Biol, 2009. **1**(5): p. a000141.
15. Akira, S., *Toll-like receptor signaling.* J Biol Chem, 2003. **278**(40): p. 38105-8.

16. Blasius, A.L. and B. Beutler, *Intracellular toll-like receptors.* Immunity, 2010. **32**(3): p. 305-15.
17. Kawai, T. and S. Akira, *Signaling to NF-kappaB by Toll-like receptors.* Trends Mol Med, 2007. **13**(11): p. 460-9.
18. Kim, K.H., et al., *Expression and significance of the TLR4/MyD88 signaling pathway in ovarian epithelial cancers.* World J Surg Oncol, 2012. **10**: p. 193.
19. Astanehe, A., et al., *Mechanisms underlying p53 regulation of PIK3CA transcription in ovarian surface epithelium and in ovarian cancer.* J Cell Sci, 2008. **121**(Pt 5): p. 664-74.

6. Publications in referred journals:

a) Published Articles.

- **Snehal M Gaikwad**, Lata Gunjal, Anitha R Junutula, Arezoo Astanehe, Sanjiv Sam Gambhir, Pritha Ray (2013) Non-invasive imaging of Phosphoinositide-3-kinase-catalyticsubunit-alpha (PIK3CA) promoter modulation in small animal models. PLOS ONE 8(2): e55971. Doi: 10.1371/journal.pone.0055971.

- Ram K Singh, **Snehal M. Gaikwad**, Smrita Chaudhury, Ankit Jinager, Amita Maheshwari, Pritha Ray, 2014, IGF-1R inhibition potentiates cytotoxic effects of chemotherapeutic agents in early stages of chemoresistant ovarian cancer cells, Cancer Letters, DOI: 10.1016/j.canlet.2014.08.

b) Accepted Articles. Not applicable

c) Communicated Articles.

Snehal M. Gaikwad, Bhushan Thakur, Asmita Sakpal and Pritha Ray, Differential activation of NF-κB signaling is associated with Platinum and Taxane resistance in MyD88 deficient epithelial ovarian cancer cells, International Journal of Biochemistry and Cell Biology **(under review)**

d) Other publications.

Review

- **Snehal M Gaikwad** and Pritha Ray (2012). Non-invasive Imaging of PI3K/AKT/mTOR signaling in Cancer'. Am J Nucl Med Mol Imaging; 2(4):418-431.

Book Chapter

- Ram K Singh, **Snehal M Gaikwad**, Subhoshree Chatterjee and Pritha Ray (2014). 'Stem cell: The Holy Grail of Regenerative Medicine', 19- 70, Engineering in Translational Medicine ISBN 978-1-4471-4371-0 ISBN 978-1-4471-4372-7 (eBook) DOI 10.1007/9781-4471-4372-7 Springer London Heidelberg New York Dordrecht Springer Publications, London

Conference abstracts

- **Snehal M. Gaikwad,** Bhushan Thakur, Asmita Sakpal and Pritha Ray, Non-invasive imaging of NF-κB activation upon cisplatin resistance in epithelial ovarian carcinoma tumor xenograft mice. World Molecular Imaging Congress, 2014, Seoul, Korea.

- **Snehal M. Gaikwad**, Asmita Sakpal and Pritha Ray, 2013, Differential activation of NFκB in cisplatin and paclitaxel resistance in ovarian cancer cells. XXXVII All India Cell Biology Conference, InStem, JN Tata Auditorium, IISC, Bangalore, India.

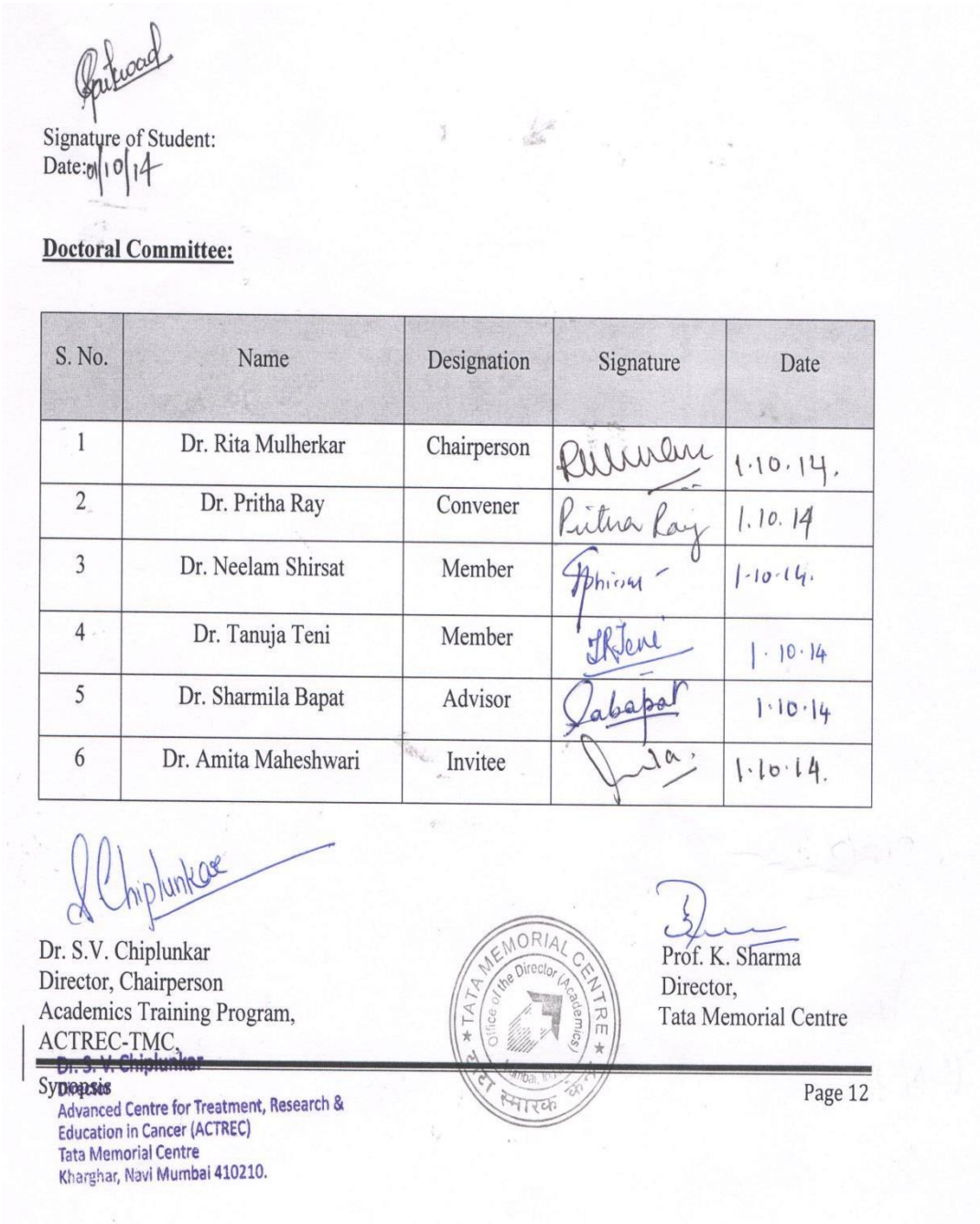

Signature of Student:
Date: 01/10/14

Doctoral Committee:

S. No.	Name	Designation	Signature	Date
1	Dr. Rita Mulherkar	Chairperson		1.10.14.
2	Dr. Pritha Ray	Convener		1.10.14
3	Dr. Neelam Shirsat	Member		1.10.14.
4	Dr. Tanuja Teni	Member		1.10.14
5	Dr. Sharmila Bapat	Advisor		1.10.14
6	Dr. Amita Maheshwari	Invitee		1.10.14.

Dr. S.V. Chiplunkar
Director, Chairperson
Academics Training Program,
ACTREC-TMC,

Prof. K. Sharma
Director,
Tata Memorial Centre

TATA MEMORIAL CENTRE
Office of the Director (Academics)

Dr. S. V. Chiplunkar
Director
Advanced Centre for Treatment, Research & Education in Cancer (ACTREC)
Tata Memorial Centre
Kharghar, Navi Mumbai 410210.

Synopsis

Page 12

Abbreviations

Gene(s)/ Acronym Description **Page No.**

List of Figures

List of Tables

Chapter 1

Introduction & Review of Literature

Cancer can be quoted as '*Achilles heel*' of the scientific progress due to the extraordinary complexity shown by the disease. Advances in prevention, diagnosis and treatment of the ailment have enabled us to understand the disease, but there is long way to cure it. Despite of decades of research and ample funds invested to overcome this deadly disease, cancer continues to be one of the principal cause of deaths worldwide and also in India, where it accounts for approximately 6% of total human deaths [20]. Even worse is the complexity of cancer and difficulty to manage the disease with its irrepressible property to recur. Over the past three decades, demographic, socioeconomic and cultural changes in India have resulted changes in lifestyles with increased longevity, delayed childbearing, lowered parity and thus have contributed to the increasing burden of cancer among women [21]. Amongst all malignancies, ovarian cancer is the fifth leading cause of cancer deaths worldwide in women. In India, it is the third most frequent gynaecological cancer after breast and cervical cancer [21, 22]. Advancement in diagnostic and treatment modalities has led to improved management of ovarian cancer, however, this improvement has not been able to mitigate relapse of the disease, which now looms as one of the major threats in ovarian cancer patients after complete remission.

Ovarian cancer: it whispers so listen carefully

Ovarian cancer (OC) is an enigma and is often termed as 'silent killer' [2]. According to the recent 2014 cancer statistics by Siegel et al., ovarian cancer attributes as fifth leading cause of death and accounts for 5% of all cancer deaths in women (lung, breast, colorectal, pancreatic are the first four respectively) [23].

The International Federation of Gynecology and Obstetrics (FIGO) has classified ovarian cancer in four stages (Stage I to 1V) and each stage has different impact on the 5 year survival rates (Table 1). If diagnosed at localised stage (Stage I) the five year survival is

very high (approximately 90%), however, the cure rate decreases substantially as the disease metastasize to pelvic organs (Stage II), abdomen (Stage III) or beyond peritoneal cavity (Stage IV) (approximately 30%) (Figure 1.1). Ovarian cancer has a distinctive biology and is a heterogeneous disease. Based on its histological features the World Health Organization (WHO) broadly classifies the ovarian tumors as:

***Epithelial Ovarian Carcinomas (EOCs)*:** The majority of the ovarian cancers (85-90%) arise from the thin layer of cuboidal cells known as germinal epithelium that sheaths the ovaries. EOCs are mostly found in women aged 45-70 years who have been through their menopause. Epithelial tumors are again classified into five broad histological sub-types: Serous (70%), Mucinous (10%), Endometrioid (5%) and Clear cell (5%), mixed or carcinosarcomatous müllerian tumours (less than 5%).

***Ovarian Germ Cell Tumors*:** Ovarian germ cell tumors develop from the cells that produce ova or eggs. Most germ cell tumors are benign (non-cancerous) in nature and accounts for 3% of all ovarian cancers. They are frequently found in young women.

***Stromal Cell Tumors*:** Ovarian stromal tumors are a rare class of tumors that develop from the connective tissue cells that hold the ovary together and those that produce the female hormones like oestrogen and progesterone. It accounts for 5% of ovarian cancer and occur in women aged 40-60 years [24].

STAGES	Relative 5 year survival rates
Stage I	80-95%
Stage II	60-80%
Stage III	30-65%
Stage IV	10-28%

Table 1: Stages of ovarian cancer showing the 5-year survival rates

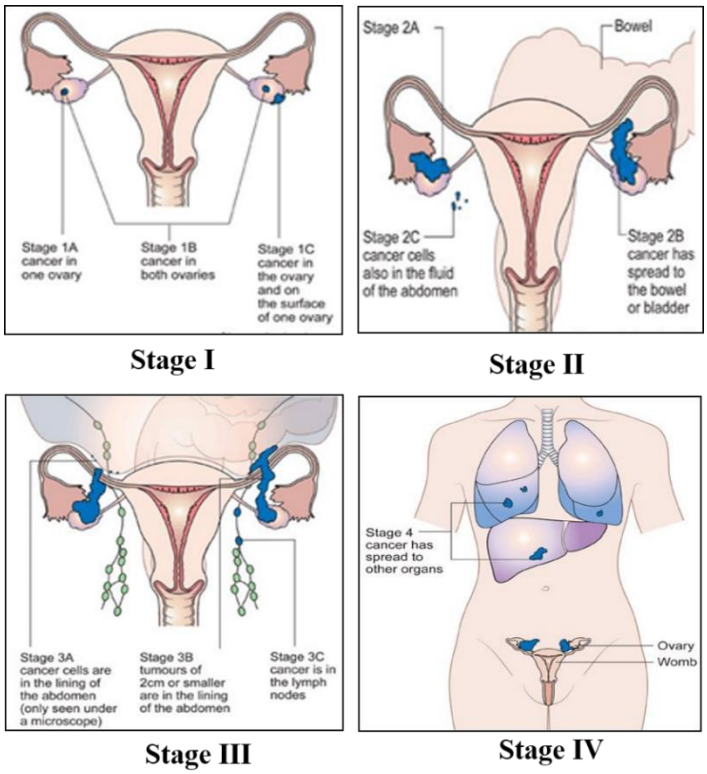

Figure 1.1. Staging of ovarian cancer. *International Federation of Gynecology and Obstetrics (FIGO) has classified ovarian cancer into four stages.* ***Stage I****: Cancer is confined to ovaries. Stage IA (one ovary) Stage IB: (both ovaries) Stage IC: (outer surface of one or both ovaries);* ***Stage II****: Cancer is ruptured from both the ovaries and lies in the pelvic region. Stage IIA: (uterus and /or fallopian tubes), Stage IIB: (bladder, rectum, or sigmoid colon) Stage IIC: uterus, fallopian tubes, bladder, sigmoid colon, or rectum and tissue or fluid of the lining of abdominal cavity;* ***Stage III****: Cancer is found in one or both ovaries and spreaded to the abdomen: Stage IIIA: (ovaries and spreaded to small part of abdomen), Stage IIIB: (ovaries, peritoneum and spreaded in amount less than 2cm, Stage IIIC: (ovaries and spread to peritoneum more than 2 cm and spreaded to the lymph nodes);* ***Stage IV****: Cancer is metastasized to lungs and liver.*

Conventional knowledge about the origin and development of ovarian cancer suggests that it originates from the ovarian surface epithelium (mesothelium) and invaginates to the other

organs by eventually undergoing malignant transformation. The differences in the morphological features of different subtypes and the histological classification have provided a basis for performing clinicopathological studies. However, the fact of no improvement in the overall survival for women with ovarian cancer has challenged the concept of histogenesis on which the clinical approaches are based. Recent series of morphologic and molecular genetic studies have evidently suggested a new paradigm of pathogenesis of ovarian carcinogenesis. This "dualistic model", as termed by Kurman et al., 2010, propose to divide EOC into two broad categories: type I and type II. The study suggests that type I and type II ovarian tumors develop independently along different molecular pathways and that both types develop outside the ovary and involve it secondarily [25].

Type I: Type I tumors include low- grade serous, low-grade endometrioid, clear cell and mucinous carcinomas. Type I tumors are clinically slow growing and usually present at a low stage. *KRAS, BRAF, and ERBB2* mutations occur in approximately two thirds of low-grade serous carcinomas whereas *TP53* mutations are rare in these tumors. Low-grade endometrioid carcinomas have aberrations in the Wnt signaling pathway involving somatic mutations of *CTNNB1* (encoding β-catenin), *PTEN* and *PIK3CA. Type I tumors exhibit clear differences in the morphological features.*

Type II: In contrast, Type II tumors comprise of high-grade serous carcinoma, high-grade endometrioid carcinoma, malignant mixed mesodermal tumors (carcinosarcomas), and undifferentiated carcinomas. They are usually present in advanced stage (stages II-IV) in more than 75% of cases. They grow rapidly and are highly aggressive. The prototypic type of (High grade serous cancer) HGSC harbours TP53 mutations in more than 95% cases. No subtle morphological differences exist between Type II tumors and the histological patterns overlap with each other.

Diagnosis

The early symptoms of ovarian cancer are very similar to other gynecological and gastrointestinal problems and therefore often go unnoticed for long. Common signs of ovarian cancer are swelling of abdomen, digestive problems such as long-term stomach pain, gas and bloating. Diagnosis is commonly performed by physical examination, transvaginal ultrasound and by measuring CA-125 levels in blood serum. Approximately, 60% of early stage ovarian cancer show elevated levels of CA-125, a glycoprotein also known as MUC16. Although, elevated levels of CA-125 are found in the cancer of fallopian tube, lungs, endometrium, and breast and in benign conditions like endometriosis, fibroids etc. it is the most widely used and available serum marker used for the detection of ovarian cancer. Another potent candidate that may be used as tumor marker is a secreted glycoprotein human epididymis protein 4 (HE4) which is highly expressed by serous and endometrioid epithelial ovarian cancer cells [26]. In premenopausal women, HE4 is the most sensitive and specific marker of ovarian malignancy, including early stage ovarian cancer. Various combinations of tumor markers (CEA, CA72-4, hCG; inhibin B and Anti-Müllerian Hormone) alongwith CA125 are under investigations for their potential in determining the disease. However, HE4 along with CA125 appears to be the strongest candidate as a tumor marker [27]. Clinical and imaging assessment of adnexal masses (which encompass ovarian and tubal lesions) influences the disease management decisions. Transvaginal or transabdominal ultrasonography (US) and Doppler US studies are the first-line non-invasive imaging method used in clinic to detect presence of tumors in ovaries. Computed tomography (CT) is widely used in preoperative evaluation of patients to predict the feasibility of primary cytoreductive surgery [27]. Magnetic resonance (MR) imaging characterizes the adnexal masses that remain indeterminate at US and improves detection of nodal metastases while evaluating the extent disease. Although the use of positron emission tomography (PET)

imaging is limited in early ovarian cancer stage, fluorine 18 fluorodeoxyglucose (18F-FDG) PET/CT is widely adopted for patients suspected with advanced disease or recurrence, offering a whole body imaging approach [28].

Management of Disease

The preferred standard management of ovarian cancer treatment is cytoreductive surgical removal of tumor followed by adjuvant chemotherapy to eliminate the residual disease [29].

Surgery: Optimal debulking (surgical resection of tumor without a macroscopic residual disease) is carried out when patients have widely disseminated and advanced disease. Surgical removal of tumor is often difficult due to the extent of the disease. In such cases neo-adjuvant chemotherapy (primary chemotherapy followed by surgery and additional chemotherapy) has become an established practice of management of ovarian cancer [29, 30].

Chemotherapy

Since late 1970s, cisplatin or carboplatin based combinations with cyclophosphamide have been used to treat ovarian cancer. In the early 1990's paclitaxel was first tested in ovarian cancer. Huinink et al., 1995, showed that paclitaxel introduction in combination with cisplatin and carboplatin into the first-line treatment strategy was effective in complete remission of the disease [31]. According to the gynecological oncology group (GOG) study by McGuire, et al., 1996, combination of cisplatin with paclitaxel was superior in terms of overall survival compared to the treatment regime with cisplatin and cyclophosphamide [32]. However, overall survival of a cohort of population treated with cisplatin-paclitaxel and carboplatin-paclitaxel combination showed equivalent response [33]. Thus, eventually, carboplatin/cisplatin and paclitaxel have become the 'backbone' of treatment of advanced ovarian cancer. Administration of chemotherapy is done either intraperitoneally or

intravenously. In its most recent consensus statements on the management of ovarian cancer during the Fourth International Ovarian Cancer Consensus Conference, the Gynaecologic Cancer Inter Group (GCIG) recommended the use of 80 mg/m^2/body weight paclitaxel, given intravenously (i.v.) over 3 h, followed by carboplatin as an i.v. infusion over 30–60 min at a dose adjusted to produce an area under the plasma concentration time curve (AUC) of 5–6 mg/ml/min and to repeat this every 3 weeks for six cycles [34-36].

Platinum based drugs kills cells by forming inter-and intrastrand DNA adducts via binding to N3 site on purine bases, arresting cell cycle at G2 phase and decreasing the ATP production in mitochondria. On the other hand, paclitaxel prevents depolymerisation of beta-tubulin subunits and blocks cell cycle at metaphase/anaphase of mitosis. Second line of chemotherapeutic agents is used in case if there is recurrence and no response after first-line agents or for the treatment of other ovarian cancer like germ cell tumors. These include etoposide, ifosfamide, cyclophosphamide, topotecan, tamoxifen, methotrexate, gemcitabine, vincristine, vinblastine, and docetaxel. With the increasing use of cytoreductive surgery and combination chemotherapy the response rate has improved with higher percentage of five year survival [2]. In spite of significant improvement in the management of ovarian cancer patients over two decades, the occurrence rate did not decline. The major debacle of ovarian cancer treatment is late diagnosis and the presence of dormant ovarian cancer cells that have resisted conventional drugs. Although the 80% patients respond to the combinatorial therapy (cisplatin/carboplatin & paclitaxel) in the beginning, 30-50% of them relapses and succumb to disease [2, 37]. Based on the response these patients can be grouped **refractory**, **resistant** and **sensitive** categories [38, 39]. Chemorefractory patients do not respond to the therapy from the very beginning since they are intrinsically resistant to it. Patient with complete remission of the disease for at least two years are termed as chemosensitive, however, many of them eventually relapse and succumb

to the disease. These chemosensitive patients respond to the first line platinum-taxol again. Chemoresistant patient shows relapse within 6 months and do not respond to same therapy again (Figure 1.2).

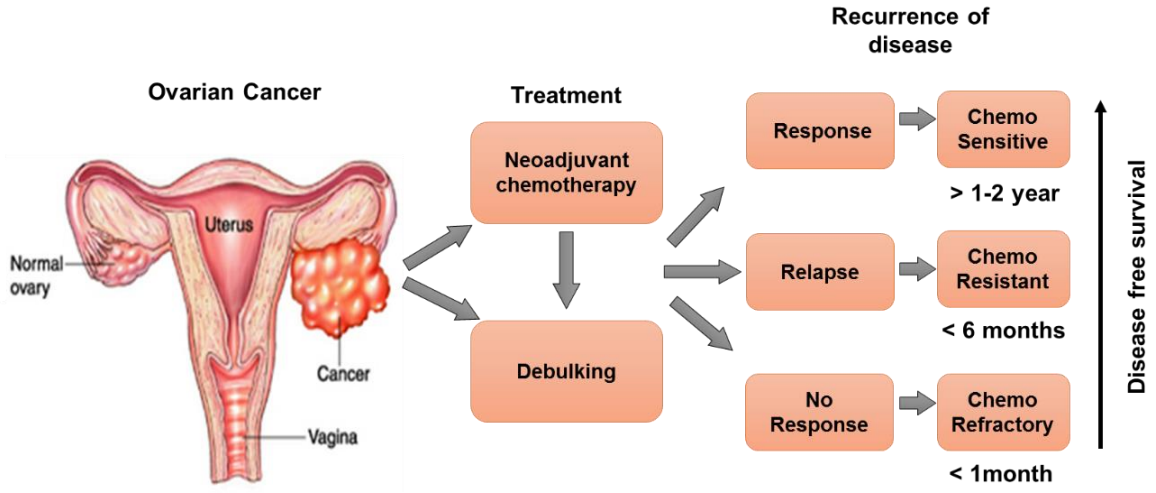

Figure 1.2: Classification of ovarian cancer patients based on recurrence after chemotherapy. *Using neoadjuvant and debulking treatment modalities patients' shows good response initially. However, 30-50% patients relapse and succumb to disease. Patients with no response and who recurs within one month of chemotherapy are called* ***chemo-refractory****. Patients which showed complete remission of the disease are termed as* ***chemo-sensitive****. They often respond to first line therapy again if relapsed after one to one and half years. Patients which relapse within 6 months of chemotherapy, are termed as* ***chemo-resistant****. They are often resistant to first line of chemotherapy and second line of agents is preferred for further treatment [39].*

Chemotherapeutic agents used for the treatment of ovarian cancer First-line chemotherapy with paclitaxel-platinum combination is usually given every 3 weeks for six cycles. A number of novel cytotoxic agents and drugs that target cell survival, drug resistance and apoptotic pathways are now entering clinical trials, and are aimed at overcoming drug resistance. The disease free interval determines the chemotherapy to be followed for the patients with the relapsed disease. If the disease free interval is more than 6 months patients can be re-treated with the same drugs (paclitaxel and carboplatin) or can be re-challenged with other agents. However, for chemo-refractory patients (if relapse of the disease is within a month) a number of drugs are used in place of platinum-taxane combination as the choice of chemotherapy (Table 2).

Drug Type	Drug(s)
Anthracyclines	Doxorubicin, Epirubicin
Topoisomerase inhibitors	Etoposide, Topotecan
Nucleoside analogue	Gemcitabine
Taxane	Docetaxel
Vinca alkaloid	Vinorelbine
Anti-oestrogen	Tamoxifen
Alkylating agent	Hexamethylamine
Anti-inflammatory phytochemicals	Apiegenin, baicalein, curcumin, genistein, luteolin, oridonin & quercetin,

Table 2: Drugs useful in relapsed disease (Adapted from [39-41])

Unfortunately, none of these agents either singly or in combination has proven to be superior for platinum-taxane resistant tumors, thereby the pressing need to investigate the molecular mechanism and development of alternate therapeutics still persists.

Mechanism of action of Cisplatin (Platinum drugs)

Cisplatin chemically known as cisplatinum or cis-diammine-dichloro-platinum (II) is a platinum based drug which is used in first-line of ovarian cancer treatment [42]. After its discovery as an anti-tumor agent, cisplatin is employed for treatment of various cancer like ovarian, bladder, head and neck, esophageal and small lung cancer. The hepato- and gastro-intestinal toxicity caused by cisplatin was minimized by aggressive prehydration and dieresis [43, 44]. Cisplatin acts as a DNA damaging agent and translates the damage into cellular effects like inhibition of DNA synthesis, suppression of RNA transcription, effects on the cell cycle and apoptosis. Thus understanding the mode of drug action is very important for strategic therapy to enhance the anti-tumor activity of cisplatin [42, 45]. Cisplatin is administered intravenously that subsequently enters into the cell evidently by active transport although passive diffusion is also postulated [46] through the cell membrane. Hydrolysis of cisplatin is important for its activity to form aquo (mono or di) species in which one or both chloride groups are replaced by water molecules inside the cell. The diaquo species is very reactive towards nucleophilic centres of intracellular macromolecules to form DNA, RNA and protein adducts because H_2O is an efficient leaving group than Cl^-. The N7 atoms of imidazole rings of guanine and adenine located in the major groove of the double helix are the most accessible and reactive nucleophilic sites for platinum binding to DNA [47]. The reaction of cisplatin with DNA leads to the formation of various structurally different adducts. Although lower percentage of adducts like 1, 3-intrastrand cross-links and interstrand cross-links and DNA-protein crosslinks exists around

65% of adducts are 1, 2-d (GpG) intrastrand cross-links and 20-25% are 1,2d (ApG) intrastrand cross-links are found due to reactivity of cisplatin [48]. Adduct formation results in inhibition of DNA replication, RNA transcription, and arrest at G_2 phase of cell cycle and/or programmed cell death. Cisplatin adducts in DNA are primarily recognised by nucleotide excision repair (NER) pathway proteins and high mobility group proteins which competes for the binding of structurally deformed DNA and cisplatin-DNA adducts and thus inhibits DNA repair [49, 50]. It is reported that DNA mismatch repair (MMR) pathway, a post replication repair system that corrects unpaired or mismatched pair, recognises the cisplatin-DNA adducts but could not remove it. On the other hand, base excision repair (BER) pathway can modulate cisplatin sensitivity. Polymerase β (Polβ), performs BER by bypassing and synthesizing cisplatin intrastrand adducts which might lead to cisplatin-DNA damage tolerance and increased mutagenicity. However, recent study demonstrated that BER and MMR pathways play an epistatic role in mediating cisplatin sensitivity where, the MMR participation in mediating cisplatin cytotoxicity is dependent on the component of BER pathway [51]. DNA-dependent protein kinase (DNA-PK) group of proteins interacts with cisplatin-DNA lesion and is required for elimination of DNA-double strand breaks [52]. Cisplatin triggers apoptosis by activation of various signal transduction pathways. These pathways originate after damage of DNA via activation of DNA repair pathways. It is unclear how DNA damage recognition results in apoptosis, however, activation of c-ABL and JNK (Jun N-terminal kinase) pathway, induction of p53 and ATM-CHK2 pathways following DNA-strand breaks often leads to apoptosis via the intrinsic pathway and contributes to the cytotoxicity of cisplatin. Apoptosis occurs due to an irreversible execution phase in which some proteins and DNA are cleaved. Bcl-2 is an oncogene that seems to be at the convergence apoptotic pathways and the ratio of Bcl-2 to Bax protein determines the cell fate. A conserved feature of the execution phase of apoptosis is the specific degradation

of a series of proteins by the cysteine-aspartate-specific proteases, or caspases. Caspases are activated when an apoptotic stimulus induces the release of cytochrome *c* from mitochondria and results in the formation of apoptosome promoting cell death [52] (Figure 1.3 a).

Mechanism of action of Paclitaxel (Taxane drugs)

Paclitaxel is another of the important antineoplastic agent which is derived from the bark of the Pacific Yew tree - *Taxus brevifolia.* It exhibits a significant toxicity against various solid tumors, including ovarian, breast, non-small cell lung cancer, head and neck carcinomas etc. Unlike other anti-microtubule agents such as vincristine and colchicine which depolymerise microtubules, paclitaxel polymerises and stabilises them [53, 54].

Due to its microtubule stabilizing properties resulting in the accumulation of cells in the G2/M phase of the cycle paclitaxel is used as cytotoxic agent. In addition, cells exposed to paclitaxel develop multiple micronuclei because the nuclear membrane reforms around unsegregated sister chromatids [55]. Paclitaxel binds into a pocket in the β-tubulin (subunit of heterodimeric tubulin) and strongly immobilise after polymerisation and thus stabilises the assembly. Binding of paclitaxel to tubulin proteins attribute to suppression of microtubule dynamics (shortening and lengthening of microtubules). This affects the functioning of cell because dynamic stability is necessary of their normal functioning. For example, during mitosis microtubules are responsible in positioning of the chromosomes during their replication and subsequent separation into the two daughter-cell nuclei [56]. Paclitaxel induced apoptosis is carried out via p53- dependent and p53-independent mechanisms [57, 58] (Figure 1.3b). Induction of apoptosis also occurs by paclitaxel induced modulation of Mitogen activated protein kinase (MAPK) pathway through dephosphorylation of the proapoptotic protein BAD and phosphorylation of Bcl2. Microtubule-associated proteins (MAPs) are the family of proteins that bind to and stabilize microtubule and are endogenous regulators of microtubule stability. One of the MAPs, *tau,*

is responsible for the bundling, spacing, and assembly of microtubules. It competes for taxane binding sites and/or may be involved in the cooperative binding of taxol to microtubules resulting in paclitaxel cytotoxicity [59]. Another MAP protein MAP4 increases microtubule polymerization after paclitaxel binding results in chemo-sensitivity. It was reported that in taxol resistant ovarian cancer cells, phosphorylation of MAP4 and its dissociation from microtubules correlated with decrease in taxol sensitivity [60, 61].

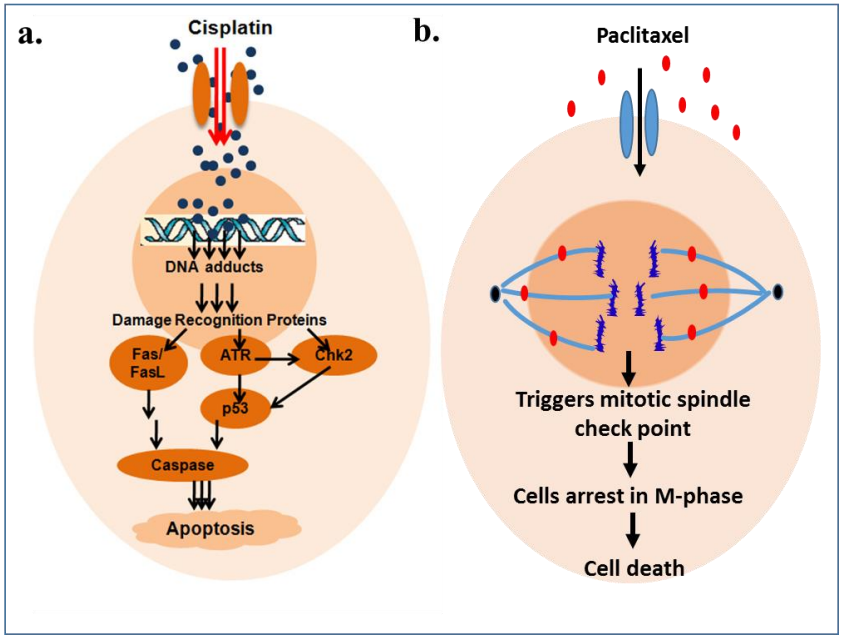

Figure 1.3: Mode of action of drugs (cisplatin and paclitaxel). *(a) Cisplatin enters cell either through active or passive diffusion and form DNA adducts in the nucleus resulting in the activation of DNA damage recognition proteins which causes cell cycle arrest. Apoptotic machinery is further activated with continuous exposure to cisplatin leading to cell death; (b) Paclitaxel stabilises the microtubule and interferes with the normal breakdown of microtubule during cell division, triggering activation of spindle checkpoint and arresting the cells in M-phase resulting in cell death (Adapted from [4, 39]).*

Chemoresistance

Chemotherapy is an inevitable option for the treatment of advanced stage ovarian cancer cases however chemoresistance in relapsed cases is the major obstacle for the clinical management of the disease. Drug resistance is a multifaceted problem and is defined as a phenomenon in which cells elude effects of chemotherapeutic drugs. Despite of high response rate to the initial meticulously designed chemotherapy regime, most of the patients develop resistance to anticancer drugs [62, 63].

De novo (intrinsic) or acquired (extrinsic) chemoresistance are the two most possible mechanism occurring in ovarian cancers [64]. The intrinsic or de novo chemoresistance shows resistance to chemotherapeutic drugs from the very beginning of treatment and is often termed as *chemo-refractory*. Intrinsic resistance originates from cells that already have abilities to limit drug uptake, enhance efflux or activate detoxification of drugs as well as to reduce apoptosis and to increase cell survival. In ovarian cancer, patients who do not respond to the first line of chemotherapy are known to possess intrinsic resistance [39, 65]. Drug inactivation or decreased formation of drug-target complexes that contribute to drug resistance can occur in one of several different ways like lowered affinity of the enzyme for the drug due to amino acid substitution or overproduction of normal substrate of enzyme or enzyme itself that decrease inhibition by the drug.

Alterations in drug efflux mechanisms commonly lead to intrinsic multidrug resistance. Overexpression of ATP-binding cassette (ABC) transporter proteins, such as P-glycoprotein (P-gp), family of multidrug-resistance proteins are involved in intrinsic drug resistance phenomenon. These transporters act by pumping anticancer agents out of the intracellular milieu into the extracellular matrix, thereby preventing the agents from reaching their minimally effective intracellular concentrations [66]. Currently, studies have elucidated the existence of subset of tumor cells with resistant properties against anticancer drugs called as

cancer stem cells (CSCs) or tumor initiating cells which can attribute to intrinsic chemoresistance. This type of cells shows high cell survival rate under chemotherapeutic challenge, quiescent and high spreading capacity under favourable conditions. Sufficient evidence supports the existence of CSCs within ovarian tumors that are capable of initiating tumors, are resistant to chemotherapy and are able to give rise to more differentiated non-tumorigenic cells [67-70].

On contrary, acquired or extrinsic chemoresistance includes genetic and epigenetic alterations of crucial genes in cancer cells during successive exposures to chemotherapy. These genetic and epigenetic modifications eventually induce the cancer cells to acclimatise the effects of apoptotic stresses due to anti-cancer drugs [71]. In ovarian cancer, platinum resistance is defined as acquirement of resistance by less than 6 months of remission following chemotherapy. Clinically, these patients show initial response to chemotherapy but experience relapse within 6 months of the last round of chemotherapy, a time course often described as platinum-free interval or treatment-free interval. Treatment free interval less than 6 months is often used as a clinical cut-off to define platinum resistant disease. Inability to mitigate and counter chemotherapy failure of these patients are majorly attributed to the mechanisms like aberrant membrane transporters, altered drug metabolism, enhanced DNA repair mechanisms, alterations in the expression of genes involved in cell proliferation, cell survival and apoptosis [3]. Novel chemotherapeutic combinations – including non-platinum based therapy, identification of biomarkers and personalized therapy based on the validated biomarkers are some of the chemotherapeutic approaches for the patients with relapse in the disease. In general, monotherapy of paclitaxel or combination with liposomal doxorubicin, topotecan, etoposide, gemcitabine, etc. or few endocrine therapies are in practice [72-74].

Recent studies have shown involvement of microRNAs (miRNAs) in gene regulation and chemoresistance in ovarian cancer. MiRNAs are group of small, non-coding RNAs that bind to the 3'UTR of their target mRNAs under base complementarity via the miRNAs seed sequence. This induces the target mRNA degradation or translational repression, depending on the complementary level of the binding between miRNA and its target mRNAs. miR-22, miR-100, and miR-93 are the few examples of miRNAs which regulate pathways likes PI3K/AKT/mTOR and Phosphatase and Tensin Homolog (PTEN) signaling, and found to be involved in chemoresistance of ovarian cancer [75, 76]. Other mechanisms that are involved in the chemoresistance of both the drugs are elaborated below:

Mechanism of Paclitaxel resistance

Acquired paclitaxel resistance is mediated by a number of mechanisms like overexpression of P-glycoprotein, modification of drug target- tubulin, changes or mutation in mitotic checkpoint signals, detoxification of cytotoxic agents, and enhanced DNA repair mechanisms [77]. The mechanisms attributing paclitaxel resistance are usually determined by *in vitro* studies as mentioned below (Figure 1.4).

Overexpression of Pgp (P- glycoprotein)

The drug transporting Pgp is a transmembrane adenosine triphosphate (ATP) dependent efflux pump encoded by a Multidrug resistance gene 1 (MDR 1) or ATP-binding cassette sub-family B member 1 (ABCB1) gene. It belongs to the ATP-binding cassette (ABC) family of transmembrane proteins involved in multidrug resistance (MDR) phenomenon. It is expressed in a wide variety of tumors and normal tissues and causes resistance to taxanes. Mechanisms by which Pgp overexpression can modulate paclitaxel resistance are amplification of the MDR-1 gene, increased transcription of the MDR-1 gene, mutation and chromosomal rearrangements in the MDR-1 gene [78-81]. Other MDR genes which are not

studied for ovarian cancer but can attribute to paclitaxel resistance are MDR related protein 1(MRP 1), MRP 2 and breast cancer resistance protein BCRP (ABCG2).

Tubulin alterations

Tubulin is a heterodimer of α- and β-tubulin subunits which forms microtubules and a significant portion of cellular cytoskeleton. The equilibrium between tubulin monomers and polymerized tubulin (i.e. the microtubule) is dynamic throughout the cell cycle. Tubulin polymerization and stability is assisted by MAPs. Each β−tubulin molecule binds to an exchangeable molecule of GTP, which leads to polymerization. Hydrolysis of GTP to GDP allows the microtubules to depolymerize. Alterations in microtubule dynamics, altered expression of β-tubulin isotypes, alterations in α-tubulin isotype composition, point mutations in tubulin leading to alterations in microtubule dynamics, post-translational modifications to tubulin, altered expression/post-translational modifications of tubulin/microtubule-regulatory proteins and altered binding of taxol to the microtubule all these mechanism results in the paclitaxel resistance. Study by Mozetti S et al., 2005, indicated that class III beta-tubulin overexpression is a prominent mechanism of paclitaxel resistance in ovarian cancer patients [82].

Genetic changes

Key proteins that mediate various signaling pathways are often localised to microtubules and microtubule targeting drugs like paclitaxel can alter these pathways [83]. Paclitaxel is known to activate mitogen activated protein kinase (MAPK) family through activation of one of the extracellular signal-regulated kinase (ERK 1 and 2) which interacts with microtubule and responds on microtubule disruption. Also, lack of functional p53 or mutations in p53 contribute to paclitaxel resistance [84]. Paclitaxel binds with Bcl-2, an anti-

apoptotic protein, which acts as an additional intracellular target of taxanes. Downregulation of Bcl-2 is found to be involved in paclitaxel resistance [85].

Chemokines and cytokines

Paclitaxel resistance is shown to be associated with overexpression of cytokines like IL6, IL8 and monocyte chemotactic protein-1 (MCP-1) [86]. Transfection of IL6 cDNA in paclitaxel sensitive ovarian cancer cell line increased resistance to paclitaxel by five folds [87]. A possible consequence of increase in IL-6 expression may be a direct consequence of activation of signal transducer and activator of transcription-3 (STAT-3), the effector transcription factor in IL-6 signaling and an important mediator in tumor cell survival in a number of tumor cell lines [88]. In EOC cells, presence of Myeloid differentiation factor 88 (MyD88) which is an adaptor molecule in the TLR-4 signaling, is shown to significantly influence drug response. In a study by Szajnik et al., 2009, paclitaxel treatment showed enhanced cell growth and tumor progression in MyD88 positive EOCs.

Activated AKT and NF-κB signaling alongwith overexpression of antiapoptotic proteins was also reported. On contrary to MyD88 positive EOC cells, MyD88 negative cells showed no proliferation rather demonstrated paclitaxel induced apoptosis by caspase activation. Patients which showed absence of MyD88 expression positively correlated with higher disease free progression interval as compared to the patients with tumors expressing MyD88. Thus MyD88 has been proposed as a potential biomarker for determining chemo-response to paclitaxel in ovarian cancer [18, 89-92].

Kinases and other regulatory proteins

Overexpression of Aurora A, a serine/threonine kinase which is involved in the centrosome separation and bipolar spindle formation, confers resistance to paclitaxel mediated apoptosis [93]. The erb/EGFR family members, HER-2/neu and EGFRVIII (an EGFR variant with a

truncated extracellular domain), are amplified and overexpressed in tumors with taxane treatment [94, 95]. Overexpression of a catalytically active subunit of PI3K in ovarian cancer cells confers taxol resistance, which is reverted upon inhibition of the PI3K pathway utilizing a selective inhibitor [96]. Activation of transcription factors like NF-κB, Interferon regulatory factor 9 (IRF 9), etc., are also responsible for paclitaxel resistance [12].

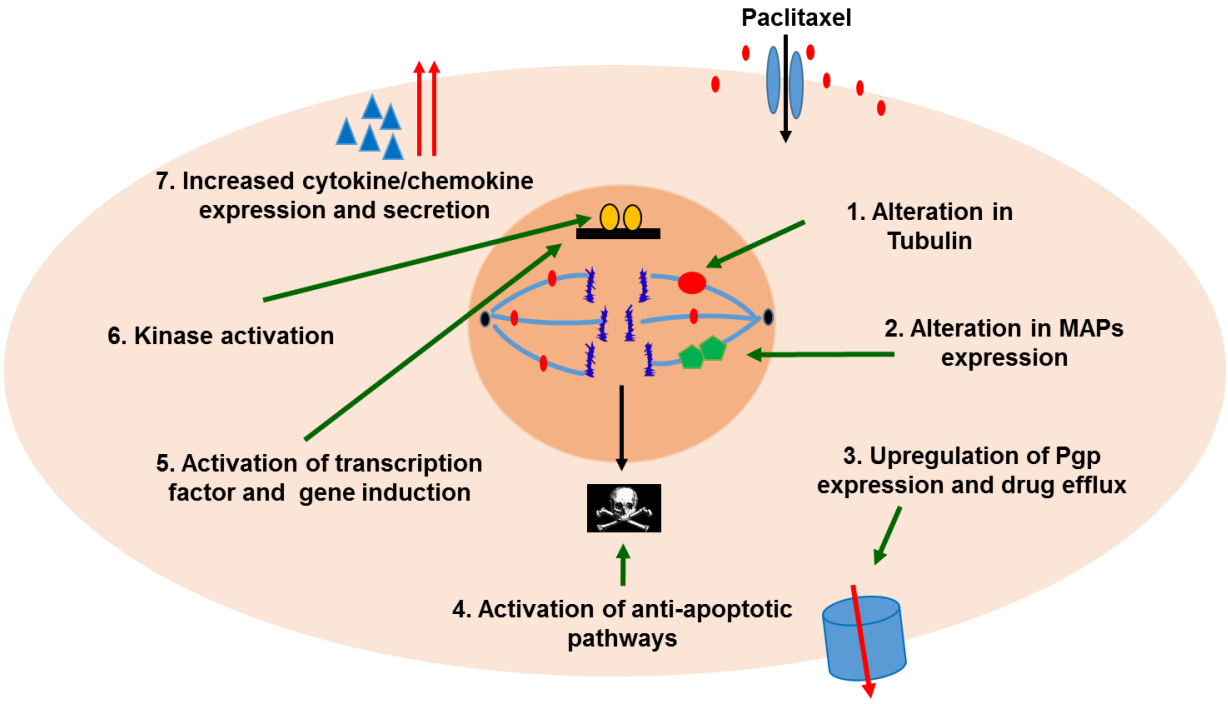

Figure 1.4. Molecular mechanism of paclitaxel resistance. *Resistance to taxanes is complex and can occur by multiple mechanisms including alteration in microtubules, transporters, proteins that regulate the cell cycle, apoptotic machinery, and signal transduction pathways (IKK: Inhibitor of nuclear factor kappa-B kinase; IAP: Inhibitor of apoptosis protein) (Adapted from Greenberger and Samarth [9])*

Mechanism of Cisplatin resistance

Like paclitaxel, cisplatin resistance is also multifactorial and relies on the activation of multiple, non-redundant molecular or cellular events. In a recent review, Galluzi et al., 2014,

classified the mechanisms of cisplatin resistance as alterations (1) which occur immediately after cisplatin enters the cell (*pre-target resistance*), (2) that directly relate to binding of cisplatin to DNA (*on-target resistance*), (3) that activate signaling pathways elicited by cisplatin-mediated DNA damage inducing cell death (*post-target resistance*) and (4) affecting molecular events that do not present obvious links with cisplatin-elicited signals (*off-target resistance*) (Figure 1.5) [97, 98].

Pre-target resistance

Resistant cancer cell elude the cytotoxic potential of cisplatin by reducing the intracellular accumulation of cisplatin and increased sequestration of cisplatin by GSH, metallothioneins, etc. Reduction in the uptake of cisplatin mainly occurs through the copper transporter 1protein (CTR 1) Downregulation and depletion of CTR1 gene had shown enhanced cisplatin resistance [99, 100]. Copper extruding P-type ATPase's like ATP 7A and ATP 7B, that are involved in the regulation of copper ion homeostasis, are upregulated in cisplatin resistant cells [101]. Multidrug-resistance associated protein 2 (MRP 2), a member of ABC family of plasma membrane transporters that mediates cellular efflux of cisplatin are overexpressed in cisplatin resistant cancer cells [102]. Increased inactivation of cisplatin occurs mainly by glutathione (GSH) and metallothioneins which are thiol containing intracellular proteins involved in detoxification of metal ions facilitating cisplatin extrusion. These are also frequently found upregulated in cisplatin resistant cells [103, 104].

On-target resistance

Cisplatin resistant cells show impairment in generation of apoptotic signals after recognition of intra- and inter-strand DNA adducts. Cisplatin resistant cells possess the ability to repair adducts in increased pace or by gaining the ability to tolerate unrepaired DNA lesions by the process of translesion synthesis (TLS). One of the mechanisms of resistance to cisplatin is due to the increased Nucleotide excision repair (NER) proficiency i.e. repair of cisplatin

adducts by excision repair cross-complementing rodent repair deficiency, complementation group 1(ERCC1) and xeroderma pigmentosum complementation group F (XPF) complex. ERCC1 expression negatively correlates with cisplatin responses in ovarian cancer patients [105]. Mismatch repair (MMR) system detects cisplatin- induced DNA damage by MSH2 and MLH1 proteins. MLH1 deficiency is sometimes associated with cisplatin resistance and MLH1 promoter methylation predicts poor survival in relapsing ovarian cancer patients [106, 107]. Increased homologous recombination (HR) repair proficiency and increased TLS repair system are some other on-target mechanism of acquired resistance [108, 109].

Post-target resistance

Plethora of alterations in the signaling cascade involved in the apoptosis and cell survival, results in resistance to cisplatin by many post-target resistance mechanisms. One of the most predominant cellular mechanisms involved in cisplatin resistance is the p53 protein or TP53. It has been shown that the ovarian cancer patients harbouring wild type TP53 respond efficiently to cisplatin based chemotherapy than the patients with TP53 mutations [110]. Another study suggests that cisplatin resistant cells exhibit an increased transcription of specific target genes for example p73 and genes involved in mitochondrial outer membrane permeabilization (MOMP) [111]. Deficiency of pro-apoptotic members of the BCL-2 protein family, BAX/BAK, confers resistance to cisplatin [112, 113].

Overexpression of Bcl-2, Bcl-XL and MCL-1 proteins, the anti-apoptotic members of the Bcl-2 family, are responsible for resistance to cisplatin. Clinical data portrays Bcl-X (L) as a key factor associated with chemotherapy failure in the treatment of ovarian cancer and correlates the expression levels of antiapoptotic Bcl-XL protein with cisplatin resistance and recurrent ovarian cancer [114]. Survivin, caspase inhibitor of the IAP family overexpression is associated with chemoresistance and poor prognosis in many cancers [115]. Several other

factors like calpain, MAPKs, ΔNp63α, X-linked inhibitor of apoptosis protein (XIAP) etc. proteins are altered during cisplatin resistance in ovarian cancer [116-120].

Off-target resistance

Although some of the cell survival signals are not directly activated by cisplatin, many cellular proteins limits the susceptibility of cancer cells to cisplatin by off-target resistance mechanisms. Erythroblastic leukemia viral oncogene homolog 2 (ERBB2) is over-expressed in ovarian carcinomas and has been found to promote cisplatin resistance by Akt murine thymoma viral oncogene homolog 1 (AKT-1) signaling axis [121]. Dual specificity Y-phosphorylation regulated kinase 1B (DYRK1B, also known as MIRK) is upregulated in multiple solid tumors and in ovarian cancer cells and its depletion potentiates the cisplatin toxicity by causing lethal oxidative stress [122]. Some of the poorly understood mechanism that can be involved in ovarian cancer cisplatin resistance includes components of the autophagy like p62/SQSTM1 (sequestosome1) or upregulation of heat shock protein 27 (Hsp 27) [123, 124]. Unfortunately, all these knowledge did not result in development of improved therapeutic molecules in last decade and thus call for more research in this area.

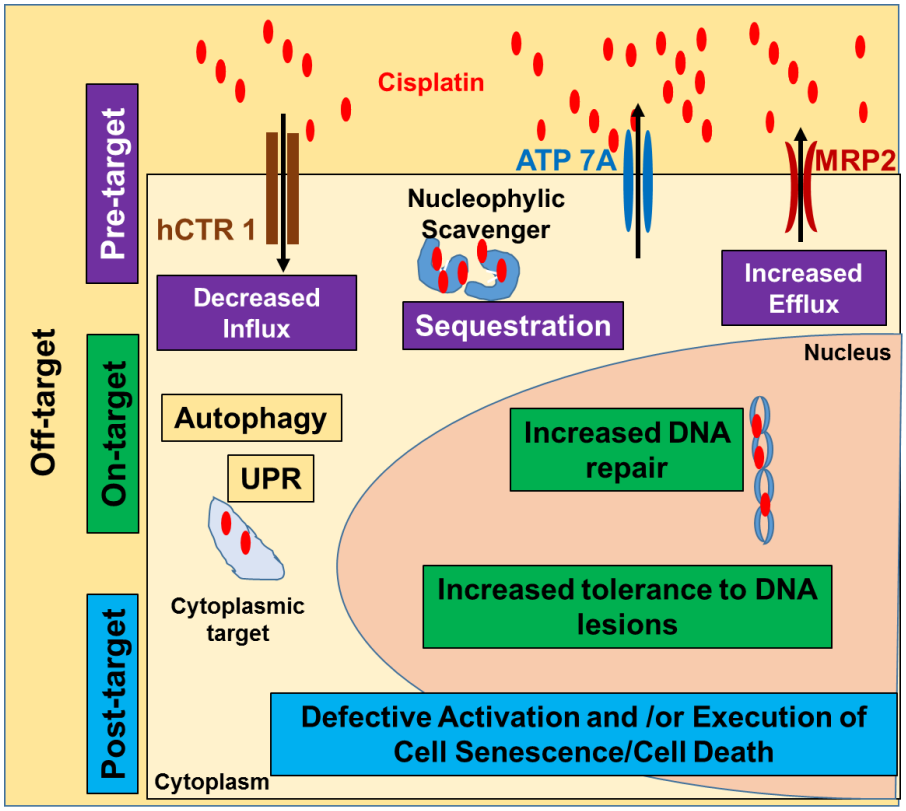

Figure 1.5. Molecular mechanisms of cisplatin resistance. *Genetic and epigenetic alterations are responsible for resistance to cisplatin. This includes pre-target resistance, on-target resistance, post-target resistance and off-target resistance. (Cu2þ transporting, b polypeptide; UPR, unfolded protein response. CDDP aquation is depicted in red) (Adapted from [97]).*

With the advent of whole genome sequencing and better understanding of the deregulated signalling pathways associated with ovarian cancer and drug resistant ovarian cancer many new therapeutic molecules are expected to be identified. To determine the efficacy of those future candidates, improved pre-clinical animal models depicting drug resistant tumor phenotypes and high throughput technologies are particularly in demand. A detail understanding on cytotoxic action of platinum and taxol drugs based on literature accelerates development of such drug resistant *in vitro* and *in vivo* models.

In this study we have made an attempt to investigate some of the common pre, on and post-target mechanisms responsible for resistance to cisplatin and paclitaxel in epithelial ovarian cancer cells. Although it is not possible to describe all the molecular alterations, few, but essential proteins in the study are broadly studied to in an effort of deciphering the mystery of drug resistance. These are tumor suppressor gene (such as TP53), oncogene (such as PI3K/AKT), and components of apoptotic machinery (such as XIAP, NF-κB and the Bcl-2 family) [2, 14, 125-131].

Tp53 (p53-Tumor suppressor gene)

The p53 is a hub of many signaling pathways which controls the cell cycle and maintains the integrity of the genome. In humans, p53 is encoded by Tp53 gene located on the short arm of chromosome 17(17p13). p53 has been called a "cellular gatekeeper" or "the guardian of the genome" because of its central role in coordinating the cellular responses to a broad range of cellular stress factors [132]. In normal cellular conditions, the major negative regulator, MDM2, binds to p53 and inhibits its transcriptional activity and provides stability. Functionally, the p53 protein acts as a transcription factor, binding to specific DNA sequences. *In vitro* data suggest that it binds as a tetramer to the consensus sequence motif RRRCWWGYYY (N 0–13) RRRCWWGYYY (where R is a purine, W is an adenine or thymine, Y is a pyrimidine and N is any base). In response to various stress signals like exposure to chemotherapeutic drugs, hypoxia, ribosomal stress, DNA damage, telomere erosion and others, p53 can be activated, principally through nullifying MDM2 (mutant double minute 2) inhibition, and transcriptionally induces the expression of an array of target genes leading to different cellular outcomes. Classically, p53 is been implicated in controlling genes involved in cell cycle arrest, DNA repair, apoptosis, senescence, autophagy and metabolism [133-135]. p53 is the most frequently mutated gene in human

cancer, but until recently was believed to be "undruggable". For example, development of drugs like PRIMA, PRIMA-1MET or nutlins, which have the property of restoring wild type functions of the mutated p53 are currently in the early-phase clinical trials [136]. Inactivation of p53 occurs by mutation in approximately 50% of all human cancers. However, triple negative breast cancer, high grade serous epithelial ovarian cancer (EOC) and squamous lung cancer the observed frequency of mutation is found to be more than 80%. According to the cancer genome atlas network data, TP53 mutations are found in approximately 80% of high grade serous EOCs [7, 137]. A few hot spot sites for mutation have been identified, especially at residues V157, R158, R175, G245, R248, R249 and R273 [137]. Mutation in p53 generally results in loss of wildtype (WT) activity and formation of a protein with a dominant negative activity against any allelic wild type protein. Mutation can give rise to gain of function such as induction of the angiogenic, metastasis and resistance to specific therapies. Binding of MDM2, promotes transfer of p53 from nucleus to cytoplasm leading to its inactivation. Inactivation of p53, in certain cancer, is caused by being bound by proteins encoded by certain DNA viruses. For example, the E6 protein of human papillomavirus (HPV) types 16/18 binds to and inactivates WT p53 in cervical cells leading to multistep formation of cervical cancer [138].

Mutant p53, which have constitutively active p53, confers cancer cells with drug resistance in several ways like elevating certain DNA repair mechanisms allowing the cells to survive; elevating expression of ABC transporters allowing efflux of drugs out of the cells; attenuating cell death by elevating the expression of antiapoptotic proteins and reducing expression of proapoptotic proteins; modulating expression of metabolic scavengers; and elevating expression of detoxifying enzymes [139]. A clinical study demonstrated that patient with gain of function (GOF) mutations in p53 have a greater likelihood of platinum treatment resistance and distant metastatic properties in HGS-OvCa. In this study, the

comprehensive somatic mutation profile obtained from The Cancer Genome Atlas (TCGA) was evaluated for the clinicopathological features of tumors with hotspot GOF mutations in p53 [140].

PI3K/AKT signaling axis

Another significant hallmark of cancer is the overexpression and/or activation of the phosphoinositide-3 kinase (PI3K)/AKT survival pathway. Improper activation of this pathway is associated with tumorigenesis in several tissue types [141-143]. AKT, the immediate effector of the PI3K activation, on activation enhances the survival of ovarian carcinoma cells and promotes chemoresistance through attenuating p53 proapoptotic signaling [118, 119, 144]. In the PI3K pathway, the inactive form of protein PI3K, composed of catalytic subunit (p110) and regulatory subunit (p85), in the cytoplasm is activated through conformational changes that occurs when ligands binds receptor tyrosine kinases (RTKs) on the cytoplasmic membrane. This interaction causes the p85-p110 complex to move to the cytoplasm tail of the RTK receptor and leads to activation of the PI3K kinase. PI3K activation causes the generation of PtdIns (3,4,5) P_3 (PIP_3) by the phosphorylation of the PtdIns (3,4,5) P_2 (PIP2), which functions as a second messenger activating multiple downstream pathways. The basic function of PIP_3 is the recruitment to the inner membrane and activation of pleckstrin homology domain–containing proteins. Among them, the most important event is the recruitment of the AKT protein. AKT is activated through two basic steps: translocation to the plasma membrane and phosphorylation at the serine/threonine residues [145, 146]. AKT activation gives rise to multiple biological activities including increased survival, proliferation, and growth of tumor cells. The tumor suppressor PTEN is the most important negative regulator of the PI3K signaling pathway which dephosphorylates the phosphorylation of PIP2 to PIP3, thus

inactivating AKT. The AKT family consists of three members (AKT1, AKT2, and AKT3) that have high sequence homology and share similar domain structures. The N-terminal pleckstrin homology (PH) domain is necessary for protein–protein interaction, a central catalytic domain is important for AKT kinase activity whereas C-terminal is the regulatory domain. AKT is activated through recruitment to the plasma membrane by PIP3, followed by phosphorylation of Thr308 and Ser473 by the phosphoinositide dependent kinase 1 (PDK1). PI3K initiated AKT signaling inactivates several proapoptotic factors including BAD, procaspase-9 and Forkhead (FKHR) transcription factors. AKT also activates IκB kinase (IKK) to phosphorylate IκB (inhibitor of NF-κB) leading to its proteasomal degradation and nuclear localization of NF-κB. AKT-mediated activation of mammalian target of rapamycin (mTOR) is important in stimulating cell proliferation. mTOR regulates translation in response to nutrients by phosphorylating components of the protein synthesis machinery. Other factors that are activated through AKT are vascular endothelial growth factor (VEGF) transcriptional activation and induced hypoxia inducible factor-1α (HIF1α) expression which are required for cell growth and angiogenesis [10, 142, 147-150].

Alterations in the PI3K/AKT pathway

Amplification in Phosphoinositol kinase catalytic subunit α (PIK3CA) gene is a more common phenomenon than mutation in EOC and it requires attention for therapeutic intervention. However, mutations are rare and clustered to the histologic subtype endometrioid and clear cell variants. The common hot spot mutations in the PIK3CA gene are present at H1047R, E542K and E545K. [7]. A transforming mutation (E17K) in the pleckstrin homology domain of AKT 1 has been reported [151]. Although no modifications or mutations in the AKT2 gene have been found in mammals, AKT2 gene amplifications

have been found in ovarian and breast tumors [152]. Similarly, no reports exist for any alterations in the AKT 3 gene. The role of PTEN in ovarian cancer is small and very few cases have PTEN focal deletion and mutation in the PTEN gene [7, 153].

PI3K pathway and chemoresistance

In a clinical study, Kolasa et al., 2009, showed that PI3KCA amplification in about 24% of 117 cases of ovarian cancer patients and was more prevalent in TP53 mutant tumors. Their findings also suggested that patients with complete remission (CR) of the disease correlated with the lower frequency of PIK3CA amplification than those treated with taxane-platinum (TP) or platinum-cyclophosphamide (PC) regimens [8]. Such observations indicated the role of PIK3CA amplification as an independent predictor of chemotherapy response in OC during development of chemoresistance. PIK3CA is expressed in non-proliferating tumor cells in ovarian cancer and is directly upregulated by NF-κB [154]. Overexpression of AKT has been demonstrated in cisplatin resistant ovarian cancer cell lines, compared to the respective cisplatin sensitive cell lines [144, 155-157]. Peng et al., 2010, showed that cisplatin treatment can activate PI3K-AKT pathway along with induction of apoptosis [10]. Many *in vitro* evidences suggest that PI3K activation is associated with decreased sensitivity to several different chemotherapeutic agents, including paclitaxel, doxorubicin and 5-fluorouracil. It was demonstrated that ovarian cancer cells overexpressing constitutively active AKT or containing AKT gene amplification were highly resistant to paclitaxel as compared to cancer cells expressing low AKT levels. Constitutively active AKT inhibits the release of cytochrome-C normally induced by paclitaxel thereby promoting apoptosis resistance [158, 159].

However, it is unclear whether an aberration in this pathway is the critical driver of cancer growth and therefore susceptible to targeted inhibition in ovarian cancer. Several agents are

being explored in clinical trials of ovarian cancer and it will be important to correlate any evidence of clinical activity with pathway alterations. A plethora of promising AKT inhibitors are being use in preclinical and clinical trials including perifosine, MK-2206, RX-0201, PBI-05204 and GSK2141795 [160]. However, none of them has reached the clinics. According to Pal et al., 2010, to optimize the activity of AKT inhibitors, identification of relevant biomarkers that predicts their activity is crucial. These potential biomarkers can be pAKT, PIK3CA mutation, and loss of PTEN expression. Although the biomarker validation is laborious, AKT inhibitors alongwith putative biomarker information can be engaged for clinical application [160, 161].

Anti-apoptotic Machinery

One of the classical hallmarks of cancer is defects in cell death signalling particularly apoptotic cell death. Apoptosis is often inhibited in tumour cells due to overexpression of anti-apoptotic proteins (e.g. Bcl-2) or decreased expression of pro-apoptotic proteins (e.g. Fas). Bcl-2 family of proteins and inhibitors of apoptosis (IAPs) are known to inhibit apoptosis.

Bcl-2

B-cell lymphoma-2 (Bcl-2) gene occurs at the t (14:18) chromosome translocation breakpoint in B-cell follicular lymphomas, where its transcription becomes excessively driven by the immunoglobulin heavy chain gene promoter and enhancer on chromosome 14 [162]. Bcl-2 does not promote cell proliferation like most oncogenes do, rather its overexpression inhibits cell death. This pathway predominantly leads to the activation of caspase-9 [163]. In humans, six anti-apoptotic members of the Bcl-2 family have been identified (Bcl-2, Bcl-x_L, Bcl-B, Bcl-W, Bfl-1, and Mcl-1) [164]. These proteins contain a

hydrophobic cleft that is able to bind to BH3-only proteins and to the pro-apoptotic Bcl-2 family members Bad, Bak, and Bax to inhibit apoptosis. The BH4 domain of Bcl-2 and Bcl-XL can bind to the C terminal part of Apaf-1, thus inhibiting the association of Caspase-9 with Apaf-1. If this binding doesn't occur, the pro-apoptotic Bcl-2 members are recruited to the outer mitochondrial membrane (OMM) at which they oligomerize and cause OMM permeabilization, releasing proapoptotic effectors such as cytochrome *c*. The released cytochrome *c* binds to Apaf-1 and pro-caspase 9 to from the apoptosome, which generates mature caspase 9 and begins a proteolytic cascade, ultimately resulting in cell death [163].

IAPs: XIAP

Inhibitor of apoptosis proteins (IAPs) are group of eight different proteins as they can bind and neutralise caspases and thus acts as anti-apoptotic proteins. Of the known human IAP related proteins, X-linked inhibitor of apoptosis (XIAP) is the most potent inhibitor. XIAP can function directly at the downstream effector caspase (caspase-3, caspase-7 and caspase-9).

Chemoresistance in ovarian cancer: role of antiapoptotic proteins

Cancer cells are typically 'addicted' to a fairly small number of anti-apoptotic proteins for their survival, providing a strong rationale for targeting these proteins therapeutically. Most prominent among these are the anti-apoptotic Bcl-2 family members, inhibitor of apoptosis proteins (IAPs) and the caspase 8 inhibitor FLIP. Mutations, amplifications, chromosomal translocations and overexpression of the genes encoding these proteins have been associated with various malignancies and linked to resistance to chemotherapy and targeted therapies [165]. Moreover, these genes are transcriptional targets for pro-survival transcription factors such as nuclear factor-κB (NF-κB) and signal transducer and activator of transcription 3

(STAT-3). During tumorigenesis, these transcription factors are activated by oncogenic mutations in kinases that regulate upstream pro-survival signalling pathways. As discussed above, cisplatin-mediated cytotoxicity is based on the recognition of DNA damage by MMR proteins and activation of p53. The activation of p53, in turn, leads to transcriptional upregulation of pro-apoptotic proteins such as BAX, BAK, and downregulation of anti-apoptotic proteins such as Bcl-2 and IAPs, resulting in cell death via apoptosis. Inactivation of p53 could therefore result in drug resistance [39]. The X-linked inhibitor of apoptosis (XIAP) is directly linked to chemoresistance as the upregulation of it confers resistance to chemotherapy. XIAP levels are elevated in many cancer cell lines, and several reports have shown that suppression of XIAP protein levels can sensitize cancer cells to chemotherapeutic drugs [166]. For both cisplatin and paclitaxel, Bcl-2 has shown to affect drug sensitivity *in vitro*. The role of Bcl-2 and the IAP survivin in mediating drug resistance is also supported by clinical studies. However, in some studies, contrary to expectation, overexpression of Bcl-2 has been found to be a good prognostic marker in EOCs [167, 168].

Pro-survival pathway: NF-κB pathway

The nuclear factor-κ light chain enhancer of activated B cells (NF-κB) signal transduction pathway is well known to regulate diverse contrasting cellular responses such as proliferation, differentiation, cell division, cell survival, apoptosis, immunity, and inflammation. The role of various cellular components in this signalling pathway is primarily to control the cellular localization of the NF-κB transcription factor. In a latent state, NF-κB dimers are held inactive in the cytoplasm through association with IκB proteins. However, diverse stimuli, including tumor necrosis factor-α (TNFα) or lipopolysaccharide (LPS), induce activation of the IκB kinase complex, leading to phosphorylation, ubiquitination, and degradation of IκB proteins. Released NF-κB dimers

translocate to the nucleus, bind specific DNA sequences, and promote transcription of target genes. Thus, the core elements of the NF-κB pathway are the ***IKK complex, IκB proteins, and NF-κB dimers*** [169].

Mechanism of activation of NF-κB

AKT activates the inhibitor of κB kinases (IKK) through phosphorylation of IKKα on Thr23, leading to IκB phosphorylation and degradation, and subsequent activation of the transcription factor NF-κB. NF-κB, in turn, promotes the transcription of several pro-survival genes [170]. Other factors which results in the activation of NF-κB are MEK and p38 [171]. Another important cellular signaling that elicits innate responses through NFκB activation is mediated through the Toll like receptor (TLR) family. All the TLRs signaling pathways culminate in activation of NF-κB transcription factor responsible for the production of array of cytokines [17].

TLR-4 signaling

Toll-like receptors (TLRs) play an essential role in the detection of invading pathogens in the body [172]. Structurally, TLRs are transmembrane proteins composed cytoplasmic C-terminal domain, known as the Toll/IL-1 receptor (TIR) domain, which is required for downstream signaling. TLRs recruit specific combination of TIR-domain containing adaptors which includes myeloid differentiation primary response gene 88 (MyD88), TIR containing adaptor protein/MyD88-adaptor like protein (TIRAP/MAL), TIR-containing adaptor inducing interferon-β (IFN-β)/TIR-domain-containing adaptor molecule 1 (TRIF/TICAM 1), Depending upon the type of adaptor moieties, TLR signaling is largely divided into two pathways: MyD88-dependent and MyD88-independent or TRIF dependent [172]. MyD88 dependent TLR-4 signaling activates distinct pathways involving the NF-κB

pathways and the mitogen-activated protein kinase (MAPK) pathway and leads to pro-inflammatory response characterized by production of cytokines and chemokines [17, 172, 173]. On the other hand, MyD88 independent pathway, or TRIF dependent pathway results in robust NF-κB activation (late phase activation). The late phase NF-κB activation is induced by a secondary response through newly synthesized TNFα and is mainly responsible for the production of type I IFN induction and other interferon response genes [17, 172, 173].

NF-κB: Role in ovarian cancer and chemoresistance

The NF-κB family of transcription factors is expressed constitutively in many tissue types and has been identified in tumors of epithelial origin including breast, colon, lung and ovarian carcinoma [174]. In many studies, NF-κB is implicated in ovarian cancer proliferation and cytokine secretion *in vitro* [175, 176]. Clinically, a correlation was observed between activation status of NF-κB and poor prognosis of EOC. Nuclear expression of NF-κB, p65 correlates with the poor differentiation and late FIGO stage in EOC tumors. Also, patients with NF-κB p65 positivity showed lower survival rates than those were negative [13, 177, 178]. Recent studies have shown that multiple mechanism are involved along with NF-κB leading to ovarian carcinogenesis. These information were achieved by *in vitro* activation or specific inhibition of the NF-κB pathway using either small-molecule inhibitors or short interfering RNA (siRNA) that has shown to affect the growth behaviour of EOC cells. For example, TNF-like weak inducer of apoptosis (TWEAK) activates NF-κB in highly metastatic human ovarian cancer cells, whereas siRNA against NF-κB1 is associated with cell growth and colony formation by human EOC cell lines [179-181]. Increased NF-κB signaling has also been reported to confer resistance to cisplatin-induced apoptosis [131]. Studies revealed that treatment of epithelial ovarian carcinomas with carboplatin upregulates NF-κB expression [182, 183]. An oncoproteomic

analysis of carboplatin resistant EOC tumors revealed an upregulation of the Rel A protein, a component of NF-κB family [184, 185]. One study showed that activation of NF-κB reduced paclitaxel induced apoptosis whereas another studies have shown to mediate paclitaxel induced apoptosis [127, 186, 187]. Thus, the overall role of NF-κB in carcinogenesis ultimately depends on whether it is proapoptotic or anti-apoptotic in particular cancer cells.

As described above several components of various pathways (influx-efflux pathway, detoxification pathway, apoptosis pathway, cell survival pathway) critically regulate acquirement of drug resistance in EOC. Majority of this information come from in vitro studies using drug resistant EOC cells or from analysis of tumor samples obtained from chemo resistant patients. However, utilization of these data for identifying druggable targets and developing appropriate therapeutics require well designed pre-clinical models and high throughput technologies. One such technology which gained tremendous popularity in drug discovery and validation field is Non-invasive Molecular Imaging that enables repeated detection of signatures of molecular events spatially and temporally from living subjects.

Non-invasive Molecular Imaging of Small Living Models

A plethora of novel imaging modalities are available for monitoring tumor responses and detecting presence of tumors [188]. Non-invasive molecular imaging techniques can be indispensable tools for the visualization, characterization and measurement of biological processes at the molecular and cellular levels in humans and other living systems [189]. Common molecular imaging techniques include Magnetic Resonance Imaging (MRI), Computed tomography (CT), Optical Bioluminescence and Fluorescence imaging, Ultrasound (US) Imaging, Single Photon Emission Computed Tomography (SPECT), and Positron Emission Tomography (PET) [190]. For imaging a molecular event in *in vivo*

condition an imaging probe is required that would interact with its target in the live animal generating specific molecular signatures. These signatures can be easily captured by specific detectors and can be analysed to gain information about the molecular event. These signatures can be radioactive rays (X-ray, gamma or beta), nuclear magnetic resonance, sound waves or light emissions. The most widely used imaging strategies are *direct* and *indirect* imaging. In direct imaging, probes are directly developed against endogenous targets like receptors or enzymes and the resultant image of probe intensity is directly proportional to the interaction with the target [5, 191]. A classic example is imaging of radiolabelled herceptin antibody (trastuzumab) developed against human epidermal growth factor receptor 2 (HER2/neu), in breast cancer patients [192-194].

Direct imaging technique requires development of probes against large number of endogenous biomolecules which is difficult to achieve. However, it is the most preferred technique for human imaging. On the other hand, in indirect imaging strategy reporter gene and probes are exogenously incorporated in living subjects to follow the molecular events. Though with the limitation of using only in small animals, indirect imaging approach is commonly used to generate information about the desired molecular event [195, 196]. Currently, various reporter genes have emerged as powerful tools for non-invasive molecular imaging [197, 198]. *In vivo* imaging using these reporter genes thereby facilitates clinical translation of novel findings related to imaging agents, gene expression, etc. [189].

Molecular imaging allows the visualization of normal and abnormal cellular processes in living subjects at the molecular or genomic level along with the anatomic level [190]. *In vivo* imaging modalities can be broadly classified into anatomical and functional imaging. Traditional anatomical imaging modalities include MRI, US and CT scanning that use the interaction of electromagnetic waves with the tissues and generate structural information. Functional molecular imaging (FMI) requires an imaging probe that is specific for a given

molecular event and produce physiological information. FMI involves non-invasive detection of molecular and metabolic factors in the living subject via probes which is made possible by radionuclide imaging (PET and SPECT) and non-radionuclide imaging (MRI, Optical bioluminescence and fluorescence imaging) and photoacoustic imaging [199]. For disease management, combined *in vivo* imaging with functional and anatomical imaging modalities is the standard clinical practice [4].

Radionuclide imaging

Radionuclide imaging that includes Positron Emission Tomography (PET) and Single photon Emission Computed Tomography (SPECT) techniques detects gamma rays emitted by a radiolabelled (positron emitter or gamma emitter) probe introduced in the body and accumulated in the tissues of interest. In PET, emission of two high-energy gamma rays (511 Kev) are simultaneously detected by two detectors situated 180° apart (an event called coincidence) in the scanner. The positron-emitting isotopes commonly used in biology are ^{11}C, ^{13}N, ^{15}O, ^{124}I, ^{64}Cu and ^{18}F. The most frequently used PET agent is ^{18}Ffluorodeoxyglucose (FDG), a glucose analog that is selectively taken up by metabolically active cells, a distinguishing feature of the malignant cells (FDG is approved by FDA for monitoring malignancies and treatment response in patients) [200].

PET (^{18}FDG)/CT plays an important role in ovarian cancer recurrence, as the metabolic tracer is able to increase lesion detection, the fusion of metabolic and anatomical imaging aids the determination of the exact location of disease and it is capable of surveying the whole body. Several studies have examined the performance of PET/CT scanning in patients with recurrent ovarian cancer and describe the distribution of metastasis [201204]. PET/CT was able to detect active disease at relatively low levels of CA125, thereby facilitating the early diagnosis of recurrence or residual disease [205, 206]. Several preclinical studies have

used microPET imaging in human xenografts of ovarian cancer models to monitor the role of therapeutics [207-210]. In a recent report, radiolabelling of anti-CA125 monoclonal antibody and anti-CA125 scFv (single chain variable fragment) with 64Cu presented specific tumor uptake rendering them as a potential immuno-PET probes for targeted *in vivo* molecular imaging of CA125 in EOC [211].

Aide et al., 2010, used SKOV3 tumor xenografts as cisplatin resistant ovarian cancer model and studied the therapeutic response of everolimus using 3-deoxy-3-^{18}Fflorothymidine (FLT) -PET imaging. This study showed that FLT-PET could be useful in monitoring the early response of inhibitors used against mammalian target of rapamycin (mTOR) pathway in preclinical model of human cisplatin resistant ovarian tumor. In SPECT, only one low-energy gamma ray is detected by single detector. To avoid detection of multiple events by the same detector, SPECT requires lead collimeters that decreases the sensitivity (a log fold lower than PET) [190]. Till date six isotopes for SPECT [Gallium-67 (^{67}Ga), Iodine-123 (^{123}I), Iodine-125 (^{125}I), Indium-111 (^{111}In), and Lutetium-177 (177Lu), and Technetium-99 m (^{99m}Tc)] are commonly used in clinics. The radionuclide imaging approaches exhibit higher spatial resolution of 1–2 mm with no limit on the depth penetration [30].

In ovarian cancer, SPECT-based imaging is extensively used for patients which are folate receptor positive. Folate receptor (FR) is a folate-binding protein expressed at high levels in ovarian cancer but minimally distributed on normal cells [212]. Etarfolatide is a ^{99m}Technetium molecularly targeted imaging agent that detects lesions expressing FRs. Etarfolatide is designed as a companion imaging agent to FR-targeted therapy of vintafolide Imaging with ^{99m}Tc-etarfolatide represents a non-invasive, real-time approach to identifying patients with FR-positive lesions. ^{99m}Tc-etarfolatide has the potential to select patients for vintafolide therapy without the need for a biopsy [213]. In a study by Scalici JM et al., 2013,

radiolabeled ^{111}In-VCAM (Vascular Cell adhesion molecule-1) specific peptide imaging probes and SPECT were used in a mouse model of resistant ovarian cancer to study peritoneal metastasis and identified VCAM-1 as a viable imaging target [214]. Another study by Muller C et al., 2008, revealed that pre-application of pemetrexed (anti-folate) with clinically tested ^{111}In-DTPA-folate (DTPA is diethylenetriaminepentaacetic acid) in a human ovarian cancer xenografted mouse model was advantageous in reducing the accumulation of radioactivity in kidney as observed by SPECT imaging [215].

MR imaging

Magnetic resonance imaging (MRI) is a non-invasive radiological technique that uses magnetic field and radio waves to form images of the organs. [190]. MRI has highest spatial resolution (25–100 μm) among all the modalities. [30, 216]. MRI with contrast enhancing agents provided the highest post-test probability of ovarian cancer when compared with CT, Doppler ultrasound, or MRI without contrast-enhancing agents in adnexal masses of suspected cases [217]. Diffusion weighted imaging (DWI) is a non-invasive functional MRI method (DWMRI) that determines diffusion of water molecules in tumors, providing information on density, volume and size. DWMRI provides sensitivity of 91.1% in predicting cytoreductive success in patients diagnosed with advanced ovarian cancer [218-220]. Hensley et al., 2007, performed a MRI imaging study, on genetically induced TgMISIIR-Tag-DR26 transgenic mice using a standard combination therapy consisting of cisplatin and paclitaxel. This study demonstrated that serial MRI with gadopentetate dimeglumine (Gd-DTPA) contrast agent is useful for quantitative analysis of tumor growth and progression and measurement of response to the therapeutic interventions in 41 ovarian cancer bearing mice [221]. MRI in combination with other modality was also used to monitor tumor-specific biology, such as protease and integrin activity [222].

CT imaging

In CT imaging, tissues with variable density differentially absorb X-rays passing through the living subject and are collected by high resolution CCD detectors. The spatial resolution is of 50–100μm [190]. Preoperative CT is the preferred technique used for accurate detection of inoperable tumor and for the prediction of suboptimal debulking in newly diagnosed epithelial ovarian cancer. It helps to select patients who might be more appropriately managed by neoadjuvant chemotherapy [223]. Another study demonstrated that CT scan has 87% precision in detection of benign or malignant tumors along with high specificity (85%) and sensitivity (90%) and 55% and 89% accuracy in detecting stage I/II and stage III/IV, respectively [224]. Small animal computed tomography was also used to visualize and quantify intraperitoneal (IP) cancer in mouse model of ovarian cancer by implantation of Hey A8 cells in the intraperitoneal cavity [225]. CT is often used as a multimodality approach for better visualisation of tumor. In a mouse model, a CXCR4-radiolabeled antibody was successfully used for tumor visualization by SPECT-CT [226].

US imaging

In ultrasound imaging reflections of high frequency sound waves (produced from a transducer) are captured by the detectors. Each tissue reflects the sound with a different frequency based on their density, and therefore, creates contrast images at 50–100 μm resolution. This is classically an anatomical imaging modality. However, Doppler imaging and micro-bubbles attached to antibodies specific for blood vessel are now also being used for functional imaging [190]. Microbubbles are tiny microspheres (<1 millimetre) filled with air or per fluorocarbon. On application of ultrasound waves it is able to oscillate and reflect the ultrasound waves. Thus microbubble has found utility as contrast agents in ultrasonography [227] and confers a functional aspect of this classical structural imaging

modality. Transvaginal sonography (TVS) transvaginal ultrasound is the preferred technique for initial evaluation because of its availability, high resolution, and lack of ionizing radiation for ovarian cancer. However, this mode of diagnosis faces limitations like inability to differentiate benign from malignant tumors and is ineffective in identifying cancerous cells in normal-sized ovaries. A wide range of sensitivities and specificities, 85–100% and 52–100%, respectively, has been reported for detection of ovarian malignancies by ultrasound [228-231]. A multimodal screening approach which combines ultrasonography (TVS) along with blood serum marker like CA125 can accelerate early stage detection of ovarian cancer [30, 232]. Ultrasound imaging was used in small animal model in combination with other imaging techniques. In a study by Cho S et al., 2013, a syngeneic epithelial mouse model was developed that replicates the characteristics seen in human ovarian cancer by using Doppler ultrasound imaging [233]. In another study by Barua et al., 2010, a laying hen was used as a preclinical model of early stage ovarian cancer to study the tumor associated neoangiogenesis Doppler ultrasonography [234].

Optical imaging

Optical imaging, such as bioluminescence and fluorescence are emerging as powerful modalities for monitoring disease and therapy in small animals. Combining innovative molecular biology and chemistry, researchers have developed optical methods for imaging a variety of cellular and molecular processes *in vivo*, including protein-protein interactions, protein degradation, and protease activity [190]. Optical imaging can primarily be categorized to bioluminescence and fluorescence based on the reporter genes and signals.

Fluorescence Imaging

In fluorescence imaging, an external light source of appropriate wavelength is used to excite a target fluorescent molecule, followed almost immediately by release of longer wavelength, lower-energy light for imaging. *In vivo* fluorescence imaging uses a sensitive camera to detect fluorescence emission from fluorophores in whole-body living small animals [235]. Cells tagged with fluorescently labeled antibodies, fluorophores designed against endogenous molecular targets, exogenous fluorescent proteins (green fluorescent protein [GFP] and related molecules), or optical contrast agents tagged with fluorescent molecules like quantum dots are used in fluorescence imaging. This modality possesses a spatial resolution of 2-5mm. Fluorescence imaging often encounters high background due to auto-fluorescence and absorption of light signals generated by the excited fluorophores (present in fluorescent proteins) or fluorochromes (present in fluorescent dyes, nanoparticles or quantum dots) and is less sensitive [190]. Fluorescent probes that 'turns on' only under specific conditions and results in emission at a certain wavelength are described as 'activatable' probes [236]. Activatable probes are commonly used for functional fluorescence imaging of enzyme activity. They often contain two or more identical or different flurochrome joined in close proximity to each other by an enzyme specific peptide linker. In the absence of the target protease, the fluorochrome is quenched by the close proximity of a second fluorochrome molecule. In the presence of the protease, the peptide substrate is cleaved releasing the fluorochromes and resulting in fluorescence [237]. An emerging new class of probes for *in-vivo* fluorescence imaging are semiconductor nanocrystals or quantum dots which are gaining popularity for wide variety of applications [238]. Quantum dots (QDs) typically have a core/ shell structure of 2–8 nm in diameter with size-dependent fluorescence emission. Fluorescent QDs require excitation from external

illumination sources to fluoresce. Such quantum dots can be conjugated to chemotherapeutic drugs to visualize drug activity [238, 239].

First in-human proof-of-principle and the potential benefit of intraoperative tumor-specific fluorescence imaging in staging and debulking surgery for ovarian cancer using the systemically administered targeted fluorescent agent folate-FITC was described in a study. FR-α–targeted fluorescent agent was used for intraoperative fluorescence imaging in patients diagnosed with ovarian tumors (malignant or benign) [240]. Recently, a novel clinical imaging strategy was demonstrated by using the dual PET and optical, FR targeted PPF (a multimodal, PET and optical, folate receptor (FR) targeted agent) for ovarian cancer management. This PPF can non-invasively delineate FR-positive, primary human serous ovarian cancer xenografts as well as micrometastases in the peritoneum using both PET and fluorescence imaging modalities [207]. QDs were used to detect the CA125 levels in ovarian cancer specimens with high specificity and sensitivity than fluorescein isothiocyanate (FITC) [241]. In another study, bioimaging of HeyA8 ovarian cancer cells was reported with the help of QDs coated with natural silk fibroin [242].

Bioluminescence Imaging

Bioluminescence refers to emission of light by the enzymatic reaction of a luciferase enzyme with its substrate. Bioluminescence imaging (BLI) requires a reporter construct to produce protein called luciferase, which catalyses the conversion of D-luciferin to oxyluciferin and provides imaging contrast by light emission. Here, luciferase is the reporter because it reports the location by emission of light under appropriate conditions [243]. The most frequently used bioluminescent reporter for research has been the luciferase obtained from the beetle Firefly (*Photinus pyralis)* which is commonly called as *firefly luciferase (Fluc).* Another luciferase from the beetle family includes the click beetle (*Pyrophorus plagaiophalum*) luciferase or *CBluc*, which has been molecularly engineered to emit light at

either red (*CBRluc*) or green (*CBGrluc*) spectra. Bioluminescence is a common phenomenon observed in many marine organisms. Several luciferase genes from sea pancy, *Renilla renifomis (Rluc),* jelly fish, *Aequorea victoria* (*Aluc*), marine copepod, *Guassia princeps (Gluc) and Metridia longa (Mluc),* have been isolated, cloned, molecularly engineered and used for many applications. All these luciferase-bearing organisms require a separate gene to encode for the substrate (luciferin or coelenterazine) which is catalyzed under appropriate circumstances to generate light. In contrary, many gram negative and luminescent bacteria like *Photorhabdus luminscens* and *Xenorhabdus luminescens* contain *lux* operon that simultaneously transcribe genes for both luciferase and luciferin [244]. The bacterial *lux* operons are widely used to noninvasively image bacterial infections from living subjects where exogenous introduction of luciferin is not required [245]. Many luciferases present in corals (*Tenilla*) and bacteria (*Vibrio fischeri* and *V. harveyi*) are yet to be cloned and exploited for applications [246].

Firefly luciferase or Fluc, the most extensively used bioluminescence reporter, is a heat stable enzyme with no post translational modification with a half-life of approximately 2-3 hours [247]. *Fluc* produces photons in a reaction that requires ATP, magnesium, and a benzothiazoyl–thiazole luciferin. Light emission from the firefly luciferase-catalyzed luciferin reaction is broad-band (530–640 nm) and peaks at 562 nm. On contrary, *Rluc* is ATP independent and uses coelenterazine (and its analogues that differ in their properties of autofluorescence). Light emission from the *Renilla luciferase*, (*Rluc)* catalysed coelenterazine reaction is in between (460-490 nm) [246].Each luciferase has its own substrate specificity, characteristic wavelength of light emission and optimal parameters. Along with the optical properties of biological tissue this emission spectrum allows light to penetrate through several centimetres of tissue, thus making it possible to detect light emitted from internal organs in mice that are express luciferase as a reporter gene. Since the

substrates for marine and beetle luciferases do not cross react with each other, it is possible to use both reporters in the same cell or animal. This can be achieved by either imaging each enzyme action sequentially or taking advantage of different spectral emission peaks to differentiate the two enzymes. Thus, more than one luciferase can be imaged simultaneously thereby allowing measurement of two molecular events at the same time; for example *Rluc* and *Fluc* can be imaged together with minimal interference. The major limitation of this approach is its inability to reach clinic. Also the signal imaged at the surface lacks information on the exact size and depth of tumor. As penetration of light is limited with depth, imaging of tumor tissues to a depth greater than 1cm is difficult. However, BLI is of low cost and non-invasive in nature and facilitates real-time analysis of disease processes at the molecular level in living organisms [247]. BLI is easy to execute and enables monitoring throughout the course of disease, allowing localization and serial quantification of biological processes without killing the experimental animal. BLI is extensively used in pre-clinical models of ovarian cancer to monitor tumor burden during the use of chemotherapy and exploiting biomarker as therapeutic intervention. A novel ErbB2-targeting bioluminescence protein was generated by fusing EC1 with *Gluc*, and was conjugated to a liposome to construct the EC1-*GLuc*-liposome. It was found that the ErbB2-targeted bioluminescence imaging and selective delivery of HPTS (fluorescent dye encapsulated in the liposome) by the EC1-GLuc-liposome was effective not only in the SKOV3 cells *in vitro*, but also in metastatic ovarian tumors *in vivo* [248]. Bioluminescence imaging studies in living mice showed that treatment with AMD3100, a clinically approved inhibitor of CXCL12-CXCR4, blocked ligand-receptor binding and reduced growth of ovarian cancer cells [249, 250]. A syngeneic mouse model by mouse ID8 ovarian cancer cells stably expressing a green fluorescent protein (GFP)/luciferase fusion product under the control of a synthetic NF-κB-dependent promoter allowed the intra-vital mapping of NF-κB activity during tumor

progression. It provided unique insight in modulating NF-κB activity on host cell immune responses in the tumor microenvironment serving powerful tool for pre-clinical testing of agents that target NFκB in ovarian cancer [251]. Recently, BLI was also used in preclinical study of ovarian cancer cells to validated intraperitoneal natural killer cell immunotherapy [252]. In another study, combined surgical intervention and adjuvant chemotherapy (carboplatin and paclitaxel) was demonstrated for the first time in an orthotopic xenograft model of ovarian cancer [253].

Bioluminescence Imaging: a modality of choice for high precision molecular imaging

Reporter gene imaging achieved by any of the above-mentioned imaging techniques: radionuclide, ultrasound, magnetic resonance or optical could be the modality of choice for pre-clinical applications. The reporter gene is introduced in mouse tissue by three principle strategies. A transgenic animal can be created for a specific reporter and imaged with appropriate modality or the reporter gene can be delivered in different tissues using gene delivery vectors like viruses. The third strategy comprised of *ex vivo* engineering of cells with specific reporter and subsequent introduction to the animal. Precise monitoring of molecular events from a multi cellular organism requires detection with high sensitivity and specificity. BLI provides significant advantages over radioactive imaging strategies such as PET and SPECT, in which the unbound or unincorporated radiotracer produces relatively high background in the host animal. The inherently low background of luciferase enables imaging of broad dynamic range at extremely low levels in biochemical assays. The necessity of substrate coupled with near absence of auto-luminescence in mammalian tissue is the reason for low background *in vivo* for BLI. Thus among all the imaging modalities, bioluminescence imaging is the most sensitive technique with a detection limit of 10^{-15}–10^{-17} mole/L. Therefore, subtle alteration in the promoter activity or gene expression level

can be best detected by bioluminescence imaging. This superior range of sensitivity allows us to image as few as 10 cells from live mice which is almost not possible with any other modalities [183]. This high level of sensitivity is conferred by the extremely low background signal thereby generating high signal to background noise ratio. In contrary, *in vivo* fluorescence imaging though achieve comparable level of sensitivity (10^{-9}–10^{-12} mole/L) does get limited due to high auto-fluorescence exhibited by biomolecules. PET, SPECT (10^{-9}–10^{-12} mole/L) and MRI (10^{-3}–10^{-5} mole/L) demonstrate much lower detection limit. Along with high detection sensitivity, bioluminescence imaging requires seconds to minute of acquisition for capturing the molecular events. Extremely low background signal and rapid turnover of luciferases (half-lives are 2-6hrs) allow repeated imaging of the same tumors within smaller time window and detect molecular changes. All the other modalities require much larger time window for repeated monitoring of the molecular events.

Bioluminescence imaging has another advantage of using different reporters to monitor two or three different molecular simultaneously and repeatedly from same tumor xenografts. No other modalities except in vivo fluorescence imaging technique can achieve this multiplexing strategy. [254]Finally, low cost instrumentation, user friendly software and scope of imaging multiple subjects at a time makes bioluminescence imaging a more preferable technique for pre-clinical imaging research. [255]. Therefore, we have adapted this imaging modality for our study.

Rationale of the study

Regardless of many improvements in the treatment of ovarian cancer, recurrent chemoresistant form of the disease remains principal phenomenon leading to the utmost cause of death from gynaecological malignancies. Although many mechanisms attribute to drug resistance, a predefined approach to mitigate this disease is still not clear. Many *in vitro* and *in vivo* studies have facilitated a better understanding of targeted therapeutics for

signaling pathways involved in drug resistance. However, due to complexity of the disease there is a constant need to investigate for more molecular and therapeutic aids to circumvent this phenomenon. *In vitro* drug resistant model of ovarian cancer can provide a better platform for understanding the intriguing molecular mechanisms of chemoresistance. Further, use of *in vivo* tumor xenografts from the drug resistant cells of ovarian cancer substantiates a preclinical model to examine new therapeutic candidates and decipher the molecular mechanisms involved in chemoresistance. Thus pre-clinical models of drug resistance can support emergence of potential target for therapeutics and diagnosis of chemoresistance in cancer. They can also furnish the need of repetitive and non-invasive monitoring of theranostic molecules used either to suppress or reverse the chemoresistant phenomenon. As described earlier, among various survival pathways, the PI3K/AKT/mTOR signaling is often found activated and plays important role in development of platinum (cisplatin or carboplatin) and paclitaxel resistance. Activating mutation in the kinase domains of PIK3CA or AKT is the underlying cause for deregulated PI3K/AKT/mTOR signalling in majority of the cancers such breast cancer, colorectal cancer, gastrointestinal cancers. In past few years, many potent small molecules of PI3K inhibitors have been developed, and at least fifteen compounds have progressed into clinical trials as new anticancer drugs [256]. It is now well proven that amplification in PIK3CA gene is a more common phenomenon than mutation in EOC and it requires attention for therapeutic intervention [8]. Gene amplification at chromosomal level may lead to increased transcript level as well as increased promoter modulation. Even with such important clinical observation, no attempt is been made to study the promoter modulation of PIK3CA in response to chemotherapeutics in cells, and during development of resistance as well as in preclinical models. The PIK3CA promoter was first isolated from normal human ovarian surface epithelium (OSE) by Astanehe et al., (2008) who showed that PIK3CA promoter

bears four p53 binding response elements and undergoes p53 mediated repression after activation of p53 [19]. Both cisplatin and paclitaxel are known to induce cell death through p53 activation. However, the effect of these drugs on PIK3CA promoter in ovarian cancer cells is yet to be understood. ***Therefore, a major objective of the current study focuses on deciphering therapeutic action on PIK3CA promoter during acquirement of resistance in in vitro and in vivo preclinical mice model using non-invasive imaging***.

Furthermore, in our quest of deciphering the molecular mechanism of chemoresistance we looked at the NF-κB pathway as one of the downstream components of PI3K signalling axis during acquired resistance. Since a large number of EOCs harbour active TLR4/MyD88 signalling which is an alternate and critical pathway to activate NF-κB and cell survival mechanism and presence of MyD88 and not TLR-4 determines the sensitivity of EOC cells to paclitaxel, MyD88 is hypothesized to cause intrinsic resistance [18]. However, a significant percentage of EOC patients (~60%) were shown to be $MyD88^{negative}$, out of which around 40% cases exhibited disease recurrence [18]. The status and role of NF-κB signaling in these chemoresistant $MyD88^{negative}$ populations is unclear and certainly requires further investigation for devising new therapeutic strategies.

Objectives:

The current investigation therefore includes four objectives, which are expanded as individual chapters in this study

1. *Construction of a PIK3CA sensor consisting of a reporter system and to study the effects of drugs in the ovarian cancer cell lines and in vivo tumor xenografts stably expressing this sensor*
2. *Development of cellular chemo-resistant models expressing the PIK3CA sensor and monitor the modulation of PIK3CA promoter activity in effect of chemotherapeutic drugs*

3. *Non-invasive optical imaging of the development of an in-vivo chemo-resistant models and monitoring dynamics of chemo-resistance in the tumors formed by the stable cells expressing the PIK3CA sensor*
4. *Characterize the chemo-resistant models by monitoring alterations in the PI3K/ AKT signaling, NF-κB pathway and antiapoptotic genes*

Chapter 2

Construction and validation of a PIK3CA sensor consisting of a reporter system in effect of drugs in ovarian cancer cells and in vivo tumor xenografts by non-invasive optical imaging

Introduction

The PI3K (Phosphoinositol 3-kinase)/AKT signaling components are frequently altered in human cancers and have been identified as crucial players in ovarian cancer. PI3Ks belong to a lipid kinase family that regulates a broad spectrum of cellular activities. These lipid kinases are known to phosphorylate the membrane phosphoinositols 4,5-biphosphate (PI(4,5)-P2) into PIP(3,4,5)3. This conversion of PIP2 to PIP3 allows AKT and PDK1 to be recruited in the cell membrane resulting in phosphorylation at Thr-308 of the kinase domain of AKT and further activation. AKT is the central molecule in the PI3K/AKT/mTOR signaling pathway which plays pivotal role in cellular functions like protein synthesis and cell growth and is involved in multiple cancer associated functions like cell survival, proliferation and migration (Figure 2.1) [257].

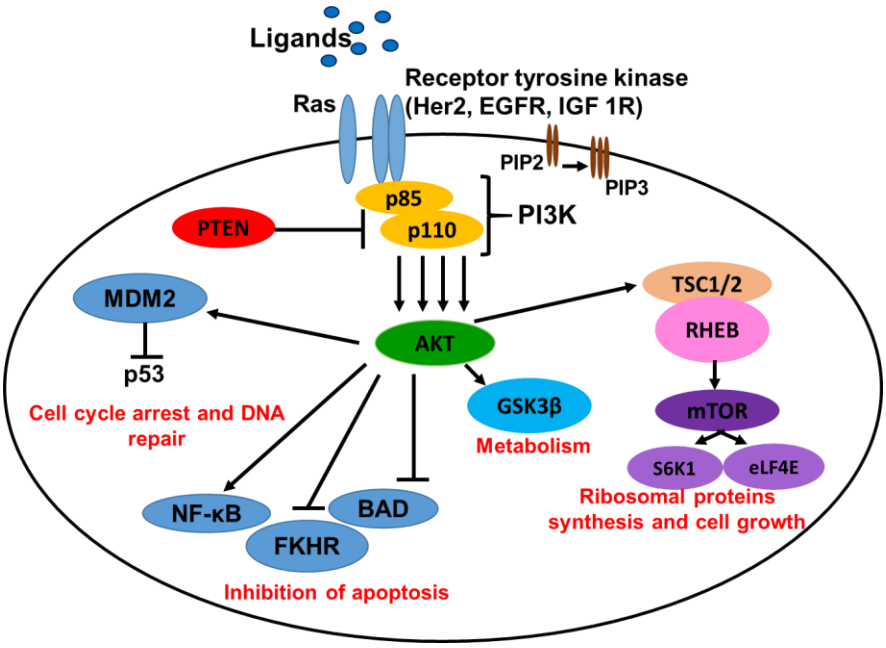

Figure 2.1: Schematic representation of the PI3K/AKT/mTOR pathway. *Growth factors such as EGF, IGF bind as ligands to the receptor tyrosine kinases like EGFR, IGF1R and Her2, thereby leading to conformational changes and further activation of PI3K. PI3K is a heterodimeric protein consisting of a regulatory subunit p85 and a catalytic subunit p110.*

PI3K initiates activation of AKT through phosphorylation which acts as a major source of activation to further downstream signalling moieties involved in various cellular processes such as (text in red) ribosomal protein synthesis and cell growth (mTOR, S6K1 and eIF4E), loss of apoptosis (through inhibition of BAD, FKHR and activation of NFkB), metabolism (activation of GSK3β), cell-cycle arrest and DNA repair mediated by p53.

Based on their structural characteristics and substrate specificity, PI3Ks are divided into three classes and each class is comprised of a regulatory and a catalytic unit. Class I PI3K is again categorised into two subclasses as IA and IB which relay cellular signalling after being activated by either receptor tyrosine kinase (RTKs) or G-protein coupled receptors (GPCRs) respectively. Class IB PI3K is a heterodimeric protein composed of a catalytic subunit p110γ and a regulatory subunit p101, expressed mainly in leukocytes. Class IA PI3K is also heterodimer consisting of three forms of p110 catalytic unit and a p85 regulatory unit. The three p110 catalytic isoforms are known as p110α, p110β and p110δ. Expression of p110δ isoform is mainly restricted to immune system whereas p110α and p110β express ubiquitously. Class III PI3K is involved in autophagy, while specific function of class II PI3K is not well understood (Figure 2.2). The focus of this study is on the regulation of the phosphatidylinositol-4, 5-bisphosphate 3-kinase catalytic subunit alpha (PIK3CA) of Class IA since PIK3CA gene is frequently altered in ovarian and other cancers and hence is implicated as oncogene [258].

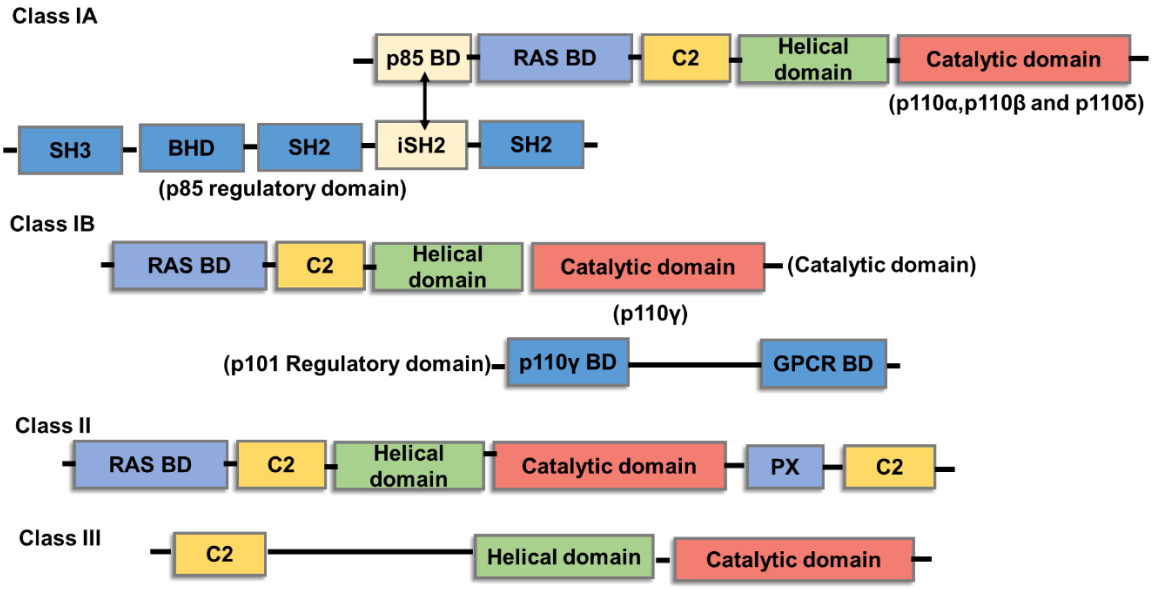

Figure 2.2: The members of the phosphoinositide 3-kinase (PI3K) family. *Based on their substrate specificities, PI3Ks have been divided into three classes.* ***Class IA*** *PI3Ks are heterodimers consisting of a p110 catalytic subunit and a p85 regulatory subunit. The catalytic subunit has three isoforms viz., p110α, p110β and p110δ which are encoded by three genes, PIK3CA, PIK3CB and PIK3CD respectively. The p110 catalytic isoforms are highly homologous and share five distinct domains: an N-terminal p85-binding domain (p85BD) that interacts with the p85 regulatory subunit, a Ras-binding domain (RasBD) that mediates activation by members of the Ras family of small GTPases, a putative membrane-binding domain C2, the helical domain and the C-terminal kinase catalytic domain. The regulatory subunit consists of three core domains including a p110-binding domain (denoted as inter-SH2 or iSH2) flanked by two Src-homology 2 (SH2) domains (N-terminal nSH2 and C-terminal cSH2). Src-homology 3 (SH3) domain and a BCR homology (BH) domain located in their extended N-terminal regions. In the basal state, p85 binds to the N-terminus of the p110 subunit via its iSH2 domain, inhibiting its catalytic activity.* ***Class IB*** *PI3K is a heterodimer composed of a catalytic subunit p110γ and a regulatory subunit p101.* ***Class II*** *PI3Ks are monomers with only a single catalytic subunit and has N-terminus*

followed by a Ras binding domain (RasBD), C2 domain, helical domain, and catalytic domain with PX and C2 domains at the C-termini. ***Class III*** *PI3Ks consists of a single catalytic subunit Vps34 (homolog of the yeast vacuolar protein-sorting defective 34) (Figure adapted from Liu et al., 2009 [258]).*

Gain-in-function mutation of PI3K signaling pathway components and amplification at 3q22–26, which harbours the PIK3CA gene are the common alterations found in non- small cell lung cancer, colorectal cancer and gastric cancer [259-262]. In epithelial ovarian cancer, around 70% cases show alterations in the PI3K signaling pathway either by gene amplifications in PIK3CA & AKT 2 or through activating mutation in AKT & PIK3CA and inactivating mutation in PTEN [263]. Approximately, 40% of ovarian cancer show amplification in at 3q26 region, which contains the PIK3CA gene [264]. Although increased PIK3CA transcript has been described in 17-35% of ovarian carcinomas, AKT activation has been emphasised in approximately 50% of the cases [151, 265, 266]. Kolasa et al., 2009, reported PIK3CA amplification in 24% of 117 cases of EOC patients and which were more prevalent in TP53 mutant tumors. Their study also revealed that this amplification occurs independent of histological subtypes and is negatively associated with platinum sensitivity [8]. According to The Cancer Genome Atlas network study, amplification (18%) rather than mutations (<1%) in PIK3CA gene is prevalent in serous adenocarcinoma, the most common EOC subtype [7]. However, the consequence of the amplification in PIK3CA gene has hardly been studied in ovarian cancer.

Gene amplification at chromosomal level may lead to increased transcript level as well as increased promoter modulation. Singh et al., 2002, showed that in head and neck squamous cell carcinoma cells, p53 negatively regulates PIK3CA transcript and protein levels in a PTEN-independent manner [267]. However, it was not known whether this inhibitory effect

of p53 on PIK3CA expression was a direct consequence or whether intermediate steps involving various signal mediators were involved. Astanehe et al., 2008, identified and characterised a PIK3CA promoter from the ovarian surface epithelial cells (OSE) containing putative p53 and Y-box transcription factor binding sites [19, 268].

Conditional suppression of p53 led to increase in PIK3CA promoter activity and p110α expression both at transcript and protein levels suggesting that p53 negatively regulates PIK3CA expression through direct binding to the promoter. This study corroborates with the clinical observations of association of p53 mutations and PI3K gene amplification in ovarian carcinoma made by Kolasa et al. [8]. However, the study by Astanehe et al., was done in primary OSE which are the precursor of EOCs [19]. The same promoter when isolated from Human Bacterial chromosome showed to bear NF-kb, hypoxia inducible factor, heat shock protein and activator protein 1(AP1) binding sites [13]. Inhibition of nuclear translocation of NF-κB or incubation with TNF-α resulted in down or up regulation of PIK3CA promoter activity [13]. Thus PIK3CA expression encounters complex regulation by several transcriptional regulators. This complex regulation becomes more intricate in neoplastic condition and therefore it is essential to understand the trend and mechanistic detail of the action of drugs on this vital promoter. Both cisplatin and paclitaxel, the standard therapeutics for ovarian cancer, are known to induce cell death through p53 activation. However, the effect of these drugs on PIK3CA promoter in ovarian cancer cells is yet to be understood.

Recently, non-invasive imaging of molecular events in small animals has become a standard practice to evaluate new drugs targets and their delivery. Combination of reporter genes which can be used with multiple imaging devices allows collection of multiple signals from deep inside the body, with higher sensitivity and specificity over reporter genes suitable for only single imaging modality [20, 34]. Over the years, the group at Molecular Imaging

Program at Stanford (MIPS), Stanford University, California have built a small library of fusion reporter vectors and have been applying to monitor tumor metastasis, cell/stem cell trafficking, stem cell therapy, and other areas [22,23,24]. These fusion vectors comprise of a bioluminescent (either *fluc* or *hrluc* and their mutants), a fluorescent (either *gfp* or red fluorescent proteins and their mutants) and a PET reporter (sr39 mutant thymidine kinase or wild type thymidine kinase) gene joined by small peptide linkers [20, 21].

To understand and monitor the PIK3CA promoter modulation by chemotherapeutic drugs used for ovarian cancer in *in vitro* and *in vivo* small animals, we used CMV-*fluc2-tdt*, one of the bi-fusion reporters and generated a PIK3CA sensor competent for both *in vitro* and *in vivo* imaging studies. Using various ovarian cancer cell lines we investigated the association of p53 with PIK3CA promoter modulation in response to drug treatments.

Materials and Methods

Cell culture and transfections: Standard aseptic practice was followed for performing cell culture. The different ovarian cancer cell lines used their respective media are shown below:

Cell line	Origin	Source	Culture Medium
PA1	Teratocarcinoma (Germ cell ovarian cancer)	NCCS,Pune, India	DMEM
A2780	Undifferentiated EOC	ATCC	DMEM
SKOV3	Serous adenocarcinoma	ATCC	McCoy's

All these medium were supplemented with 10% FBS, 1% penicillin-streptomycin solutions.

Prior to the day of transfection, cells were seeded to achieve ~60 % confluency.

Transfection was carried out using Superfect transfection reagent and following the manufacturer guideline. Post 48 hrs of transfection, cells were analysed for the expression of both luciferase and red fluorescence protein (*tdt*). For producing stable expression, cells were carried out for G418 selection after transfection. Detailed experimental details are given in the section 8.1.

Drug Treatments

Treatments of cisplatin and paclitaxel of different concentration were given to cells according to the need of experiment. Cisplatin (30 µg/µl) stock is freshly prepared every time by diluting in DMSO. Paclitaxel (10 µg/µl) is diluted in DMSO, aliquoted and stored in -20°C. Repeated freezing and thawing of paclitaxel stock is avoided.

Plasmids:

The *pcDNA 3.1(+)-CMV-fluc2-tdt* plasmid comprises of a fusion reporter competent for both *in vitro* and *in vivo* imaging studies. It consists of a mutant red fluorescent proteins with better photon efficiency (*tandem dimer Tomato (tdt*)) and a codon optimized highly sensitive bioluminescence reporter (*firefly luciferase 2* or *fluc2*).

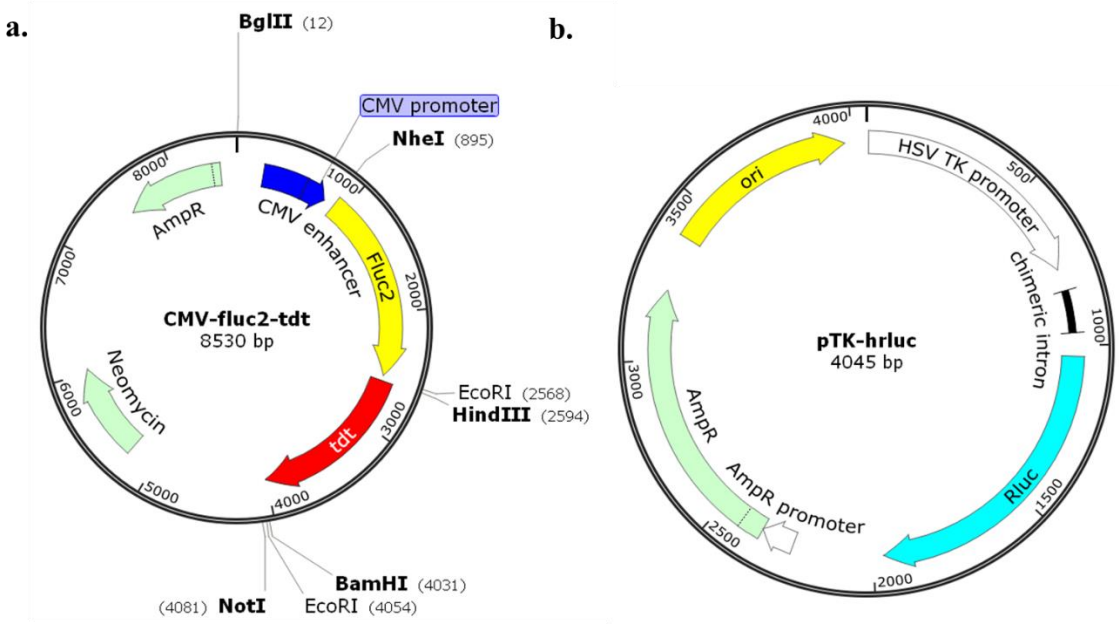

Figure 2.3. Plasmid map of CMV-fluc2-tdt (a) and pTK-hrluc (b). *This plasmid was used as a vector for the construction of PIK3CA sensor. pTK-hrluc (Thymidine kinase (TK) promoter driving humanized renilla luciferase) was used as an internal control for every luciferase assay reaction (Figure 2.3).*

Construction of a PIK3CA sensor

PCR amplification and standard cloning techniques were used to generate the PIK3CA sensor. The PIK3CA promoter [12] was PCR amplified from pGL3 vector (carrying PIK3CA promoter driven luciferase gene) using primers given below:

Primer	Sequences
Forward primer	GTAAGATCTACTGCTCCTACGCTTC
Reverse primer	GCAGCTAGCTCGTGTAAACAAACAACG

Primers used for the amplification of the PIK3CA promoter

The PCR reaction mixture used for the amplification of PIK3CA promoter is as follows:

Reagents	**Sample (µL)**	**Negative Control(µL)**
H2O	13	14
5x GC Buffer	5	5
dNTPs	1	1
Forward primer (10pM)	2	2
Reverse primer (10pM)	2	2
Plasmid DNA (50ng)	1	--
DNA Polymerase	1	1

The thermal cycler program for the amplification of the PIK3CA promoter is as follows:

Sr.No.	**Steps**	**Temperature (°C)**	**Time (sec)**
1	Initial Denaturation	95	120
2	Denaturation	95	30
3	Annealing	52	30
4	Extension	68	60
5	Repeat (2-4)	Cycle 29	
6	Final Extension	68	300
7	Hold	4	Forever

The 934 bp of PCR product (expected size of PIK3CA promoter) was visualised on 1% agarose gel and eluted using QIAGEN plasmid purification kit. The PCR product was then digested with both NheI and BglII restriction enzymes. Simultaneously, the vector CMV*fluc2-tdt* bifusion plasmid was digested with the same enzymes and ligation reaction

was set at 3:1 (insert: vector) ratio (Figure 2.4). After transformation, positive clones were confirmed by PCR amplification, restriction digestion (EcoRI) and sequencing. Detailed protocol for the restriction digestion and ligation is described in the section 8.9.

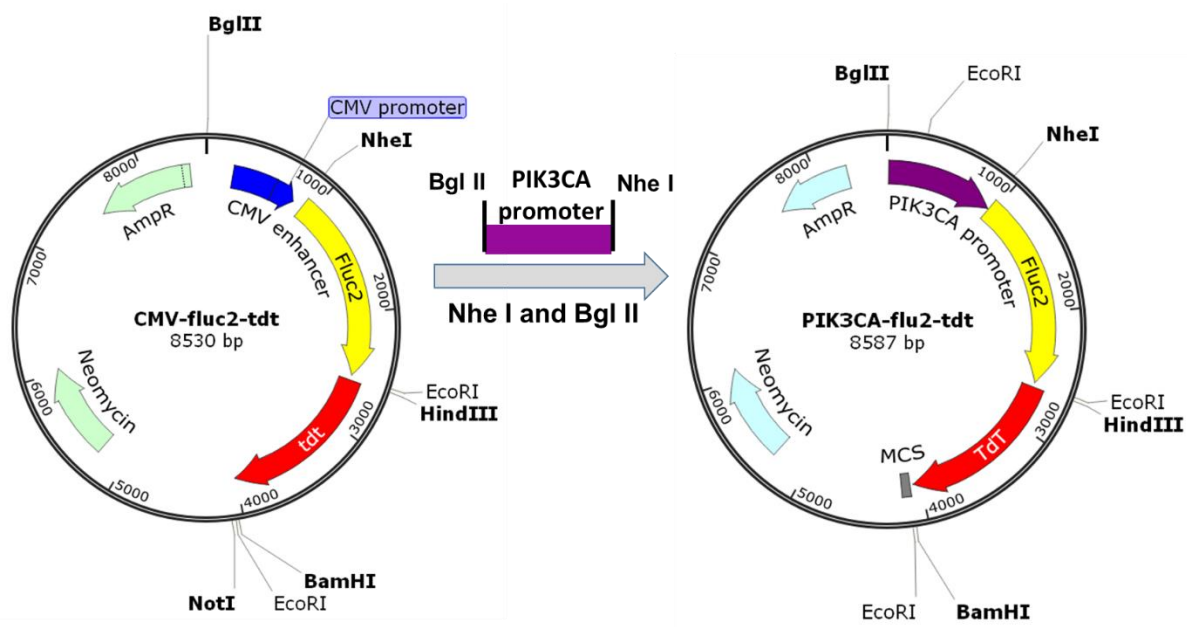

Figure 2.4. Cloning strategy for the construction of the PIK3CA sensor. *Map of the vector CMV-fluc2-tdt (left) and amplified PIK3CA promoter (middle). Both vector and PIK3CA promoter were digested with restriction enzymes NheI and BglII to construct the PIK3CA-fluc2-tdt (right).*

Luciferase assay

Cells from both transient transfections and the stable indicator lines were cultured in 24 well flat bottom plate at an equal density. The detailed procedure for luciferase assay is given in the section 8.14. The lysates were used for *renilla* and *firefly luciferase* assays using Dual–Luciferase Reporter Assay System from Promega. The relative light unit per second (RLU/sec) was normalised with protein estimated by Bradford method. Each of the luciferase reactions was measured in a Berthold luminometer for period of 60 sec. All the transfection and drug treatment experiments were done in triplicates and repeated at least twice.

Western blotting / Immunoblotting:

The protein lysates were prepared by using passive lysis buffer and concentration of proteins was estimated by Bradford assay. The proteins were resolved in SDS PAGE and transferred to nitrocellulose membrane. Membrane was probed with the appropriate primary antibodies and HRP-conjugated secondary antibodies. The immune complexes were detected using Pierce ECL systems according to instructions supplied by the manufacturer. The detailed procedure of western blotting is given in the section 8.15.

Antibodies	Company	Dilution
Anti-p53	Cell Signaling Technologies	1:1000
Anti-p110α	Cell Signaling Technologies	1:1000
Anti-β-actin	Sigma, USA	1:10000
Secondary Antirabbit	Cell Signaling Technologies	1: 4000
Secondary Antimouse	Sigma, USA	1:15000 or 1:10000

Immunofluorescence:

The detailed procedure of immunofluorescence is given in the section 8.16. Briefly, 24 hrs of treatments of drugs at desired concentrations, cells were fixed with 4% PFA for 10 min. Cells were then washed in 1X PBS and blocked in 5% BSA followed by overnight incubation with anti-p53 primary antibody (1:200). Cover slips were then washed, incubated with secondary antibody for 2 h (anti-mouse antibody conjugated with Dylight 633 or FITC) and finally counter stained with 0.05% DAPI was used as a counter stain for the nuclei.

Images were captured using 63X objective. At least five representative fields were studied for p53 and DAPI staining.

Genomic DNA isolation and copy number evaluation

Genomic DNA from all the cell lines (IOSE, PA1 and A2780) were isolated by using a hypotonic lysis buffer containing EDTA, a detergent (Tween-20) and proteinase K followed by phenol chloroform extraction and alcohol precipitation. The detailed protocol of genomic DNA isolation is given in the section 8.4. The copy number changes in the PIK3CA gene in all the cell lines were studied by using the real-time quantitative PCR. PIK3CA gene copy number calculation was performed using the comparative C_t method [269]. Copy number of PIK3CA gene in the reference cell line was set as 2 and a copy number more than 4 was considered to be a gain. A detail description of the copy number evaluation and analysis is given in the section 8.5.

Site directed mutagenesis (SDM)

Standard SDM protocol was used to generate the mutations at the p53 binding site in the PIK3CA promoter. A detailed protocol for the SDM is given in the section 8.18. We designed four pairs of mutagenic primers following several guidelines described in section 8.18. Table 3 shows the sequence of the mutagenic primers used for the SDM of all the p53 binding sites. A number of modification in SDM protocol were required to amplify the whole PIK3CA-*fluc2*-*tdt* (WT-PFT) with the desired mutations which includes the use of $MgCl_2$, formamide, buffers (5X HF and GC buffer) and PCR reaction conditions. The PCR conditions and the cycling parameters used are given as follows:

p53 binding sites	Mutagenic primers
Site 1 AAACAGACTT CACCAAGACA	5’ GGTACGCAGCACTGTGACACTACCTTG 3’ F 5’ CAAGGTAGTGTTACAGTGCTGCGTACC 3’ R
Site 2 TGGCATTACG CCCCACGTCT	5’ CGCGAAAAATCCCCAGAATCTTCTGAATAG 3’ F 5’ CTATTCAGAAGATTCTGGGGATTTTTCGC 3’ R
Site 3 ACGCTGGTTA CGGTTAGCCA	5’ TCCATAACCACGAGAATTAGCCACTGAC 3’ F 5’ GTCAGTGGCTAATTCTCGTGGTTATGGA 3’ R
Site 4 AAGCAAGACG GCACATATTG	5’ TCGGGCGGAAAAGTGTGACGCAGGCG 3’F 5’ CGCCTGCGTTACACTTTTCCGCCCGA 3’R

Table 3: The p53 binding sites in the PIK3CA promoter with core sequence (underlined) and the mutagenic primers.

Sr. No.	Steps	Temperature(°C)	Time (sec)
1	Initial Denaturation	95	300
2	Denaturation	95	30
3	Annealing	55	50
4	Extension	68	900
5	Repeat (2-4)	18 Cycles	
6	Final Extension	68	600
7	Hold	4	Forever

Thermo Cycler Parameters

PCR conditions

The PCR conditions used for development of all the mutant constructs are given as follows:

Reagents	**MPFT 1**	**MPFT 2**	**MPFT 3**	**MPFT 4**
Primer 5' (125ng/µl)	1	1	1	1
Primer 3'(125ng/µl)	1	1	1	1
DNA (50-100ng/µg)	1	1	1	1
dNTP(10nmol/µl)	1	1	1	1
HF Buffer (µl)	-	5	5	5
GC Buffer (µl)	5	-	-	-
MQ water (µl)	38	38.5	38.5	38.5
MgCl2 (µl)	-	1.5	1.5	1.5
Formamide (µl)	2	-	-	-
Enzyme (µl)	1	1	1	1
Total volume (µl)	50	50	50	50

A series of stepwise mutations were created in the PIK3CA promoter of the PIK3CA*fluc2-tdt* (WT-PFT) vector to abolish the binding of p53. The four p53 binding sites in the PIK3CA promoter are schematically depicted in the Figure 2.5a. MPFT 1 carries mutation at Site 3, MPFT 2 bears mutation at Site 3 and 4, MPFT 3 has mutation at Site 3, 4 and 1 and finally the fourth construct MPFT 4 bears mutation at Site 3,4,1 and 2 (Figure 2.5b).

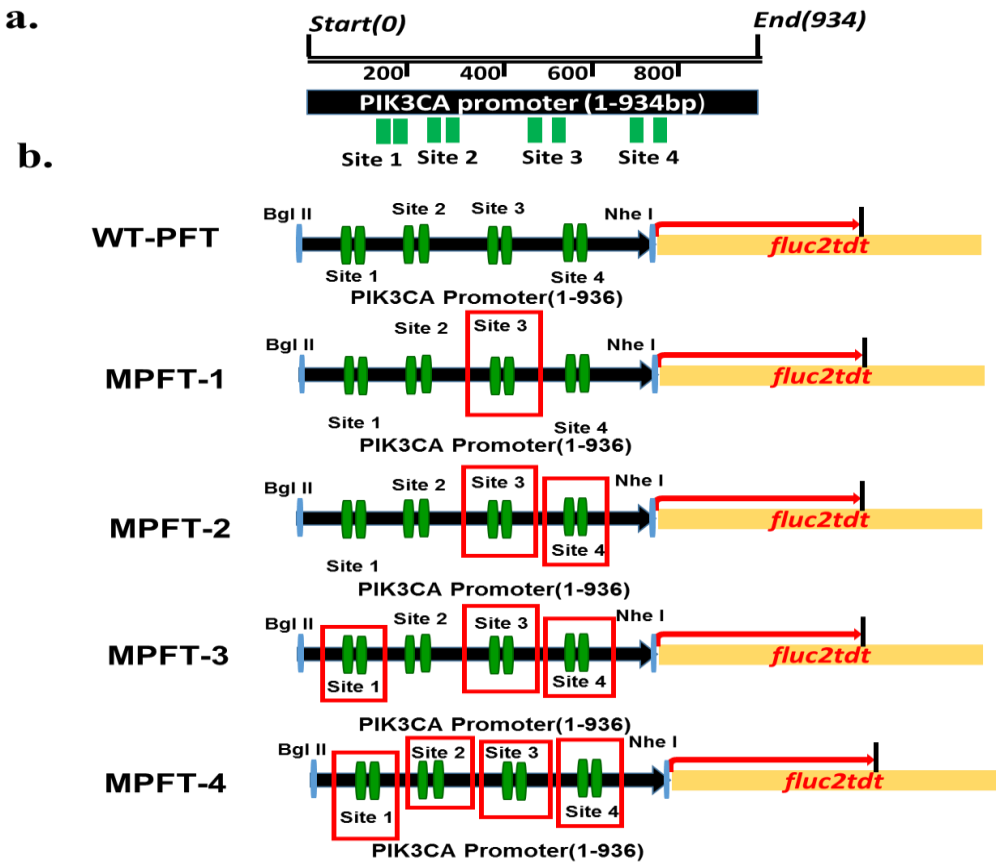

Figure 2.5. Sequential mutations at the p53 binding sites. *a) Schematic representation of the PIK3CA promoter bearing the four p53 binding sites; b) Sequential site directed mutagenesis were performed on PIK3CA-fluc2-tdt reporter (WT- PFT) to obtain four mutant PIK3CA-fluc2-tdt reporters (MPFT 1, MPFT 2, MPFT 3 and MPFT 4) by successive substitution in the core sequence of the p53 binding sites.*

The wild type PIK3CA-*fluc2tdt* and the mutant constructs were amplified using mutagenic primers for the respective sites in the PCR conditions and cycling parameters were described above. The products were confirmed by agarose gel electrophoresis (Figure 2.6a-d). The amplified products of each mutation were further digested by DpnI endonuclease and transformed in competent cells. The colonies after this transformation were screened for the desired mutation by EcoRI digestion and by sequencing (Figure 2.6e).

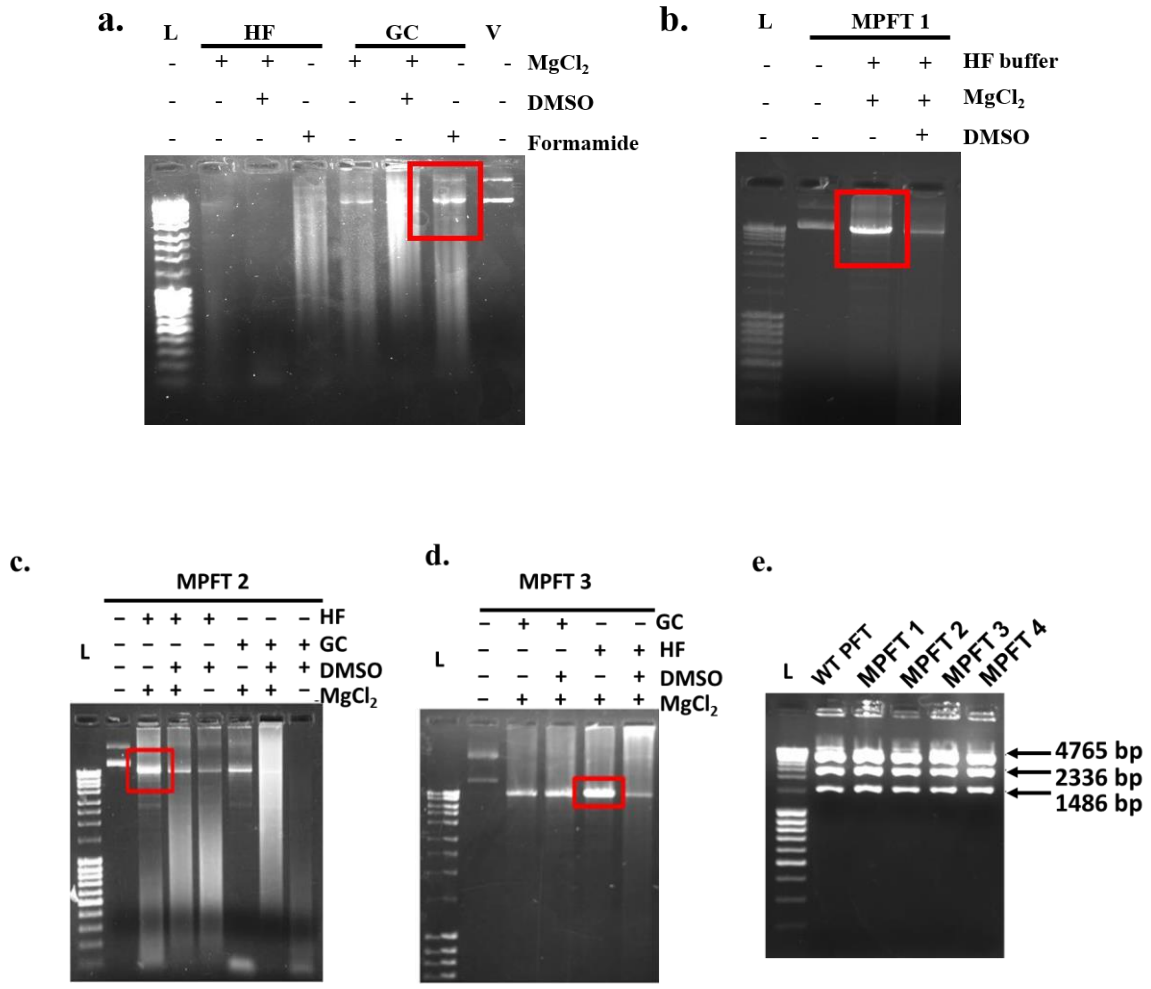

Figure 2.6: Establishment of sequential mutations in the p53 binding site of the PIK3CA promoter. *a) PIK3CA–fluc2-tdt plasmid was used for SDM with mutagenic primer set of Site 3. $MgCl_2$, formamide and DMSO along with either of the two buffers (GC and HF) were added in the PCR reaction as shown in the gel picture (Lane L: 10kb DNA ladder and Lane V: PIK3CA–fluc2-tdt plasmid). The amplified product, highlighted in red, was subjected to the DpnI digestion, transformed and colonies were screened by sequencing for desired mutation. The construct was named as MPFT 1; b) MPFT 1 was used for sequentially mutating the site 4, the PCR conditions used for the same are shown in the gel picture. The PCR product amplified, highlighted in red, was used for further study. Similar to MPFT 1, MPFT 2 was constructed; c) MPFT 2 construct was used for mutation on Site 1, as shown in the figure several modifications were performed and the amplified product, highlighted*

in red, was DpnI digested and transformed, which was later finalised as MPFT 3 construct upon screening through colonies; d) Similarly, MPFT 4 construct was made by SDM at Site 2 using MPFT 3 vector; e) All the four mutated constructs and wild type promoter were confirmed and verified by the EcoRI digestion.

Bioluminescence imaging in living mice

Ovarian cancer cells stably expressing the PIK3CA-*fluc2-tdt* ($6x10^6$) were implanted in nude mice. In this study, Berthold's NightOwl II LB 983 optical imaging system was used. The tumor formation and growth was monitored by repetitive bioluminescence imaging (BLI). A detailed description of *in vivo* BLI is given in the Appendix (Material and methods). Mice bearing tumor xenografts were segregated into two groups, control and test group. An intraperitoneal cisplatin treatment (8mg/kg/week three days a week.) was given to the test group. BLI was acquired for 1 min after intraperitoneal administration of D-Luciferin (3mg/mouse). ROIs were drawn over the tumors of control and cisplatin treated mice and quantified by using the Winlight Optimas Live Image Software 32. Bioluminescence signal was recorded as maximum (photons/sec/cm2) with a fixed angle at 2*pi.

RESULTS

Construction of a PIK3CA sensor: Astanehe *et al*., (2009) [19], demonstrated that binding of p53 suppresses PIK3CA promoter activity in normal ovarian surface epithelial (OSE) cells. Both cisplatin and paclitaxel are known to induce p53 mediated cell death. In order to study the modulation of PIK3CA promoter by chemotherapeutic drugs in ovarian cancer cells, we constructed a PIK3CA sensor i.e. PIK3CA promoter driving bifusion reporter. The original bifusion reporter system is described before and mentioned as CMV-*fluc2-tdt* vector. Characterization of the reporter activities of CMV-*fluc2-tdt* was earlier conducted

by Dr. Pritha Ray at Molecular Imaging Program at Stanford (MIPS), Stanford University, California. The cloning strategy for construction of PIK3CA sensor is described earlier in material and methods and in figure 2.7a. Among the three clones obtained, one turned out to be positive which was further verified by restriction digestion and sequencing (Figure2.7b).

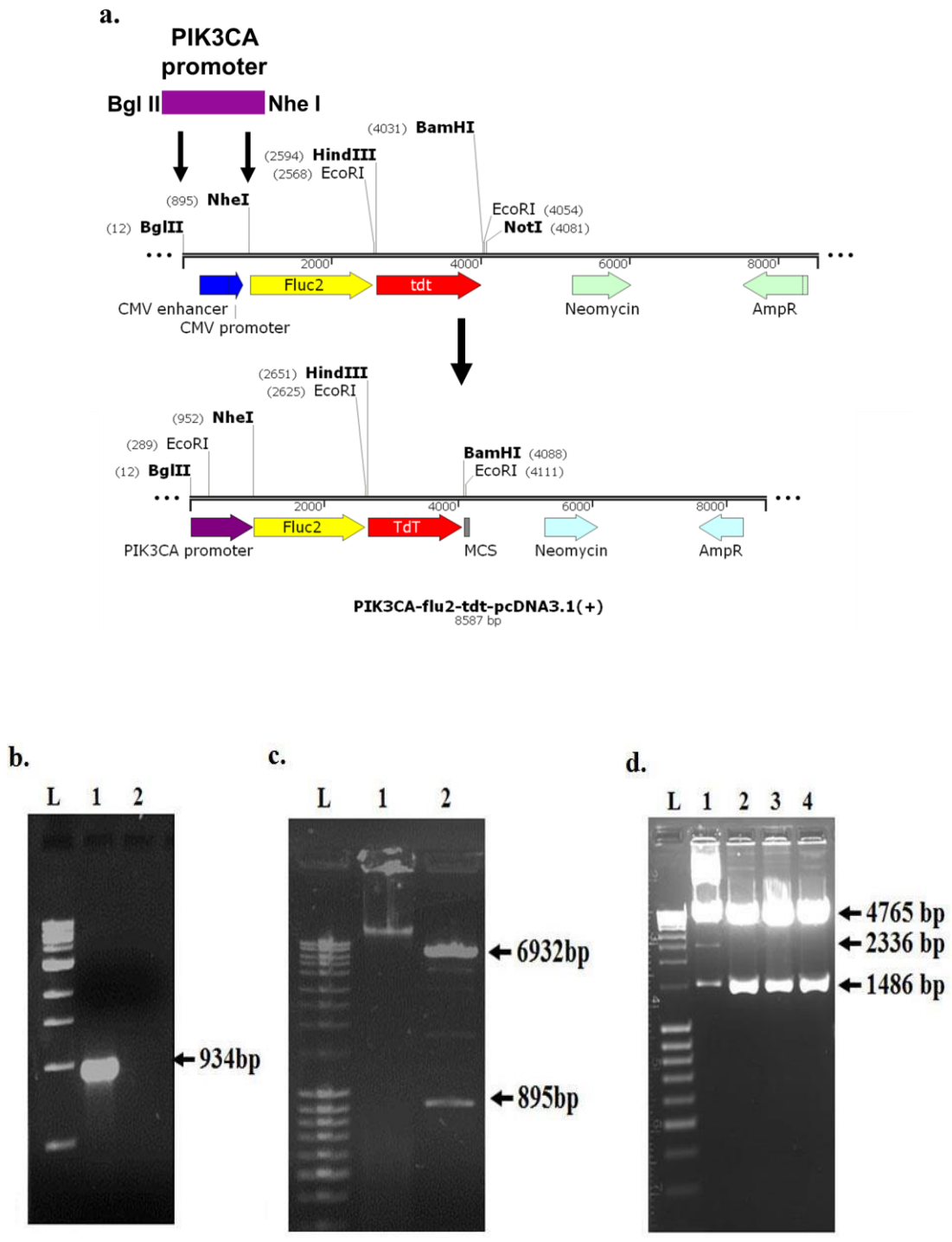

Figure 2.7. Construction of a PIK3CA sensor. *a) Schematic of the strategy used to clone PIK3CA promoter in a pcDNA 3.1(+) vector by replacing the CMV promoter; b) Amplification of PIK3CA promoter (Insert): LaneL-1kb DNA ladder, Lane1-PCR amplified product of the PIK3CA promoter; Lane2-negative control. c) Pre and post backbone removal vector configuration by NheI and BglII digestions: Lane L: 10kb DNA ladder; Lane1: undigested CMV-fluc2-tdt, Lane2: CMV-fluc2-tdt double digested with NheI and BglII; d) Restriction endonuclease analysis of plasmids after cloning:: Lane L10kb DNA ladder, Lane1-3-EcoRI digestion of clones obtained after ligation, lane1 bears the positive clone; lane4- vector CMV-fluc2-tdt EcoRI digested.*

Expression status of the PIK3CA sensor (PIK3CA-fluc2-tdt): To check the functional ability of the positive clone expressing the PIK3CA sensor, PA1 cells were transiently transfected for 24 h and imaged using a rhodamine filter in fluorescent microscope. Strong expression of *tdt* gene was observed as shown in figure 2.8. Simultaneously, the luciferase assay showed high activity as compared to the untransfected cells. The PIK3CA sensor was also validated *in vivo* in SCID mice which showed bioluminescence signal from the site of transplanted cells indicating the efficient functioning of the sensor.

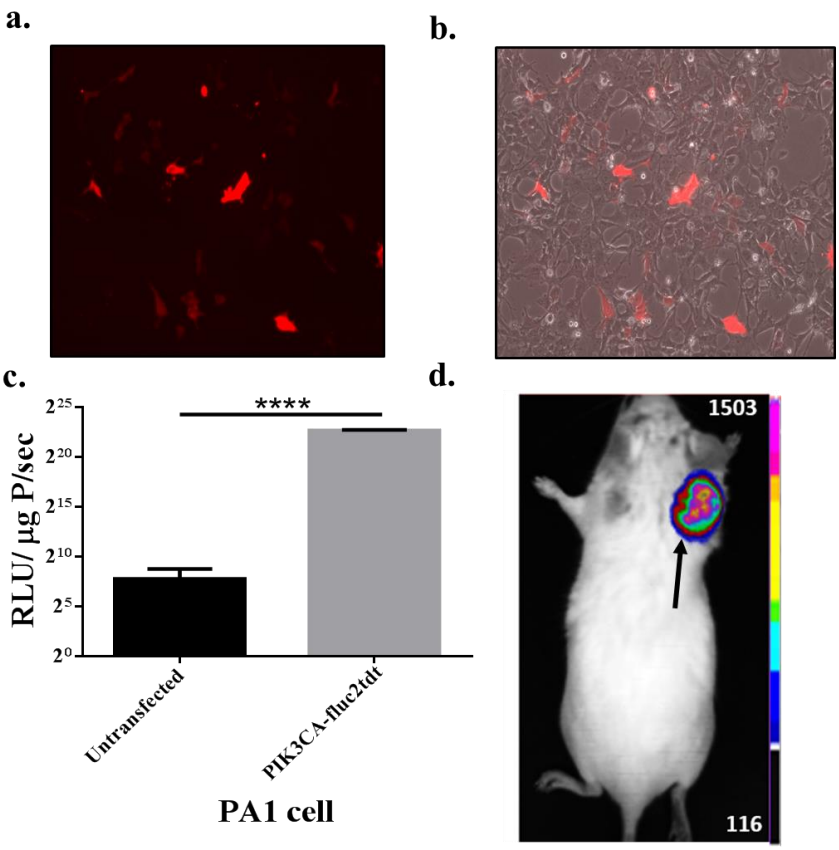

Figure 2.8.: Functional activity of the PIK3CA sensor. *a) Fluorescent Imaging of PA1 cells after transient transfection of PIK3CA sensor expressing TDT protein as visualized with Rhodamines filter (magnification 10x); b) Bright field image of the same field. c. Luciferase assay of PA1 cells after transient transfection of PIK3CA sensor demonstrated high (****p<0.0001) luciferase activity (Relative light unit (RLU)/ concentration of Protein (µg P)/time (sec)) as compared to the untransfected cells. d) In vivo validation of the PIK3CA sensor by bioluminescence imaging (arrow denotes the signal).*

Monitoring drug induced modulation of PIK3CA promoter of the PIK3CA sensor: After the *in vitro* and *in vivo* validation of the PIK3CA sensor, the modulation of the PIK3CA promoter upon exposure to the chemotherapeutics was evaluated. The PIK3CA promoter contains four p53 binding sites which upon direct binding of p53 represses the promoter activity. Since cisplatin and paclitaxel are known to induce cell death through p53

activation, it would have been intriguing to understand the alteration in PIK3CA promoter activity caused by these chemotherapeutics. A dose dependent treatment of cisplatin, paclitaxel (common drugs used for the treatment of ovarian cancer) and adriamycin (a drug known to activate p53) for 2h indicated that 5 µg/ml concentration of both drugs were able to decrease the promoter activity in PA1 cells. Treatments with three drugs [cisplatin, paclitaxel and adriamycin (1 mM), significantly decreased the PIK3CA promoter activity (Figure 2.9a). However, TK promoter driven renilla luciferase activity (pTK-*hrluc*), which was co-transfected and used as an internal control, did not show any change upon drug treatments (Figure 2.9b) in PA1 cells. Similar results were observed in A2780 cells transiently co-transfected with PIK3CA-*fluc2-tdt* & pTK-*hrluc* and treated with cisplatin (Figure 2.9c and d). Paclitaxel treatment to the A2780 cells transiently transfected with *PIK3CA-fluc2-tdt* demonstrated decrease in promoter activity, however similar decrease was also obtained in the pTK–*hrluc* activity used as an internal control (Figure 2.9e and f). This unanticipated attenuating effect on TK promoter is surprising and could be a cell line specific event.

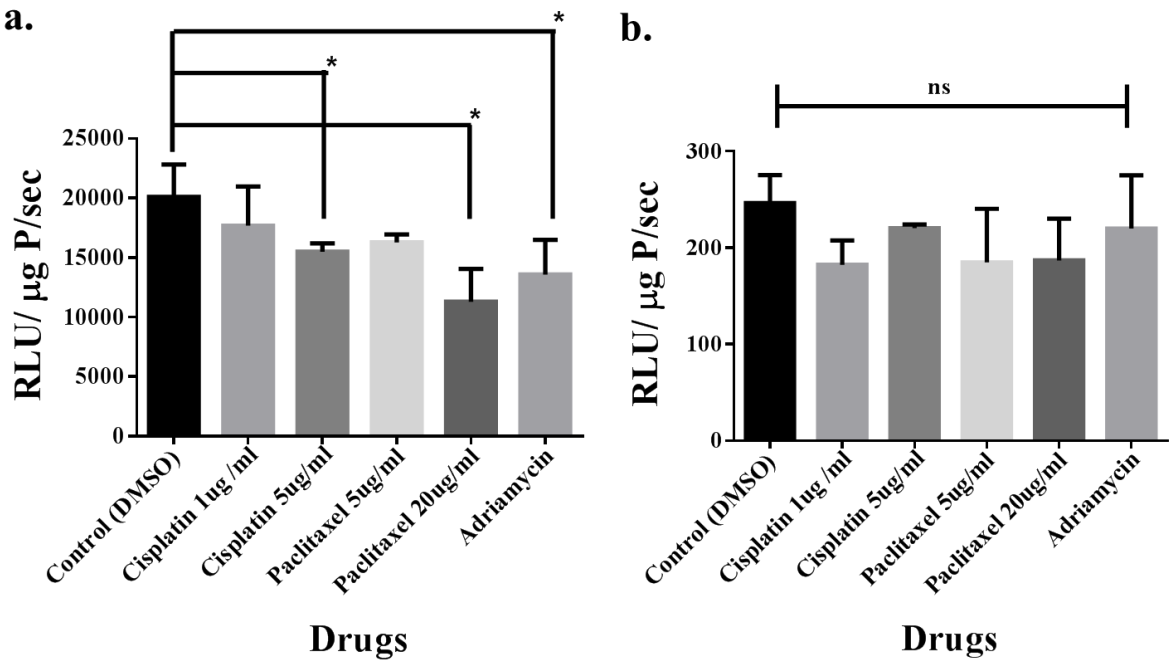

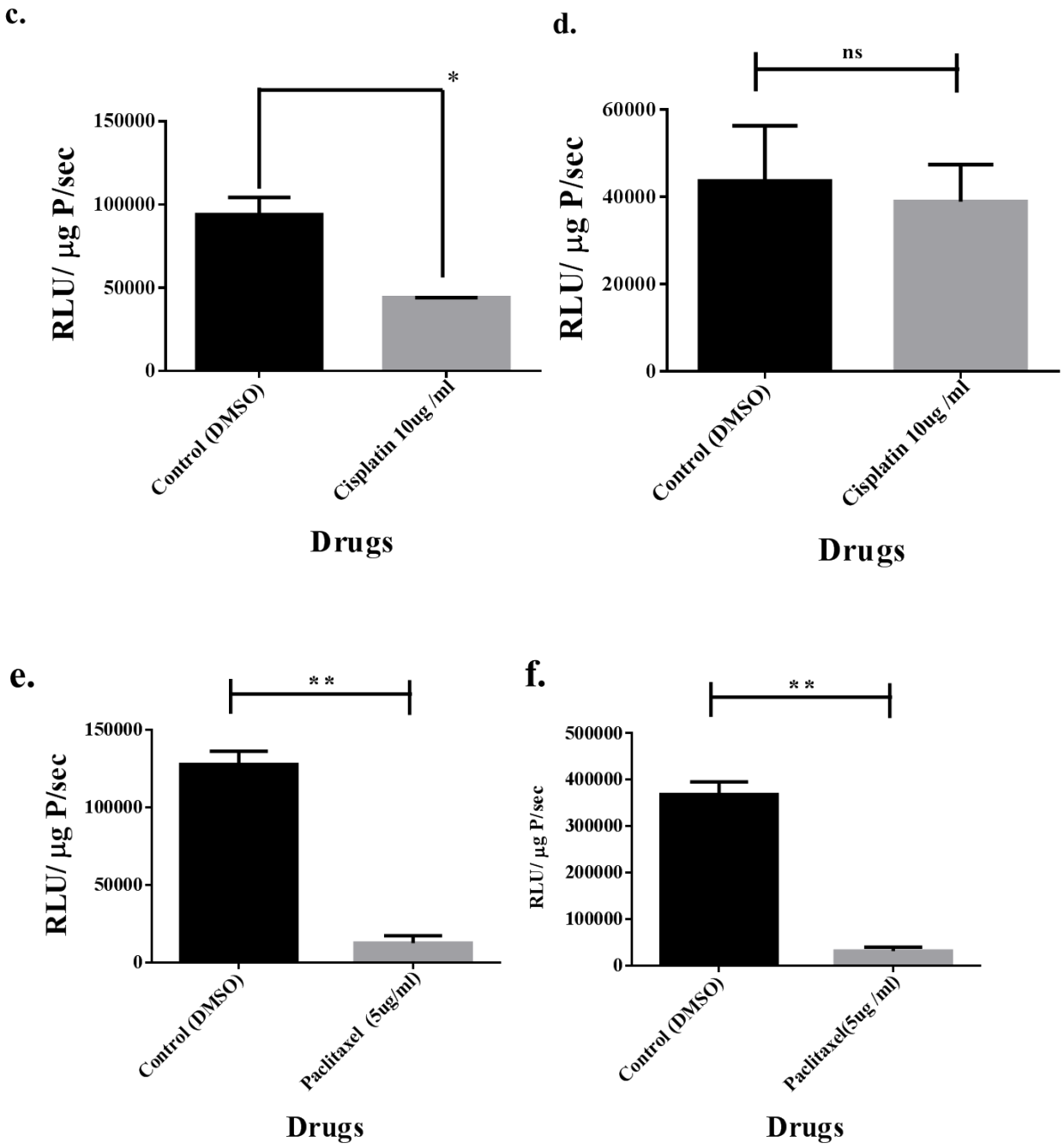

Figure 2.9. PIK3CA promoter modulation after drug treatment. *a) PIK3CA sensor (PIK3CA promoter driven fluc2-tdt) showed attenuation in promoter activity (luciferase activity) on treatment with cisplatin, paclitaxel and adriamycin of transiently transfected PA1 cells (*p<0.030.03). b) Humanized renilla luciferase driven by the TK promoter (pTK-hrluc) co-transfected in PA1 cells does not show any change in luciferase activity after drug treatment (p=ns); c) A2780 cell transiently transfected with the PIK3CA sensor showed*

*repression in promoter activity upon cisplatin treatment (*p<0.03); d) pTK-hrluc plasmid which was co-transfected and cisplatin treated did not show any modulation (p=ns). e) A2780 cell transiently transfected with the PIK3CA sensor showed repression in promoter activity upon paclitaxel treatment (**p<0.001); f) pTK-hrluc plasmid which was co-transfected and paclitaxel treated showed similar modulation (**p<0.001).*

Generation of clones of A2780, PA1 (wild type p53 background) and SKOV3 (p53 null background) cells stably expressing PIK3CA sensor: In order to understand the modulation of PIK3CA promoter in varied endogenous p53 expression, three cell lines (A2780, PA1 & SKOV3) were chosen. Both A2780 and PA1 cells have p53 wild type background, while SKOV3 cells are known to have a p53 null (homozygous deletion) background [270]. All these cell lines were transfected with PIK3CA sensor and were allowed to grow in the G418 (400µg/ml) selection media. Many clones were obtained in a span of 10-15 days, which were grown and then screened for their luciferase activity. Single clones from all the cell lines with highest luciferase activity, were selected and further used to carry out the experiments. These cells were named as PA1-*PIK3CA-fluc2tdt* (PPF), A2780-PIK3CA-*fluc2-tdt* (APFT) and SKOV3-PIK3CA-*fluc2-tdt* (SPFT) (Figure 2.10a-c). The p53 deficient status of SPFT was confirmed by western blotting (Figure 2.10d).

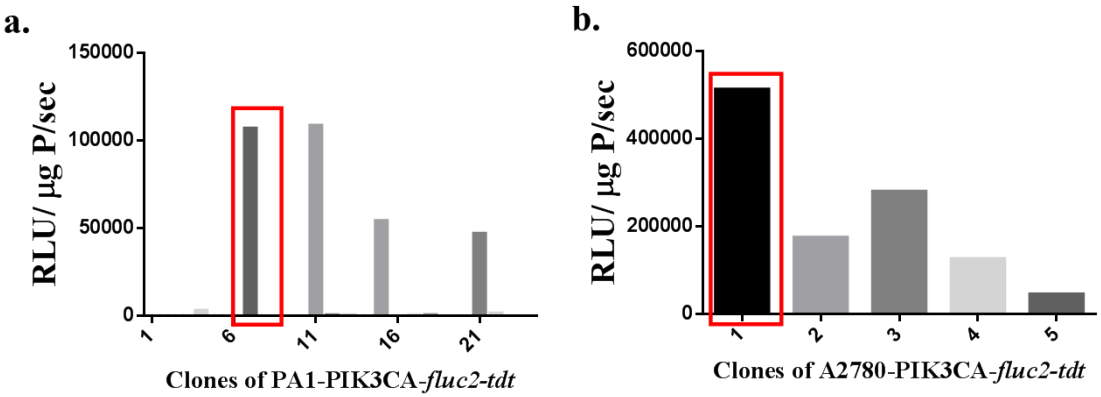

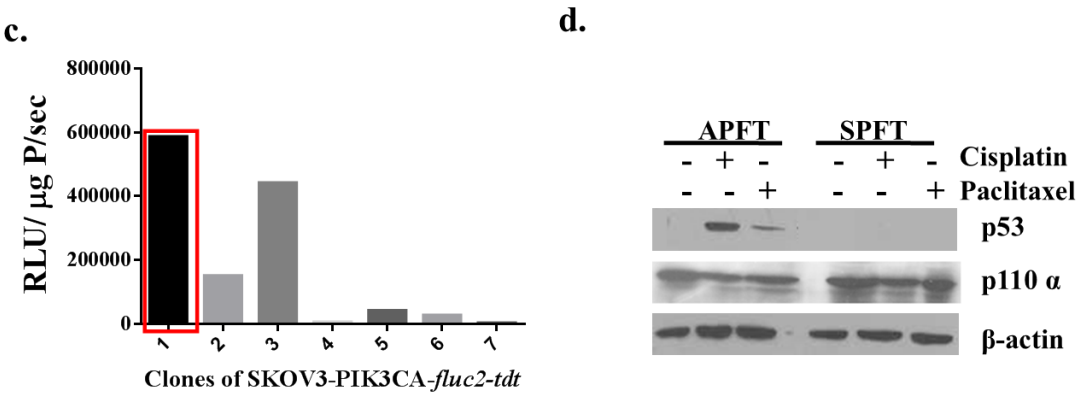

Figure 2.10. Screening of PA1, A2780 and SKOV3 cells for stable expression of the PIK3CA sensor through G418 selection. *a) Screening of clones from PA1 cells by luciferase assay. Colony number 7 with highest luciferase activity was selected as PA1-PIK3CA-fluc2-tdt (PPF); b) Screening of clones from A2780 cells through luciferase assay, Colony number 1 was selected as A2780-PIK3CA-fluc2-tdt (APFT); c) Screening of clones from SKOV3 cells through luciferase assay. Colony number 1 was selected as SKOV3-PIK3CA-fluc2-tdt (SPFT); d) Western blotting to verify the mutant status of the p53 in SPFT cells.*

Effects of cisplatin and paclitaxel treatment on PIK3CA promoter activity in A2780, PA1 and SKOV3 cells: Transient transfection of PIK3CA sensor showed attenuation upon cisplatin and paclitaxel treatment in PA1 and A2780 cells. To explore the kinetics of PIK3CA promoter in presence or absence of functional p53, stable cells expressing PIK3CA sensor were developed in three cell lines PA1, A2780 (wild type) and SKOV3 (null). PA1 cells are originated from teratocarcinoma and are highly sensitive to the treatment. On contrary, A2780 cell line is obtained from epithelial carcinoma patient which is comparatively less sensitive. A dose dependent attenuation of the PIK3CA promoter activity was observed after cisplatin and paclitaxel treatments in PPF and APFT cells corroborating with our transient expression results. It was observed that at same concentration of drug (5

µg/ml) (either cisplatin or paclitaxel for 2 h) exerted different levels of promoter attenuation in A2780 (less sensitive) and PA1 (highly sensitive) cells (Figure 2.11 a-d). On contrary, the PIK3CA promoter activity in the SPFT cells did not show any attenuation when treated with increasing concentrations of cisplatin and paclitaxel for 2 h (Figure 2.11e & f).

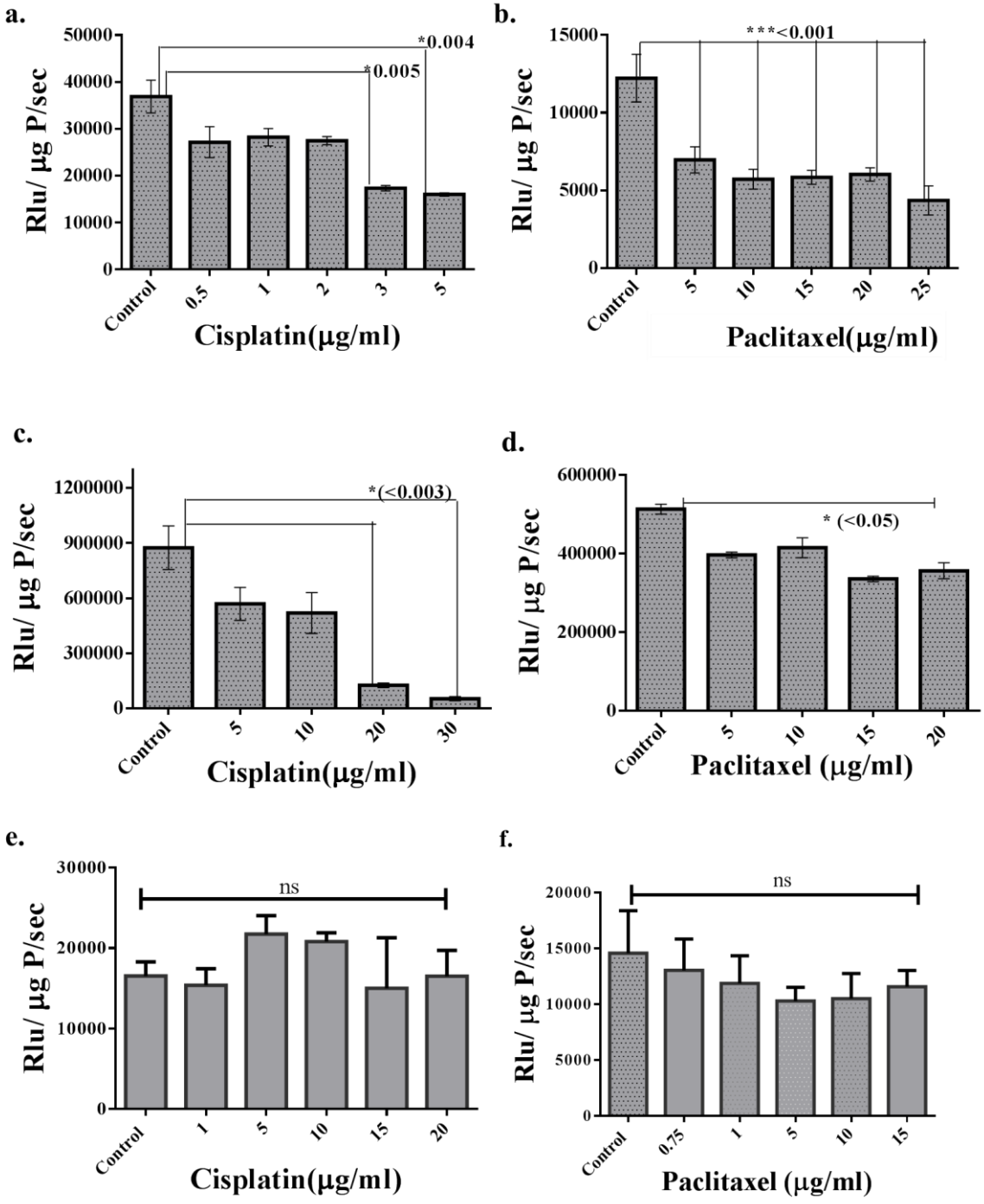

Figure 2.11. In vitro studies on effect of cisplatin and paclitaxel on PIK3CA promoter.

a) & b) PPF cells were treated with increasing concentration of cisplatin and paclitaxel. A dose dependent decrease in luciferase activity (promoter activity) was observed on increasing concentrations of cisplatin (3 and 5 µg/ml, p≤0.005) and paclitaxel (upto 25 µg/ml,***p≤0.001); c and d) Similar observation were also made with APFT cells, however, the concentration of cisplatin (20 and 30 µg/ml, *p≤0.003) and paclitaxel (upto 20 µg/ml, *p≤0.051) were much higher; e and f) In SPFT cells no such change in luciferase activity was observed with increasing concentration of cisplatin and paclitaxel.*

Cisplatin and paclitaxel treatments in PA1 and A2780 exhibit p53 activation: It is reported conditional activation of p53 demonstrate attenuation of PIK3CA promoter. In this study, p53 level significantly was increased after 24h of drug treatments as compared to 2h in PPF, with no change in the endogenous p110α levels (Figure 2.12a). Similar observations were also made in APFT cells (Figure 2.12b). Densitometric analysis of the blot with PPF cell lysates showed 5.3 and 6.3 fold p53 activation after cisplatin and paclitaxel treatment respectively (Figure 2.12c). Similarly, in APFT cells, the fold change in the level of p53 activation by cisplatin was 8.1 as compared to paclitaxel (4.4 fold). The p53 activation by cisplatin seemed to be higher than that induced by paclitaxel (Figure 2.12d). Activation of p53 leads to its nuclear accumulation inducing or repressing transcription of many target genes. Immunofluorescence study clearly demonstrated nuclear localisation of p53 protein in cisplatin and paclitaxel treated PPF and APFT cells (Figure 2.12e & f).

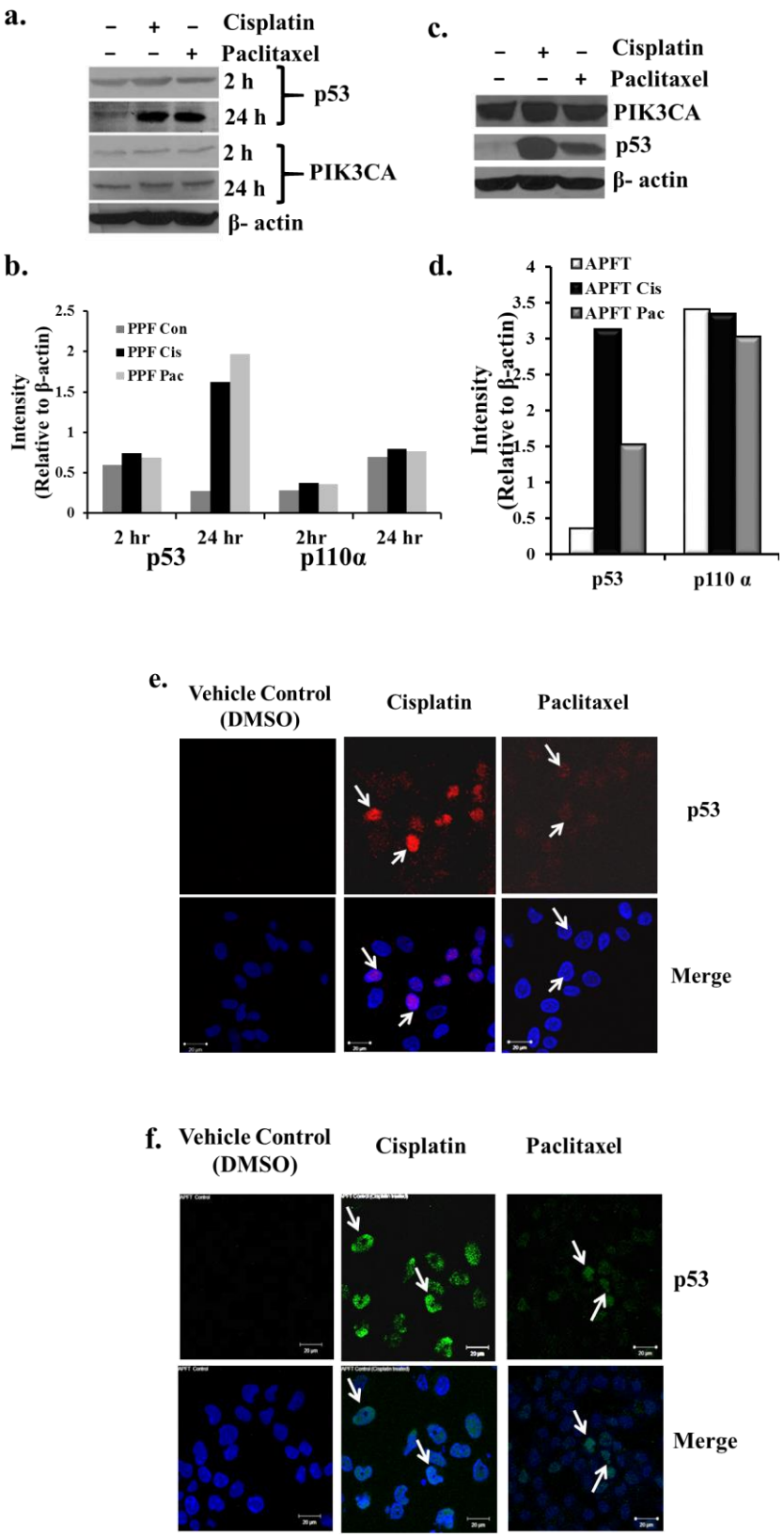

Figure 2.12. Evaluating the endogenous levels of p53 in PPF and APFT cells upon cisplatin and paclitaxel treatment. *a) & c) Western blot analysis of p53 protein from lysates*

of cisplatin and paclitaxel treated PPF and APFT cells showed induction in p53 level after 24h, however no change was observed after 2h. The p110a levels did not show any change after drug treatment; b) & d) the densitometric analysis representing the same are shown; e) & f) nuclear localization of p53 after treatment in cisplatin treated cells. p53 protein (red in e and green in f) showed nuclear localization upon treatment with cisplatin and paclitaxel for 2h as compared to the vehicle treatment in PPF and APFT cells. DAPI (blue) indicated the nuclear staining.

Copy number evaluation of PIK3CA in PA1 cells: According to the TCGA data, 18% of ovarian cancer patients have amplification in the PIK3CA gene. Amplification in PIK3CA gene can be a result of increase in copy number which is often a feature of malignant cells. Copy number of ovarian cells A2780 and SKOV3 are known to be 2 and 3 respectively [264] which is not reported for PA1 cells. In order to evaluate the copy number of PIK3CA gene in PA1 cells, a comparative C_t method after quantitative real-time PCR was used [271]. Briefly PIK3CA copy number calculation was carried out using the comparative C_t method after validating the efficiencies of PCR reactions of both PIK3CA and COL8A1 (used as an internal control) genes. IOSE 364 (a normal ovarian cell line) genomic DNA was used as reference whose copy number of PIK3CA gene is known as 2. A relative quantification method was used to find the copy number change. Real-time PCR analysis (analysis described in detail in the Appendix, Material and methods) showed no fold change in the PIK3CA gene expression compared to the reference cell line indicating that the copy number of PIK3CA gene in PA1 cells is similar to IOSE 364 cell line which is equal to 2.

Cells	COL8A1	PIK 21 E	ΔCt	ΔΔCt	2ΔΔCt
A2780	24.09	22.83	-1.25	0.04	0.78
IOSE	23.06	21.45	-1.61	0	1
PA1	22.12	20.90	-1.21	0.04	0.759

Table 4: Representation of the analysis performed for evaluating the copy number of PIK3CA gene*. PIK 21E is the region encoding exon 21 of the PIK3CA gene; COL8A1 is used as an internal control, as it is located on the same arm of chromosome as that of PIK3CA gene.* $\Delta C_t = C_t$ *(PIK 21E)*$_{Gene}$ $- C_t$ *(COL8A1)*$_{Reference\ gene}$; $\Delta\Delta C_t = (C_{t\ PIK3CA} - C_{t\ COLA81})_{Target\ cell\ line} - (C_{t\ PIK3CA} - C_{t\ COLA81})_{IOSE\ (reference\ cell\ line).}$; $2^{-\Delta\Delta Ct}$ *relative fold change* **.**

Non-invasive imaging of cisplatin induced modulation of PIK3CA promoter activity in tumor xenografts of PA1 and A2780 cells. *In vitro* studies demonstrated that the PIK3CA promoter showed repression upon cisplatin treatment. To explore the kinetics of PIK3CA promoter modulation by cisplatin *in vivo*, we used two different tumor xenograft models (PA1-PIK3CA-*fluc2-tdt* and A2780-PIK3CA-*fluc2-tdt*). For each model, six million cells were subcutaneously implanted in nude mice were allowed to grow tumors. The tumor growth was monitored by repetitive BLI. The mice were divided in control group and test groups. The control group were treated with vehicle solvent whereas the cisplatin treatment was given to the test group. The concentration of cisplatin given was (8 mg/kg/week) [272]. To avoid toxicity, it was decided to divide each dose in three parts. Once the tumors were palpable, either one or two cycles of cisplatin were injected intraperitoneally in nude mice for three days a week. Since ovarian germline tumors are more sensitive to cisplatin in comparison to epithelial ovarian tumors and PA1 cells in our *in vitro* study showed higher promoter attenuation mediated by cisplatin (Figure 2.13a and c), it was decided to treat the PA1 tumor bearing mice (n = 6) with one cycle and A2780 tumor bearing mice (n= 7) with two cycles of cisplatin. Decrease in luciferase activities for PA1 model ($4.4 \times 10^8 \pm 2.2 \times 10^8$

p/sec/cm^2 to 3x10^8 ±1.9 x10^8 p/sec/cm^2) (0.7 fold) were detected at 14th day of completion of treatment which further decreased (0.82 x 10^8 ± 5.7 x 10^7 p/sec/cm^2) (0.2 fold) with time (22nd day). The control mice, however, had increased luminescence and tumor growth with time (5.8x10^8 ± 4.1x10^8 p/sec/cm^2 to 8.7x10^8 ±4.5x10^8 p/sec/cm^2 to 1.3x10^9±7.4x10^8 p/sec/cm^2) (Figure 2.13 a & b). The shaded region in the Figure 2.13a depicts the duration of the cisplatin treatment. Figure 2.13c shows representative bioluminescent images of the mice bearing PPF tumors. Mice from the control and treated group exhibited specific and similar intensity signals which decreased after cisplatin treatment (arrowhead).

In the A2780 tumor model, cisplatin treated mice (n=4), exhibited a faster growth kinetics. The bioluminescence signal did not decrease after first treatment (6.93x10^9 ±1x10^9 p/sec/cm^2 to 6.1x10^9±1x10^{9}p/sec/cm^2) (0.9 fold) at 11 days but decreased rapidly (1.9x10^9±3x10^8 p/sec/cm^2) (0.27 fold) after the completion of two treatments at 15 days. The control mice (n= 3) showed increased bioluminescence and tumor growth (1.2x10^9±3x10^8 p/sec/cm^2 to 4x10^9±7.6x10^8 p/sec/cm^2 to 7.4x10^9±2x10^9 p/ sec/cm^2) over time (Figure 2.13d & e). The bioluminescence signals in the cisplatin treated mice at day 15 post-treatment showed a significant decrease (p= 0.025) as compared to the control mice (Figure 2.13e). Representative bioluminescent images of the mice bearing APFT tumors exhibited specific signals which decreased only in treated mouse (Figure 2.13 e & f).

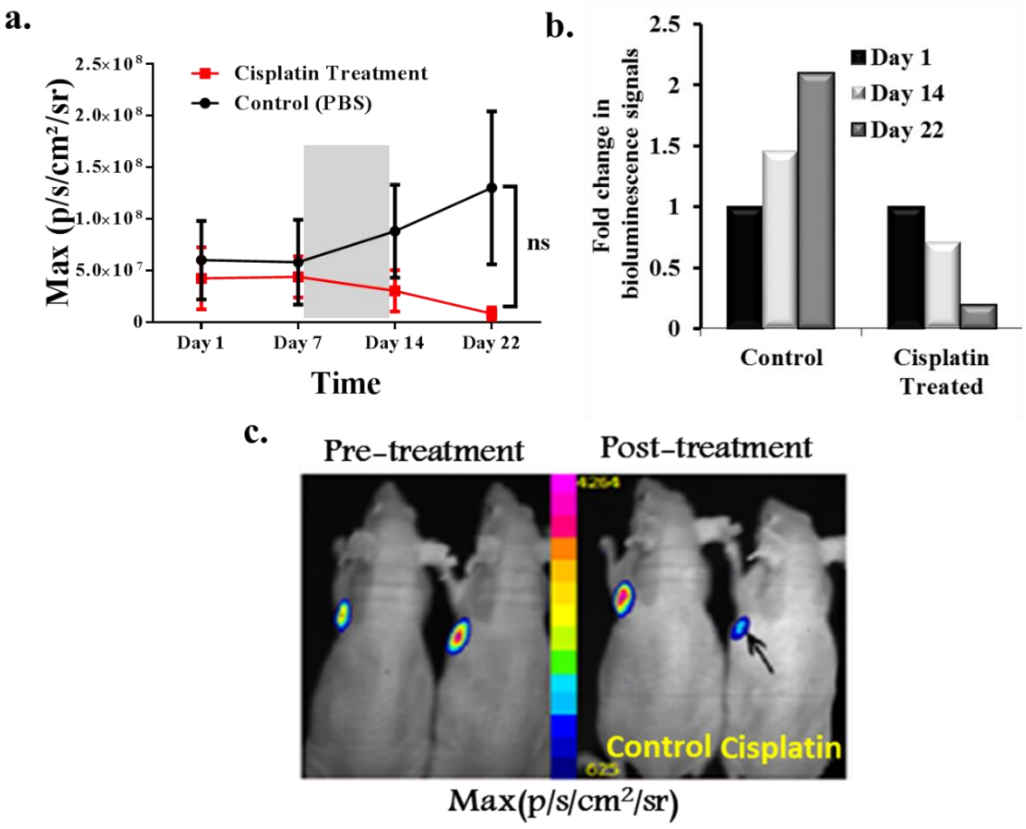
a.
Cisplatin Treatment
Control (PBS)
Max (p/s/cm²/sr)
2.5×10⁸
2.0×10⁸
1.5×10⁸
1.0×10⁸
5.0×10⁷
0
ns
Day 1
Day 7
Day 14
Day 22
Time
b.
Fold change in bioluminescence signals
2.5
2
1.5
1
0.5
0
Day 1
Day 14
Day 22
Control
Cisplatin Treated
c.
Pre-treatment
Post-treatment
Control Cisplatin
Max(p/s/cm²/sr)

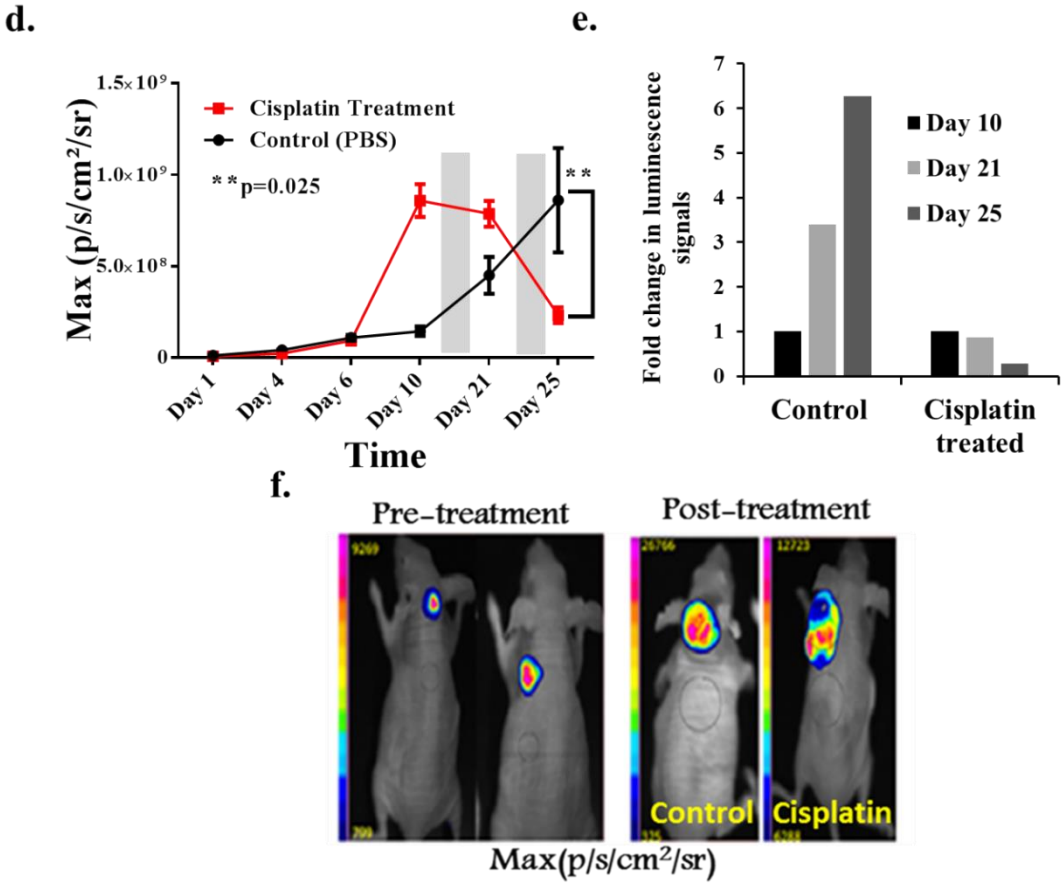
d.
Cisplatin Treatment
Control (PBS)
**p=0.025
Max (p/s/cm²/sr)
1.5×10⁹
1.0×10⁹
5.0×10⁸
0
**
Day 1
Day 4
Day 6
Day 10
Day 21
Day 25
Time
e.
Fold change in luminescence signals
7
6
5
4
3
2
1
0
Day 10
Day 21
Day 25
Control
Cisplatin treated
f.
Pre-treatment
Post-treatment
Control
Cisplatin
Max(p/s/cm²/sr)

Figure 2.13. Non-invasive imaging of PIK3CA promoter for modulation in PA1 and APFT tumor xenografts upon cisplatin treatment. *a) Graphical representation of the promoter modulation in PPF tumor xenografts, the luminescence signal in the control group increased with time while that of the cisplatin treated group (n=3) attenuated from the fourteenth day of treatment till 22nd (endpoint) day after one treatment (shaded area represented the duration of the treatment). At 22nd day, measurable attenuation of bioluminescence signal the control and treated mice was evident however it did not reach statistical significance. (Day 1 represents the pre-treatment signals);b) Graphical representation of temporal fold-change bioluminescence signal (post-treatment signal/pre-treatment signal) showed increased luciferase activity in the control group and attenuation in the treated group; c) Representative bioluminescent images of the mice bearing PPF tumors; d) Graphical representation of the PIK3CA promoter modulation in APFT tumors, the control mice (n = 3) showed increased bioluminescence with time while that of the treated group (n = 4) showed a slight decrease at 11th day after first treatment and significant repression at 15th day after second treatment (p=0.025); e) Graphical representation of the temporal fold change in bioluminescence signals (post-treatment signal/pre-treatment signal) demonstrated augmented bioluminescence in the control group and but attenuation in the treated (Day 10 represented signal prior to treatment); f) Representative bioluminescent images of the mice bearing APFT tumors.*

Non-invasive imaging of cisplatin induced modulation of PIK3CA promoter activity in tumor xenografts of SKOV3 cells: In a wild type p53 background, the PIK3CA promoter activity demonstrated attenuation in *in vitro* and *in vivo* studies. To understand the *in vivo*

kinetics of PIK3CA promoter modulation in a p53 null background, SPFT cells implanted in nude mice for tumor xenografts. Similar to the PA1 and APFT tumor xenografts, the SPFT the control mice (n=5) showed increased bioluminescence and tumor growth ($4.4x10^7 \pm 2.9x10^7$ p/sec/cm^2 to $1.1x10^8 \pm 4.5x10^7$ p/sec/cm2 at day 7 to $1.3x10^8 \pm 5.9x10^7$ p/sec/cm^2) (3 fold) over time. However, in contrast to the PPF and APFT tumor models, the bioluminescence signals of SPFT tumor xenografts (n=5) did not decrease rather exhibited an increase after first treatment ($3.9x10^7 \pm 2.7x10^7$ p/sec/cm^2 to $9.6x10^7 \pm 3.8x10^7$ sec/cm^2) (2.4 fold) of cisplatin at 7th day, which further increased to $1.2x10^8 \pm 8x10^7$ p/sec/cm^2 (3.1 fold) after completion of two treatments at 24 days (Figure 2.14a&b). The representative images of the SPFT tumor xenografts for bioluminescence are shown in the Figure 2.14c.

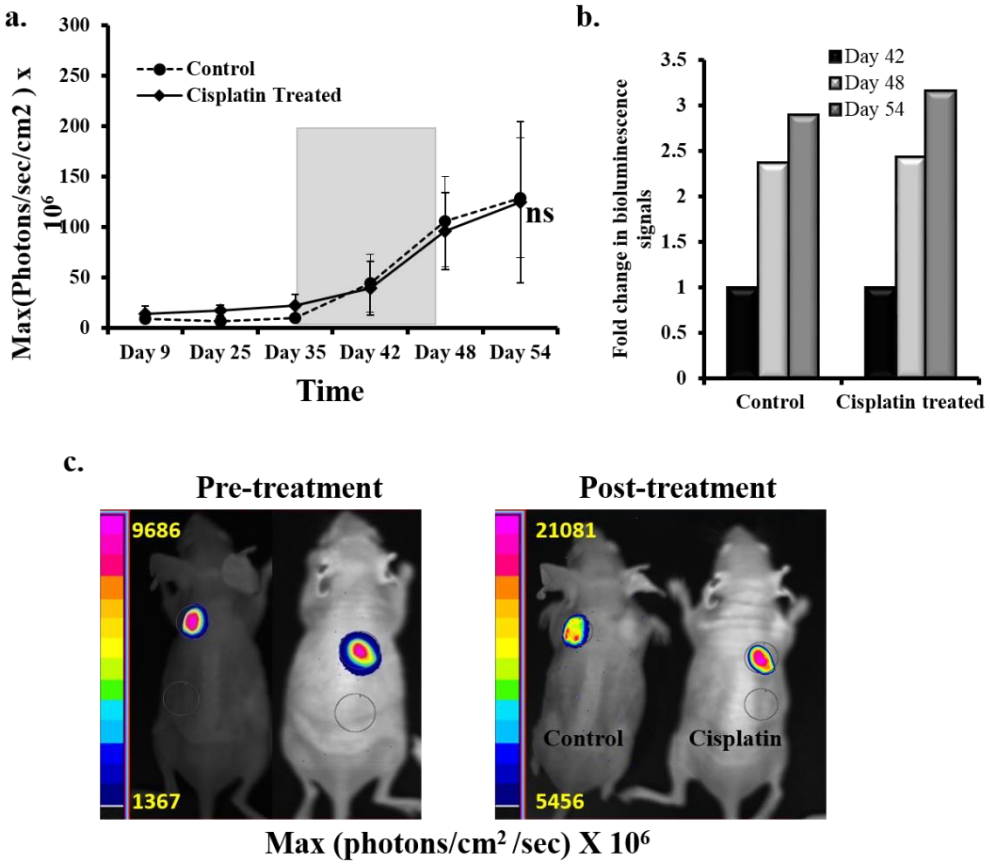

Figure 2.14. Bioluminescence imaging of SPFT tumor xenografts upon cisplatin treatment. *a) Graphical representation of modulation of PIK3CA promoter in the control*

and cisplatin treated mice. The BLI signals of both control (n=5) and cisplatin treated mice (n=5) showed rapid increase with time; b) Graphical representation of temporal fold-change in bioluminescence signal (post-treatment signal/pre-treatment signal) exhibited increased luciferase activity in the both control and cisplatin treated group (Day 42 exhibit the signals prior to the treatment); c) Representative bioluminescent images of SPFT tumor xenograft from control and treated group which exhibited specific (pre-treatment) signals, which did not decrease even after two round of cisplatin treatment (post-treatment) (shaded area in the Figure a).

Mutations in the p53 binding sites augment PIK3CA promoter activity: Our earlier results indicated dependence of PIK3CA promoter activity on the activation status of p53. To understand the mechanistic association of p53 and PIK3CA promoter sequence, we sought to generate mutations in the p53 binding sites. As reported by Astanehe et al**.,** the PIK3CA promoter bears four p53 binding sites which were further confirmed by us through sequencing and four clusters of p53 half sites within the PIK3CA promoter (934 bp) were identified (Figure 2.5a). These half sites are separated by 0-13bp and in each cluster either one or both half site consists of the core sequence CNNG in its consensus site. The list of p53 binding sites is provided in the following Table 5 wherein, the exact location of the binding sites are denoted and the core sequence are highlighted in red.

p53 binding sites	**Sequence on PIK3CA promoter**	**Location (bp)**
Site 1	AAACAGACTT	118-127
	CACCACGACA	141-150
Site 2	TGGCATTACG	200-209
	CCCCACGTCT	219-228

Site 3	ACGCTGGTTA	456-465
	CGGTTAGCCA	480-489
Site 4	AAGCAAGACG	731-740
	GCACATATTG	752-761

Table 5: The p53 binding sites in the PIK3CA promoter with their location and core sequence (highlighted in red)

Astanehe et al., reported that mutation in one of the four p53 binding sites (site 4) in PIK3CA promoter showed 50% less attenuation in presence of conditionally activated p53 protein [12]. Their study showed that changing the core (CNNG) nucleotides of the p53binding site significantly reduced *PIK3CA* promoter activity, suggesting that the integrity of the p53-binding site in the *PIK3CA* promoter plays a role in its repression by p53. Thus a series of site directed mutagenesis (SDM) were performed to sequentially abolish the binding of p53 in the PIK3CA promoter. (Figure 2.5b). MPFT 1 carries mutation at Site 3, MPFT 2 bears mutation at Site 3 and 4, MPFT 3 has mutation at Site 3, 4 and 1 and finally the fourth construct MPFT 4 bears mutation at Site 3, 4, 1 and 2.

A2780 cells were transiently transfected with all the constructs and their luciferase activities were measured. Cisplatin treatment to the transfected cells demonstrated that mutation at site 3 (MPFT 1), sites 3&4 (MPFT 2), sites 3, 4 & 1 (MPFT 3) and sites 3, 4, 1 & 2 (MPFT 4) did not exhibit any signal attenuation in comparison to the 20% reduction (***$p<0.0005$) showed by the wild type promoter (Figure 2.15). Surprisingly, three of these mutant promoters (MPFT-1, 2, 3) showed gradual augmentation of *PIK3CA* expression in comparison to the wild type promoter with MPFT-3 showing the maximal increase (2.5 fold **$p<0.03$). The MPFT 4 promoter showed overall decrease in *PIK3CA* expression in

comparison to the wild type and other mutants. For all these experiments, pTK-*hrluc* was used as an internal control.

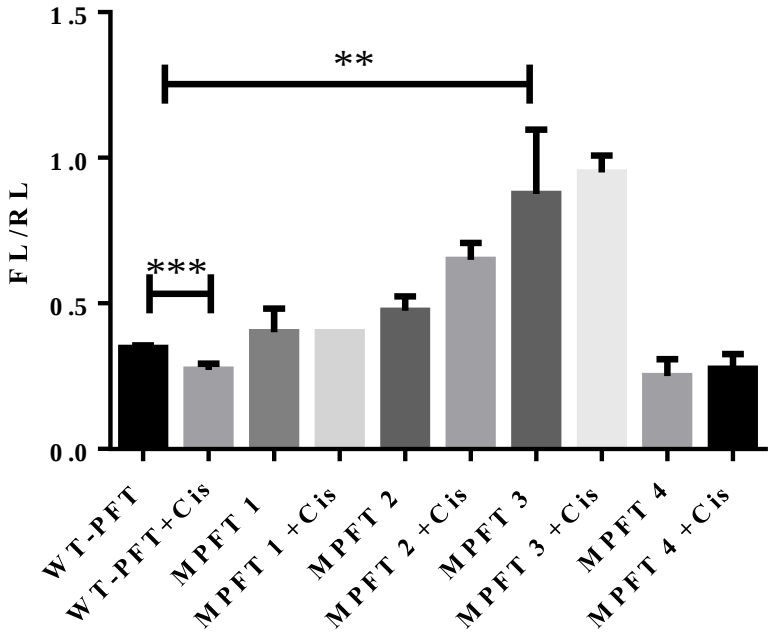

Figure 2.15. Sequential mutations in the p53 binding site increases PIK3CA promoter activity. *Graphical representation of the ratiometric analysis of the wild type and mutant PIK3CA-fluc2-tdt reporters with the pTK-hrluc from transiently transfected A2780 cells with and without cisplatin treatment (2 h). A reduction of 20% was obtained in WT-PFT activity ($p<0.005$) without any attenuation in the mutant promoters (MPFT-1, MPFT-2 and MPFT-3) after cisplatin treatment (10µg/ml). These mutant promoters showed a gradual increase of PIK3CA expression compared to WT-PFT with MPFT 3 showing a maximum of 2.5-fold increase. The MPFT-4 promoter showed an overall decrease in PIK3CA expression in comparison to WT-PFT. The SEM represents triplicate experiments.*

In silico analysis of the PIK3CA promoter for the presence of transcription factor binding sites other than p53: Since the MPFT 4 construct showed overall decrease in the luciferase activity, it was needed to analyse this promoter sequence for the presence of other

transcription factor binding sites that might be involved in the regulation of the promoter. With the help of Genomatix (trial version) software it was observed that two important transcription factor binding (NF-κB & HIF-1 ancillary sequence) sites overlap at site 2 p53 binding site. (Table 6). Similarly presence of other transcription factor binding sites in the promoter region as mentioned in the table below signifies that they can be potential regulators of the promoter.

Sequence	Transcription factors	Position
TTACAACAAAAGACCAGTAGG GGGA	SOX/SRY-sex/testis determining and related HMG box factors	24-48
CACCAAGACA	Site 1 (half p53 binding element)	142-151
TGGCATTACG CCCCACGTCT	Site 2 (p53 binding site)	201-210 220-229
CGCGAAAAATCCCCC	NF-κB	209-223
CCCCACGTCTT	HIF-1 ancillary sequence family	220-230
AAGTGAGTCAAAG	AP1	320-332
ACGCTGGTTA CGGTTAGCCA	Site 3 (p53 binding site)	457-466 481-490
TAGAAACAAATATACTA	Fork head domain factors	608-624
CACGTACGCTGT	HIF- 1	624-636
GATGACACAACA	Activating protein-1	642-653
AAGCAAGACG GCACATATTG	Site 4 (p53 binding site)	732-741 753-762

Table 6. Transcription binding sites in PIK3CA promoter with help of genomatix software and references from Astanehe et al. and Yang et al.

In vivo study of PIK3CA promoter modulation upon cisplatin treatment after mutations in the p53 binding sites: The MPFT 3 plasmid had showed augmented promoter activity and no effect upon cisplatin treatment. To evaluate the modulation of this mutant PIK3CA promoter *in vivo*, stable clone of A2780 cells expressing the MPFT 3 construct was generated, A2780-MPFT 3 cells (Figure 2.16) and treated with cisplatin and paclitaxel. Similar to earlier transient transfection result (Figure 2.15), the A2780-MPFT 3 cells showed higher luciferase activity (approximately 1.4 fold) than APFT cells. When treated with increasing concentrations of cisplatin and paclitaxel APFT cells exhibited attenuated luciferase activity with no significant change in activities of A2780-MPFT 3 cells (Figure 2.16 b & c). However, at higher concentration of cisplatin (15µg/ml), the A2780-MPFT 3 cells did show slight attenuation (Figure 2.16b).

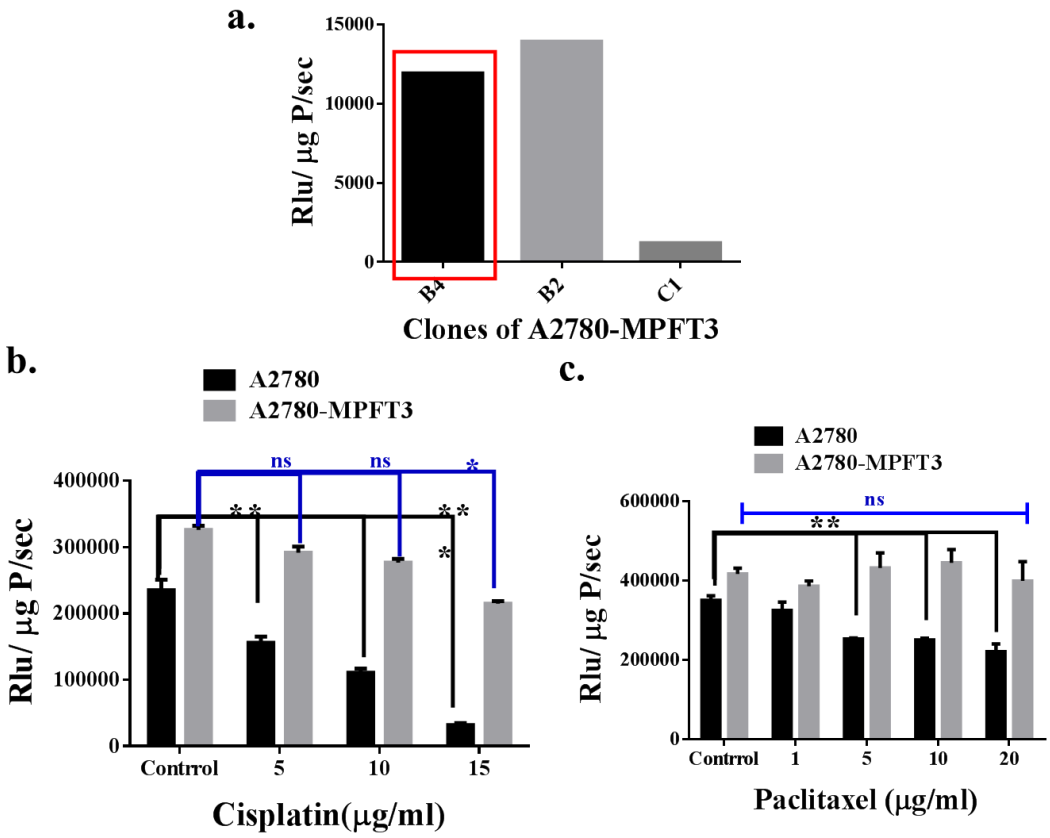

Figure 2.16: Effect of chemotherapeutics on the mutant PIK3CA promoter. *a) Screening of clones from A2780 cells by luciferase assay from MPFT 3 construct. Colony B4 was used as stable A2780-MPFT 3 cells; b and c) Treatment with increasing concentrations of cisplatin (5 and 10 mg/ml) and paclitaxel (1–20 mg/ml) exhibited attenuated luciferase activity in APFT cells (*p<0.005) but not in A2780-MPFT3 cells except at very high dose of cisplatin (15 mg/ml). The SEM represents triplicate experiments.*

To observe the effect of cisplatin on the MPFT 3 promoter *in vivo,* six million A2780MPFT3 cells were implanted in nude mice (n=6) and tumors xenografts were developed. Similar to our earlier *in vivo* studies, the A2780-MPFT 3 tumor xenograft models were grouped into two: control and test. The test group (n=2) were given the same dose of cisplatin treatment. It was observed that the bioluminescence signals in treated mice did not decrease rather exhibited an increase after first round of cisplatin treatment ($4x10^8 \pm 1.4x10^8$ p/sec/cm^2 to $7.5x10^8 \pm 2.3x10^8$ p/sec/cm^2) (2.4 fold) at 7th day, which remained constant to $7.5x10^8 \pm 2.5x10^8$ p/sec/cm^2 after completion of two treatments at 24 days. The control mice (n =3) also showed increased bioluminescence and tumor growth ($2.3x10^8 \pm 2x10^8$ p/sec/cm^2 to $4.4x10^8 \pm 2.2x10^8$ p/sec/cm^2 at day 7 to $9.2x10^8 \pm 4.5x10\pm$ p/sec/cm^2) (4 fold) over time (Figure 2.17a and b). The representative images of the bioluminescence signal in mice pre- and post-treatment in A2780-MPFT3 tumor models are shown in the Figure 2.17c.

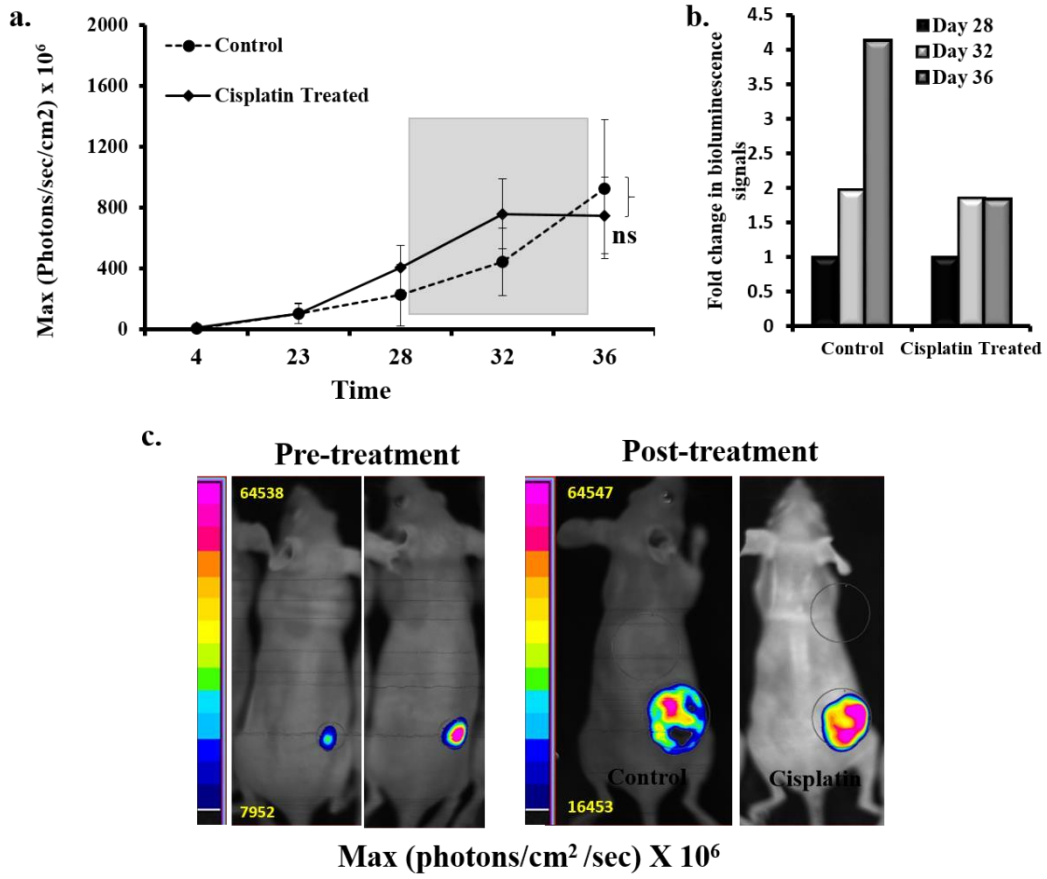

Figure 2.17. Bioluminescence imaging of cisplatin treated A2780-MPFT 3 tumor xenografts. *a) Graphical representation of the kinetics of MPFT 3 promoter wherein, the bioluminescence signal in both control (n=3) and treated mice (n=3) increased with time even after two rounds of cisplatin treatment (shaded area denotes the duration of cisplatin treatment); b) Graphical representation of fold-changes in the bioluminescence signals calculated ratiometrically (post treatment signal/pre-treatment signal) demonstrate augmented bioluminescence in both the control and treated group (Day 28 of b represents Day1 i.e. signal prior to treatment); c) Representative bioluminescent images of the mice bearing tumors of A2780-MPFT3 cells. Mouse from control and treated group exhibited specific [Figure: c (pre-treatment)] signals which did not decrease even after two treatments of cisplatin [Figure: c (post-treatment)].*

Discussion

Ovarian cancer is commonly treated with the combinatorial therapy of platinum (cisplatin and carboplatin) and taxol followed by debulking of tumor. [39]. Both cisplatin and paclitaxel have different modes of action for their cell killing activity. Cisplatin induces cell death by forming DNA adducts on the other hand paclitaxel induce cell cycle arrest causing cell death. However, both drugs are known to induce p53 activation. [42]. Activation of p53 might down-regulate the PIK3CA/AKT signaling as indirectly evidenced by association of PIK3CA gene amplification with p53 mutations in ovarian carcinoma [7, 8]. Alterations in the p110α, the catalytic subunit of class I PI3K and encoded by PIK3CA gene through mutation or gene amplification initiates a signal transduction pathway that promotes growth, metabolism, and survival in cancer cells [7, 273]. The ~900 bp upstream region of PIK3CA gene carries several important binding sites for p53, NF-κB, HIF, and AP1 transcription factors [19, 154]. Inhibition of nuclear translocation of NF-κB or incubation with TNF-α resulted in down or up-regulation of PIK3CA promoter activity [154]. P53 was shown to be involved in the negative regulation of PIK3CA promoter by direct physical interaction in ovarian surface epithelial cells. However, there are no reports to understand the effect on the activity of PIK3CA promoter by chemotherapeutic drugs that induce p53 activation. Non-invasive molecular imaging of living animals with reporter genes has opened new approaches for understanding molecular events [190, 274]. A variety of reporter genes has constantly been developed for different imaging modalities to study specific biological processes and monitor disease progression and therapy [275-277]. Multimodality imaging vectors generated by ‘fusion gene’ approach are most suitable for visualizing molecular events from both live cells and living organisms. One of such fusion vector, CMV-*fluc2-tdt* was used in this study to understand the regulation of *PIK3CA* promoter in ovarian cancer cells by cisplatin and paclitaxel from intact cells to living animals. To best of our knowledge

this is the first report of understanding the kinetics of drug induced PIK3CA promoter modulation. PIK3CA *(*PIK3CA-*fluc2-tdt)* sensor exhibited significant attenuation after treatment with three chemotherapeutic drugs (cisplatin, paclitaxel and adriamycin) commonly used for ovarian cancer patients in two different cancer cells but with same copy number for PIK3CA gene. Similar treatments did not affect the *TK* (Thymidine kinase) promoter in PA1 and A2780 cells. PA1 and A2780 cells are derived from patients with different types of ovarian cancer. While PA1 cells are derived from germ cell tumors and are sensitive to chemotherapeutics, A2780 cells are derived from serous adenocarcinoma and are comparatively more resistant to the chemotherapeutics. The level of attenuation varied between the cell lines with PA1 cells being more sensitive (2.3 fold reduction in promoter activity) than A2780 cells (1.3 fold) at same concentrations of cisplatin (5µg/ml) reflecting their respective clinical behaviour.

Since reporter gene technology is extremely sensitive and can measure minute molecular changes, the bifusion reporter used here was able to detect changes in the PIK3CA promoter activity while similar variation in the endogenous p110α protein level after cisplatin or paclitaxel treatments were not observed. The drug mediated attenuation of PIK3CA activity due to increased binding of activated p53 was not detected in a p53 deficient EOC (SKOV3) cell line. Both cisplatin and paclitaxel with increasing concentrations were not able to attenuate the PIK3CA promoter in these cells.

We further evaluated the endogenous levels of p53 upon drug treatment in PA1 and A2780 cells. Cisplatin and paclitaxel both significantly induced the p53 which was reflected by immunoblotting. Activation of p53 by these drugs thereby led to increased binding of p53 to the PIK3CA promoter and its suppression. This promoter suppression was not detected in SKOV3 cells which are deficient in p53 indicating that presence of p53 is important for the modulation of PIK3CA promoter. The *in vivo* imaging kinetics showed a decrease in

bioluminescence signal in both PA1 and A2780 tumors (expressing *PIK3CA-fluc2-tdt*) after cisplatin treatment. While a single treatment of cisplatin caused measurable reduction in luminescence activity in PA1 tumors at 14th day, it did not effectively reduce the PIK3CA promoter activity in A2780 tumors. Two successive treatments were required to achieve significant reduction in luminescence activity in A2780 tumors. This differential effect of cisplatin on two different tumor types correlates well with their origin as ovarian germline tumors are known to be more sensitive to cisplatin in comparison to epithelial ovarian tumors. In corroboration with the *in vitro* results, cisplatin treatment *in vivo* also did not reduce the bioluminescence signals of SKOV3 tumor xenografts stably expressing the PIK3CA sensor indicating that presence of p53 protein is essential for PIK3CA regulation in ovarian cancer.

Detailed bioinformatics study of the PIK3CA promoter showed that along with the putative p53 binding sites, the promoter also bears transcription factor binding sites for NF-κB, HIF-1 ancillary sequence, Activating protein-1 (AP 1), etc. that may alter the promoter modulation. Dependence of PIK3CA promoter on p53 resulting in its repression led us to generate mutations in the p53 binding sites. Surprisingly, sequential deletion of the p53 binding sites exhibited a gradual increase in the normal promoter activity indicating a temporary relief of p53 mediated suppression. Cisplatin induced attenuation of these mutant promoters were abolished. The promoter carrying mutations at all the four p53 binding sites showed an overall attenuation which might occur due to destabilization of co-operative bindings of other transcription factors required for PIK3CA expression.

Further studies are needed to understand the exact p53 binding site playing role in PIK3CA promoter repression and to investigate other potential targets in the PIK3CA promoter modulating its activity.

In this part of the study, we observed that the PIK3CA promoter activity is attenuated upon drug treatment in chemo-sensitive ovarian cancer cells and tumor xenografts. Since, such a negative correlation is reported to exist between PIK3CA gene amplification and platinum sensitivity in EOCs [8], there is a need to understand the regulation of this promoter during acquirement of chemo-resistance. In the following chapters, a detailed study on role and regulation of PIK3CA signalling in chemo resistant ovarian cancer are undertaken.

Chapter 3

Development of cellular chemo-resistant models expressing the PIK3CA sensor and monitor the modulation of PIK3CA promoter activity in effect of chemotherapeutics

Introduction

Ovarian cancer is the leading cause of gynecological cancer mortality and the prognosis for women with ovarian cancer is very poor. Majority of the patients are diagnosed at an advanced stage of disease and long-term survival rate is as low as 10-30% [62]. The conventional treatment strategy for EOC includes cytoreductive surgery followed by cisplatin/carboplatin and paclitaxel based combination adjuvant therapy however, neoadjuvant therapy which involves chemotherapy treatment of patients prior to surgery is also practiced [3]. Despite of promising therapeutic response at initial stages, majority of the patients show recurrence due to development of chemoresistance. Overall survival (OS) for patients is thus short (5 year OS: 30-40% for all stages) and has remained stable for last two decades [3]. Even after a significant effort undertaken by many investigators worldwide, no improvement in OS rate was observed. Therefore, late detection and development of drug resistance are still the two major clinically observed obstacles for effective treatment of EOC [278]. Platinum and taxane, the most common therapeutics for ovarian cancer have different mechanism of action. Cisplatin binds to the DNA strand, hindering both DNA replication and RNA translation and eventually triggers apoptosis, and on the other hand, paclitaxel causes cytotoxicity by binding to and stabilising polymerised microtubules. Drug resistance is a multifactorial phenomenon with many unknown and poorly understood mechanisms and thus difficult to overcome. Many tumor cells gradually acquire resistance to chemotherapy and to mimic this clinical scenario use of drug resistant cellular model is the best possible approach for investigating the mechanisms that modulate drug resistance [279]. The first *in vitro* drug resistant cellular model was established in 1970 by selection through anti-tumor agents. In this study, the development of resistance to actinomycin-D (AD) in Chinese Hamster cells was found due to alteration in cell membrane resulting in decreased permeability to AD [280]. Since then many such resistant cell lines are established

that exhibited acquired resistance to antitumor agents and are constantly being used to evaluate and understand the different mechanisms of chemoresistance. According to McDermott et al., (2014) drug-resistant cell models can be categorized into two groups: 1. clinically relevant models or 2. high-level laboratory or conventional models. The conventional and the most common method of establishing resistant cell lines is to use continuous administration of drugs at low-dosage intermittent incremental inducement for a long time. This high-level laboratory models are established with the purpose of understanding possible mechanisms of resistance to chemotherapy agents and show 10-20 fold high resistant index. Clinically relevant drugresistant cell lines are usually developed by employing a pulsed treatment strategy and mimic the conditions cancer patients experience during chemotherapy and these cell lines usually display between 2-8 fold resistances compared to their parental cell line. [281].

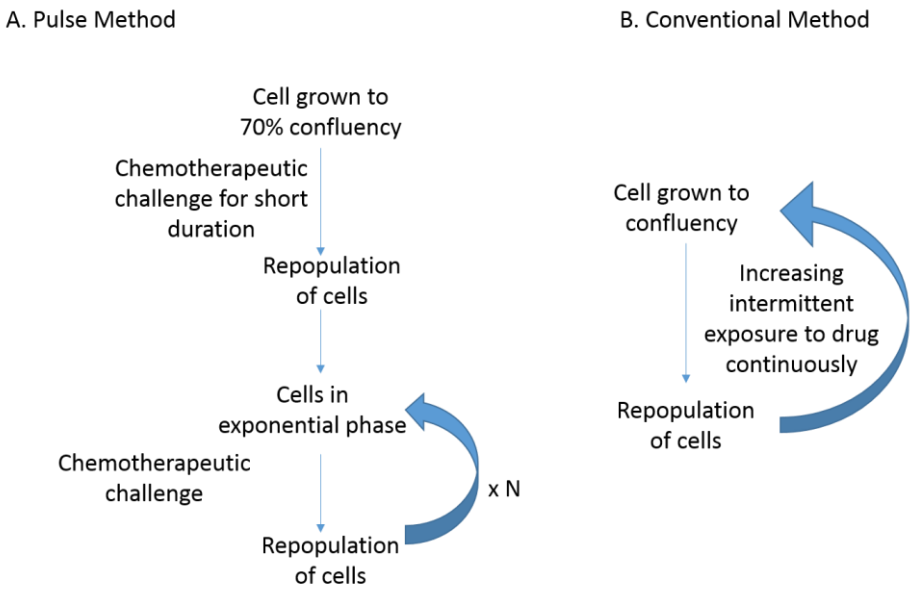

Both the type of models have their own advantages and disadvantages. Pulse treatment mimics the cycles of chemotherapy a patient receives in the clinic, however, often it creates unstable

and low–level resistance with few molecular changes to detect and analyse. Stable highly resistant cells are obtained with the conventional method which can be easily maintained in culture and the molecular changes are easily identified, however, such high resistance is less relevant to clinic. The heterogeneity observed in drug-resistant models produced from the same parent cell line with the same chemotherapy agent by two different methods indicates existence of differential mechanism of drug resistance [279]. Considering that pulse method is closely relevant to clinic, in our laboratory, we employed pulse method with a little modification to develop a set of isogenic ovarian cancer cell lines resistant to either cisplatin or paclitaxel. Rather than using the same dose repeatedly for chemotherapeutic challenge in the next cycles of pulse treatment, the concentration of drug was increased manifold in each cycle rendering the selection and repopulation of only the surviving cells. Thus the possibility of heterogeneity within the surviving population was avoided and only resistant cells were selected.

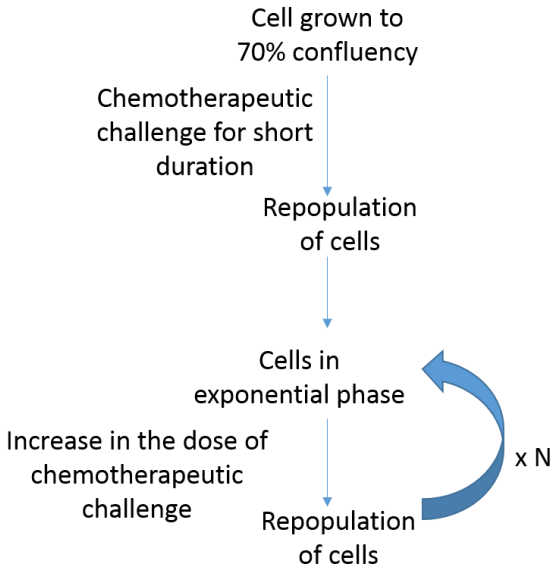

The thrust of our study is to improve our knowledge about the underlying mechanism of the multifactorial phenomenon of chemoresistance in ovarian cancer. Several reviews have elaborated many factors that are responsible for this chemoresistance like aberrant membrane transporters, altered drug metabolism, and enhanced DNA repair mechanisms, suppression of apoptosis and upregulation in many cell survival pathway components. Since

ovarian cancer patients are treated with a combination of two different drugs i.e., paclitaxel and cisplatin, it is important to develop resistant models for both in an isogenic background which would enable us to understand the common or differential features. As described in earlier sections, PI3K/AKT/mTOR signaling is one of the major pathway that plays an important role in the development of cisplatin and paclitaxel resistance in ovarian cancer [9, 10]. Chemotherapeutic drugs are known to induce activated AKT in several cancer cell lines, including ovarian, breast, glioma and pancreatic cancer cells. Constitutively active AKT has also been found in chemoresistant lung, glioma and ovarian cancer cell lines, compared with their sensitive parental counterparts [144, 282, 283]. EOCs harbour PIK3CA amplification irrespective of histological subtypes and are negatively associated with platinum sensitivity. However, little is known about the role of PI3K gene amplification or its promoter in acquirement of chemoresistance in ovarian carcinoma.

In the previous chapter it was observed that PIK3CA promoter exhibited attenuated activity after cisplatin and paclitaxel treatment in A2780 cells. Tumor xenografts of A2780 cells stably expressing PIK3CA sensor also displayed similar attenuation after cisplatin treatment corroborating with the *in vitro* results. In order to understand the molecular alterations occurring in the acquirement of chemoresistance and to address the question of monitoring the modulation of the PIK3CA sensor in the acquired chemoresistance to these drugs, isogenic cisplatin and paclitaxel resistant models in A2780 cells stably expressing PIK3CA sensor were established in a brief period of 6 months by the clinically relevant pulse method. These resistant cellular models were then compared to the parental sensitive cells using a cell viability assay (MTT) or clonogenic assay. In this study we describe the establishment and characterization of the acquired cisplatin and paclitaxel resistance in A2780 cells.

Materials and Methods:

Generation/Establishment of the cisplatin and paclitaxel resistance in A2780 cells

Following the pulse method strategy, 2 x 10^6 A2780 cells were treated with incremental doses either cisplatin or paclitaxel for a period of six months. Briefly, cells were treated with fixed concentration of cisplatin and paclitaxel for 2h and were allowed to grow in drug free medium. The surviving cells were subcultured and again treated with the same concentration of drug for three successive cycles. These repeated cycles of drug treatment helped the cells to acquire stable chemoresistance over time. The dose of cisplatin and paclitaxel were increased after every three cycles of drug treatments (Figure 3.1a). The concentration of cisplatin and paclitaxel used to develop the respective isogenic variant of A2780 cells were as shown table below with a schematic representation of the procedure followed for the development of chemoresistance. Figure 3.1b demonstrates the number of drug treatment cycles and concentration of cisplatin and paclitaxel used for cisplatin and paclitaxel resistant isogenic variants of A2780 cells.

a.

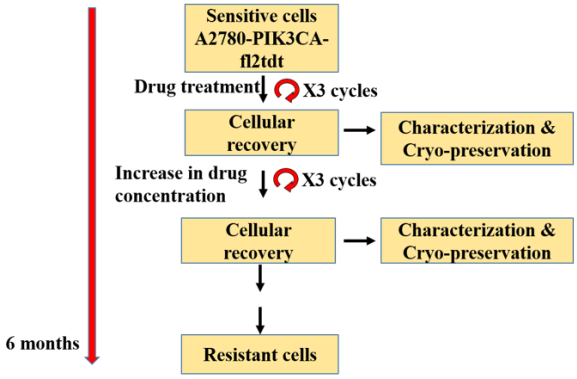

b.

Concentration of Cisplatin (µg/ml)	Concentration of Paclitaxel (nM)	Number of Cycles
1	60	1
1	60	2
1	60	3
1	100	4
5	100	5
5	100	6
5	150	7
10	150	8
10	150	9
10	200	10
15	200	11
15	200	12
15	350	13
20	350	14
20		15
20		16

Figure 3.1.Development of cellular chemoresistant model. *a) Illustration of stepwise development of individual cisplatin and paclitaxel resistant model. Cells were exposed to drug treatment (either cisplatin or paclitaxel) of one concentration for three times (3X) and*

the surviving cells were subcultured subsequently with increased concentration; b) Tabular illustration of drug concentration used for each treatment cycle.

Cell cycle analysis

For cell cycle analysis, cells were harvested by trypsinisation, washed once with phosphate-buffered saline (pH 7.4), pelleted down and resuspended in ice-cold 70% ethanol (v/v) for fixation. After incubation at room temperature for 1h, cells were centrifuged and the supernatant was removed. The cells were then resuspended in 1 mL of PBS containing 50 µg/mL PI and 100 µg/mL ribonuclease A and incubated at 37°C for 30 min. After centrifugation, cells were resuspended in PBS and analyzed using a flow cytometer (LSR II, BD Bioscience, San Jose, CA). The detailed procedure for flow cytometric assay is described in the section 8.3.

MTT assay or cell viability assay

The percentage viability of cells calculated by MTT assay was used to determine the cell proliferation rate. Sensitive and resistant cells were seeded (500 cells) in each well of 96 well plate and cell growth was assessed at 0, 24, 48, 72, 96, 120 and 144h. The absorbance was recorded using SPECTRA MAX190 at 560 and 670 nm. The percent viability of cells was calculated as follows:

(A560nm – A670nm) sample / (A560nm – A670nm) control x 100.

Measurement of cellular uptake of cisplatin

A2780 and A2780-Cis ^{LR} ($10x10^5$ cells) were treated with 10 µg/mL of cisplatin 24h at 37^0C. Untreated cells of both stages were used as controls. Cells were lysed using concentrated HCl as described in the protocol mentioned in Appendix (Material and methods). The platinum content in control and cisplatin treated samples was measured using cisplatin (2000ppm) as a

standard in VGPQ2 plus, Inductively coupled plasmon mass spectrometer (ICPMS) system, placed in Bhabha Atomic Research Centre (BARC), Mumbai, India.

DCFDA assay

Endogenous levels of reactive oxygen species (ROS) was measured by 2', 7'dichlorofluorescein diacetate (DCFDA) dye. The detailed procedure of measurement of ROS by DCFDA dye is given in section 8.7. Briefly, 7.5×10^4 cells/well were grown and were processed for DCFDA assay, according to the kit guidelines. The ROS formation was analyzed using 10000 events/sample by flow cytometry after establishing the forward and side scatter gates that excluded debris and cellular aggregates.

Immunofluorescence

Cells were seeded on the sterilized coverslips a day prior to the experiment. The detailed procedure of immunofluorescence is given in the section 8.16. Briefly, desired treatments of drugs were given to the cells which were then fixed by with 4% PFA after 24 h. After permeabilizing with 0.025% Triton X100 in 4% PFA for 10 minutes, the coverslips were washed in 1X PBS and blocked in 5% BSA followed by overnight incubation with antiγH2AX antibody (1:200). Cover slips were then washed, incubated with secondary antibody (2 h) anti-rabbit (Dylight 633 or FITC). 0.05% DAPI was used to counter stain the nuclei. Images were captured using 63X objective in LSM Zeiss microscope. At least five representative fields were studied for γH2AX and DAPI staining. Mean fluorescent intensity for γH2AX staining was calculated by counting approximately 40 nuclei for each sample.

Quantitative real-time PCR (q RT-PCR) from cell line

Total RNA was extracted from cultured cells using RNease kit (Qiagen, Netherlands).

Two micrograms of total RNA was reverse transcribed using cDNA synthesis kit (Invitrogen, Carlsbad, CA). qRT-PCR analysis was performed using SYBR Green method as described in section 8.12. GAPDH was used as an internal control. Primer sequences used were as follows: hCTR1 (Forward: GCTGGAGAAATGGCTGGAG, Reverse: GCTCTCTCGGGCTATCTTGA), ATP7A (Forward GCACAAACATCAAAGGCTCC, Reverse: GAGGGTGGCAATGGAAACAA) ATP7B (Forward: CGTTGGTGGTATGGATTGTA Reverse: GTGCTTGTTGGGGTTAGGAA), ABCB1 (Forward: CACCCGACTTACAGATGATG and Reverse: CCCAGTGAAAAATGTTGCCA), OATP1B3 (Forward CCGTATTTTTTGGAAGGGTCTAC Reverse: TTCTTTCATTGTCCGATGCC) and GAPDH (Forward: TGCACCACCAACTGCTTAGC, Reverse GGCATGGACTGTGGTCATGAG).

The relative expression levels of mRNAs were calculated by the ΔCt for relative quantification and ΔΔCt method for fold change measurement.

Clonogenic Assay/ Colony Forming Assay

The detailed procedure for colony forming assay is described in the section 8.17. Briefly, single-cell suspension of A2780 cells and its isogenic resistant variants were plated in six well dishes at a density of 500 cells/well. Once adhered, the cells were treated with increasing concentrations of either cisplatin or paclitaxel respectively for 24h. The plates were further incubated for 7days and the colonies were stained with 0.01% crystal violet and counted under inverted microscope.

Results

Determination of the IC_{50} concentration of cisplatin and paclitaxel for the A2780 cells:

Drugs (cisplatin and paclitaxel) were added at increasing concentrations and the half minimal inhibitory concentrations i.e. IC_{50} were calculated for the sensitive A2780 cells for 72h by

MTT assay. IC_{50} concentration for cisplatin at 72 h was found to be 500ng/ml which showed approximately 56% viability. This IC_{50} concentration was further used to determine the resistance index of the cisplatin resistant A2780 cells (Figure 3.2a). Similarly, IC_{50} concentration for paclitaxel at 72h was calculated as 80ng/ml, which showed 49.4% viability which was further used to monitor the acquirement of paclitaxel resistant A2780 cells (Figure 3.2b).

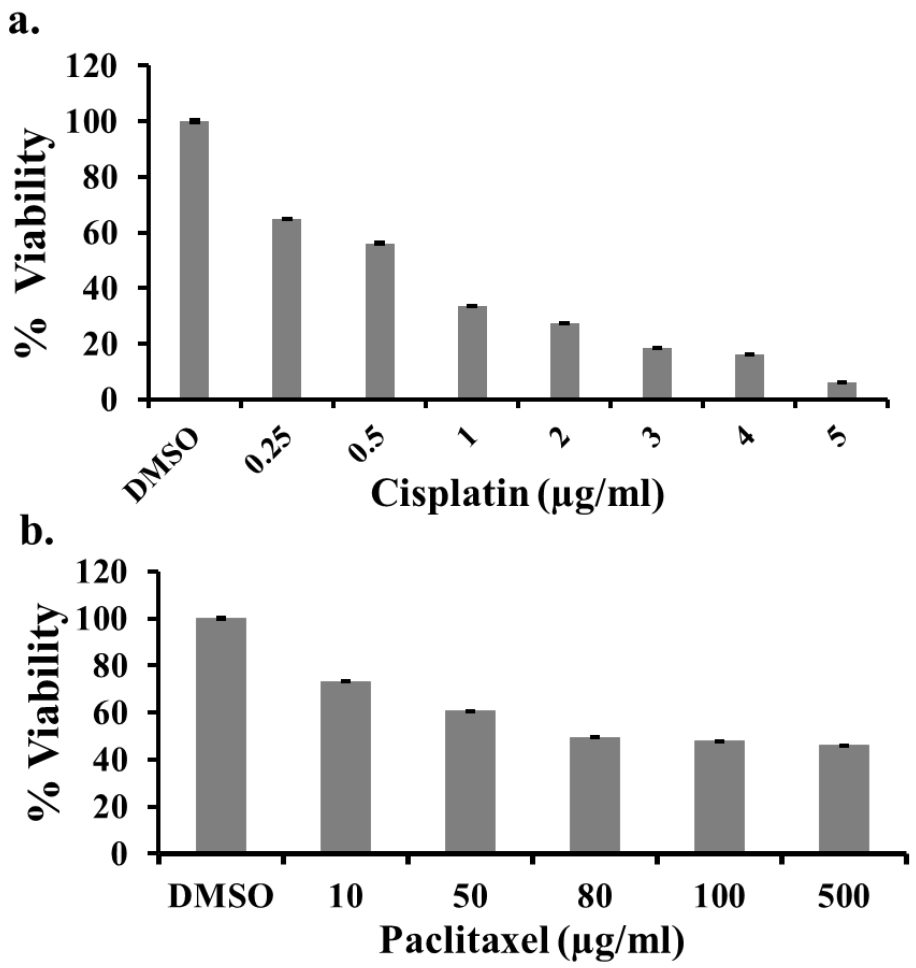

Figure 3.2. IC_{50} dose determination for cisplatin and paclitaxel on A2780 cells. *a and b) Graphical representations of the percent viability of cells treated with different doses of cisplatin (0.25-5µg/ml) and paclitaxel (10-500ng/ml). Concentration of the drugs at which*

the cells showed 50% viability were considered as the IC_{50} value and were further used to determine the level of chemoresistance.

Development of isogenic cellular models of cisplatin and paclitaxel resistance in A2780 cells: As described earlier in method section, two cellular models of cisplatin and paclitaxel resistance were developed using pulse method with incremental doses. Percent viability of these cells at different stages during the development of resistance were assessed by MTT assay using the IC_{50} concentrations of both cisplatin and paclitaxel. As shown in Figure 3.3, cells gradually acquired resistance with increasing concentrations of drugs. The cisplatin late resistant cells, A2780-Cis^{LR} demonstrated 92% viability whereas, paclitaxel late resistant cells, A2780-Pac^{LR} demonstrated 86% (Figure 3.3).

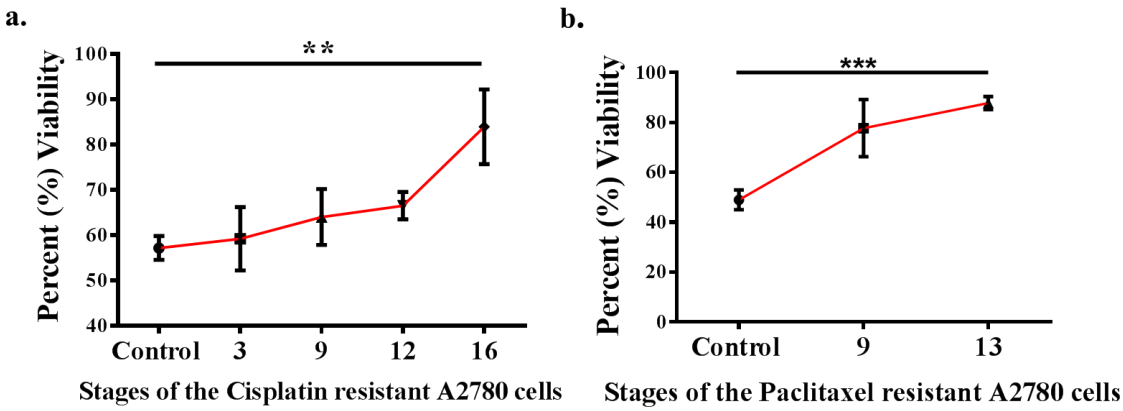

Figure 3.3. MTT assay to determine the chemoresistance. *a and b) Graphical representations of the percent viability of cells at different stages of development of resistance. Cellular viability was calculated with IC_{50} concentration of drugs for 72h. A2780-Cis^{LR} cells showed 97% viability (**p<0.05) upon cisplatin treatment whereas A2780-Pac^{LR} (***p<0.001) cells showed approximately 86% viability upon paclitaxel treatment.*

Resistance indices (RI) for both models were calculated using the standard formula (IC_{50} of resistant cells/ IC_{50} of sensitive cells). It was found that the RI for late cisplatin resistant cells (A2780-Cis^{LR}) were 7.5 fold higher than the sensitive A2780 cells. The RIs of intermediate stages of developing cisplatin resistant cells were also measured and cells with intermediate RI value was termed as early resistant cells (A2780-Cis^{ER}) as described in the table 7.

Sr. No.	Stages in the development of cisplatin resistance	IC_{50} concentration of cisplatin(ng/ml)	Resistance Index (RI)
1	A2780	500	1
2	3	750	1.5
3	6(A2780-CisER)	1500	3
4	12	3000	4.5
5	16 (A2780-CisLR)	3750/5000	7.5/10

Table 7. Determination of the Resistant Indices (RI) in the cisplatin resistant model.

Similarly, the RI value for paclitaxel resistant model was also calculated and was found to be 5 fold higher in the late paclitaxel resistant cells (A2780-Pac^{LR}) (Table 8). Similar to cisplatin resistance, the cells at intermediate RI value was termed as early resistant cells (A2780-Pac^{ER}).

Sr. No.	Stages in the development of paclitaxel resistance	IC_{50} concentration of paclitaxel (ng/ml)	Resistance Index (RI)
1	A2780	80	1
2	9(A2780-PacER)	200	2.5
3	14 (A2780-PacLR)	400	5

Table 8.Determination of the Resistant Index (RI) in the paclitaxel resistant model.

In order to gain insight whether the isogenic resistant variants of A2780 cells demonstrate cross resistance, we used IC_{50} concentrations of cisplatin and paclitaxel to check cellular toxicity in A2780-Pac^{LR} and A2780-Cis^{LR} cells. As expected both cisplatin and paclitaxel treatment to A2780 cells showed approximately 50% viability. Interestingly, A2780-Pac^{LR} cells showed 85% viability upon treatment with IC_{50} concentration of cisplatin indicating that these paclitaxel resistant cells have also developed resistance to cisplatin (Figure 3.4b). In contrast, the A2780-Cis^{LR} cells demonstrated hypersensitivity upon paclitaxel treatment with survival of only 25% cells (Figure 3.4a).

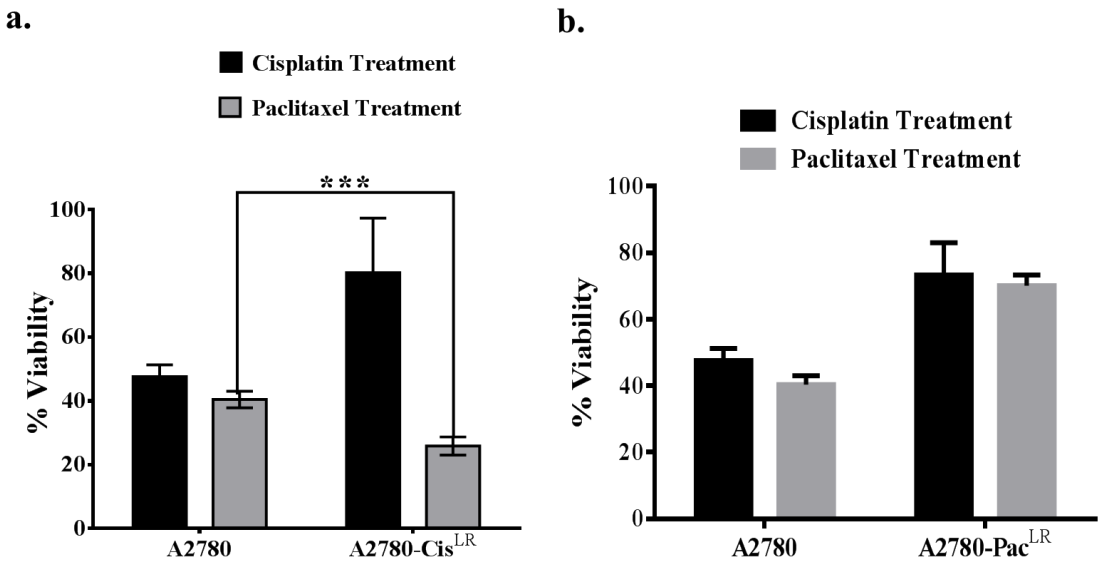

Figure 3.4. Determination of cross-resistance for cisplatin and paclitaxel in the resistant models. *a and b) A2780, A2780-Cis^{LR} and A2780-Pac^{LR} were treated with IC_{50} concentration of both cisplatin and paclitaxel. Cisplatin resistant cells showed higher sensitivity to paclitaxel (25%) (***p<0.005) whereas cisplatin had no effect on the paclitaxel resistant cells.*

Isogenic cisplatin and paclitaxel resistant cells exhibit slower proliferation: Drug resistant cells often show changes in their proliferative capacity and doubling time. In our study, both the isogenic cisplatin and paclitaxel resistant variants of the A2780 cells were monitored for

the changes in proliferation rate and doubling time. Changes in proliferation were markedly observed after 48h between the sensitive, early and late resistant cells. Interestingly, the early resistant cells showed comparable proliferation rate as sensitive cells but the late resistant ones demonstrated a much slower proliferation (** $p<0.004$) (Figure 3.5a and b). Table 9 shows the different growth doubling times of the sensitive and resistant sublines of A2780 cells. The doubling time was calculated from assessing the cell proliferation for 144 h. The growth doubling time for the sensitive A2780 cells were about 26h and that of resistant cell lines (A2780-Cis^{LR} and A2780Pac^{LR}) were significantly longer (33h and 37h). In both the resistant models, the early resistant cells showed cell proliferation similar to the parental cells and their doubling times are comparable to the A2780 parental cell line whereas the late resistant cells were less proliferative with higher doubling time.

Cell lines	Doubling time (h)
A2780	**25.59 ± 1.53**
A2780-CisER	**21.35 ± 0.27**
A2780-CisLR	**33.44 ± 1.35****
A2780-PacER	**24.63± 0.53**
A2780-PacLR	**37.55 ± 1.86****

Legend: ** ($p<0.005$) compared with A2780 cells

Table 9: Doubling time of the cisplatin and paclitaxel isogenic variant of A2780 cells.

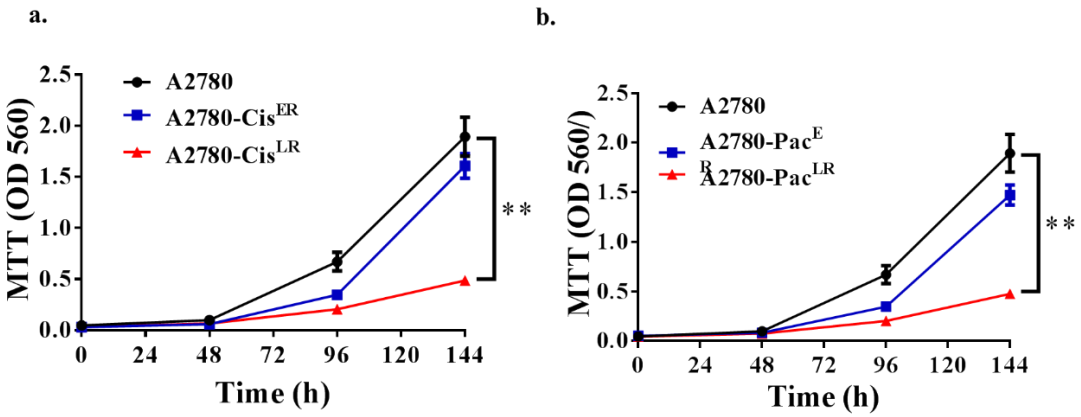

Figure 3.5. Cell growth and proliferation rate. *a and b) Graphical representations of the growth curves of cells from cisplatin and paclitaxel resistant models as assessed for 144h by MTT assay. The A2780-Cis^{LR} cells showed a drastic decrease (**p<0.004) in the proliferation as compared to A2780 and A2780-Cis^{ER}. Similarly, A2780-Pac^{LR} demonstrated decrease in proliferation as compared to the sensitive and A2780-Pac^{ER}.*

Cisplatin and paclitaxel resistant variants of ovarian cancer cells exhibited enhanced clonogenic survival: The superior endurance capacity of drug resistant cells is often been measured by clonogenic assay in presence of drugs. The survival ability of sensitive A2780 cells and its isogenic cisplatin and paclitaxel resistant variants (A2780-Cis^{LR} and A2780-Pac^{LR}) were assessed with increasing concentration of cisplatin and paclitaxel for 24h using the clonogenic survival assay. In cisplatin and paclitaxel resistant cells, significantly higher (****p<0.0001) fraction of colonies were observed in the highest concentration of drugs (2µg/ml cisplatin and 500ng/ml paclitaxel) as compared to the sensitive A2780 cells. While both the sensitive and resistant cells formed comparable number of colonies at lower concentration (0.02ug/ml), around 10 fold reduction in colony numbers was observed in the sensitive cells at higher drug concentrations. However, the late resistant cells were able to form colony at 2µg/ml of cisplatin or 500ng/ml paclitaxel (Figure 3.6 a and c). The representative images of the colonies obtained after staining with crystal violet are given in the Figure 3.6 b and d.

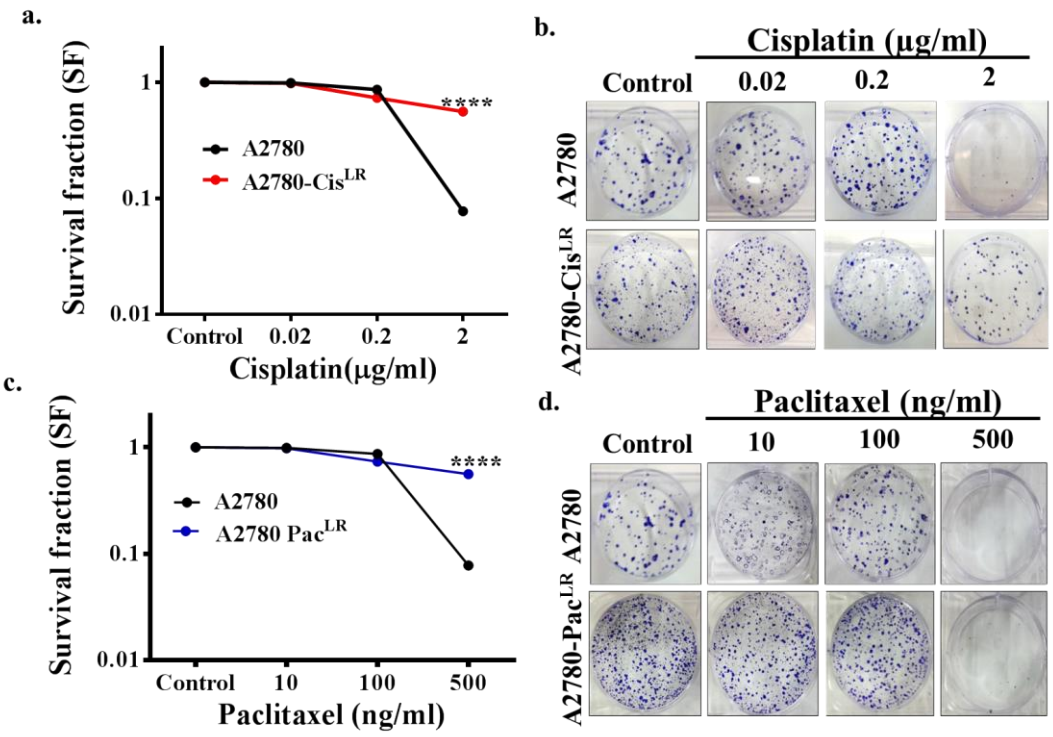

Figure 3.6. Cisplatin and paclitaxel resistant variants of A2780 showed high clonogenic potential. *a and c)Clonogenic assays were carried out to assess the effects of increasing concentrations of either cisplatin or paclitaxel on A2780 and the respective isogenic resistant variants. Survival fractions demonstrated that of A2780-Cis^{LR} and A2780-Pac^{LR} show higher colony forming abilities with increasing concentration of cisplatin and paclitaxel (****p<0.0001). The representative images of the clonogenic plates are shown in b and d.*

Cisplatin and Paclitaxel Resistant A2780 cells demonstrate alterations in cell cycle and aneuploidy: Ovarian cancer is characterized with global genomic instability and presence of such aneuploid population often contributes to its drug resistance. Slower proliferation rate observed in our resistant models also indicates for an altered cell cycle. Hence, to further understand the cell cycle progression in the sensitive and resistant cells, A2780 and both the resistant cells were analysed by propidium iodide staining. The cell cycle phases were

analysed in an unsynchronized population of all the cell lines, and the late resistant cells showed an elongation in G0/G1 phase and slight decrease in G2-M phase (Figure 3.7 a-c). Ploidy level was assessed by using peripheral blood lymphocytes as diploid control. A2780 was found to be slightly hypo-ploid compared to PBC, however both the cisplatin and paclitaxel resistant cells showed aneuploidy (Figure 3.7d and e).

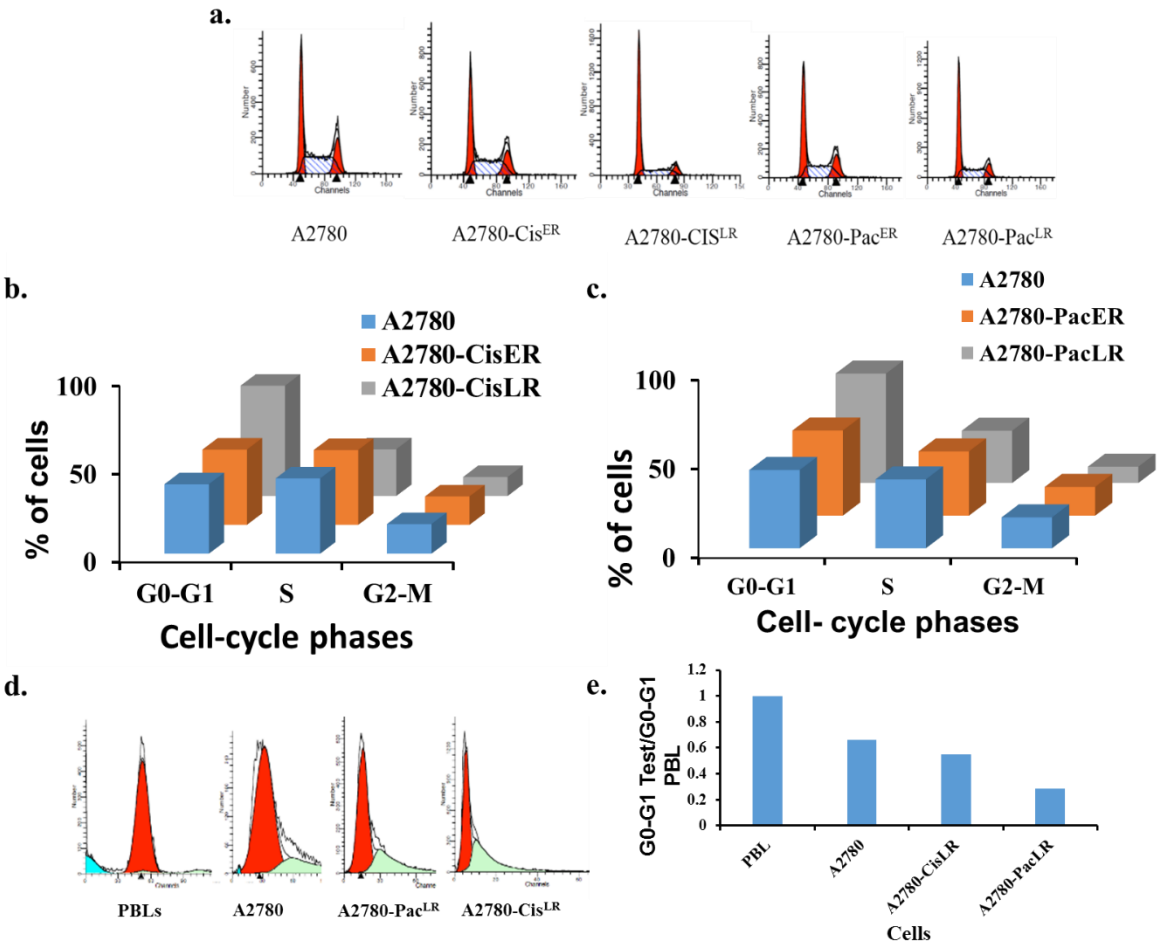

Figure 3.7. Cell cycle analysis of the Cisplatin and paclitaxel resistant variants of A2780.

a) Cell cycle distribution for each resistant models is shown in the histogram; b and c) A2780-Cis^{LR} and A2780-Pac^{LR} cells showed marked increase in G0-G1 phase and slight decrease in G2-M .d and e) DNA content analysis by DAPI staining showed hypo-ploid nature of the parental cell line as compared to the peripheral blood lymphocytes (PBLs)

used as diploid control but the resistant cells showed aneuploidy. Ploidy was deciphered by the ratiometric analysis of (G0-G1) channels of test cells verses PBLs.

Expression of membrane transporter genes in cisplatin and paclitaxel resistance: Cellular uptake of drugs may occur by passive diffusion or via active transport, which is controlled by membrane transporter proteins. These transporters are of two types: influx transporters and efflux transporters. Aberrant expression of these membrane transporters may result in drug resistance. Two copper homeostasis proteins ATPase Copper transporting α-polypeptide (ATP7A) and ATPase Copper transporting β-polypeptide (ATP7B) are assumed to be involved in the intracellular transport (efflux) of cisplatin and may account for acquired resistance to cisplatin. ATP7A sequesters platinum agents in intracellular compartments, inhibiting their reaction with nuclear DNA. Ovarian cancer patients with higher ATP7A expression have lower survival rate than patient which show low levels of expression. ATP7A is found to over express in several cisplatin resistant ovarian cancer cells [284]. ATP7B protein is involved in blockade of drug access to the nucleus. ATP7B mRNA or protein expression has been reported in several human malignancies like ovarian cancer, gastric cancer and breast cancer. Over expression of ATP7B in primary ovarian cancer cell lines imparts resistance to cisplatin [285, 286]. On the other hand, the major human copper (Cu) influx transporter (hCTR1) controls the uptake of cisplatin in mammalian cells. Studies have shown a significantly high level of hCTR1 in the plasma membrane of sensitive cells compared to resistant cells [287-290]. Another membrane transporter P-glycoprotein 1 (permeability glycoprotein), (Pgp) also known as multidrug resistance protein 1 (MDR1) or ATP-binding cassette sub-family B member 1 (ABCB1) or cluster of differentiation 243 (CD243), functions as an ATP dependent efflux pump with broad substrate specificity. It is mainly involved in resistance against paclitaxel [78]. To understand the role of membrane transporter genes in the development of

resistance, the mRNA expression of cisplatin influx (hCTR1) and efflux (ATP7A and ATP7B) membrane protein were studied (Figure 3.8a). A significant reduction in the expression of hCTR1 gene was observed in cisplatin resistant cells as compared to the parental cell line. However, there was no change in the expression of the efflux membrane transporters. Surprisingly, the expression of ABCB1 transporter gene was extremely high in paclitaxel resistant cells as compared to the A2780 and A2780Cis^{LR} cells (Figure 3.8b). When these A2780-Pac^{LR} cells were treated with Verapamil, a known inhibitor of ABCB1 transporter, along with paclitaxel, decrease in viability was observed (Figure 3.8c).We also validated the expression levels of one of the influx transporter specific for paclitaxel, OATP1B3, which is down-regulated in the paclitaxel resistant cells. The cisplatin resistant cells showed a significantly high expression of this gene giving a possible reason of hypersensitivity of these cells to paclitaxel (Figure 3.8d).

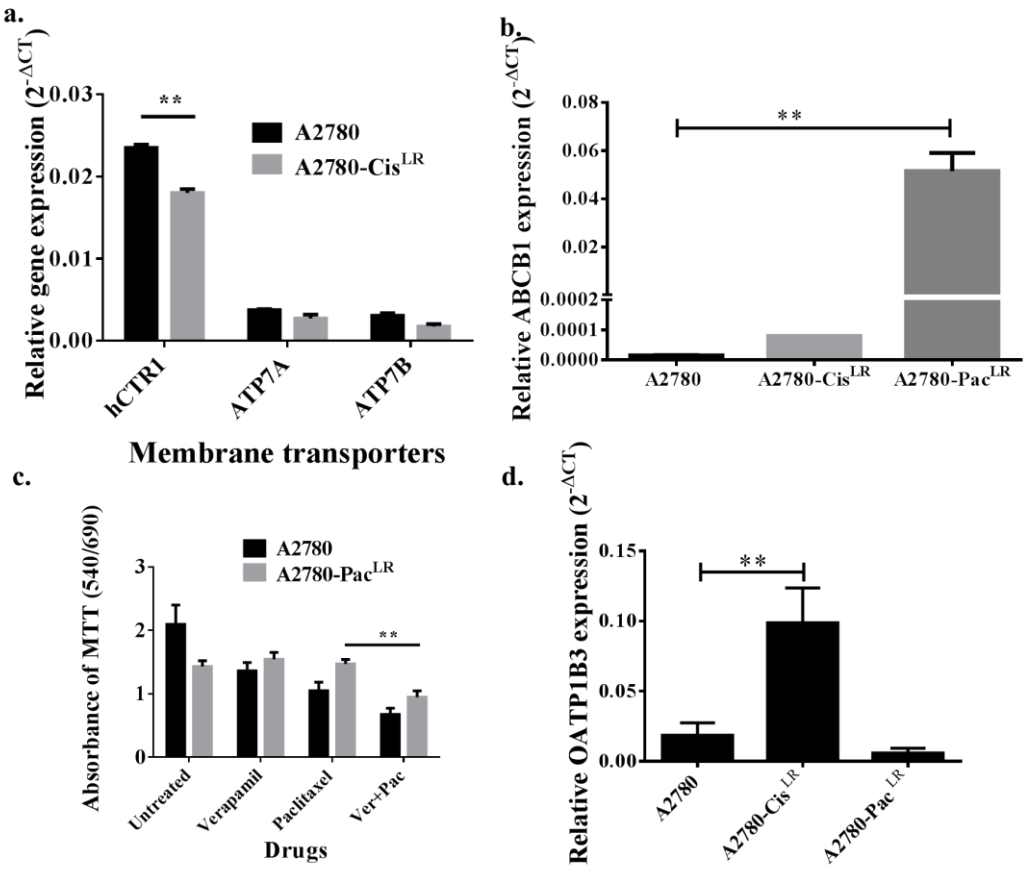

Figure 3.8: Expression of membrane transporters in resistant cells. *a)Real time PCR analysis of membrane transporter genes: Significant (**p<0.05) decrease in hCTR1(influx) gene expression is observed in the cisplatin resistant cells with no change in ATP 7A and ATP7B (efflux)expression as compared to A2780 cells; b)Paclitaxel resistant cells demonstrated a significant (**p<0.001)increase in the ABCB1 expression as validated by real time PCR analysis ;c) MTT assay showed that verapamil (2ug/ml) and paclitaxel at IC_{50} concentration (80ng/ml) together can sensitize the paclitaxel resistant cells (***p<0.0003).d) Hypersensitivity of cisplatin resistant cells to paclitaxel is validated by the higher expression (**p<0.005) of influx transporter OATP1B3, specific for paclitaxel, however, paclitaxel resistant cells did not show any change in the expression.*

High ROS production, less DNA damage and lower uptake of cisplatin are the characteristics of cisplatin resistant cells:

Cisplatin is known to induce reactive oxygen species (ROS) generation and DNA damage in sensitive cells. Cisplatin induced DNA damage response is commonly examined by pγH2AX foci formation assay. We therefore examined the formation of foci in A2780 and A2780-Cis^{LR} cells in response to cisplatin treatment. The result showed an increase in the mean fluorescence intensity of γH2AX foci with 2 h and 24 h cisplatin treatments in A2780 cells, whereas the levels of p-γH2AX foci remained relatively constant in the A2780-Cis^{LR} cells. Intriguingly, we observed that the untreated A2780 cells exhibited higher γH2AX foci formation as compared to the A2780-Cis^{LR} cells (Figure 3.9 a and b).

We also compared the endogenous levels of ROS in sensitive and cisplatin resistant A2780 cells. A two-fold higher ROS generation was found in A2780- Cis^{LR} cells as measured by flow cytometry (Figure 3.9c).

In order to measure the total cisplatin uptake in the resistant cells we used inductively coupled plasmon mass spectrometry (ICPMS) analysis method. Both sensitive and resistant cell were treated with high concentration of cisplatin and the platinum content was measured. As expected Cisplatin resistant cells showed a significantly 4 fold low level of accumulation of platinum than the sensitive cells (Figure 3.9d).

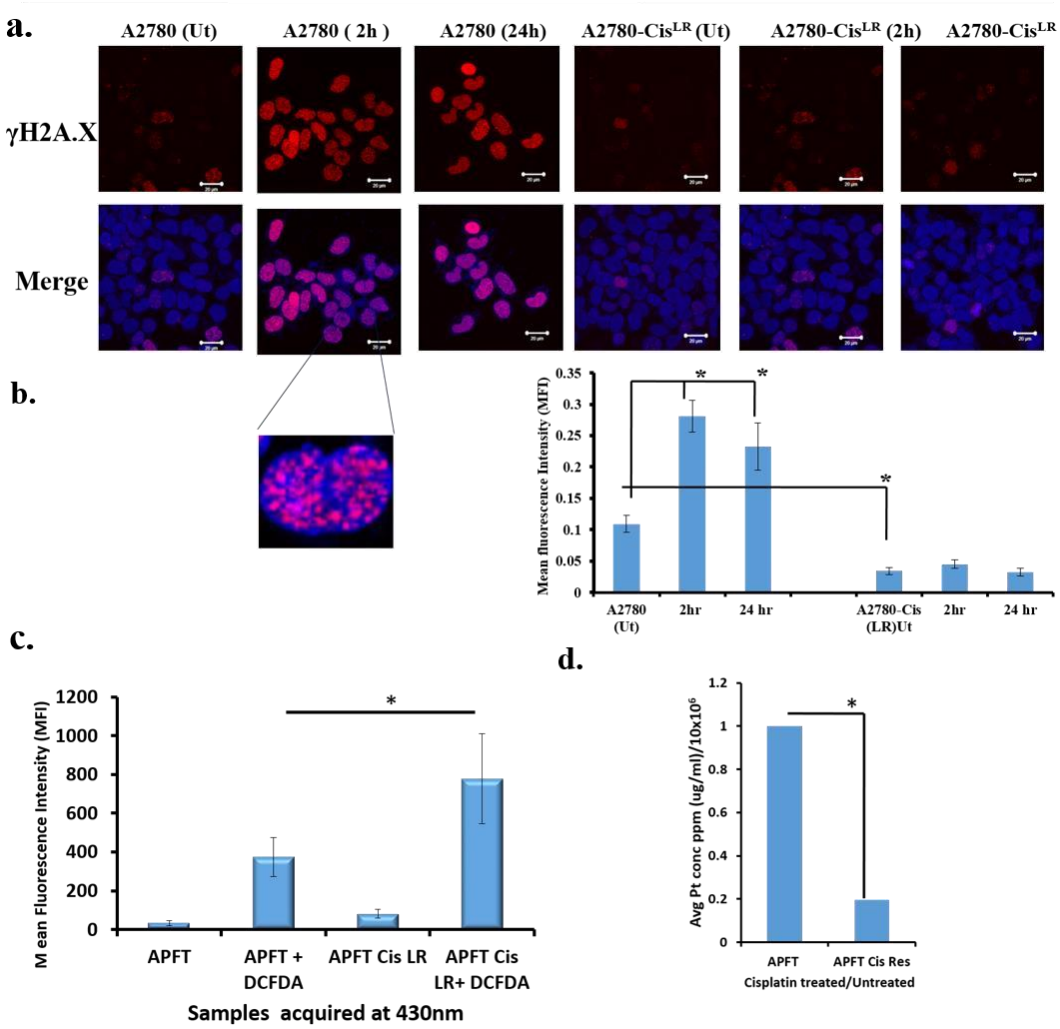

Figure 3.9. Monitoring DNA damage and ROS in cisplatin resistant cells. *a and b) A2780 and A2780-Cis^{LR} treated with cisplatin (10µg/ml) for 2h and 24h were stained with p-γH2Ax antibody and DAPI. Images were visualized and scored by LCM 510 software (Zeiss). A magnified image of foci formation in the nucleus is shown in the inset. The foci formation was significantly reduced (*p<0.0001) in the cisplatin resistant cells; c) ROS quantification*

by the DCFDA dye demonstrate that Cisplatin resistant cells have high ROS (2 fold) content as compared to sensitive cells; d) ICPMS analysis showed that as compared to the sensitive cells the uptake of cisplatin is (*4 fold) lower in Cisplatin resistant cells.*

Monitoring the modulation of PIK3CA promoter in the cisplatin and paclitaxel resistant cells: The main interest in developing and characterising the cisplatin and paclitaxel resistant cells was to understand the alterations in the PIK3CA promoter activity during resistance. As mentioned earlier both the resistant cells were developed from A2780 cells stably expressing the PIK3CA sensor. Thus the promoter activity was monitored with luciferase assay in presence and absence of drugs. It was observed that attenuation obtained in PIK3CA promoter activity upon drug treatment in sensitive cells was abolished across both the resistant models. Surprisingly, the early paclitaxel resistant cells showed an increase 2 folds in the PIK3CA promoter activity (Figure 3.10).

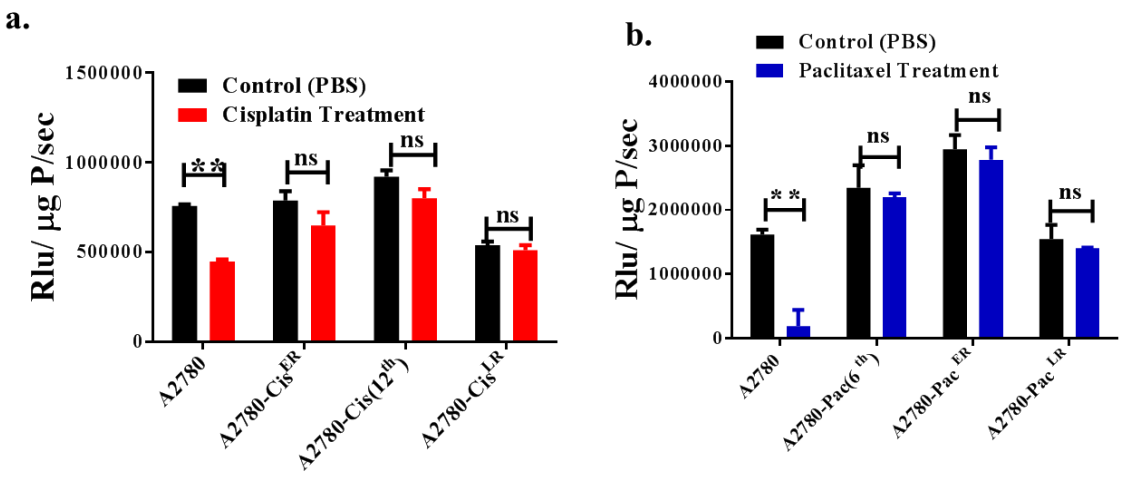

Figure 3.10. Modulation of the PIK3CA promoter in the cisplatin and paclitaxel resistant cells. *a) The PIK3CA promoter activity measured by luciferase assay showed attenuation (* $p<0.05$) upon cisplatin treatment, however such attenuation was abolished in the increasing stages of cisplatin resistance. There was no attenuation in the A2780Cis^{LR} cells;*

b) similar observations were also made with paclitaxel resistant A2780 cells. Early stages of paclitaxel resistance showed an increase of 2 fold in the promoter activity.

Discussion

The cornerstone of chemotherapy of ovarian cancer is combination of platinum and paclitaxel, however, disease recurrence due to chemoresistance is the common phenomenon which is difficult to mitigate. Mechanism underlying the development of resistance to platinating agents like cisplatin and taxanes like paclitaxel have been well characterized. Altered gene expression affecting cellular transport, DNA repair, reduction in apoptosis, altered expression or mutations in the drug target are some of the reasons for either acquired or intrinsic chemoresistance. In this study, we have developed a set of isogenic ovarian cancer cell lines resistant to either cisplatin or paclitaxel in order to delineate the underlying molecular mechanisms responsible for chemoresistance. The A2780 ovarian cancer cells are derived from a chemo-naïve patient and are thus sensitive to many chemotherapeutics. However, an acquired resistance can be developed *in vitro*. Establishment of isogenic cell line eliminates the variability occurring due to intrinsic genetic differences in cell lines and help to understand the common and differential mechanisms involved in development of resistance against different therapeutic molecules. Although numerous studies have investigated the mechanism of drug resistance to individual chemotherapeutics, the use of isogenic cell line is not so popular and comparison usually occurs between different cellular matrices [131]. During the selection of drug resistance, the gradual increase in the drug concentration generated a population of resistant cells and in turn avoided selection of few drug resistant clones. Although this strategy may not seem to reflect the typical clinical approach, the gradual increasing concentration of the drug might select for a population of

drug resistant cells representative of the cellular heterogeneity present in the tumors. Using this selection method, the A2780 cisplatin and paclitaxel resistant cell lines were developed.

Firstly, the IC_{50} concentration of the both the drugs in the A2780 cells were deduced and this was further used to monitor the development of resistance by MTT assay. Increasing resistance for both the drugs showed increase in cellular viability at IC_{50} concentrations of the drugs (Figure 3.3). Steady increase in the RI values of early and late resistant cells of both cisplatin and paclitaxel models suggest gradual acquirement of resistance. The RI for A2780-Cis^{ER} to A2780-Cis^{LR} cells increased form 3fold - 7.5/10 fold. Similarly, in paclitaxel model A2780-Pac^{ER} and A2780-Pac^{LR} cells demonstrated 2.5 and 5 fold increase in RI values, respectively.

Cross resistance to completely different drugs or completely different compound in cell lines selected for resistance to a specific drug is a recognised phenomenon [291, 292]. Strodal et al., 2007, suggests that when acquired cisplatin resistance was produced in various cell lines, 17% were also found to be resistant to paclitaxel. 41% of cisplatin drug resistant models reported till today were not resistant to paclitaxel and 28% of these cellular models became hypersensitive to paclitaxel [278]. Hypersensitivity occurs when a resistant cell line is more sensitive to a drug than the parental cell line it was derived from [278, 293]. Another recent study by the same group showed that IGROV, an ovarian cancer cell line when modelled to be cisplatin resistance (IGROV-Cis) was found to be paclitaxel resistant and these IGROV-Cis cells developed depicted the resistance phenotype of relapsed ovarian cancer patients after first-line platinum/taxane chemotherapy [294]. Similarly, in our study, A2780-Pac^{LR} showed cross resistance to cisplatin. Interestingly, the A2780-Cis^{LR} cell line showed a trend towards hypersensitivity towards paclitaxel. Hypersensitivity of A2780-Cis^{LR} cells corroborates with the findings by Strodal et al., in which hypersensitivity was observed in

30% of models of acquired drug resistance [278, 293]. Similarly, a study by Rahman et al., elucidated hypersensitivity of cisplatin resistant ovarian cancer cell line (KFr13) to paclitaxel by 40% in comparison to the parental KF28 cells [295]. A major reason for cells being resistant to cisplatin but hyper-sensitive to paclitaxel could be due to attenuated expression of efflux transporters like MDR genes (MDR 1, MRP 1) or upregulated expression of influx proteins (OATP1B3 etc), specific to paclitaxel transport that can lead to altered intake and sequestration [296]. In contrary lack of resistance towards cisplatin in A2780-Pac^{LR} suggests that the resistant characteristic developed is exclusive to paclitaxel and other drugs do not perturb this acquired resistance.

Both the cisplatin and paclitaxel resistant lines showed a reduced rate of proliferation (Cis^{LR}: 33.44 ± 1.35h & Pac^{LR}: 37.55 ± 1.86h) compared to the A2780 parental line (Figure 3.5). Reports of reduced cell proliferation associated with increased drug resistance and an association between multi-drug resistances with decreased proliferation exists, which supports our observation of decreased proliferation in resistant cell lines [297-299].

Clonogenic potential of A2780 cells along with its cisplatin and paclitaxel resistant variants upon treatment with increasing concentration of drugs was used to monitor resistance. Higher colony formation or the survival fractions of resistant cells at increased concentration of drugs indicates that they can sustain and initiate cell growth even at high drug concentration. Although there were subtle differences in G2/M phase between the resistant cells as compared to the A2780 cells, both the resistant variants had a significant increase in G0/G1 phase compared with their parent cells. Thus, it can be guessed that the alteration of cell cycle arrest in G0/G1 phase is important to the development of drug resistance. Studies indicate whole chromosome aneuploidy is important contributor to genetic variability in human diseases, as well as to the acquisition of resistance to chemotherapeutic

agents by tumor cells [300, 301]. We observed that the both cisplatin and paclitaxel resistant cells are aneuploids. Aneuploids seem to be either quiescent or less proliferative, and the capacity to proliferate in drug refractory manner contribute to the drug resistance [302].

Membrane transporters play an important role in cellular uptake of various drugs. Many membrane transporters and their aberrant expression are involved in the drug resistance [101, 165, 287, 288]. Low expression of hCTR1, influx membrane transporter, is associated with cisplatin resistance [287] In our study, we found significant low expression of hCTR1 in the cisplatin resistant cells without any change in ATP7A and ATP7B efflux transporters. This suggests involvement of other membrane transporters and/or different mechanism of resistance in cisplatin resistance. Similarly, in paclitaxel resistant cells high expression of ABCB1 transporter was observed which is already known to be associated with paclitaxel resistance [78].

Both cisplatin and paclitaxel are known to induce production of reactive oxygen species (ROS) [303, 304]. Cancer cells exhibit greater ROS stress than normal cells do, partly due to oncogenic stimulation, increased metabolic activity and mitochondrial malfunction. ROS is a double-edged sword. On one hand, at low levels, ROS facilitates cancer cell survival since cell-cycle progression driven by growth factors and receptor tyrosine kinases (RTK) require ROS for activation and chronic inflammation, a major mediator of cancer, is regulated by ROS. On the other hand, a high level of ROS can suppress tumor growth through the sustained activation of cell-cycle inhibitor [305]. Studies have shown that cisplatin resistant tumors and cells have high levels of ROS and show increased secretion of the antioxidant thioredoxin-1 (TRX1) [306]. We also have found similar trend in ROS generation in our model. After entering the cancer cell, the distribution of platinum compounds between the cytoplasm and the nucleus could affect their anti-cancer potential. In our study, the influx pump in cisplatin resistant cells showed decreased ($p=0.06$)

expression, although not significant. The total platinum content measured in cisplatin resistant cells suggests that the cisplatin uptake is lowered .This could be probably due to downregulation of influx pump or upregulation of efflux membrane transporters. However, to explain this phenomenon a detail examination of the other membrane transporters is required.

The main aim of the development of cisplatin and paclitaxel resistant model was to monitor the changes occurring at the PIK3CA promoter level. Intriguingly, we found that the Cisplatin/paclitaxel induced attenuation in PIK3CA promoter activity observed in A2780 cells was abolished in both these A2780-Cis^{LR} and A2780-Pac^{LR} cells. However, unlike cisplatin resistant cells the early paclitaxel resistant cells showed a two-fold increase in PIK3CA promoter activity which later decreased at late stages of resistance. Since pharmacokinetics of distribution of therapeutic molecules is an important criteria for ultimate action of drugs on tumor sites, monitoring the modulation of the PIK3CA promoter in the drug resistant tumor xenografts will be the next step for our study.

Chapter 4

Non-invasive optical imaging of the dynamics of in-vivo chemo-resistant models of ovarian cancer cells expressing PIK3CA sensor

Introduction

Conventional *in vitro* cancer models offer appealing advantage of high reproducibility and responsiveness to drugs. However, this two dimensional model has limitation of portraying the three dimensional *in vivo* cellular environment and therefore does not reflect the true response that occurs in physiological condition [307]. Tumor xenografts of human cancer cell lines overcome this limitation and act as a preclinical models that are relevantly close to replicate the histology, biochemical pathways and metastasis pattern of the same human tumor type [307, 308]. A tumor is a three dimensional (3D) structure comprising several cell types, which secretes extracellular matrix (ECM) and contains vascularisation. An *in vivo* human xenograft model is a 3D entity featuring phenotypic and ECM similarity and mimics the vulnerability of drug penetration in tumor [309]. Such preclinical human xenograft models are used to extrapolate the outcomes of any potential therapeutics and allow the clinical predictability. Thus human xenografts model can also serve as pre-clinical models to predict factors that attributes for the development of acquired chemoresistance.

Standard first line chemotherapy for ovarian cancer patients is platinum-taxane based chemotherapy that shows high percentage of initial response to treatment but patients eventually develop resistance to these chemotherapeutics. The mechanism of acquired chemoresistance includes many genetic and epigenetic changes in the crucial genes of cancer cells that may induce cells to adapt to the apoptotic stresses of the drugs [64]. Human xenograft mouse models provide approach for determining genetic changes associated with acquired resistance to anticancer drugs. Many reports have summarized the phenotypes of mouse models for ovarian cancer that have been generated either induction through carcinogen, allografts of syngeneic ovarian epithelial tumor models or genetically engineered epithelial ovarian cancer models [310-312]. Carcinogens like 7,12-Dimethylbenz (a) anthracene (DMBA) and N-methyl-N'-nitrosourea are frequently used for

the development of tumor models. However, chemical carcinogens mediated neoplasms did not attribute to ovarian cancer etiology [310]. In syngeneic tumor models, mouse ovarian surface epithelial (MOSE) cells isolated from the ovaries of virgin wildtype mice are cultured repeatedly *in vitro* before transplantation into recipient mice. These MOSE cells can spontaneously transform with repeated passages and show tumorigenic capacity alongwith generation of ascitic fluid upon injection into athymic mice. The intact immune system of this model helps to understand the anti-tumor immune response and to study tumor microenvironment, epithelial-stromal cell interactions, tumor-secreting factors, immune cell infiltrations and vasculature. Although human and mouse tumors share similar features, the complexity of human disease coupled with the heterogeneity of cancer often prove difficult to translate the findings to clinic [313].

A more appropriate pre-clinical model to portray human disease biology is the genetically engineered mouse model (GEMMs). These are immuno-competent mice with genetic defects introduced using RNA interference, inducible gene expression, viruses, or DNA recombination techniques. GEMMs of ovarian epithelial mouse models provide efficient reproducibility and can be used to analyse the functional role of oncogenes or tumor suppressor genes [311]. These genetic modifications are often performed using inducible gene expression systems which provides the flexibility to turn on or off gene(s) for e.g. transgenic mice carrying both the tetracycline-regulated transcriptional transactivator and its respective binding site linked to a gene of interest. When mice are provided with tetracycline in their drinking water, gene expression is reversibly suppressed. Several genes (TP53, C-MYC, K-RAS, AKT, and BRCA1 and BRCA2) known to be associated with various EOC subtypes have been used to develop ovarian cancer specific GEMM models. Orsulic et al., 2002, crossbred mice expressing the avian retroviral receptor (TVA) selectively on the surface ovarian cells (OSE) with transgenic mice which are genotypically

Trp53+/+ or *Trp53*−/−. Exposing the cells to replication competent avian leukosis viral-derived vectors expressing c-*Myc*, *Kras*, or AKT or other combinations, resulted in transformation of the OSE. Tumor formation from OSE was observed by Flesken-Nikitin et al., 2003, in concurrent inactivation of p53 and Rb1 by skilfully injecting an adenoviral vector expressing cytomegalovirus (CMV)-Cre recombinase under the ovarian bursal sac of mice expressing conditional floxed-P alleles of *Trp53*, *Rb*, or both [314]. Dinulescu et al., 2005, generated mice that have a transcriptionally silent oncogenic allele of *K-ras* (*LSL-K-rasG*^{12}*D*$^{/+}$) which can be conditionally expressed through administration of an adenovirus containing Cre. When the *LSL-K-rasG*^{12}*D*$^{/+}$ mice were crossed with *PTEN*$^{loxP/loxP}$ mice, they developed invasive primary ovarian endometrioid adenocarcinomas (OEA), a subtype of EOC, suggesting that phosphate and tensin homologue deletion on chromosome 10 (PTEN) plays a role in tumorigenesis when combined with other oncogenes [315]. To drive site specific overexpression of transgenes, keratin 5 promoter, β-actin promoter, Mullerian inhibitory substance type 2 receptor promoter (MISIIR), ovarian specific promoter1 (OSP-1) and mouse oviduct glycoprotein (OGP) promoter were utilized. However, some of these promoters show leakiness. For example, transcription from the OSP-1 promoter occurs predominantly in ovary, but permits their tumorigenic conversion by SV40-TAg. Thus to understand the complexity of OC, a mouse model representing each subtype is required [310, 311, 313]. However, developments of these models are quite tedious and require specialised expertise. The most common and convenient mouse model to study ovarian cancer biology is developed by transplantation of human ovarian tumor cells either under the skin (subcutaneous), or in the abdominal cavity (intraperitoneal), or in the organ of origin i.e., ovary (orthotopic) in an immune-compromised host. Intraperitoneal and orthotopic injections can mimic metastatic dissemination whereas, subcutaneously injected cells allows tumor formation at the site of injection. These xenograft models help to study tumorigenesis

and effect of drugs in real time. Earlier efficacy measurement was relied on tumor volume and histological analysis, lacked longitudinal kinetics and required a large number of mice. Implementation of non-invasive molecular imaging nowadays overcomes these drawbacks and monitor tumor response in real-time following systemic targeted therapy.

Ideally, *in vivo* development of acquired chemoresistance to anticancer drugs in immunocompromised mice is achieved by implantation of cancerous cells and administration of chemotherapeutics at the maximum tolerated dose (MTD). Such technique was used in the study by Yoshida et al., 2009, in which changes in gene expression related to chemoresistance during chemotherapy was studied in an acquired chemoresistant xenograft model established using SCID mice with human esophageal cancer cells. This model system elucidated the mechanism of resistance during chemotherapy without immune influence [316]. Previous report by Masazza et al., 1991 described the development of unique intraperitoneal xenograft model in nude mice obtained from an ovarian cancer patient. It was a representative of patient's tumor progression, malignant behaviour and drug response [317]. In this study, three tumor cell lines were obtained from a single ovarian cancer patient during the course of therapy and disease progression. Of the three tumor lines, one cell line was derived from pleural effusion of chemo-naive patient, second cell line was derived after chemotherapy and the third cell line was derived after relapse in abdominal cavity. These three tumor variants when xenografted and studied in nude mice reflected the varying drug response and mimicked the clinical development of drug resistance [317].

Drug resistant tumor lines can be developed *in vitro* by continuous or intermittent exposure to a single or dual drug and implanted in mouse to understand their resistant characteristics and influence on therapy [37, 279]. Several studies have used A2780 ovarian cancer cell line and its resistant variants to study the mechanism underlying chemoresistance [318-321]. In our study, we have used A2780 cell line stably expressing the PIK3CA sensor to establish

a cisplatin and paclitaxel resistance by following a pulse method to develop acquired resistance. As described in chapter 3, the observed attenuation in PIK3CA promoter activity in response to drugs was abolished in the late cisplatin and paclitaxel resistant cells. In order to study this promoter alteration *in vivo*, where pharmaco-distribution of cisplatin and tumor development might influence the drug resistant conditions, we implanted A2780 Cis^{LR} cells in nude mice and monitored the promoter activity upon drug treatment by non-invasive bioluminescence imaging. We also intended to observe the PIK3CA promoter modulation in A2780-Pac^{LR} tumor xenografts upon paclitaxel treatment but due to unavailability of mice the experiments were not conducted.

Material and Methods

Cell line and culture from tumors:

The A2780-Cis^{LR} cells as mentioned in chapter 3, were frequently maintained under selection of cisplatin at the IC_{50} concentration but removed from selection for at least two passages prior to any experimental use. For explants culture, tumors were minced thoroughly and cultured in appropriate media.

MTT assay:

The percentage viability of cells cultured from the tumor was determined using MTT assay at IC_{50} concentration (500ng/ml) of cisplatin. The absorbance was recorded using SPECTRA MAX190 at 560 and 670 nm. The percent viability of cells was calculated as follows:

(A560nm – A670nm) sample / (A560nm – A670nm) control *100.

Bioluminescence imaging in living mice:

A2780-Cis^{LR} cells stably expressing the PIK3CA-*fluc2-tdt* ($6x10^6$) were implanted in nude mice. In this study, IVIS Spectrum optical imaging system was used. Mice bearing tumor

xenografts were segregated into two groups, control and test group. An intraperitoneal cisplatin (8mg/kg) treatment was given to the test group and the control group was treated with DMSO. BLI was performed by intraperitoneal administration of D-Luciferin (3mg/mouse) for 1minute. ROIs were drawn over the tumors of control and cisplatin treated mice and quantified by using the Live Image (4.4) software. Bioluminescence signal was recorded as maximum p/sec/cm^2/sr. A detailed procedure for bioluminescence is given in the section 8.18.

Results

Non-invasive optical imaging of the development of an *in vivo* cisplatin resistant model:

To compare the tumorigenic potential of the A2780-Cis^{LR} cells with the parental cells, six million cells for both group were subcutaneously implanted in nude mice and tumor growth was measured over time. Palpable tumor appeared within 10 days of implantation for the A2780 cells (n=4) which increased vigorously over time and had to be sacrificed in next three weeks because of heavy tumor burden (Figure 4.1a). In contrast, the A2780-Cis ^{LR} (n=4) tumor xenografts were developed with a delay of almost 20 days (Figure 4.1b). In corroboration to the observed slower proliferating capacity of these resistant cells, no tumor growth was observed for initial 3-4 weeks and palpable tumors were observed only after 28 days. BLI was performed repeatedly for three weeks and signals were rapidly increased over time as shown in the figure 4.1c. The representative images of BLI performed on the same mice are shown in the figure 4.1d.

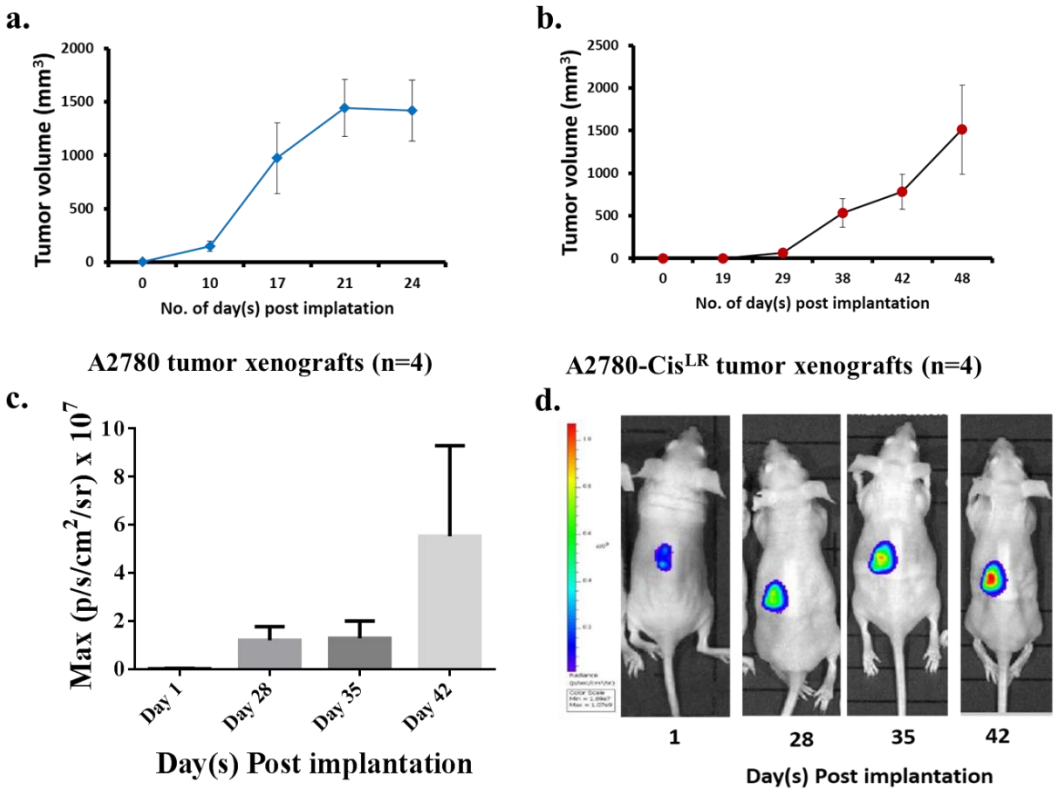

Figure 4.1 Bioluminescence imaging of the development of cisplatin resistant tumor xenografts. *a) Graphical representation of tumor volume (mm^3) of A2780 tumor xenografts grown from day 10 after implantation over time. b) Graphical representation of tumor volume of A2780-Cis^{LR} tumor xenografts grown at 29th day after implantation over time. Comparison between the two growth curves demonstrates that the cisplatin resistant tumor formation showed a delay of almost 20 day; c) Graphical representation of PIK3CA promoter driven bioluminescence signals over time showing an increase in promoter activity in A2780-Cis^{LR} tumor xenografts (n=4); d) Representative images of the BLI taken from the same mouse over time.*

Culture established from A2780-Cis^{LR} cells maintains resistant property: Drug resistant cells often exhibit reversal of their resistant phenotype especially when they remain without the selection pressure for long time. To check and negate the possibility of reversal of resistance in the A2780-Cis^{LR} cells, we established explant culture directly from the

tumor xenografts. Since these cells were stably expressing the PIK3CA-fluc2-tdt reporter, they were easily segregated from the mouse stromal cells by fluorescence imaging. In fact only the fluorescent cells were able to proliferate in culture. These cells proliferated were further assessed for cellular cytotoxicity to cisplatin. MTT assay at the IC_{50} concentration of cisplatin for A2780 cells (500ng/ml) showed 80% cellular viability indicating a highly resistant phenotype. Further, at previously determined IC_{50} concentration of A2780-Cis^{LR} cells i.e., 5µg/ml also showed approximately 60% cellular viability for this explant culture. This implies that the resistant characteristics of these cells were retained even after growing them *in vivo)* (Figure 4.2).

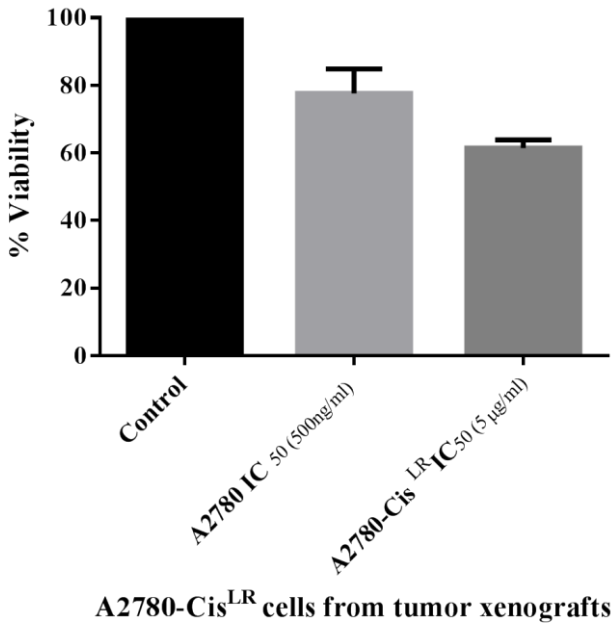

Figure 4.2. A2780-Cis^{LR} cell obtained from tumor retains resistant characteristics.

Cells obtained from explant culture of resistant tumors showed approximately 80% and 60% cellular viability when treated with 500ng/ml (IC_{50} concentration of A2780) and 5µg/ml (IC_{50} concentration of A2780-Cis^{LR}) of cisplatin for 72h as assessed by MTT assay.

Monitoring the modulation of PIK3CA promoter activity in cisplatin resistant tumor xenografts by non-invasive optical imaging

In our earlier chapter, we have measured the repressive effect of Cisplatin on PIK3CA promoter activity in A2780 tumor xenografts by non-invasive imaging. We have also observed that this repressive effect was abolished as the cells gained resistance towards Cisplatin in culture. To understand the behaviour of these cells in vivo condition, modulation in PIK3CA promoter activity in the A2780-Cis^{LR} tumors was measured upon treatment with cisplatin (8 mg/kg) using bioluminescence imaging. The treatment was given in two doses as described earlier. Bioluminescence signals of these A2780-Cis^{LR} tumor xenografts (n=3) did not decrease after first treatment rather increased ($3.72x10^8 \pm 2x10^8$ p/sec/cm^2 to $1.2x10^9 \pm 4.31x10^8$ p/sec/cm^2) and remained constant even after the second dose of cisplatin ($3.36x10^9 \pm 1.26x10^9$ p/sec/cm^2) (Figure 3b). The control mice (n=3) showed increased bioluminescence and tumor growth ($2.46x10^8 \pm 4.8x10^7$ p/sec/cm^2 to $9.9x10^8 \pm 2.78x10^8$ p/sec/cm^2 to $5.6x10^9 \pm 1.03x10^9$ p/sec/cm^2) over time (Figure 3b). Representative bioluminescent images of the mice bearing A2780-Cis^{LR} tumors are given in the Figure 3a. Tumor volume of the treated A2780-Cis^{LR} tumors remained stable whereas the untreated tumor xenografts exhibited gradual increase (Figure 3c).

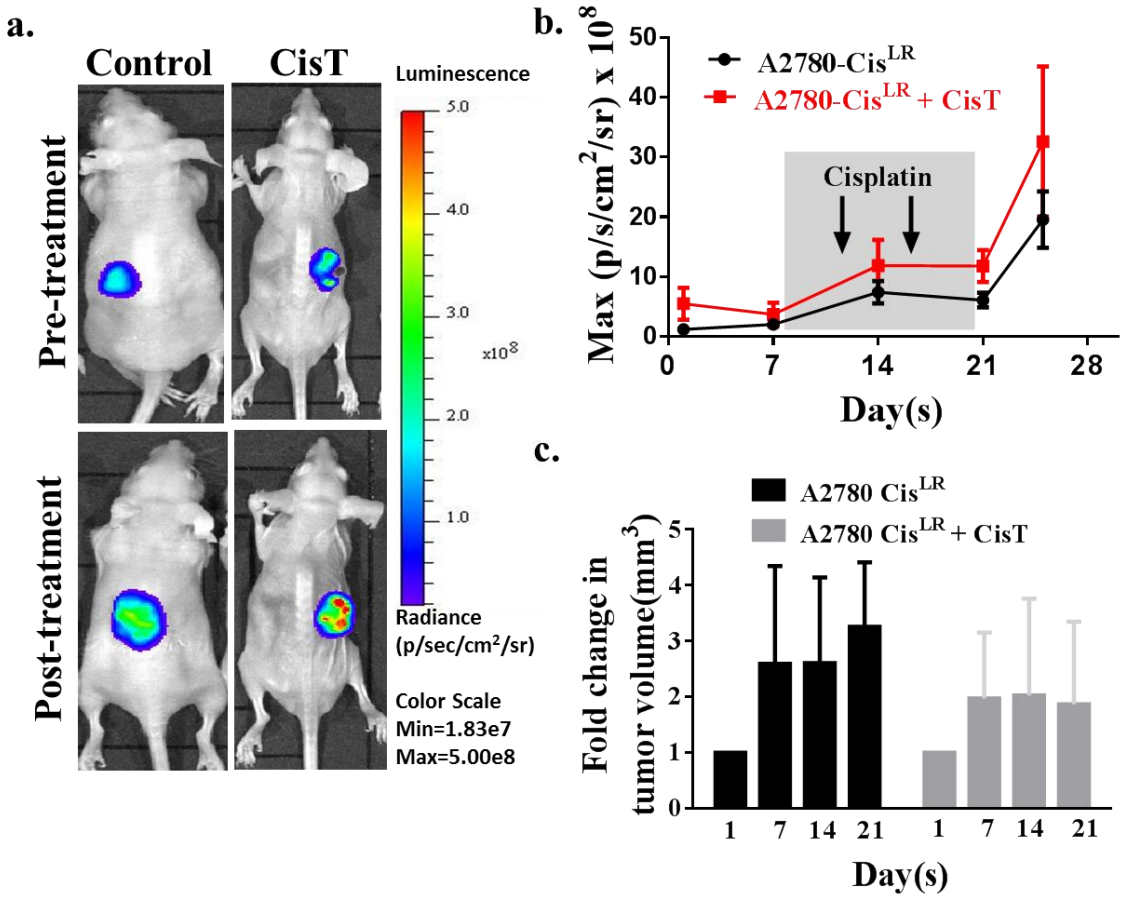

Figure 4.3. Non-invasive imaging of A2780-Cis^{LR} tumor xenografts demonstrated resistant property after cisplatin treatment. *a) Representative bioluminescent images of A2780-Cis^{LR} tumor xenografts bearing mice before and after treatment did not exhibit attenuated luciferase activity after two treatments of cisplatin (post-treatment). The control group was injected with normal saline and exhibited increased luciferase activity.*

b) Graphical representation of the bioluminescent signals of pre and post-treated A2780Cis^{LR} tumor xenografts showed increased luminescence with time after two rounds of cisplatin treatment in both control (n=3) and treated mice (n=3). Shaded area with arrow displays the day/s of cisplatin treatment. c) Measurement of fold change in tumor volume (mm3) of cisplatin treated mice showed steady increase in tumor growth of both control mice, treated mice showed stationary tumor growth.

Discussion

Xenograft models are particularly useful for evaluating tumorigenesis in real-time manner. As discussed in previous chapter, the drug resistant cell lines developed by exposing the cells with increasing intermittent exposure to drug is closely relevant to clinical scenario. Development of tumor xenografts from these drug resistant cells in immunocompromised mice facilitates to translate the *in vitro* systemic targeted therapeutic study to *in vivo.* These models, thus become accessible to study the mechanisms underlying drug resistance. In our study, we have used cisplatin resistant tumor xenografts to study the modulation of the PIK3CA promoter in response to cisplatin. The resistant cells were used to develop tumor xenografts and the growth of tumor was non-invasively monitored by repeated bioluminescence imaging. Initially for a period of 28-30 days there was no palpable tumor observed, however, after tumor formation, rapid increase in tumor growth was observed. Thus A2780-Cis^{LR} tumor xenografts showed a delayed kinetics as compared to A2780 tumor xenografts. The delayed kinetics of tumor formation can be corroborated with the *in vitro* studies (as described in Chapter 3), where cisplatin resistant cells demonstrated slower proliferation rate and high doubling time. Since most of the drugs demonstrate cytotoxicity by targeting the proliferating cells, slow proliferation or quiescence possibly could be one way to acquire the resistant phenotype.

It is always a question of debate whether and how long the resistant cells can retain their resistant property. The possibility of loss of resistant phenotype by cisplatin resistant cells could be negated by *in vitro* culture of tumor xenografts and assessing the cytotoxicity of cisplatin. The resistant characteristic was monitored by the cisplatin treatment to the explant cultured cells which demonstrated 80% viability. Our results thus indicate that the method by which the resistant cells were developed is substantial and the cells retain the resistant

property even under *in vivo* conditions simulating the phenotype of acquired chemoresistance.

Our early *in vivo* BLI results, suggests that the A2780 tumor xenografts showed attenuation in PIK3CA promoter activity upon cisplatin treatment. Also, in our *in vitro* studies, this attenuation was abolished in the resistant cells after cisplatin treatment. By non-invasive imaging, we demonstrated that the cisplatin resistant tumors could effectively retain their resistant phenotype without any selection. Corroborating with *in vitro* results, *in vivo* models did not exhibit attenuation in PIK3CA promoter driven luciferase signal or tumor regression after cisplatin treatment.

The mechanisms underlying drug resistance are attributed to efficient DNA repair, alterations in membrane transporters and changes in the expression of signaling pathways pertaining to apoptosis and cell growth. In the next chapter, we sought to investigate molecular alterations in some candidate proteins associated with PI3K signaling axis during the maintenance of chemoresistance.

Chapter 5

Molecular Characterization of the chemo-resistant models by monitoring alterations in the PI3K-AKT signaling, NF-κB pathway and antiapoptotic genes

Introduction

Chemotherapy is the principal mode of treatment for ovarian cancer and the efficacy of the chemotherapy is limited by the development of drug resistance. The underpinning mechanisms of resistance to conventional chemoresistance are attributed to alterations in drug targets, activation of pro-survival pathways and ineffective induction of cell death. As described in introductory chapter, apparent drug resistance is broadly due to the pharmacokinetics, processes that are involved in the distribution and metabolism in the cancer cells. Along with pharmacokinetics, defects in common signaling and effector pathway downstream of drug-target interactions are the probable causes of maintenance of resistance in clinical practice. They include insufficient DNA binding, increased detoxification, enhanced DNA repair, deregulated expression of transporters, altered expression and activation of genes involved in cell survival pathways, such as p53, AKT/mTOR, Bcl-2, and NF-κB, etc.

It is established that PI3K/AKT is an essential signaling pathway that intervenes plethora of cellular processes, including cell proliferation, metabolism, survival and motility. Mechanisms leading to deregulation of the PI3K/AKT pathway in human cancers including ovarian cancer are diverse and include activating mutations, amplification of PIK3CA and AKT1/2/3, mutation in the p85 regulatory subunit of PI3K, loss of PTEN expression or function, Ras mutation and perturbation of integrin signaling. AKT is the key player of PI3K pathway, which on phosphorylation mediates many cellular functions leading to tumor progression. Immunohistochemical studies demonstrate that AKT activation is common in high-grade, late-stage serous ovarian carcinomas [322-324]. Moreover, recently, a multiplatform genomic analysis by The Cancer Genome Atlas (TCGA) Research Network

identified alterations in the PI3K/AKT and RAS pathways in approximately 45% of high-grade, serous ovarian tumors [7].

Increased activation, deregulation, and mutation of the components in the PI3K/AKT pathway have also been implicated conferring resistance to chemotherapy [142, 325]. Elevated levels of phosphorylated AKT can protect cells from undergoing apoptosis induced by chemotherapy and contributes to drug resistance [10]. The best-characterized substrate of AKT is the serine/ threonine kinase mTOR (mammalian target of rapamycin). It is known that activation of the AKT/mTOR pathway can increase cell survival and resistance to apoptosis [326]. Perturbation of this pathway by inhibitors can have significant therapeutic potential. Wortmannin, a fungal metabolite, is one of the known inhibitors of PI3K that binds the p110 catalytic subunit of PI3K noncompetitively and irreversibly inhibiting its enzymatic activity [327]. In many human cancers, wortmannin has shown to be a potent inducer of apoptosis [328, 329]. However, until recent Zhao et al., 2014, study, it was unclear whether the wortmannin could suppress growth, invasion and apoptosis in chemoresistant ovarian cancer. This study examined the *in vitro* effects of wortmannin on AKT phosphorylation, invasion and apoptotic effect of cisplatin. They had shown that wortmannin sensitises ovarian cancer cells to the apoptotic effect of cisplatin [330]. Rapamycin, is a bacterial drug that have immunosuppressant functions and leads to cell cycle arrest in the G1 phase by inhibiting the mammalian target of rapamycin complex 1 (mTORC1). mTORC1 controls protein translation and several cytokine-driven signaling pathways involved in cell cycle progression. Many studies have suggested that rapamycin is efficient in suppressing ovarian cancer cell growth and in combination with carboplatin it can antagonize the development of drug resistance [331-333]. In this study we first monitored the status AKT phosphorylation in the sensitive and isogenic chemoresistant

model for cisplatin and paclitaxel and studied the effects of wortmannin and rapamycin on their cellular viability.

Another important cell survival regulatory factor, often activated by the PI3K signaling pathway is NF-κB (nuclear factor kappa light chain enhancer of activated B cells). NF-κB activation facilitates cell death in sensitive OC cells, but has shown to switch to an antiapoptotic 'oncogenic' pathway in chemoresistant isogenic variants [11]. Studies in the last few years have unraveled that multiple mechanisms that enable NF-κB to sustain carcinogenesis and drug resistance [12-14]. As mentioned in the introductory chapter, a clinical correlation was observed between activation status of NF-κB and poor prognosis of EOC. Nuclear expression of NF-κB p65 correlates with the poor differentiation and late FIGO stage in EOC tumors. Also, the patients with positive NF-κB p65 subunit staining had lower cumulative survival rates than those were negative [13, 177, 178]. NF-κB pathway is also activated by the Toll-like receptor (TLR) family which plays a central role in initiation of innate immunity via MyD88 (myeloid differentiation factor 88) dependent or independent pathways [15-17]. TLR-4/MyD88 signaling is also found on epithelial ovarian cancer cells and presence of MyD88 but not TLR-4 significantly influences the drug response [89-92]. Studies revealed that EOC cells possess an active TLR-4 signaling and presence of MyD88 mediated NF-κB signaling may lead to intrinsic paclitaxel resistance and poor survival [18]. However, a significant percentage of EOC patients (~60%) were shown to be $MyD88^{negative}$, out of which around 40% cases exhibited disease recurrence [18]. The status and role of NF-κB in governing resistance and survival in MyD88 deficient EOC patients is still unclear and requires attention for devising new therapeutic interventions. In this study, we also tried to examine the response of cisplatin and paclitaxel on NF-κB activity in MyD88 negative chemoresistant A2780 cells. Next we used non-invasive imaging to monitor the modulation in NF-κB activity in real time from cisplatin resistant tumor xenografts. We further tried to

decipher the function of the downstream targets of active NF-κB pathway which could be critical in determining and maintenance of cisplatin resistance. This part of the study thus emphasize the molecular complexity observed in generation of cisplatin resistance in cellular and pre-clinical models.

Materials and methods

Cell line, transfections and drug treatments

A2780, A2780-Cis^{LR} and A2780-Pac^{LR} cells stably expressing PIK3CA promoter driving firefly luciferase were engineered for stable expression of the NF-κB sensor. The NF-κB sensor was constructed in our laboratory. It consists of a 160bp sequence of NF-κB response element (composed of four tandem copies of the NF-κB consensus binding sequence) followed by a minimal TA promoter which is cloned in a *hrluc*-eGFP bifusion background. All the transient and stable transfections with NF-κB sensor were carried out using Superfect transfection reagent (Qiagen, Valencia, CA) and stable cells were selected were using puromycin. For all the drug treatments, cells were incubated for 24h with cisplatin, paclitaxel, wortmannin and rapamycin diluted in DMSO. All transfection and drug treatment experiments were performed in triplicates and repeated at least twice.

Luciferase Reporter assay

Renilla and Firefly luciferase activities were measured using luciferase assay system (Promega) and coelenterazine in a Berthold luminometer as described in section 8.14.

MTT assays

Cell viability was assessed using the standard thiazolyl blue tetrazolium bromide (MTT) method and percent viability was counted using the formula ([Absorbance $^{(Test)}$ ÷Absorbance $^{(Control)}$] ×100).

Immunofluorescence

Immunofluorescence studies were performed as described in earlier chapters. Briefly, cells plated on coverslips were fixed with 4% paraformaldehyde, permeabilized with 0.025% Triton-X and probed with NF-κB antibody for overnight at 4^0 C. Next day, after two hours of incubation with secondary antibody, cells were counterstained with DAPI and images were observed under Carl Zeiss, LSM 710 microscope. At least five representative fields were studied for NF-κB and DAPI staining. The detailed protocol for the immunofluorescence is described in the section 8.16.

Preparation of nuclear and cytosolic proteins and western blotting

$1x10^8$cells were lysed with 400µl (five times the cells pellet volume) of Cytoplasmic Extract (CE) buffer [(10mM KCl, 0.1 mM EDTA, 10 mM HEPES and 0.3% NP-40 with proteinase inhibitor cocktail (Sigma)] at 4°C for 10 minutes. The lysate was centrifuged for 15 minutes at 2,000 rpm at 4°C and supernatants were collected as cytosolic extract. The resulting pellet was re-suspended in CE buffer and washed for 2-3 times for 15 minutes at same conditions. Further, the pellet was resuspended in 50µl of ice-cold 20mM HEPES (pH 7.9), 420mM NaCl, 20% (v/v) glycerol, 1mM EDTA and proteinase inhibitor cocktail. After 5 minutes incubation at 4°C, the lysate was centrifuged for 10 minutes at 14,000 rpm at 4°C, and the supernatant was collected as nuclear extract. The concentrations of cytosolic and nuclear extracts were determined using Bradford Reagent (Sigma). Western blot analysis was done as described in the section 815.

Semi-quantitative RT-PCR

2µg of total RNA extracted from cells using RNease kit (Qiagen, Netherland) was reverse transcribed using cDNA synthesis kit (Invitrogen, Carlsbad, CA). GAPDH was used as an internal control. Primer sequences used were as follows: GAPDH (forward TGCACCACCAACTGCTTAGC, reverse GGCATGGACTGTGGTCATGAG); XIAP

(forward GATGATGTGAGTTCTGATAGG and reverse CTTAATGTCCTTGAAACTGAAC). The RT coupled PCR reaction was used for the semiquantification of the mRNA expression.

Bioluminescence imaging of tumor xenografts

Animal care and euthanasia were performed with the approval from Institutional Animal Ethics Committee of ACTREC. A2780-Cis^{LR} ($6x10^6$) cells stably expressing the dual reporters: PIK3CA-*fluc2-tdt* and NF-κB-*hrluc-eGFP* were implanted in mice. Tumor formation and growth was monitored by repeated BLI by the IVIS Spectrum Optical Imaging system. A detailed description of *in vivo* BLI is given in the section 8.18. Mice bearing tumor xenografts were segregated into two groups, control and test group. An intraperitoneal cisplatin treatment was given to the test group. Whole body images of anaesthetized mice were obtained after 100µl intra-peritoneal injection of D-luciferin (3mg/mouse) or tail-vein injection of coelenterazine (50µg/mouse) diluted in phosphate buffered saline. Region of Interests (ROIs) were drawn over the tumors and quantified by using the Live Image (4.4) software. BLI of the same mouse was acquired in sequence (first NF-κB-renilla luciferase followed by firefly luciferase). Bioluminescence signals were recorded as maximum (photons/s/cm^2/sr).

Results

Chemoresistant cells show enhanced AKT phosphorylation and cisplatin resistant cells are sensitised by PI3K/AKT inhibitor, wortmannin: Constitutively active PI3K/AKT pathway show enhanced cell survival and drug resistance [10]. Phosphorylation of AKT denotes activation which in turn mediates activation of downstream effectors responsible for various cellular functions. When the phosphorylation status of AKT was verified in the cisplatin and

paclitaxel chemo-resistant models, both showed gradual activation of AKT with acquirement of resistance without any significant change in total AKT level. The activation of AKT seemed to occur at much earlier stages for cisplatin resistance than paclitaxel resistance (Figure 5.1a). It is important to find alternative therapeutics along with cisplatin or paclitaxel for the treatment of ovarian cancer. We monitored the response of wortmannin and rapamycin which are known inhibitors of PI3K/AKT/mTOR pathway on cisplatin and paclitaxel resistant cells. The cisplatin resistant cells were more sensitive (only 30%viability at IC_{50}) to Wortmannin (0.1μM) as compared to the control A2780 cells. However no effect was observed on the Paclitaxel resistant cells. Surprisingly, no effect was observed on cellular viability of resistant cells with the Rapamycin (0.1μM) treatment.

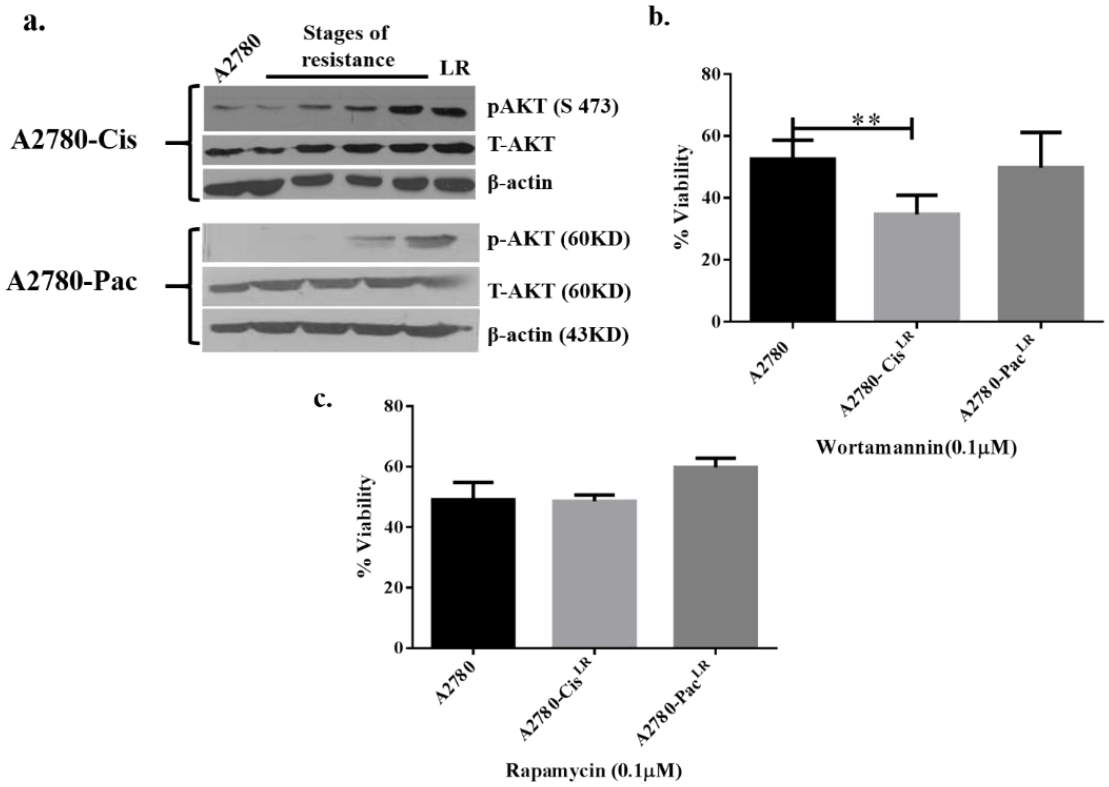

Figure 5.1: Enhanced AKT phosphorylation by the chemoresistant cells. ***a)*** *With the increase in the development of resistance, phosphorylated AKT levels increased in cisplatin resistant model (upper panel) and paclitaxel resistant model (lower panel);* ***b and c)*** *Wortmannin and rapamycin treatment of IC_{50} concentration on the sensitive A2780, A2780-*

*Cis^{LR} and A2780-Pac^{LR}.Wortmannin treatment sensitizes the cisplatin resistant cells (**p<0.005).*

Differential activation of NF-κB was associated with differential drug treatments: Cisplatin and paclitaxel have different mode of action but they converge to induce certain similar signaling pathways at their effector end i.e. induction of apoptosis. In order to understand the status of NF-κB activation by these drugs, A2780 cells were transiently transfected with NF-κB sensor and treated with various drugs and inducers. While 2 hours of TNF-α treatment induced 2.5 fold increase, cisplatin treatment resulted in significant (4 fold) decrease in NF-κB-renilla luciferase activity. No change in luciferase activity was observed after paclitaxel treatment (Figure 5.2a and b).

Since the transient expression of any reporter gene is often influenced by the heterogeneity of the experimental procedure, A2780 cell stably expressing the NF-κB sensor were generated wherein TNF-α showed increased (6-7 fold) NF-κB activity while LPS, a paclitaxel analogue did not induce NF-κB activation (Figure 5.2c). The stable A2780-NFκB sensor cells displayed no change in NF-κB reporter activity after paclitaxel treatment but significant attenuation was observed after cisplatin (Figure 5.2d). In corroboration with luciferase activity, changes in NF-κB expression in nuclear extracts were found after paclitaxel and cisplatin treatments by western blotting (Figure 5.2e). Nuclear localisation of NF-κB, a key event for NF-κB transcriptional action was differentially altered by various drug treatments. Minimal nuclear localisation of NF-κB was found after cisplatin treatment while enhanced localisation was observed after paclitaxel treatment. An overall increase in NF-κB expression was evident in paclitaxel treated cells (Figure 5.2f). Higher basal level of phosphorylated IκBα was observed in the cytoplasmic extracts of paclitaxel treated A2780 cell lysates which also corroborates with enhanced activation of NF-κB. However, the levels of pIκBα after cisplatin treatment did not show any change. Total levels of IκBα

did not differ among the lanes, suggesting that either of the drug had any effect on the degradation of IκBα. High levels of pIκBα and no change in the NF-κB activity upon paclitaxel treatment and reduction in pIκBα and NF-κB activity by cisplatin suggests that both the drugs effect NF-κB signaling differentially (Figure 5.2e).

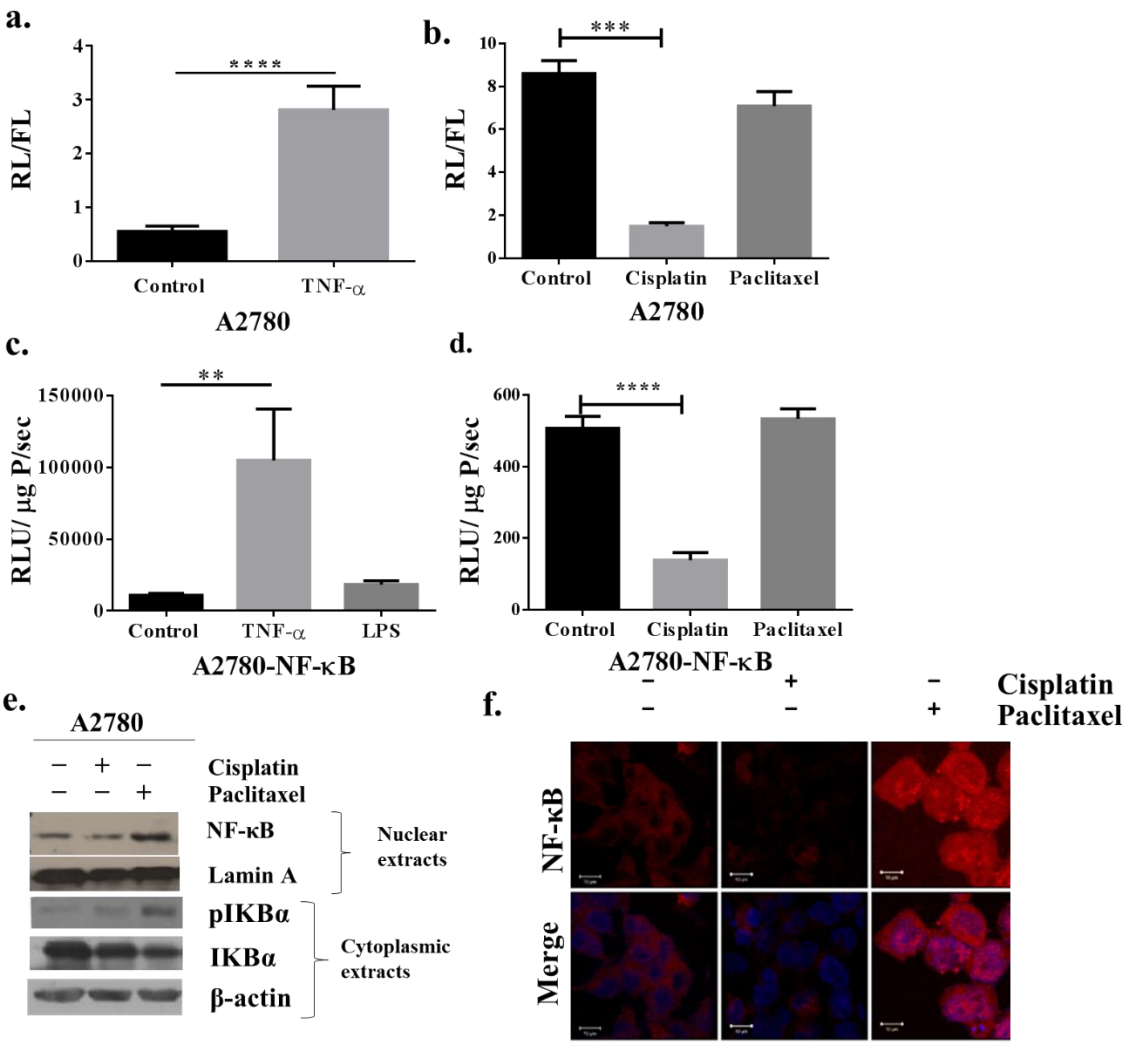

Figure 5.2. Different drug treatments show different pattern of NF-κB activation. *a and b) Transient transfection of NF-κB driven-renilla luciferase in A2780 cells followed by TNF-α treatment (20ng/ml for 2h) showed significant increase (****p<0.0001); Cisplatin (10µg/ml) showed decreased activity (***p<0.002) whereas no change was observed after paclitaxel(5µg/ml) for 24h; c and d) A2780 cells stably expressing NF-κB (A2780-NF-κB*

*cells) showed increased luciferase activity upon TNF-α (**p<0.01)treatment whereas decreased activity was observed with cisplatin treatment (****p<0.0001). No change was observed with Lipopolysaccharide (LPS) and paclitaxel treatment; e) Western blot analysis showed increased NF-κB levels in paclitaxel treated nuclear lysates but not after cisplatin treated A2780 cells. LaminA was used as loading control. High levels of pIKBαα upon paclitaxel treatment while reduction in pIKBαα by cisplatin was observed in the cytoplasmic extracts. The levels of IκBα did not change with treatments, β-actin was used as loading control; f) Immunofluorescence showed increased nuclear localisation of NFκB in A2780 cells after paclitaxel treatment, however, such localisation was absent in cisplatin treated cells. Upper panel showed the staining pattern of NF-κB and lower panel showed merged images with DAPI.*

Validation of MyD88 status in A2780 chemoresistant cells:

Though control A2780 cells are reported to be MyD88 deficient cells, the status is not known for chemoresistant cells [89, 92]. We therefore checked the expression of MyD88 in the cisplatin and paclitaxel resistant cells and observed that resistant cells too did not express MyD88 (Figure 5.3).

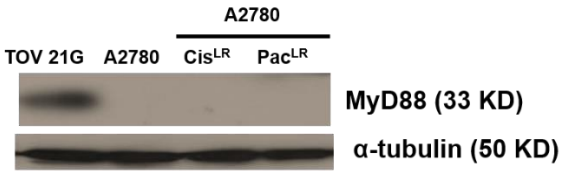

Figure 5.3. Determination of MyD88 status in isogenic chemoresistant A2780 cell. *Western blot analysis showed absence of MyD88 protein in A2780 and its resistant variants. TOV21G cells were used as positive control and α-tubulin as a loading control.*

Acquirement of cisplatin resistance augmented NF-κB activity: Absence of MyD88 expression is thought to associate with effective paclitaxel treatment and longer survival in epithelial ovarian cancer patients. However, a significant number of them exhibit disease recurrence [18]. Presence or absence of MyD88 regulates NF-κB is activation resulting in production of either cytokines or interferons. The two chemotherapeutics (cisplatin and paclitaxel) showed differential pattern of NF-κB activation in A2780 cells. NF-κB is also activated by AKT, which exhibited a gradual increase in phosphorylated state during acquirement of cisplatin and paclitaxel resistance in our models (Figure 5.1a). In order to understand the role of NF-κB in the response to drug in chemoresistant cells, we sought to monitor the changes in the NF-κB signaling by stably expressing the NF-κB sensor in these (A2780-Cis^{LR} and A2780-Pac^{LR}) cells (Figure 5.4a). Both A2780-Cis^{LR} and A2780-Pac^{LR} cells showed increased levels in the NF-κB protein in nuclear lysates (Figure 5.4b). Interestingly, the A2780-Cis^{LR} cells stably expressing the NF-κB sensor exhibited a significant increase in luciferase activity (~10 fold) (an indirect measure of NF-κB activity) after cisplatin treatment (Figure 5.4d).

Though NF-κB showed distinct nuclear localization in A2780-Cis^{LR} cells with or without cisplatin treatment (Figure 5.4f) There was no in NF-κB level after cisplatin treatment to the A2780-Cis^{LR} cells (Figure 5.4c). On contrary, A2780-Pac^{LR} cells demonstrated a significant decrease in NF-κB activity after paclitaxel treatment (Figure 5.4e). In contrast to the sensitive cells, where paclitaxel could induce nuclear localization, the A2780 Pac^{LR} cells did not exhibit nuclear localisation of NF-κB in pre and post treatment (Figure 5.4f). Western blot analysis showed decreased nuclear NF-κB after treatment (Figure 5.4c).

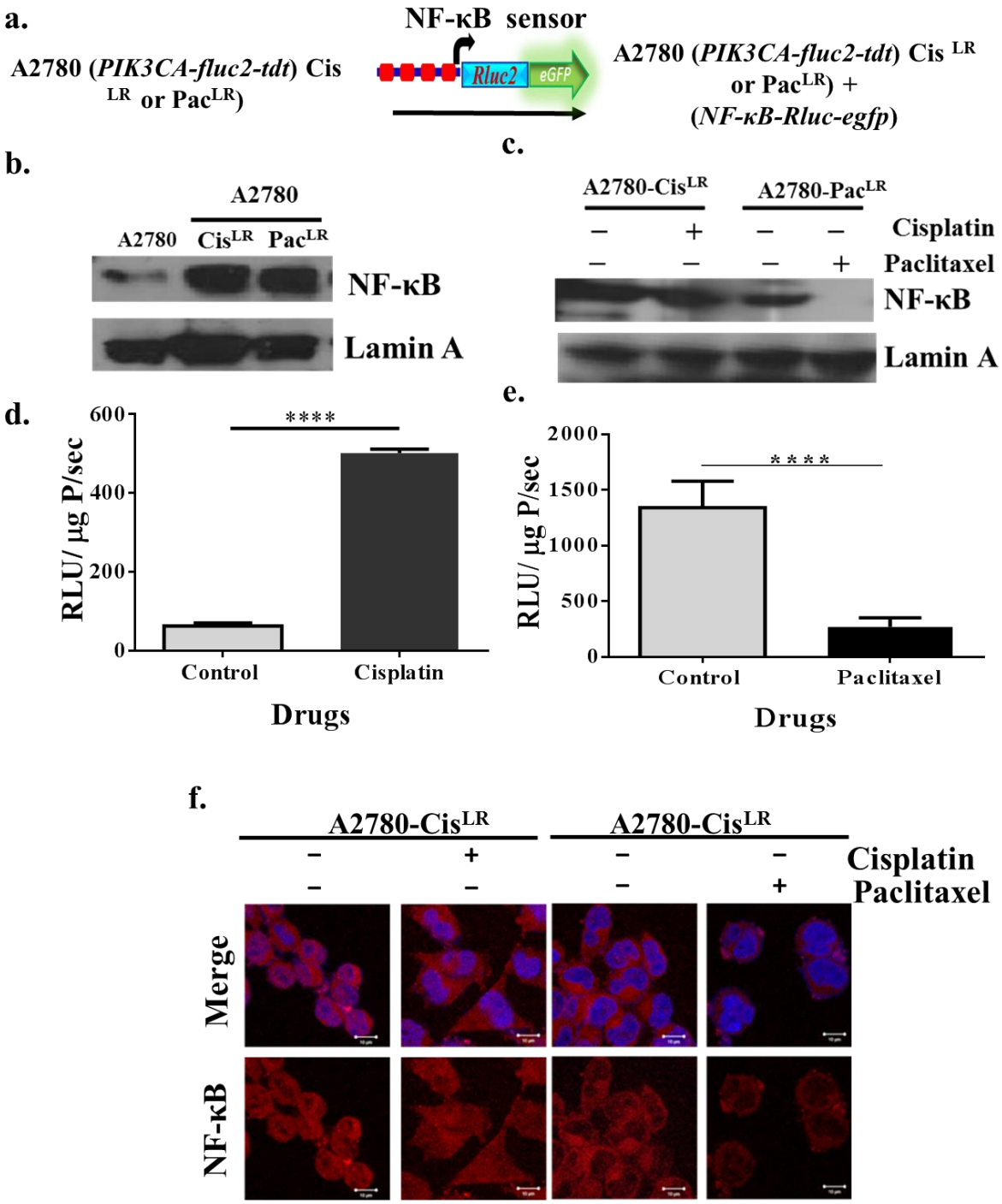

Figure 5.4. NF-κB activity was upregulated/enhanced in the cisplatin resistant cells. *a) Schematic representation for understanding the functioning of the dual reporter cells; b) Nuclear lysates from A2780, A2780-Cis^{LR} and A2780-Pac^{LR} showed augmented levels of*

*NF-κB in the resistant cells; c) Western blotting showed decreased NF-κB levels in nuclear cell lysates of drug treated of A2780-Pac^{LR}. However, no obvious change was observed after cisplatin treatment in A2780-Cis^{LR}. d and e) A2780-Cis^{LR} cells stably expressing NF-κB sensor showed significant increase (****p<0.0001) in luciferase activity after cisplatin treatment. On contrary A2780-Pac^{LR} cells showed significant decrease (****p<0.0001) in luciferase activity after paclitaxel; f) Immunofluorescence showed no change in the nuclear staining in A2780-Cis^{LR} after cisplatin treatment. However, decreased NF-κB staining was observed in A2780-Pac^{LR} cells after paclitaxel treatment. Lower panel showed the merged images with DAPI.*

Differential expression of Bcl2 was associated with differential resistance:

Activated NF-κB controls apoptosis by directly regulating various antiapoptotic proteins like Bcl-2 and XIAP. When investigated only Bcl-2 expression was found to be enhanced in cisplatin resistant cells but was down-regulated in paclitaxel and dual resistant cells (Figure 5.5a). In contrary, anti-apoptotic protein XIAP transcripts though decreased after cisplatin treatment did not show any changes after drug treatments to A2780-Cis^{LR} and A2780-Pac^{LR} cells (Figure 5.5b). Paclitaxel also did not enhance XIAP transcription in sensitive or A2780-Pac^{LR} cells.

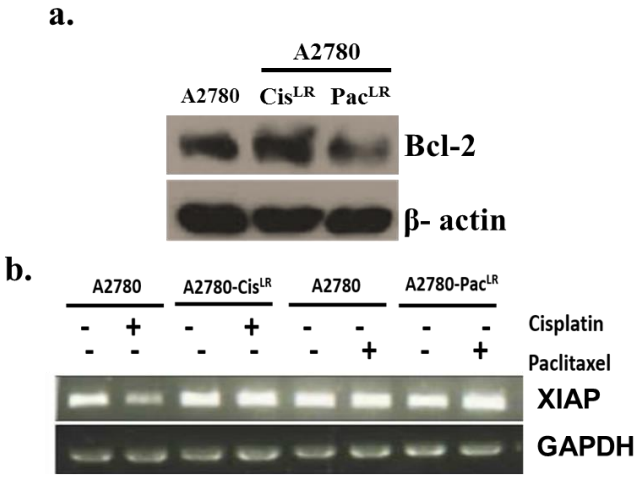

Figure 5.5. Expression of downstream target of NF-κB in the chemoresistant cells.

a*) Immunoblotting demonstrate that endogenous Bcl-2 expression was highest in A2780Cis^{LR} in comparison to A2780 and paclitaxel resistant cells; b) Semi-quantitative analysis of XIAP expression in the same cells showed no change in expression levels even after drug treatments.*

Cisplatin treatment to the A2780-Cis^{LR} cells augmented NF-κB activity *in vivo*:

Quantitative measurements of NF-κB activation through non-invasive BLI in *in vivo* would provide sufficient evidence of NF-κB augmentation. To non-invasively monitor the NF-κB activation in cisplatin resistant cells, subcutaneous tumor xenografts of A2780-Cis^{LR} cells stably expressing the NF-κB sensor were developed in nude mice (n=7) and sequential bioluminescence imaging for firefly and renilla luciferase were performed. A schematic representation of the procedure followed is shown in the figure 5.6a. As expected firefly luciferase activity of A2780-Cis^{LR} tumor xenografts (n=4) showed no change after cisplatin treatment ($6.2 \times 10^6 \pm 1.6 \times 10^5$ p/sec/cm^2/sr to $7.1 \times 10^6 \pm 2.1 \times 10^5$ p/s/cm^2/sr) in comparison to control tumor xenografts ($8.7 \times 10^6 \pm 1.3 \times 10^5$ to $6.8 \times 10^6 \pm 1.7 \times 10^5$ p/s/cm^2/sr) (n=3). However, a 14 fold increase in NF-κB-RL activity was found after cisplatin treatment (n=4) ($5.43 \times 10^5 \pm 8.4 \times 10^3$ p/sec/cm^2/sr to $4.31 \times 10^6 \pm 1.4 \times 10^4$ p/sec/cm^2/sr) as compared to the control tumor xenografts (n=3) ($3.8 \times 10^5 \pm 1.3 \times 10^4$ to $3.8 \times 10^5 \pm 1.2 \times 10^4$) (Figure 5.6c). The RL/FL ratio of the pre and post treatment luciferase activities of control and cisplatin treated group showed increased NF-κB driven RL activity (Figure 5.6d). The representative images of same mouse scanned for *firefly* and *renilla luciferase* pre- and post-cisplatin treatment phases were shown in figure 5.6b.

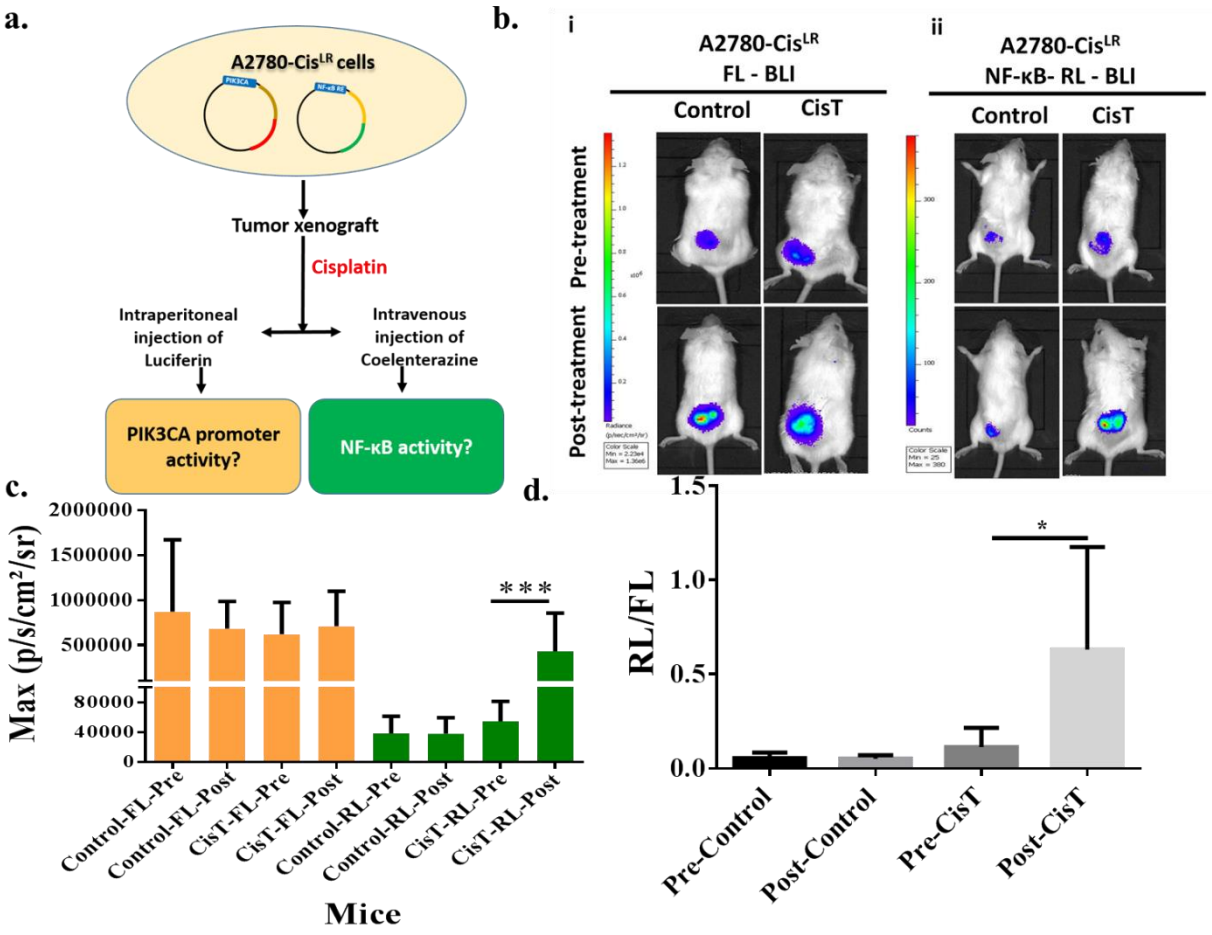

Figure 5.6. Non-invasive imaging of NF-κB activation in cisplatin resistant tumor xenografts. ***a)*** *Schematic representation of strategy followed for the dual BLI;* ***b)*** *Representative bioluminescent images of the same mouse bearing A2780-CisLR tumors are shown for pre- and post- cisplatin treatment. The left panel (i) showed the mouse imaged for firefly luciferase signal and the right panel showed the same mouse imaged sequentially for the renilla luciferase signal (ii). The upper panel depicts images before treatment and lower panel depicts images after treatment;* ***c)*** *Graphical representation of bioluminescence signals for both firefly luciferase and NF-κB-renilla luciferase were calculated for the respective ROIs drawn over tumors of control and cisplatin treated mice. No change was observed for firefly luminescence (before and after treatment), however, a 14 fold increased luminescence was observed for NF-κB-renilla luciferase after cisplatin treatment; d)*

Graphical representation of the fold change of RL/FL activities obtained from the tumors of control and cisplatin treated mice.

Discussion

AKT plays a crucial key player in cancer therapy by promoting resistance to the apoptosis inducing effects of chemotherapy. Thus, PI3K/AKT-targeted molecular therapy has become an intense area of research in ovarian cancers. The addition of a PI3K pathway inhibitor to the standard cytotoxic chemotherapy might not only target tumor cell growth, but also antagonize the development of drug resistance. Over the past years, PI3K pathway inhibitors are used in the treatment of many human cancers and many inhibitors are under phase I/ II clinical trials.

Specific small molecule inhibitors of PI3K/AKT pathway developed in an attempt to facilitate therapy are LY294002, wortmannin or rapamycin. These inhibitors are either tested in combination with cisplatin or carboplatin on ovarian carcinoma cells or given individually. In this study, the role of commonly used PI3K/AKT/mTOR pathway inhibitors like wortmannin and rapamycin in the cisplatin and paclitaxel resistant cells were studied. We found that cisplatin resistant cells were more sensitive to the wortmannin. However, no effect was observed in the paclitaxel resistant cells. Our results corroborates with the recently reported study, wherein wortmannin was used as adjuncts to conventional chemotherapy in the treatment of cisplatin resistant ovarian cancer cells [330]. We observed that rapamycin alone could not affect the cellular viability of cells of resistant cells. As observed by Schlosshauer et al., 2009, rapamycin along with carboplatin demonstrated effective apoptosis in ovarian cancer cells. Probably, such combinatorial treatment would have showed efficacious cell killing in our study. However, we have not attempted such

combinatorial treatment as our major interest lies in understanding the cause and consequence of chemoresistance and validate in pre-clinical model.

The IKK family of proteins is also known be induced by various compounds through the Toll like Receptors (TLRs) present on myeloid and non-myeloid cells [15]. TLR-4 driven signaling cascade which primarily triggers inflammatory and immune response by production of NF-κB, is known to be found in epithelial ovarian cancer cells [90]. TLR-4 driven signaling pathway is shown to influence the drug response towards paclitaxel, a TLR-4 ligand and analogue of lipopolysaccharide (LPS). MyD88, an essential adapter protein in TLR-4 mediated NF-κB signaling pathway has shown to influence the response of EOC cells to paclitaxel treatment [89, 92].

A recent study by Liang et al.,2013 have shown that elevated expression of MyD88 may promote tumor growth and metastasis via both TLR/IL-1R–dependent and –independent signaling and may serve as a biomarker for prognosis of patients with Hepatocellular carcinoma. In $MyD88^{positive}$ EOC cells, treatment with LPS and paclitaxel showed enhanced cell proliferation, activation of NF-κB, constitutive secretion of proimflammatory cytokines promoting tumor growth and thus renders paclitaxel resistance. In contrast, $MyD88^{negative}$ cells undergo apoptosis and do not secrete cytokines/chemokines in response to paclitaxel treatment. Overexpression of MyD88 expression in $MyD88^{negative}$ EOC cells contributed to paclitaxel resistance [92]. A large cohort of ovarian cancer patient showed that $MyD88^{negative}$ population (~40 % of total EOC patients) show better prognosis and longer survival, a significant proportion of them (~40%) acquire resistance over time [18]. Moreover, NF-κB signaling shows a delayed kinetics in MyD88-independent pathway and induces IFN-γ and IFN-responsible genes [172].

Luciferase assay and western blot demonstrated that cisplatin down-regulated NF-κB level and activity in chemosensitive A2780 cells. We have also observed reduced nuclear

localisation of NF-κB after 24 hours of cisplatin treatment by western blotting and immunofluorescence assay. Such decrease was also observed in MyD88 deficient A2780 cells exhibited after six hours of cisplatin treatment in study by Mabuchi et al., 2004 [131]. Conversely, paclitaxel treatment showed no change in expression of NF-κB in sensitive cells by reporter assay in the sensitive cells. Also increased nuclear localization of NF-κB protein was found in paclitaxel treated cells. However, these results contradict with the earlier reported study wherein, paclitaxel treatment showed no nuclear localisation in the A2780 cells by Szajnik *et al.*,2009 [92]. The reason for such discrepancy could be due to differential exposure time of the drug used by us. These data suggests that NF-κB could be differentially induced by different drugs in MyD88 deficient cells.

Study by Kim *et al.*, 2012, showed an association of TLR-4/MyD88 /NF-κB with survival and disease recurrence in a cohort of 123 patients. Although higher disease recurrence was found in MyD88 positive tumors (~36%), around 68 of the MyD88 negative patients (60% of total population) showed relapse and 65% of these patients were turned to be NF-κB positive. However, it is unclear how platinum and taxane resistant MyD88 deficient EOC cells alter NF-κB signaling. We investigated the state of NF-κB activation in MyD88 deficient EOC cell lines after making them resistant towards cisplatin and paclitaxel treatments.

Surprisingly we found that NF-κB activation pattern in both the resistant cells upon drug treatments vary with resistance. We treated these cisplatin and paclitaxel resistant cells with high dose of drugs for longer time period. While cisplatin treatment augmented NFκB in cisplatin resistant cells, paclitaxel treatment down regulated NF-κB. This contrary effect was evident from luciferase, western and immunofluorescence data.

Enhanced expressions of anti-apoptotic genes have been found to sustain the resistance properties of cancer cells [334]. Bcl-2, but not XIAP, a downstream target of NF-κB showed

differential expression in cisplatin and paclitaxel/platinum-taxol resistant cells. Thus our data indicates that an active NF-κB signaling and over expression of Bcl-2 is an essential phenomenon for acquirement of cisplatin resistance but not for paclitaxel resistance in $MyD88^{negative}$ epithelial ovarian cancer cells. Thus our data indicate that MyD88 expression is dispensable for acquirement of resistance towards cisplatin in epithelial ovarian cancer.

The activation NF-κB in cisplatin resistant tumor xenografts was studied *in vivo* by non-invasive imaging. In the previous chapter, using BLI modality, we demonstrated that the cisplatin resistant tumors could effectively retained their resistant phenotype and did not exhibit attenuation in luciferase signal or tumor regression after cisplatin treatment. When these resistant cells were further engineered to stably express the NF-κB sensor, a fourteen fold increase in NF-κB activity was observed after cisplatin treatment. Real time monitoring of NF-κB activity in animal models using various luciferases (renilla luciferase or gaussia luciferase) have already been demonstrated using TNF alpha as an inducer [335, 336]. However, to the best of our knowledge this is the first report in which NF-κB reporter activity was studied non-invasively in effect of cisplatin treatment.

Earlier study hypothesized that MyD88 expression is an indispensable molecule that imparts crucial influence on intrinsic taxol resistance in epithelial ovarian carcinoma. Our results demonstrated that paclitaxel, a TLR-4 ligand did not induce NF-κB in sensitive or in taxol/platinum resistant cells without MyD88 indicating an absolute dependency. In contrary, NF-κB upregulation by cisplatin and high Bcl-2 expression in MyD88 deficient cisplatin resistant cells indicated dispensability of MyD88 in acquired cisplatin resistance.

Acquirement of cisplatin resistance does require an active NF-κB signalling which could also be envisaged from *in vivo* tumor xenografts by non-invasive optical imaging. NF-κB upregulation by cisplatin and high Bcl-2 expression in MyD88 deficient cisplatin resistant cells demonstrated reliance of cisplatin resistance on the NF-κB pathway. This *in vivo* tumor

xenografts model would be useful in screening therapeutic molecules against NFκB or Bcl-2 for platinum resistant ovarian cancer cells particularly in a MyD88 compromised background.

Thus our data has provided a new insight into the molecular complexity associated with chemoresistance which may be exploited for developing better therapeutic strategy for ovarian cancer in future.

Chapter 6

Summary and Conclusions

Acquirement of chemoresistance towards platinum based drugs is a common phenomenon and a major hurdle in combating the relapse of the ovarian cancer often involve deregulation of one of the prime cell survival pathways, the PI3K/AKT/mTOR signaling cascade. The genetic alterations related to this pathway are often responsible for initiation and/or maintenance of carcinogenesis. To develop novel therapeutics against the key molecules of PI3K pathway, rigorous validation is required using both *in-vitro* and *in-vivo* models. *In vivo* tumor xenografts generated from *in vitro* drug resistant cells can act as a preclinical model to examine new therapeutic candidates and decipher the potential targets in this pathway. Activating mutation in the kinase domains of PIK3CA or AKT is the underlying cause for deregulated PI3K/AKT/mTOR signalling in majority of the cancers.

However, amplification in PIK3CA gene is a more common phenomenon than mutation in EOC. In recent clinical studies, PIK3CA gene amplification is observed in 16–24% of epithelial ovarian cancer (EOC) patients in conjunction with p53 mutations. Gene amplification at chromosomal level results to increased transcript level as well as increased promoter modulation. Although many *in vitro* and *in vivo* studies have facilitated a better understanding of targeted therapeutics against this pathway in drug resistance, there is a constant need to discover more molecular and therapeutic aids to circumvent this phenomenon due to the intricacy of the disease. However, till today no attempt has been made to understand the modulation in PIK3CA promoter activity in ovarian cancer cells as well as pre-clinical models in response to drugs and in context to acquirement of drug resistance. The only study conducted by Arezoo et al, demonstrated that a PIK3CA promoter isolated from ovarian surface epithelial cells is negatively regulated by p53.

Since the consequence of chemotherapeutic drug treatments on this promoter in ovarian cancer cells and during chemoresistance is unclear we aim to study the modulation of this

promoter by cisplatin and paclitaxel in ovarian cancer cells and tumor xenografts by non-invasive imaging approach. A PIK3CA sensor was developed using a bi-fusion reporter of red fluorescent protein (tdTomato/tdt), a mutant firefly luciferase (*fluc2*). Repression of the PIK3CA sensor by drugs was inversely proportional to cellular p53 level in a germline (PA1) and in an EOC (A2780) cell line but not in a p53 deficient EOC (SKOV3) cell line. Bioluminescence imaging of tumor xenografts stably expressing the PIK3CA sensor in PA1 and A2780 cells exhibited attenuating activity without any change in SKOV3 tumors expressing the PIK3CA sensor after cisplatin treatment. Sequential mutation at p53 binding sites showed gradual increase in promoter activity and decreased effects of the drugs indicating the importance of p53 governed regulation of PIK3CA promoter. These newly developed PIK3CA-fluc2-tdt and the mutant reporter sensors thus would be extremely useful for screening new drugs and for functional assessment of PIK3CAexpression from intact cells to living subjects.

In order to understand the molecular alterations occurring in the acquirement of chemoresistance and to address the question of monitoring the modulation of the PIK3CA sensor in the acquired chemoresistance to these drugs, isogenic cisplatin and paclitaxel resistant models in A2780 cells stably expressing PIK3CA sensor were established in a brief period of 6 months by the clinically relevant pulse method. These resistant cellular models were then compared to the parental sensitive cells using a cell viability assay (MTT) or clonogenic assay. Further, we found that AKT is highly activated in the cisplatin and paclitaxel resistant cells and observed that cisplatin resistant cells are more sensitive to wortmannin, a PI3K/AKT inhibitor.

In addition, we looked at the NF-κB pathway as one of the downstream components of PI3K signaling axis during acquired resistance. NF-κB activation facilitates cell death in sensitive

OC cells, but has shown to switch to an antiapoptotic 'oncogenic' pathway in chemoresistant isogenic variants. Studies in the last few years have unravelled multiple mechanisms that enable NF-κB to sustain carcinogenesis and drug resistance. Another pathway involved in NF-kb activation which is also active in EOCs other than immune cells is the TLR-4 pathway. Presence of MyD88, a component of TLR-4/MyD88 mediated NF-κB signaling in EOC tumors is reported to cause intrinsic paclitaxel resistance and poor survival. However, 50-60% of EOC patients do not express MyD88 and one-third of these patients finally relapses and dies due to disease burden. The status and role of NF-κB signaling in this chemoresistant MyD88^{negative} population was unknown. The isogenic cisplatin and paclitaxel resistant model we developed was using A2780 cells, a MyD88^{negative} background. Expressing a NF-κB reporter sensor, we showed that enhanced NF-κB activity was required for cisplatin but not for paclitaxel resistance. Immunofluorescence and western blotting demonstrated enhanced nuclear localization of NF-κB and subsequent binding to NF-κB response element in cisplatin resistant cells. In contrast, paclitaxel resistant cells showed down regulation in NF-κB activity. This study signifies that though acquired drug resistance involves alteration/activation of certain major signalling pathways (such as PI3KCA/AKT), the ultimate maintenance of resistance might require presence/absence of other effector molecules. This intrinsic molecular complexity has been observed in respect to the difference in generation of cisplatin and paclitaxel resistance in our cellular models.

Our study thus opens the future scope of incorporating these drug resistant models with non-invasive imaging strategies for *in-vivo* high throughput screening across PI3K/AKT/ mTOR pathway and NF-κB pathway to identify novel molecules for therapy and diagnosis of acquired chemoresistance in epithelial carcinoma of ovarian cancer.

Chapter 7

Bibliography

1. Tomao, F., et al., *Investigating molecular profiles of ovarian cancer: an update on cancer stem cells.* J Cancer, 2014. **5**(5): p. 301-10.
2. Bast, R.C., Jr., B. Hennessy, and G.B. Mills, *The biology of ovarian cancer: new opportunities for translation.* Nat Rev Cancer, 2009. **9**(6): p. 415-28.
3. Chaudhury S , M.A., Ray P, *Ovarian Cancer: An ever challenging malady.* Biomedical Research Journal, 2014 **1**(1): p. 34-55.
4. Gaikwad, S.M. and P. Ray, *Non-invasive imaging of PI3K/AKT/mTOR signalling in cancer.* Am J Nucl Med Mol Imaging, 2012. **2**(4): p. 418-31.
5. Blasberg, R.G., *In vivo molecular-genetic imaging: multi-modality nuclear and optical combinations.* Nucl Med Biol, 2003. **30**(8): p. 879-88.
6. Karakas, B., K.E. Bachman, and B.H. Park, *Mutation of the PIK3CA oncogene in human cancers.* Br J Cancer, 2006. **94**(4): p. 455-9.
7. Network, T.C.G.A., *Integrated genomic analyses of ovarian carcinoma.* Nature, 2011. **474**(7353): p. 609-15.
8. Kolasa, I.K., et al., *PIK3CA amplification associates with resistance to chemotherapy in ovarian cancer patients.* Cancer Biol Ther, 2009. **8**(1): p. 21-6.
9. Orr, G.A., et al., *Mechanisms of Taxol resistance related to microtubules.* Oncogene, 2003. **22**(47): p. 7280-95.
10. Peng, D.J., et al., *Role of the AKT/mTOR survival pathway in cisplatin resistance in ovarian cancer cells.* Biochem Biophys Res Commun, 2010. **394**(3): p. 600-5.
11. Yang, G., et al., *The biphasic role of NF-kappaB in progression and chemoresistance of ovarian cancer.* Clin Cancer Res, 2011. **17**(8): p. 2181-94.
12. Alvero, A.B., *Recent insights into the role of NF-kappaB in ovarian carcinogenesis.* Genome Med, 2010. **2**(8): p. 56.

13. Annunziata, C.M., et al., *Nuclear factor kappaB transcription factors are coexpressed and convey a poor outcome in ovarian cancer.* Cancer, 2010. **116**(13): p. 3276-84.

14. Karin, M., *NF-kappaB as a critical link between inflammation and cancer.* Cold Spring Harb Perspect Biol, 2009. **1**(5): p. a000141.

15. Akira, S., *Toll-like receptor signaling.* J Biol Chem, 2003. **278**(40): p. 38105-8.

16. Blasius, A.L. and B. Beutler, *Intracellular toll-like receptors.* Immunity, 2010. **32**(3): p. 305-15.

17. Kawai, T. and S. Akira, *Signaling to NF-kappaB by Toll-like receptors.* Trends Mol Med, 2007. **13**(11): p. 460-9.

18. Kim, K.H., et al., *Expression and significance of the TLR4/MyD88 signaling pathway in ovarian epithelial cancers.* World J Surg Oncol, 2012. **10**: p. 193.

19. Astanehe, A., et al., *Mechanisms underlying p53 regulation of PIK3CA transcription in ovarian surface epithelium and in ovarian cancer.* J Cell Sci, 2008. **121**(Pt 5): p. 664-74.

20. Dikshit, R., et al., *Cancer mortality in India: a nationally representative survey.* Lancet, 2012. **379**(9828): p. 1807-16.

21. Dhillon, P.K., et al., *Trends in breast, ovarian and cervical cancer incidence in Mumbai, India over a 30-year period, 1976-2005: an age-period-cohort analysis.* Br J Cancer, 2011. **105**(5): p. 723-30.

22. Murthy, N.S., et al., *Changing trends in incidence of ovarian cancer - the Indian scenario.* Asian Pac J Cancer Prev, 2009. **10**(6): p. 1025-30.

23. Siegel, R., et al., *Cancer statistics, 2014.* CA Cancer J Clin, 2014. **64**(1): p. 9-29.

24. Kaku, T., et al., *Histological classification of ovarian cancer.* Med Electron Microsc, 2003. **36**(1): p. 9-17.

25. Kurman, R.J. and M. Shih Ie, *The origin and pathogenesis of epithelial ovarian cancer: a proposed unifying theory.* Am J Surg Pathol, 2010. **34**(3): p. 433-43.

26. Drapkin, R., et al., *Human epididymis protein 4 (HE4) is a secreted glycoprotein that is overexpressed by serous and endometrioid ovarian carcinomas.* Cancer Res, 2005. **65**(6): p. 2162-9.

27. Mohaghegh, P. and A.G. Rockall, *Imaging strategy for early ovarian cancer: characterization of adnexal masses with conventional and advanced imaging techniques.* Radiographics, 2012. **32**(6): p. 1751-73.

28. Rockall, A.G., et al., *The role of FDG-PET/CT in gynaecological cancers.* Cancer Imaging, 2012. **12**: p. 49-65.

29. William R. Robinson, G.B., April S. Rogers, *Neoadjuvant chemotherapy prior to intraperitoneal chemotherapy in women with advanced ovarian cancer.* COMMUNITY ONCOLOGY, 2008. **5**: p. 376–38.

30. Chaudhury S, T.B., Chatterjee S and Ray P, *Molecular Imaging Aided Improvement in Drug Discovery and Development.* Current Biotechnology, 2014. **3**(3): p. 20.

31. ten Bokkel Huinink, W., et al., *Paclitaxel plus carboplatin in the treatment of ovarian cancer.* Semin Oncol, 1995. **22**(3 Suppl 6): p. 97-100.

32. McGuire, W.P., et al., *Cyclophosphamide and cisplatin compared with paclitaxel and cisplatin in patients with stage III and stage IV ovarian cancer.* N Engl J Med, 1996. **334**(1): p. 1-6.

33. du Bois, A., et al., *A randomized clinical trial of cisplatin/paclitaxel versus carboplatin/paclitaxel as first-line treatment of ovarian cancer.* J Natl Cancer Inst, 2003. **95**(17): p. 1320-9.

34. Thigpen, T., et al., *First-line therapy in ovarian cancer trials.* Int J Gynecol Cancer, 2011. **21**(4): p. 756-62.

35. Katsumata, N., *Dose-dense therapy is of benefit in primary treatment of ovarian cancer? In favor.* Ann Oncol, 2011. **22 Suppl 8**: p. viii29-viii32.

36. Jelovac, D. and D.K. Armstrong, *Recent progress in the diagnosis and treatment of ovarian cancer.* CA Cancer J Clin, 2011. **61**(3): p. 183-203.

37. Armstrong, D.K., et al., *Intraperitoneal cisplatin and paclitaxel in ovarian cancer.* N Engl J Med, 2006. **354**(1): p. 34-43.

38. Colombo, P.E., et al., *Sensitivity and resistance to treatment in the primary management of epithelial ovarian cancer.* Crit Rev Oncol Hematol, 2014. **89**(2): p. 207-16.

39. Agarwal, R. and S.B. Kaye, *Ovarian cancer: strategies for overcoming resistance to chemotherapy*. Nat Rev Cancer, 2003. **3**(7): p. 502-16.

40. Chen, S.S., A. Michael, and S.A. Butler-Manuel, *Advances in the treatment of ovarian cancer: a potential role of antiinflammatory phytochemicals.* Discov Med, 2012. **13**(68): p. 7-17.

41. Harries, M. and S.B. Kaye, *Recent advances in the treatment of epithelial ovarian cancer.* Expert Opin Investig Drugs, 2001. **10**(9): p. 1715-24.

42. Siddik, Z.H., *Cisplatin: mode of cytotoxic action and molecular basis of resistance.* Oncogene, 2003. **22**(47): p. 7265-79.

43. Hayes, D.M., et al., *High dose cis-platinum diammine dichloride: amelioration of renal toxicity by mannitol diuresis.* Cancer, 1977. **39**(4): p. 1372-81.

44. Rosenberg, B., et al., *Platinum compounds: a new class of potent antitumour agents.* Nature, 1969. **222**(5191): p. 385-6.

45. Siddik, Z.H., *Biochemical and molecular mechanisms of cisplatin resistance.* Cancer Treat Res, 2002. **112**: p. 263-84.

46. Gately, D.P. and S.B. Howell, *Cellular accumulation of the anticancer agent cisplatin: a review.* Br J Cancer, 1993. **67**(6): p. 1171-6.

47. Yang, X.L. and A.H. Wang, *Structural studies of atom-specific anticancer drugs acting on DNA.* Pharmacol Ther, 1999. **83**(3): p. 181-215.

48. Fichtinger-Schepman, A.M., et al., *Adducts of the antitumor drug cis-diamminedichloroplatinum(II) with DNA: formation, identification, and quantitation.* Biochemistry, 1985. **24**(3): p. 707-13.

49. Bowden, N.A., *Nucleotide excision repair: why is it not used to predict response to platinum-based chemotherapy?* Cancer Lett, 2014. **346**(2): p. 163-71.

50. Huang, J.C., et al., *HMG-domain proteins specifically inhibit the repair of the major DNA adduct of the anticancer drug cisplatin by human excision nuclease.* Proc Natl Acad Sci U S A, 1994. **91**(22): p. 10394-8.

51. Kothandapani, A., et al., *Epistatic role of base excision repair and mismatch repair pathways in mediating cisplatin cytotoxicity.* Nucleic Acids Res, 2013. **41**(15): p. 7332-43.

52. Gonzalez, V.M., et al., *Is cisplatin-induced cell death always produced by apoptosis?* Mol Pharmacol, 2001. **59**(4): p. 657-63.

53. Schiff, P.B., J. Fant, and S.B. Horwitz, *Promotion of microtubule assembly in vitro by taxol.* Nature, 1979. **277**(5698): p. 665-7.

54. Sharma, S., et al., *Promotion of tubulin assembly by poorly soluble taxol analogs.* Anal Biochem, 2007. **360**(1): p. 56-62.

55. Long, B.H. and C.R. Fairchild, *Paclitaxel inhibits progression of mitotic cells to G1 phase by interference with spindle formation without affecting other microtubule functions during anaphase and telephase.* Cancer Res, 1994. **54**(16): p. 4355-61.

56. Dumontet, C. and B.I. Sikic, *Mechanisms of action of and resistance to antitubulin agents: microtubule dynamics, drug transport, and cell death.* J Clin Oncol, 1999. **17**(3): p. 1061-70.

57. Blagosklonny, M.V., et al., *Taxol induction of p21WAF1 and p53 requires c-raf-1.* Cancer Res, 1995. **55**(20): p. 4623-6.

58. Wang, L.G., et al., *The effect of antimicrotubule agents on signal transduction pathways of apoptosis: a review.* Cancer Chemother Pharmacol, 1999. **44**(5): p. 355-61.

59. Rouzier, R., et al., *Microtubule-associated protein tau: a marker of paclitaxel sensitivity in breast cancer.* Proc Natl Acad Sci U S A, 2005. **102**(23): p. 8315-20.

60. Zhang, C.C., et al., *The role of MAP4 expression in the sensitivity to paclitaxel and resistance to vinca alkaloids in p53 mutant cells.* Oncogene, 1998. **16**(12): p. 1617-24.

61. Poruchynsky, M.S., et al., *Accompanying protein alterations in malignant cells with a microtubule-polymerizing drug-resistance phenotype and a primary resistance mechanism.* Biochem Pharmacol, 2001. **62**(11): p. 1469-80.

62. Hennessy, B.T., R.L. Coleman, and M. Markman, *Ovarian cancer.* Lancet, 2009. **374**(9698): p. 1371-82.

63. Yap, T.A., C.P. Carden, and S.B. Kaye, *Beyond chemotherapy: targeted therapies in ovarian cancer.* Nat Rev Cancer, 2009. **9**(3): p. 167-81.

64. Liu MX, C.D., Ngan HYS, *Mechanisms of Chemoresistance in Human Ovarian Cancer at a Glance.* Gynecology & Obstetrics, 2012. **2**(3): p. 104.

65. Gottesman, M.M., *Mechanisms of cancer drug resistance.* Annu Rev Med, 2002. **53**: p. 615-27.

66. Giaccone, G. and H.M. Pinedo, *Drug Resistance.* Oncologist, 1996. **1**(1 & 2): p. 82-87.

67. Boman, B.M. and M.S. Wicha, *Cancer stem cells: a step toward the cure.* J Clin Oncol, 2008. **26**(17): p. 2795-9.

68. Foster, R., R.J. Buckanovich, and B.R. Rueda, *Ovarian cancer stem cells: working towards the root of stemness.* Cancer Lett, 2013. **338**(1): p. 147-57.

69. Zhou, B.B., et al., *Tumour-initiating cells: challenges and opportunities for anticancer drug discovery.* Nat Rev Drug Discov, 2009. **8**(10): p. 806-23.

70. Zhan, Q., C. Wang, and S. Ngai, *Ovarian cancer stem cells: a new target for cancer therapy.* Biomed Res Int, 2013. **2013**: p. 916819.

71. Szakacs, G., et al., *Targeting multidrug resistance in cancer.* Nat Rev Drug Discov, 2006. **5**(3): p. 219-34.

72. Jordan, S., et al., *Patterns of chemotherapy treatment for women with invasive epithelial ovarian cancer--a population-based study.* Gynecol Oncol, 2013. **129**(2): p. 310-7.

73. Ledermann, J.A. and R.S. Kristeleit, *Optimal treatment for relapsing ovarian cancer.* Ann Oncol, 2010. **21 Suppl 7**: p. vii218-22.

74. Lisianskaia, A.S., *[Rationale for the approach to the choice of hormone therapy for ovarian cancer]*. Vopr Onkol, 2014. **60**(3): p. 274-9.

75. Fu, X., et al., *Involvement of microRNA-93, a new regulator of PTEN/AKT signaling pathway, in regulation of chemotherapeutic drug cisplatin chemosensitivity in ovarian cancer cells.* FEBS Lett, 2012. **586**(9): p. 1279-86.

76. Nagaraja, A.K., et al., *A link between mir-100 and FRAP1/mTOR in clear cell ovarian cancer.* Mol Endocrinol, 2010. **24**(2): p. 447-63.

77. Yusuf, R.Z., et al., *Paclitaxel resistance: molecular mechanisms and pharmacologic manipulation.* Curr Cancer Drug Targets, 2003. **3**(1): p. 1-19.

78. Schondorf, T., et al., *Induction of MDR1-gene expression by antineoplastic agents in ovarian cancer cell lines.* Anticancer Res, 2002. **22**(4): p. 2199-203.

79. Parekh, H., K. Wiesen, and H. Simpkins, *Acquisition of taxol resistance via Pglycoprotein- and non-P-glycoprotein-mediated mechanisms in human ovarian carcinoma cells.* Biochem Pharmacol, 1997. **53**(4): p. 461-70.

80. Choi, K.H., et al., *An altered pattern of cross-resistance in multidrug-resistant human cells results from spontaneous mutations in the mdr1 (P-glycoprotein) gene.* Cell, 1988. **53**(4): p. 519-29.

81. Mickley, L.A., et al., *Gene rearrangement: a novel mechanism for MDR-1 gene activation.* J Clin Invest, 1997. **99**(8): p. 1947-57.

82. Mozzetti, S., et al., *Class III beta-tubulin overexpression is a prominent mechanism of paclitaxel resistance in ovarian cancer patients.* Clin Cancer Res, 2005. **11**(1): p. 298305.

83. Gundersen, G.G. and T.A. Cook, *Microtubules and signal transduction.* Curr Opin Cell Biol, 1999. **11**(1): p. 81-94.

84. Giannakakou, P., et al., *Paclitaxel selects for mutant or pseudo-null p53 in drug resistance associated with tubulin mutations in human cancer.* Oncogene, 2000. **19**(27): p. 3078-85.

85. Ferlini, C., et al., *Bcl-2 down-regulation is a novel mechanism of paclitaxel resistance.* Mol Pharmacol, 2003. **64**(1): p. 51-8.

86. Duan, Z., et al., *Discovery of differentially expressed genes associated with paclitaxel resistance using cDNA array technology: analysis of interleukin (IL) 6, IL-8, and monocyte chemotactic protein 1 in the paclitaxel-resistant phenotype.* Clin Cancer Res, 1999. **5**(11): p. 3445-53.

87. Duan, Z., et al., *Overexpression of IL-6 but not IL-8 increases paclitaxel resistance of U-2OS human osteosarcoma cells.* Cytokine, 2002. **17**(5): p. 234-42.

88. Sampath, G.a., *Resistance to Taxanes*, in *Cancer Drug Discovery and Development: Cancer Drug Resistance*, T. B. Teicher © Humana Press Inc., NJ, Editor 2006.

89. Kelly, M.G., et al., *TLR-4 signaling promotes tumor growth and paclitaxel chemoresistance in ovarian cancer.* Cancer Res, 2006. **66**(7): p. 3859-68.

90. Muccioli, M., et al., *Toll-like receptors as novel therapeutic targets for ovarian cancer.* ISRN Oncol, 2012. **2012**: p. 642141.

91. Silasi, D.A., et al., *MyD88 predicts chemoresistance to paclitaxel in epithelial ovarian cancer.* Yale J Biol Med, 2006. **79**(3-4): p. 153-63.

92. Szajnik, M., et al., *TLR4 signaling induced by lipopolysaccharide or paclitaxel regulates tumor survival and chemoresistance in ovarian cancer.* Oncogene, 2009. **28**(49): p. 4353-63.

93. Anand, S., S. Penrhyn-Lowe, and A.R. Venkitaraman, *AURORA-A amplification overrides the mitotic spindle assembly checkpoint, inducing resistance to Taxol.* Cancer Cell, 2003. **3**(1): p. 51-62.

94. Slamon, D.J., et al., *Human breast cancer: correlation of relapse and survival with amplification of the HER-2/neu oncogene.* Science, 1987. **235**(4785): p. 177-82.

95. Moscatello, D.K., et al., *Transformational and altered signal transduction by a naturally occurring mutant EGF receptor.* Oncogene, 1996. **13**(1): p. 85-96.

96. Hu, L., et al., *Inhibition of phosphatidylinositol 3'-kinase increases efficacy of paclitaxel in in vitro and in vivo ovarian cancer models.* Cancer Res, 2002. **62**(4): p. 1087-92.

97. Galluzzi, L., et al., *Systems biology of cisplatin resistance: past, present and future.* Cell Death Dis, 2014. **5**: p. e1257.

98. Galluzzi, L., et al., *Molecular mechanisms of cisplatin resistance.* Oncogene, 2012. **31**(15): p. 1869-83.

99. Holzer, A.K., et al., *The copper influx transporter human copper transport protein 1 regulates the uptake of cisplatin in human ovarian carcinoma cells.* Mol Pharmacol, 2004. **66**(4): p. 817-23.

100. Ishida, S., et al., *Uptake of the anticancer drug cisplatin mediated by the copper transporter Ctr1 in yeast and mammals.* Proc Natl Acad Sci U S A, 2002. **99**(22): p. 14298-302.

101. Safaei, R., et al., *The role of copper transporters in the development of resistance to Pt drugs.* J Inorg Biochem, 2004. **98**(10): p. 1607-13.

102. Liedert, B., et al., *Overexpression of cMOAT (MRP2/ABCC2) is associated with decreased formation of platinum-DNA adducts and decreased G2-arrest in melanoma cells resistant to cisplatin.* J Invest Dermatol, 2003. **121**(1): p. 172-6.

103. Lewis, A.D., J.D. Hayes, and C.R. Wolf, *Glutathione and glutathione-dependent enzymes in ovarian adenocarcinoma cell lines derived from a patient before and after the onset of drug resistance: intrinsic differences and cell cycle effects.* Carcinogenesis, 1988. **9**(7): p. 1283-7.

104. Kelley, S.L., et al., *Overexpression of metallothionein confers resistance to anticancer drugs.* Science, 1988. **241**(4874): p. 1813-5.

105. Dabholkar, M., et al., *ERCC1 and ERCC2 expression in malignant tissues from ovarian cancer patients.* J Natl Cancer Inst, 1992. **84**(19): p. 1512-7.

106. Aebi, S., et al., *Loss of DNA mismatch repair in acquired resistance to cisplatin.* Cancer Res, 1996. **56**(13): p. 3087-90.

107. Brown, R., et al., *hMLH1 expression and cellular responses of ovarian tumour cells to treatment with cytotoxic anticancer agents.* Oncogene, 1997. **15**(1): p. 45-52.

108. Alt, A., et al., *Bypass of DNA lesions generated during anticancer treatment with cisplatin by DNA polymerase eta.* Science, 2007. **318**(5852): p. 967-70.

109. Edwards, S.L., et al., *Resistance to therapy caused by intragenic deletion in BRCA2.* Nature, 2008. **451**(7182): p. 1111-5.

110. Gadducci, A., et al., *Molecular mechanisms of apoptosis and chemosensitivity to platinum and paclitaxel in ovarian cancer: biological data and clinical implications.* Eur J Gynaecol Oncol, 2002. **23**(5): p. 390-6.

111. Vousden, K.H. and D.P. Lane, *p53 in health and disease.* Nat Rev Mol Cell Biol, 2007. **8**(4): p. 275-83.

112. Castedo, M., et al., *Apoptosis regulation in tetraploid cancer cells.* EMBO J, 2006. **25**(11): p. 2584-95.

113. Tajeddine, N., et al., *Hierarchical involvement of Bak, VDAC1 and Bax in cisplatininduced cell death.* Oncogene, 2008. **27**(30): p. 4221-32.

114. Williams, J., et al., *Expression of Bcl-xL in ovarian carcinoma is associated with chemoresistance and recurrent disease.* Gynecol Oncol, 2005. **96**(2): p. 287-95.

115. Ryan, B.M., N. O'Donovan, and M.J. Duffy, *Survivin: a new target for anti-cancer therapy.* Cancer Treat Rev, 2009. **35**(7): p. 553-62.

116. Wang, Y., et al., *Calpain activation through galectin-3 inhibition sensitizes prostate cancer cells to cisplatin treatment.* Cell Death Dis, 2010. **1**: p. e101.

117. Mansouri, A., et al., *Sustained activation of JNK/p38 MAPK pathways in response to cisplatin leads to Fas ligand induction and cell death in ovarian carcinoma cells.* J Biol Chem, 2003. **278**(21): p. 19245-56.

118. Fraser, M., et al., *Chemoresistance in human ovarian cancer: the role of apoptotic regulators.* Reprod Biol Endocrinol, 2003. **1**: p. 66.

119. Fraser, M., et al., *p53 is a determinant of X-linked inhibitor of apoptosis protein/AKTmediated chemoresistance in human ovarian cancer cells.* Cancer Res, 2003. **63**(21): p. 7081-8.

120. Yuan, M., et al., *c-Abl phosphorylation of DeltaNp63alpha is critical for cell viability.* Cell Death Dis, 2010. **1**: p. e16.

121. Hengstler, J.G., et al., *Contribution of c-erbB-2 and topoisomerase IIalpha to chemoresistance in ovarian cancer.* Cancer Res, 1999. **59**(13): p. 3206-14.

122. Hu, J. and E. Friedman, *Depleting Mirk Kinase Increases Cisplatin Toxicity in Ovarian Cancer Cells.* Genes Cancer, 2010. **1**(8): p. 803-811.

123. Yamamoto, K., et al., *Heat shock protein 27 was up-regulated in cisplatin resistant human ovarian tumor cell line and associated with the cisplatin resistance.* Cancer Lett, 2001. **168**(2): p. 173-81.

124. Yu, H., et al., *p62/SQSTM1 involved in cisplatin resistance in human ovarian cancer cells by clearing ubiquitinated proteins.* Eur J Cancer, 2011. **47**(10): p. 1585-94.

125. Brozovic, A., et al., *Long-term activation of SAPK/JNK, p38 kinase and fas-L expression by cisplatin is attenuated in human carcinoma cells that acquired drug resistance.* Int J Cancer, 2004. **112**(6): p. 974-85.

126. Koti, M., et al., *Identification of the IGF1/PI3K/NF kappaB/ERK gene signalling networks associated with chemotherapy resistance and treatment response in highgrade serous epithelial ovarian cancer.* BMC Cancer, 2013. **13**: p. 549.

127. Mabuchi, S., et al., *Inhibition of inhibitor of nuclear factor-kappaB phosphorylation increases the efficacy of paclitaxel in in vitro and in vivo ovarian cancer models.* Clin Cancer Res, 2004. **10**(22): p. 7645-54.

128. Nehra, R., et al., *BCL2 and CASP8 regulation by NF-kappaB differentially affect mitochondrial function and cell fate in antiestrogen-sensitive and -resistant breast cancer cells.* FASEB J, 2010. **24**(6): p. 2040-55.

129. Tang, G., et al., *Inhibition of JNK activation through NF-kappaB target genes.* Nature, 2001. **414**(6861): p. 313-7.

130. Beale, P.J., et al., *BCL-2 family protein expression and platinum drug resistance in ovarian carcinoma.* Br J Cancer, 2000. **82**(2): p. 436-40.

131. Mabuchi, S., et al., *Inhibition of NFkappaB increases the efficacy of cisplatin in in vitro and in vivo ovarian cancer models.* J Biol Chem, 2004. **279**(22): p. 23477-85.

132. Kruse, J.P. and W. Gu, *Modes of p53 regulation.* Cell, 2009. **137**(4): p. 609-22.

133. Hao, Q. and W.C. Cho, *Battle Against Cancer: An Everlasting Saga of p53.* Int J Mol Sci, 2014. **15**(12): p. 22109-22127.

134. Marchenko, N.D. and U.M. Moll, *The role of ubiquitination in the direct mitochondrial death program of p53.* Cell Cycle, 2007. **6**(14): p. 1718-23.

135. Zilfou, J.T. and S.W. Lowe, *Tumor suppressive functions of p53.* Cold Spring Harb Perspect Biol, 2009. **1**(5): p. a001883.

136. Duffy, M.J., et al., *p53 as a target for the treatment of cancer.* Cancer Treat Rev, 2014. **40**(10): p. 1153-1160.

137. Kandoth, C., et al., *Mutational landscape and significance across 12 major cancer types.* Nature, 2013. **502**(7471): p. 333-9.

138. Hengstermann, A., et al., *Complete switch from Mdm2 to human papillomavirus E6mediated degradation of p53 in cervical cancer cells.* Proc Natl Acad Sci U S A, 2001. **98**(3): p. 1218-23.

139. Shetzer, Y., et al., *The paradigm of mutant p53-expressing cancer stem cells and drug resistance.* Carcinogenesis, 2014. **35**(6): p. 1196-208.

140. Kang, H.J., et al., *Clinical relevance of gain-of-function mutations of p53 in highgrade serous ovarian carcinoma.* PLoS One, 2013. **8**(8): p. e72609.

141. Testa, J.R. and A. Bellacosa, *AKT plays a central role in tumorigenesis.* Proc Natl Acad Sci U S A, 2001. **98**(20): p. 10983-5.

142. Vivanco, I. and C.L. Sawyers, *The phosphatidylinositol 3-Kinase AKT pathway in human cancer.* Nat Rev Cancer, 2002. **2**(7): p. 489-501.

143. Banerjee, S. and S.B. Kaye, *New strategies in the treatment of ovarian cancer:*

current clinical perspectives and future potential. Clin Cancer Res, 2013. **19**(5): p. 961-8.

144. Abedini, M.R., et al., *AKT promotes chemoresistance in human ovarian cancer cells by modulating cisplatin-induced, p53-dependent ubiquitination of FLICE-like inhibitory protein,* in *Oncogene*2009. p. 11-25.

145. Marte, B.M. and J. Downward, *PKB/AKT: connecting phosphoinositide 3-kinase to cell survival and beyond.* Trends Biochem Sci, 1997. **22**(9): p. 355-8.

146. Scheid, M.P. and J.R. Woodgett, *PKB/AKT: functional insights from genetic models.* Nat Rev Mol Cell Biol, 2001. **2**(10): p. 760-8.

147. Yuan, T.L. and L.C. Cantley, *PI3K pathway alterations in cancer: variations on a theme.* Oncogene, 2008. **27**(41): p. 5497-510.

148. Hennessy, B.T., et al., *Exploiting the PI3K/AKT pathway for cancer drug discovery.* Nat Rev Drug Discov, 2005. **4**(12): p. 988-1004.

149. Kim, D., et al., *AKT/PKB signaling mechanisms in cancer and chemoresistance.* Front Biosci, 2005. **10**: p. 975-87.

150. Denley, A., et al., *Oncogenic signaling of class I PI3K isoforms.* Oncogene, 2008. **27**(18): p. 2561-74.

151. Carpten, J.D., et al., *A transforming mutation in the pleckstrin homology domain of AKT1 in cancer.* Nature, 2007. **448**(7152): p. 439-44.

152. Bellacosa, A., et al., *Molecular alterations of the AKT2 oncogene in ovarian and breast carcinomas.* Int J Cancer, 1995. **64**(4): p. 280-5.

153. Obata, K., et al., *Frequent PTEN/MMAC mutations in endometrioid but not serous or mucinous epithelial ovarian tumors.* Cancer Res, 1998. **58**(10): p. 2095-7.

154. Yang, N., et al., *Transcriptional regulation of PIK3CA oncogene by NF-kappaB in ovarian cancer microenvironment.* PLoS One, 2008. **3**(3): p. e1758.

155. Servidei, T., et al., *Chemoresistant tumor cell lines display altered epidermal growth factor receptor and HER3 signaling and enhanced sensitivity to gefitinib.* Int J Cancer, 2008. **123**(12): p. 2939-49.

156. Yang, H., et al., *Aurora-A induces cell survival and chemoresistance by activation of AKT through a p53-dependent manner in ovarian cancer cells.* Int J Cancer, 2006. **119**(10): p. 2304-12.

157. Lee, S., et al., *Activation of PI3K/Akt pathway by PTEN reduction and PIK3CA mRNA amplification contributes to cisplatin resistance in an ovarian cancer cell line.* Gynecol Oncol, 2005. **97**(1): p. 26-34.

158. Hafsi, S., et al., *Gene alterations in the PI3K/PTEN/AKT pathway as a mechanism of drug-resistance (review).* Int J Oncol, 2012. **40**(3): p. 639-44.

159. Page, C., et al., *Overexpression of AKT/AKT can modulate chemotherapy-induced apoptosis.* Anticancer Res, 2000. **20**(1A): p. 407-16.

160. Pal, S.K., et al., *AKT inhibitors in clinical development for the treatment of cancer.* Expert Opin Investig Drugs, 2010. **19**(11): p. 1355-66.

161. Carden, C.P., et al., *The association of PI3 kinase signaling and chemoresistance in advanced ovarian cancer.* Mol Cancer Ther, 2012. **11**(7): p. 1609-17.

162. Tsujimoto, Y., N. Ikegaki, and C.M. Croce, *Characterization of the protein product of bcl-2, the gene involved in human follicular lymphoma.* Oncogene, 1987. **2**(1): p. 3-7.

163. Youle, R.J. and A. Strasser, *The BCL-2 protein family: opposing activities that mediate cell death.* Nat Rev Mol Cell Biol, 2008. **9**(1): p. 47-59.

164. Scarfo, L. and P. Ghia, *Reprogramming cell death: BCL2 family inhibition in hematological malignancies.* Immunol Lett, 2013. **155**(1-2): p. 36-9.

165. Holohan, C., et al., *Cancer drug resistance: an evolving paradigm.* Nat Rev Cancer, 2013. **13**(10): p. 714-26.

166. Obexer, P. and M.J. Ausserlechner, *X-linked inhibitor of apoptosis protein - a critical death resistance regulator and therapeutic target for personalized cancer therapy.* Front Oncol, 2014. **4**: p. 197.

167. Sui, L., et al., *Survivin expression and its correlation with cell proliferation and prognosis in epithelial ovarian tumors.* Int J Oncol, 2002. **21**(2): p. 315-20.

168. Mano, Y., et al., *Bcl-2 as a predictor of chemosensitivity and prognosis in primary epithelial ovarian cancer*. Eur J Cancer, 1999. **35**(8): p. 1214-9.

169. Hayden, M.S. and S. Ghosh, *NF-kappaB, the first quarter-century: remarkable progress and outstanding questions.* Genes Dev, 2012. **26**(3): p. 203-34.

170. Ali, A.Y., et al., *Molecular determinants of ovarian cancer chemoresistance: new insights into an old conundrum.* Ann N Y Acad Sci, 2012. **1271**: p. 58-67.

171. Lagunas, V.M. and J. Melendez-Zajgla, *Nuclear Factor-kappa B as a Resistance Factor to Platinum-Based Antineoplasic Drugs.* Met Based Drugs, 2008. **2008**: p. 576104.

172. Kawai, T. and S. Akira, *TLR signaling.* Cell Death Differ, 2006. **13**(5): p. 816-25.

173. Chen, R., et al., *Inflammation, cancer and chemoresistance: taking advantage of the toll-like receptor signaling pathway.* Am J Reprod Immunol, 2007. **57**(2): p. 93-107.

174. Karin, M., *Nuclear factor-kappaB in cancer development and progression.* Nature, 2006. **441**(7092): p. 431-6.

175. Lin, Y.G., et al., *Curcumin inhibits tumor growth and angiogenesis in ovarian carcinoma by targeting the nuclear factor-kappaB pathway.* Clin Cancer Res, 2007. **13**(11): p. 3423-30.

176. Chou, C.H., et al., *Up-regulation of interleukin-6 in human ovarian cancer cell via a Gi/PI3K-Akt/NF-kappaB pathway by lysophosphatidic acid, an ovarian canceractivating factor*. Carcinogenesis, 2005. **26**(1): p. 45-52.

177. Darb-Esfahani, S., et al., *Expression of classical NF-kappaB pathway effectors in human ovarian carcinoma.* Histopathology, 2010. **56**(6): p. 727-39.

178. Guo, R.X., et al., *Increased staining for phosphorylated AKT and nuclear factorkappaB p65 and their relationship with prognosis in epithelial ovarian cancer.* Pathol Int, 2008. **58**(12): p. 749-56.

179. Guo, L.M., et al., *MicroRNA-9 inhibits ovarian cancer cell growth through regulation of NF-kappaB1.* FEBS J, 2009. **276**(19): p. 5537-46.

180. Dai, L., et al., *TWEAK promotes ovarian cancer cell metastasis via NF-kappaB pathway activation and VEGF expression.* Cancer Lett, 2009. **283**(2): p. 159-67.

181. Hernandez, L., et al., *Activation of NF-kappaB signaling by inhibitor of NF-kappaB kinase beta increases aggressiveness of ovarian cancer.* Cancer Res, 2010. **70**(10): p. 4005-14.

182. Aghajanian, C., et al., *Phase I trial of bortezomib and carboplatin in recurrent ovarian or primary peritoneal cancer.* J Clin Oncol, 2005. **23**(25): p. 5943-9.

183. Konstantinopoulos, P.A., et al., *Carboplatin-induced gene expression changes in vitro are prognostic of survival in epithelial ovarian cancer.* BMC Med Genomics, 2008. **1**: p. 59.

184. Jinawath, N., et al., *Oncoproteomic analysis reveals co-upregulation of RELA and STAT5 in carboplatin resistant ovarian carcinoma.* PLoS One, 2010. **5**(6): p. e11198.

185. Gagne, J.P., et al., *Proteome profiling of human epithelial ovarian cancer cell line TOV-112D.* Mol Cell Biochem, 2005. **275**(1-2): p. 25-55.

186. Huang, Y., et al., *The possible correlation between activation of NF-kappaB/IkappaB pathway and the susceptibility of tumor cells to paclitaxel-induced apoptosis.* Oncol Res, 2002. **13**(2): p. 113-22.

187. Huang, Y. and W. Fan, *IkappaB kinase activation is involved in regulation of paclitaxel-induced apoptosis in human tumor cell lines.* Mol Pharmacol, 2002. **61**(1): p. 105-13.

188. Brindle, K., *New approaches for imaging tumour responses to treatment.* Nat Rev Cancer, 2008. **8**(2): p. 94-107.

189. Hong, H., et al., *Non-invasive cell tracking in cancer and cancer therapy.* Curr Top Med Chem, 2010. **10**(12): p. 1237-48.

190. Massoud, T.F. and S.S. Gambhir, *Molecular imaging in living subjects: seeing fundamental biological processes in a new light.* Genes Dev, 2003. **17**(5): p. 545-80.

191. Blasberg, R.G., *Molecular imaging and cancer.* Mol Cancer Ther, 2003. **2**(3): p. 335-43.

192. Yoshimoto, M., H. Kurihara, and H. Fujii, *Theragnostic Imaging Using Radiolabeled Antibodies and Tyrosine Kinase Inhibitors.* The Scientific World Journal.

193. Dijkers, E.C., et al., *Biodistribution of 89Zr-trastuzumab and PET imaging of HER2positive lesions in patients with metastatic breast cancer.* Clin Pharmacol Ther, 2010.

87(5): p. 586-92.

194. Oude Munnink, T.H., et al., *(89)Zr-trastuzumab PET visualises HER2 downregulation by the HSP90 inhibitor NVP-AUY922 in a human tumour xenograft.* Eur J Cancer, 2010. **46**(3): p. 678-84.

195. Ray, P., *Multimodality molecular imaging of disease progression in living subjects.* J Biosci, 2011. **36**(3): p. 499-504.

196. Ray, P., *The pivotal role of multimodality reporter sensors in drug discovery: from cell based assays to real time molecular imaging.* Curr Pharm Biotechnol, 2011. **12**(4): p. 539-46.

197. Gambhir, S.S., et al., *Imaging transgene expression with radionuclide imaging technologies.* Neoplasia, 2000. **2**(1-2): p. 118-38.

198. Massoud, T.F., et al., *Reporter gene imaging of protein-protein interactions in living subjects.* Curr Opin Biotechnol, 2007. **18**(1): p. 31-7.

199. Shah, K., et al., *Molecular imaging of gene therapy for cancer.* Gene Ther, 2004. **11**(15): p. 1175-87.

200. Salminen, E., et al., *Investigations with FDG-PET scanning in prostate cancer show limited value for clinical practice.* Acta Oncol, 2002. **41**(5): p. 425-9.

201. Dragosavac, S., et al., *Staging recurrent ovarian cancer with (18)FDG PET/CT.* Oncol Lett, 2013. **5**(2): p. 593-597.

202. Fulham, M.J., et al., *The impact of PET-CT in suspected recurrent ovarian cancer: A prospective multi-centre study as part of the Australian PET Data Collection Project.* Gynecol Oncol, 2009. **112**(3): p. 462-8.

203. Nanni, C., et al., *(18)F-FDG PET/CT in the evaluation of recurrent ovarian cancer: a prospective study on forty-one patients.* Eur J Surg Oncol, 2005. **31**(7): p. 792-7.

204. Bilici, A., et al., *Clinical value of FDG PET/CT in the diagnosis of suspected recurrent ovarian cancer: is there an impact of FDG PET/CT on patient management?* Eur J Nucl Med Mol Imaging, 2010. **37**(7): p. 1259-69.

205. Palomar, A., et al., *Value of FDG PET/CT in patients with treated ovarian cancer and raised CA125 serum levels.* Mol Imaging Biol, 2012. **14**(1): p. 123-9.

206. Ghosh, J., et al., *Role of FDG PET-CT in asymptomatic epithelial ovarian cancer with rising serum CA-125: a pilot study.* Natl Med J India, 2013. **26**(6): p. 327-31.

207. Liu, T.W., et al., *Biologically-targeted detection of primary and micro-metastatic ovarian cancer.* Theranostics, 2013. **3**(6): p. 420-7.

208. Munk Jensen, M., et al., *Imaging of treatment response to the combination of carboplatin and paclitaxel in human ovarian cancer xenograft tumors in mice using FDG and FLT PET.* PLoS One, 2013. **8**(12): p. e85126.

209. Niu, G., et al., *Monitoring therapeutic response of human ovarian cancer to 17DMAG by noninvasive PET imaging with (64)Cu-DOTA-trastuzumab.* Eur J Nucl Med Mol Imaging, 2009. **36**(9): p. 1510-9.

210. Jensen, M.M., et al., *[18F]FDG and [18F]FLT positron emission tomography imaging following treatment with belinostat in human ovary cancer xenografts in mice.* BMC Cancer, 2013. **13**: p. 168.

211. S K Sharma, M.W., M Wang, D Glubrecht, B Andrais, S E Lapi, F Wuest, *ImmunoPET of epithelial ovarian cancer: harnessing the potential of CA125 for non-invasive imaging.* EJNMMI Research, 2014. **4**.

212. Toffoli, G., et al., *Expression of folate binding protein as a prognostic factor for response to platinum-containing chemotherapy and survival in human ovarian cancer.* Int J Cancer, 1998. **79**(2): p. 121-6.

213. Morris, R.T., et al., *Phase II study of treatment of advanced ovarian cancer with folate-receptor-targeted therapeutic (vintafolide) and companion SPECT-based imaging agent (99mTc-etarfolatide).* Ann Oncol, 2014. **25**(4): p. 852-8.

214. Scalici, J.M., et al., *Imaging VCAM-1 as an indicator of treatment efficacy in metastatic ovarian cancer.* J Nucl Med, 2013. **54**(11): p. 1883-9.

215. Muller, C., et al., *Pemetrexed improves tumor selectivity of 111In-DTPA-folate in mice with folate receptor-positive ovarian cancer.* J Nucl Med, 2008. **49**(4): p. 623-9.

216. Gross, S. and D. Piwnica-Worms, *Molecular imaging strategies for drug discovery and development.* Curr Opin Chem Biol, 2006. **10**(4): p. 334-42.

217. Kinkel, K., et al., *Indeterminate ovarian mass at US: incremental value of second imaging test for characterization--meta-analysis and Bayesian analysis.* Radiology, 2005. **236**(1): p. 85-94.

218. Michielsen, K., et al., *Whole-body MRI with diffusion-weighted sequence for staging of patients with suspected ovarian cancer: a clinical feasibility study in comparison to CT and FDG-PET/CT.* Eur Radiol, 2014. **24**(4): p. 889-901.

219. Espada, M., et al., *Diffusion-weighted magnetic resonance imaging evaluation of intra-abdominal sites of implants to predict likelihood of suboptimal cytoreductive surgery in patients with ovarian carcinoma.* Eur Radiol, 2013. **23**(9): p. 2636-42.

220. Motoshima, S., et al., *Diffusion-weighted MR imaging in gynecologic cancers.* J Gynecol Oncol, 2011. **22**(4): p. 275-87.

221. Hensley, H., et al., *Magnetic resonance imaging for detection and determination of tumor volume in a genetically engineered mouse model of ovarian cancer.* Cancer Biol Ther, 2007. **6**(11): p. 1717-25.

222. Hensley, H.H., et al., *Combined in vivo molecular and anatomic imaging for detection of ovarian carcinoma-associated protease activity and integrin expression in mice.* Neoplasia, 2012. **14**(6): p. 451-62.

223. Qayyum, A., et al., *Role of CT and MR imaging in predicting optimal cytoreduction of newly diagnosed primary epithelial ovarian cancer.* Gynecol Oncol, 2005. **96**(2): p. 301-6.

224. Byrom, J., et al., *Can pre-operative computed tomography predict resectability of ovarian carcinoma at primary laparotomy?* BJOG, 2002. **109**(4): p. 369-75.

225. Rampurwala, M., et al., *Visualization and quantification of intraperitoneal tumors by in vivo computed tomography using negative contrast enhancement strategy in a mouse model of ovarian cancer.* Transl Oncol, 2009. **2**(2): p. 96-106.

226. Nimmagadda, S., M. Pullambhatla, and M.G. Pomper, *Immunoimaging of CXCR4 expression in brain tumor xenografts using SPECT/CT.* J Nucl Med, 2009. **50**(7): p. 1124-30.

227. Dijkmans, P.A., et al., *Microbubbles and ultrasound: from diagnosis to therapy.* Eur J

Echocardiogr, 2004. **5**(4): p. 245-56.

228. Rehn, M., K. Lohmann, and A. Rempen, *Transvaginal ultrasonography of pelvic masses: evaluation of B-mode technique and Doppler ultrasonography.* Am J Obstet Gynecol, 1996. **175**(1): p. 97-104.

229. Kurjak, A. and M. Predanic, *New scoring system for prediction of ovarian malignancy based on transvaginal color Doppler sonography.* J Ultrasound Med, 1992. **11**(12): p. 631-8.

230. Bromley, B., H. Goodman, and B.R. Benacerraf, *Comparison between sonographic morphology and Doppler waveform for the diagnosis of ovarian malignancy.* Obstet Gynecol, 1994. **83**(3): p. 434-7.

231. Iyer, V.R. and S.I. Lee, *MRI, CT, and PET/CT for ovarian cancer detection and adnexal lesion characterization.* AJR Am J Roentgenol, 2010. **194**(2): p. 311-21.

232. Menon, U., et al., *Sensitivity and specificity of multimodal and ultrasound screening for ovarian cancer, and stage distribution of detected cancers: results of the prevalence screen of the UK Collaborative Trial of Ovarian Cancer Screening (UKCTOCS).* Lancet Oncol, 2009. **10**(4): p. 327-40.

233. Cho, S., et al., *Characterization and evaluation of pre-clinical suitability of a syngeneic orthotopic mouse ovarian cancer model.* Anticancer Res, 2013. **33**(4): p. 1317-24.

234. Barua, A., et al., *Detection of tumor-associated neoangiogenesis by Doppler ultrasonography during early-stage ovarian cancer in laying hens: a preclinical model of human spontaneous ovarian cancer.* J Ultrasound Med, 2010. **29**(2): p. 173-82.

235. Rao, J., A. Dragulescu-Andrasi, and H. Yao, *Fluorescence imaging in vivo: recent advances.* Curr Opin Biotechnol, 2007. **18**(1): p. 17-25.

236. Drake, C.R., D.C. Miller, and E.F. Jones, *Activatable Optical Probes for the Detection of Enzymes.* Curr Org Synth, 2011. **8**(4): p. 498-520.

237. Sutton, E.J., et al., *Cell tracking with optical imaging.* Eur Radiol, 2008. **18**(10): p. 2021-32.

238. Giepmans, B.N., et al., *The fluorescent toolbox for assessing protein location and function.* Science, 2006. **312**(5771): p. 217-24.

239. Tian, H., et al., *A high throughput drug screen based on fluorescence resonance energy transfer (FRET) for anticancer activity of compounds from herbal medicine.* Br J Pharmacol, 2007. **150**(3): p. 321-34.

240. van Dam, G.M., et al., *Intraoperative tumor-specific fluorescence imaging in ovarian cancer by folate receptor-alpha targeting: first in-human results.* Nat Med, 2011. **17**(10): p. 1315-9.

241. Wang, H.Z., et al., *Detection of tumor marker CA125 in ovarian carcinoma using quantum dots.* Acta Biochim Biophys Sin (Shanghai), 2004. **36**(10): p. 681-6.

242. Nathwani, B.B., et al., *Fabrication and characterization of silk-fibroin-coated quantum dots.* IEEE Trans Nanobioscience, 2009. **8**(1): p. 72-7.

243. Zinn, K.R., et al., *Noninvasive bioluminescence imaging in small animals.* ILAR J, 2008. **49**(1): p. 103-15.

244. Lake, M.C. and E.O. Aboagye, *Luciferase fragment complementation imaging in preclinical cancer studies.* Oncoscience, 2014. **1**(5): p. 310-25.

245. Yoshioka, K., et al., *A novel mouse model of soft-tissue infection using bioluminescence imaging allows noninvasive, real-time monitoring of bacterial growth.* PLoS One, 2014. **9**(9): p. e106367.

246. Hastings, J.W., *Chemistries and colors of bioluminescent reactions: a review.* Gene, 1996. **173**(1 Spec No): p. 5-11.

247. Sadikot, R.T. and T.S. Blackwell, *Bioluminescence imaging.* Proc Am Thorac Soc, 2005. **2**(6): p. 537-40, 511-2.

248. Han, X.J., et al., *Development of a novel liposomal nanodelivery system for bioluminescence imaging and targeted drug delivery in ErbB2-overexpressing metastatic ovarian carcinoma.* Int J Mol Med, 2014. **34**(5): p. 1225-32.

249. Ray, P., et al., *Noninvasive imaging reveals inhibition of ovarian cancer by targeting CXCL12-CXCR4.* Neoplasia, 2011. **13**(12): p. 1152-61.

250. Salomonnson, E., et al., *Imaging CXCL12-CXCR4 signaling in ovarian cancer therapy.* PLoS One, 2013. **8**(1): p. e51500.

251. Wilson, A.J., et al., *Tracking NF-kappaB activity in tumor cells during ovarian cancer progression in a syngeneic mouse model.* J Ovarian Res, 2013. **6**(1): p. 63.

252. Geller, M.A., et al., *Intraperitoneal delivery of human natural killer cells for treatment of ovarian cancer in a mouse xenograft model.* Cytotherapy, 2013. **15**(10): p. 1297-306.

253. Helland, O., et al., *First in-mouse development and application of a surgically relevant xenograft model of ovarian carcinoma.* PLoS One, 2014. **9**(3): p. e89527.

254. Liu, H., et al., *Molecular optical imaging with radioactive probes.* PLoS One, 2010. **5**(3): p. e9470.

255. Gaikwad, S.M., et al., *Non-invasive imaging of phosphoinositide-3-kinase-catalyticsubunit-alpha (PIK3CA) promoter modulation in small animal models.* PLoS One, 2013. **8**(2): p. e55971.

256. Akinleye, A., et al., *Phosphatidylinositol 3-kinase (PI3K) inhibitors as cancer therapeutics.* J Hematol Oncol, 2013. **6**(1): p. 88.

257. Zhao, L. and P.K. Vogt, *Class I PI3K in oncogenic cellular transformation.* Oncogene, 2008. **27**(41): p. 5486-96.

258. Liu, F.S., *Mechanisms of chemotherapeutic drug resistance in cancer therapy--a quick review.* Taiwan J Obstet Gynecol, 2009. **48**(3): p. 239-44.

259. Jehan, Z., et al., *Frequent PIK3CA gene amplification and its clinical significance in colorectal cancer.* J Pathol, 2009. **219**(3): p. 337-46.

260. Ji, M., et al., *Highly frequent promoter methylation and PIK3CA amplification in nonsmall cell lung cancer (NSCLC).* BMC Cancer, 2011. **11**: p. 147.

261. Kawano, O., et al., *PIK3CA gene amplification in Japanese non-small cell lung cancer.* Lung Cancer, 2007. **58**(1): p. 159-60.

262. Shi, J., et al., *Highly frequent PIK3CA amplification is associated with poor prognosis in gastric cancer.* BMC Cancer, 2012. **12**: p. 50.

263. Kinross, K.M., et al., *An activating Pik3ca mutation coupled with Pten loss is sufficient to initiate ovarian tumorigenesis in mice.* J Clin Invest, 2012. **122**(2): p. 553-7.

264. Shayesteh, L., et al., *PIK3CA is implicated as an oncogene in ovarian cancer.* Nat Genet, 1999. **21**(1): p. 99-102.

265. Abubaker, J., et al., *PIK3CA alterations in Middle Eastern ovarian cancers.* Mol Cancer, 2009. **8**: p. 51.

266. Liang, S., et al., *Expression of activated PIK3CA in ovarian surface epithelium results in hyperplasia but not tumor formation.* PLoS One, 2009. **4**(1): p. e4295.

267. Singh, B., et al., *p53 regulates cell survival by inhibiting PIK3CA in squamous cell carcinomas.* Genes Dev, 2002. **16**(8): p. 984-93.

268. Astanehe, A., et al., *The transcriptional induction of PIK3CA in tumor cells is dependent on the oncoprotein Y-box binding protein-1.* Oncogene, 2009. **28**(25): p. 2406-18.

269. Livak, K.J. and T.D. Schmittgen, *Analysis of relative gene expression data using realtime quantitative PCR and the 2(-Delta Delta C(T)) Method.* Methods, 2001. **25**(4): p. 402-8.

270. Ryu, S.Y., et al., *Synergistic growth inhibition by combination of adenovirus mediated p53 transfer and cisplatin in ovarian cancer cell lines.* J Gynecol Oncol, 2009. **20**(1): p. 48-54.

271. Yamamoto, H., et al., *PIK3CA mutations and copy number gains in human lung cancers.* Cancer Res, 2008. **68**(17): p. 6913-21.

272. Khynriam, D. and S.B. Prasad, *Cisplatin-induced genotoxic effects and endogenous glutathione levels in mice bearing ascites Dalton's lymphoma.* Mutat Res, 2003. **526**(1-2): p. 9-18.

273. Campbell, I.G., et al., *Mutation of the PIK3CA gene in ovarian and breast cancer.* Cancer Res, 2004. **64**(21): p. 7678-81.

274. Min, J.J., et al., *In vivo bioluminescence imaging of cord blood derived mesenchymal stem cell transplantation into rat myocardium.* Ann Nucl Med, 2006. **20**(3): p. 165-70.

275. Ray P, B.E., Iyer M, Barrio JR, Satyamurthy N, Phelps ME, Herschman HR, Gambhir SS, *Monitoring gene therapy with reporter gene imaging.* Semin Nucl Med., 2001 **31**(4): p. 312-20.

276. Doubrovin, M., et al., *Multimodality in vivo molecular-genetic imaging.* Bioconjug Chem, 2004. **15**(6): p. 1376-88.

277. Mayer-Kuckuk, P., et al., *Role of reporter gene imaging in molecular and cellular biology.* Biol Chem, 2004. **385**(5): p. 353-61.

278. Stordal, B., N. Pavlakis, and R. Davey, *A systematic review of platinum and taxane resistance from bench to clinic: an inverse relationship.* Cancer Treat Rev, 2007. **33**(8): p. 688-703.

279. Yan, X.D., et al., *Biological comparison of ovarian cancer resistant cell lines to cisplatin and Taxol by two different administrations.* Oncol Rep, 2007. **17**(5): p. 1163-9.

280. Biedler, J.L. and H. Riehm, *Cellular resistance to actinomycin D in Chinese hamster cells in vitro: cross-resistance, radioautographic, and cytogenetic studies.* Cancer Res, 1970. **30**(4): p. 1174-84.

281. McDermott, M., et al., *In vitro Development of Chemotherapy and Targeted Therapy Drug-Resistant Cancer Cell Lines: A Practical Guide with Case Studies.* Front Oncol, 2014. **4**: p. 40.

282. Clark, A.S., et al., *Constitutive and inducible Akt activity promotes resistance to chemotherapy, trastuzumab, or tamoxifen in breast cancer cells.* Mol Cancer Ther, 2002. **1**(9): p. 707-17.

283. Prasad, G., et al., *Inhibition of PI3K/mTOR pathways in glioblastoma and implications for combination therapy with temozolomide.* Neuro Oncol, 2011. **13**(4): p. 384-92.

284. Samimi, G., et al., *Increase in expression of the copper transporter ATP7A during platinum drug-based treatment is associated with poor survival in ovarian cancer patients.* Clin Cancer Res, 2003. **9**(16 Pt 1): p. 5853-9.

285. Nakayama, K., et al., *Copper-transporting P-type adenosine triphosphatase (ATP7B) as a cisplatin based chemoresistance marker in ovarian carcinoma: comparative analysis with expression of MDR1, MRP1, MRP2, LRP and BCRP.* Int J Cancer, 2002. **101**(5): p. 488-95.

286. Rabik, C.A., et al., *Role of copper transporters in resistance to platinating agents.* Cancer Chemother Pharmacol, 2009. **64**(1): p. 133-42.

287. Holzer, A.K., et al., *Cisplatin rapidly down-regulates its own influx transporter hCTR1 in cultured human ovarian carcinoma cells.* Clin Cancer Res, 2004. **10**(19): p. 6744-9.

288. Kalayda, G.V., et al., *Altered localisation of the copper efflux transporters ATP7A and ATP7B associated with cisplatin resistance in human ovarian carcinoma cells.* BMC Cancer, 2008. **8**: p. 175.

289. Ivy, K.D. and J.H. Kaplan, *A re-evaluation of the role of hCTR1, the human highaffinity copper transporter, in platinum-drug entry into human cells.* Mol Pharmacol, 2013. **83**(6): p. 1237-46.

290. Song, I.S., et al., *Role of human copper transporter Ctr1 in the transport of platinumbased antitumor agents in cisplatin-sensitive and cisplatin-resistant cells.* Mol Cancer Ther, 2004. **3**(12): p. 1543-9.

291. Jensen, P.B., et al., *In vitro cross-resistance and collateral sensitivity in seven resistant small-cell lung cancer cell lines: preclinical identification of suitable drug partners to taxotere, taxol, topotecan and gemcitabin.* Br J Cancer, 1997. **75**(6): p. 869-77.

292. Mizuno, K., et al., *Mitomycin C cross-resistance induced by adriamycin in human ovarian cancer cells in vitro.* Cancer Chemother Pharmacol, 1990. **26**(5): p. 333-9.

293. Stordal, B. and R. Davey, *A systematic review of genes involved in the inverse resistance relationship between cisplatin and paclitaxel chemotherapy: role of BRCA1*. Curr Cancer Drug Targets, 2009. **9**(3): p. 354-65.

294. Stordal, B., et al., *Resistance to paclitaxel in a cisplatin-resistant ovarian cancer cell line is mediated by P-glycoprotein.* PLoS One, 2012. **7**(7): p. e40717.

295. Rahman, M.T., et al., *Notch3 overexpression as potential therapeutic target in advanced stage chemoresistant ovarian cancer.* Am J Clin Pathol, 2012. **138**(4): p. 535-44.

296. Takano, M., et al., *Paclitaxel-resistance conferred by altered expression of efflux and influx transporters for paclitaxel in the human hepatoma cell line, HepG2.* Drug Metab Pharmacokinet, 2009. **24**(5): p. 418-27.

297. Peters, D., J. Freund, and R.L. Ochs, *Genome-wide transcriptional analysis of carboplatin response in chemosensitive and chemoresistant ovarian cancer cells.* Mol Cancer Ther, 2005. **4**(10): p. 1605-16.

298. Kaaijk, P., et al., *Cell proliferation is related to in vitro drug resistance in childhood acute leukaemia.* Br J Cancer, 2003. **88**(5): p. 775-81.

299. Shain, K.H. and W.S. Dalton, *Cell adhesion is a key determinant in de novo multidrug resistance (MDR): new targets for the prevention of acquired MDR.* Mol Cancer Ther, 2001. **1**(1): p. 69-78.

300. Duesberg, P., R. Stindl, and R. Hehlmann, *Origin of multidrug resistance in cells with and without multidrug resistance genes: chromosome reassortments catalyzed by aneuploidy.* Proc Natl Acad Sci U S A, 2001. **98**(20): p. 11283-8.

301. Duesberg, P., R. Stindl, and R. Hehlmann, *Explaining the high mutation rates of cancer cells to drug and multidrug resistance by chromosome reassortments that are catalyzed by aneuploidy.* Proc Natl Acad Sci U S A, 2000. **97**(26): p. 14295-300.

302. Kusumbe, A.P. and S.A. Bapat, *Cancer stem cells and aneuploid populations within developing tumors are the major determinants of tumor dormancy.* Cancer Res, 2009. **69**(24): p. 9245-53.

303. Alexandre, J., et al., *Novel action of paclitaxel against cancer cells: bystander effect mediated by reactive oxygen species.* Cancer Res, 2007. **67**(8): p. 3512-7.

304. Berndtsson, M., et al., *Acute apoptosis by cisplatin requires induction of reactive oxygen species but is not associated with damage to nuclear DNA.* Int J Cancer, 2007. **120**(1): p. 175-80.

305. Martindale, J.L. and N.J. Holbrook, *Cellular response to oxidative stress: signaling for suicide and survival.* J Cell Physiol, 2002. **192**(1): p. 1-15.

306. Wangpaichitr, M., et al., *The relationship of thioredoxin-1 and cisplatin resistance: its impact on ROS and oxidative metabolism in lung cancer cells.* Mol Cancer Ther, 2012. **11**(3): p. 604-15.

307. Voskoglou-Nomikos, T., J.L. Pater, and L. Seymour, *Clinical predictive value of the in vitro cell line, human xenograft, and mouse allograft preclinical cancer models.* Clin Cancer Res, 2003. **9**(11): p. 4227-39.

308. Cespedes, M.V., et al., *Mouse models in oncogenesis and cancer therapy.* Clin Transl Oncol, 2006. **8**(5): p. 318-29.

309. Ricci C, M.L., Danti S., *Cancer tissue engineering new perspectives in understanding the biology of solid tumours: a critical review.* OA Tissue Engineering 2013. **1**(1): p. 4.

310. Fong, M.Y. and S.S. Kakar, *Ovarian cancer mouse models: a summary of current models and their limitations.* J Ovarian Res, 2009. **2**(1): p. 12.

311. Mullany, L.K. and J.S. Richards, *Minireview: animal models and mechanisms of ovarian cancer development.* Endocrinology, 2012. **153**(4): p. 1585-92.

312. Orsulic, S., et al., *Induction of ovarian cancer by defined multiple genetic changes in a mouse model system.* Cancer Cell, 2002. **1**(1): p. 53-62.

313. House, C.D., L. Hernandez, and C.M. Annunziata, *Recent technological advances in using mouse models to study ovarian cancer.* Front Oncol, 2014. **4**: p. 26.

314. Flesken-Nikitin, A., et al., *Induction of carcinogenesis by concurrent inactivation of p53 and Rb1 in the mouse ovarian surface epithelium.* Cancer Res, 2003. **63**(13): p.59-63.

315. Dinulescu, D.M., et al., *Role of K-ras and Pten in the development of mouse models of endometriosis and endometrioid ovarian cancer.* Nat Med, 2005. **11**(1): p. 63-70.

316. Yoshida, T., et al., *Gene expression changes in a chemoresistant model with human esophageal cancer xenografts using cDNA microarray.* Anticancer Res, 2009. **29**(4): p. 1163-8.

317. Masazza, G., et al., *Malignant behavior and resistance to cisplatin of human ovarian carcinoma xenografts established from the same patient at different stages of the disease.* Cancer Res, 1991. **51**(23 Pt 1): p. 6358-62.

318. Aird, R.E., et al., *In vitro and in vivo activity and cross resistance profiles of novel ruthenium (II) organometallic arene complexes in human ovarian cancer.* Br J Cancer, 2002. **86**(10): p. 1652-7.

319. Parker, R.J., et al., *Acquired cisplatin resistance in human ovarian cancer cells is associated with enhanced repair of cisplatin-DNA lesions and reduced drug accumulation.* J Clin Invest, 1991. **87**(3): p. 772-7.

320. Rattan, R., et al., *Metformin suppresses ovarian cancer growth and metastasis with enhancement of cisplatin cytotoxicity in vivo.* Neoplasia, 2011. **13**(5): p. 483-91.

321. Tang, X.H., et al., *Cross-reacting material 197, a heparin-binding EGF-like growth factor inhibitor, reverses the chemoresistance in human cisplatin-resistant ovarian cancer.* Anticancer Drugs, 2014. **25**(10): p. 1201-10.

322. Altomare, D.A., et al., *AKT and mTOR phosphorylation is frequently detected in ovarian cancer and can be targeted to disrupt ovarian tumor cell growth.* Oncogene, 2004. **23**(34): p. 5853-7.

323. Cristiano, B.E., et al., *A specific role for AKT3 in the genesis of ovarian cancer through modulation of G(2)-M phase transition.* Cancer Res, 2006. **66**(24): p. 11718-25.

324. Kurose, K., et al., *Frequent loss of PTEN expression is linked to elevated phosphorylated Akt levels, but not associated with p27 and cyclin D1 expression, in primary epithelial ovarian carcinomas.* Am J Pathol, 2001. **158**(6): p. 2097-106.

325. West, K.A., S.S. Castillo, and P.A. Dennis, *Activation of the PI3K/Akt pathway and chemotherapeutic resistance.* Drug Resist Updat, 2002. **5**(6): p. 234-48.

326. Hay, N., *The Akt-mTOR tango and its relevance to cancer.* Cancer Cell, 2005. **8**(3): p.

179-83.

327. Powis, G., et al., *Wortmannin, a potent and selective inhibitor of phosphatidylinositol-3-kinase.* Cancer Res, 1994. **54**(9): p. 2419-23.

328. Yun, J., et al., *Wortmannin inhibits proliferation and induces apoptosis of MCF-7 breast cancer cells.* Eur J Gynaecol Oncol, 2012. **33**(4): p. 367-9.

329. Kim, W., et al., *Enhancement of tumor radioresponse by wortmannin in C3H/HeJ hepatocarcinoma.* J Radiat Res, 2007. **48**(3): p. 187-95.

330. Zhao, J.X., et al., *Wortmannin enhances cisplatin-induced apoptosis in human ovarian cancer cells in vitro.* Eur Rev Med Pharmacol Sci, 2014. **18**(17): p. 2428-34.

331. Shi, Y., et al., *Rapamycin enhances apoptosis and increases sensitivity to cisplatin in vitro.* Cancer Res, 1995. **55**(9): p. 1982-8.

332. Huynh, H., C.C. Teo, and K.C. Soo, *Bevacizumab and rapamycin inhibit tumor growth in peritoneal model of human ovarian cancer.* Mol Cancer Ther, 2007. **6**(11): p. 59-66.

333. Schlosshauer, P.W., et al., *Rapamycin by itself and additively in combination with carboplatin inhibits the growth of ovarian cancer cells.* Gynecol Oncol, 2009. **114**(3): p. 516-22.

334. Cepeda, V., et al., *Biochemical mechanisms of cisplatin cytotoxicity.* Anticancer Agents Med Chem, 2007. **7**(1): p. 3-18.

335. Badr, C.E., et al., *Real-time monitoring of nuclear factor kappaB activity in cultured cells and in animal models.* Mol Imaging, 2009. **8**(5): p. 278-90.

336. Roth, D.J., et al., *A novel method of monitoring response to islet transplantation: bioluminescent imaging of an NF-kB transgenic mouse model.* Transplantation, 2006. **81**(8): p. 1185-90.

Chapter 8

Appendix: Materials and Methods

8.1 .Cell culture: Cell lines and Subculturing

Reagents and Chemicals

Reagents/Chemicals	Source
DMEM, MEM, McCoy's Culture medium	Gibco/Invitrogen, USA
Foetal Bovine Serum (FBS)	Gibco/Invitrogen, USA; Hi media, India
Penicillin-Streptomycin	Gibco/Invitrogen, USA;
Trypsin-EDTA	Gibco/Invitrogen, USA;
Puromycin, G418	Sigma, USA;
DMSO	Sigma, USA;
Superfect transfection reagent	Qiagen, Valencia, CA

Composition of Phosphate Buffered Saline (PBS) (pH 7.4) 10X / 1L:

80g NaCl, 2g KCl, 14.4g Na_2HPO_4, 2.4g KH_2PO_4, Dissolve in 800ml autoclaved water. Adjust the pH 7.4. Make up the volume to 1L.

Cell culture

Standard aseptic practice was followed for performing cell culture. The different ovarian cancer cell lines used their respective media are shown below:

Cell line	Origin	Source	Culture Medium
PA1	Teratocarcinoma (Germ cell ovarian cancer)	NCCS, Pune, India	DMEM
A2780	Undifferentiated EOC	ATCC	DMEM
SKOV3	Serous Adeno-carcinoma	ATCC	McCoy's

All of these adherent cell lines were maintained and sub-cultured in their respective media supplemented with 10% FBS, 100U/ml penicillin and 100 µg/ml streptomycin solutions as shown in Table. For experimental procedure, each of these cell lines were seeded to achieve ~60 % confluency.

Procedure of Subculturing

1. Cell culture media from culture plates were aspirated and cells were gently washed with 1X sterile PBS twice.
2. 1ml trypsin (for 10cm dish) was added and the cells were incubated at 37^0C for 5 to 7 min (till cells started detaching from substratum).
3. 3ml complete medium was added to neutralize trypsin action (complete medium contains serum which neutralizes trypsin action).
4. Single cell suspension was made by gently pipetting and cells were centrifuged at 1000rpm for 5min. Supernatant was discarded and the cells were resuspended in 1ml complete medium to make a single cell suspension culture.
5. Viable cell count from cell suspension was estimated by trypan blue dye exclusion method. In brief, viable cells (bright cells due to exclusion of dye) were counted from 10µl mixture of cell suspension and trypan blue dye (1:1 ratio) using haemocytometer and number of cells per ml were calculated using following formula:

No of cells/ml= average number of cells per WBC chamber x 10^4.

6. Further cells were either sub cultured with 1:4 slit ratio into new culture vessel(s) or seeded according to the requirement for experimental purpose.
7. Cells were fed with complete medium and incubated at 37^0C in 5% CO_2.

Cryopreservation

Cryopreservation is a method used for long term storage of cell cultures. . Cryopreservation media generally consists of a base medium, cryo-protective agent, and a protein source.

Cryoprotective agents reduce the freezing point of the medium and reduces the risk of ice crystal formation, which can damage cells and cause cell death during freezing.

1. Cells were trypsinized as described above and single cell suspension was made by gently aspirating the cells.
2. Cell number was calculated using haemocytometer.
3. Cell suspension was centrifuged at 1200 rpm for 5min at 4°C and the supernatant was discarded.
4. Freezing medium was prepared by adding 50-70% serum to complete medium along with 5%-8% of DMSO.
5. 1×10^6 - 2×10^6 cells were gently resuspended in 1ml of chilled freezing medium with gentle pippeting and immediately transferred to a cryopreservation vial (cryo vials).

9. Cryo vials were then transferred to chiller were temperature reduces $1\text{-}2^0$/hr at -80^0C for overnight and then transferred to liquid nitrogen for cryopreservation.

Revival of cryopreserved cells

1. Cryo vial from the liquid nitrogen was thawed at room temperature for approximately 35 minutes and immediately added to microfuge tube containing medium.
2. DMSO is toxic to cells. Thus to remove DMSO, cells were centrifuged at 700 rpm for 5min at 4°C and the cell pellet was resuspended in complete media with gentle pipetting. Then the cell suspension was transferred to a new culture vessel or plate.
3. Cells were incubated at 37°C in 5% CO2 and allowed to adhere to the substratum.

Transfection

Transfection is the process of deliberately introducing nucleic acids in eukaryotic cells by non-viral methods. Transfection was done using superfect transfection reagent as per

manufacturer's instructions. In brief, the following procedure was followed for transient/stable transfection of cell lines :

1. Prior to the day of transfection, a required amount of viable cell were seeded in culture vessel, primarily in 24well plate.

2. DNA-Superfect reagent complex were prepared by adding required amount of plasmid/s and transfection reagent in appropriate amounts of incomplete medium with gentle mixing. This mixture was then incubated for 10 minutes at room temperature.

4. In the meantime. the medium was aspirated from the culture vessel and washed twice with 1X PBS.

5. Definite amount of complete media was added to the transfection mixture and this was administered in the culture vessel. The plate was swirled gently to uniformly distribute the complex and incubated at 37°C, 5% CO2.

6. After 3hours, the transfection media was aspirated, washed with 1X PBS and complete media was added to the cells.

For stable transfection, after 24-48 h of transfection, the cells are trypsinized and are subcultured in the selection media containing antibiotics like puromycin or G418.

8.2 MTT Assay

MTT assay is a colorimetric assay for assessing cell viability. Cellular enzymes like NAD(P)H-oxidoreductase enzyme reflects the number of viable cells present. These enzymes are capable of reducing the tetrazolium dye MTT 3-(4,5-dimethylthiazol-2-yl)2,5-diphenyltetrazolium bromide) into its insoluble formazan crystals. The absorbance of the coloured solution can be quantified by the spectrophotometer at wavelength 560-670nm.

Source of reagents

Reagents/Chemicals	Source
DMSO	Sigma, USA
MTT	Sigma, USA

Procedure

1. The cells were seeded in 96 well plate at density of 2000 cells per well. The experiment was done in quadruplet.

2. According to the need of experiment either cytotoxicity of drugs or cell proliferation the cells were proceeded for the experiment and incubated for required duration at 37ºC, 5% CO_2.

3. All the cytotoxicity test were performed after drug treatment and the cells were incubated for 72h. For cell proliferation assay, the cell were seeded in required amount and incubated for different time points like (0, 24,48 h ,etc.)

4. At end points, cells were treated with 20µl of 5mg/ml MTT and incubated for 3 hours.

5. The spent media from each well were removed completely.

6. 100µl DMSO per well was added to solubilise the dye.

7. It was then kept in shaker for 15-20 minutes until the whole dye solubilised and then preceded for measuring the absorbance at wavelength 560nm and 670nm.

Note- The absorbance at 560nm is subtracted from the absorbance at 670nm to remove the background caused by the presence of DMSO.

8.3. Propidium Iodide (PI) Staining & Cell Cycle Analysis

Source of reagents

Reagent/chemicals	Source
Propidium Iodide (PI)	Sigma, USA
RNase A	Sigma, USA
DAPI	Sigma, USA

Preparation of PI buffer

Reagents	Stock	Use (for 500µl)
1×PBS	-	470µl
RNAse A	1µg/µl	5µl
PI stain	1 µg/µl	25µl

Cell-cycle analysis is a method in cell biology that employs flow cytometry to distinguish cells in different phases of the cell cycle. It is quantification of DNA by DNA-binding fluorescent dyes. The premise of these dyes is that they are stoichiometric i.e. they bind in proportion to the amount of DNA present in the cell. In this way cells that are in S phase will have more DNA than cells in G1. They will take up proportionally more dye and will fluoresce more brightly until they have doubled their DNA content. The cells in G2 will be approximately twice as bright as cells in G1. The detailed procedure for flow cytometry is given as below.

1. The cells (1 x 10^6) were harvested were washed with 1×PBS after centrifugation at 1200rpm for 5 minutes and supernatant was discarded.
2. Ice cold 70% alcohol was added (1ml/10^6 cells) dropwise with gentle tapping and cells pellet was resuspended.
3. The cells were stored at -20ºC for at least 1 h or long after proper labelling on the centrifuge tubes.

4. Fixed cells were collected in another centrifuge tube and were pelleted by spinning at 1200 rpm for 5 minutes and alcohol as supernatant was discarded.
5. The cells were washed thrice with 1×PBS, centrifuged and supernatant discarded.
6. **For staining with PI:** 500µl of PI buffer was poured in each centrifuge tube, pipetted gently and collected in dark condition.
7. The cells in PI buffer were incubated in pre-warmed incubator/water-bath at 37ºC for 1h.
8. The FACS-tubes were tapped every 10 minutes to mix the cell and buffer properly. The cells were passed through a 26 gouge needle followed by PI fluorescence acquisition using FACS Caliber.

(Note: PI is light sensitive. So, PI buffer was made fresh before use. PI buffer in tube were stored in amber coloured bottle to minimise light exposure.)

9. **For staining with DAPI:** 500µl of DAPI buffer (0.5µg/ ml) along with RNase A (0.1 µg/ ml) was poured in each centrifuge tube and transferred to FACS-tubes. The FACS-tubes were tapped every 10 minutes to mix the cell and buffer properly. The cells were passed through26 gouge needle. Followed by DAPI fluorescence acquisition using FACS Caliber.

8.4 Genomic DNA Isolation

Source of reagents

Reagent/chemicals	Source
RNase A (10µg/µl)	Sigma, USA
Phenol	ThermoFischer, USA
Chloroform	Fischer Scientific, India
Proteinase K	Sigma, USA
Sodium Acetate (3M)	HiMedia, India
Isopropanol	Fischer Scientific, India

Composition of Digestion Buffer

50mM Tris, pH 8, 1mM EDTA, 0.5% Tween 20) along with Proteinase K (50ug/ml)

Procedure

Genomic DNA from mammalian cells is usually isolated by using a hypotonic lysis buffer containing EDTA, a detergent (Tween 20) and proteinase K followed by extraction with phenol chloroform and alcohol precipitation. This method yields genomic DNA fragments ranging from 100-150 kb, suitable as a source for amplification of required DNA fragments. The detailed procedure for genomic isolation is as follows.

1.1x10^6cells were harvested by cell scrapper and pelleted by centrifuging at 1200rpm for 5min at 4°C.

2.The cells was completely resuspended in 500µl of Digestion buffer by vortex mixing and the reaction was incubated over night at 55°C in a water bath.

3. 10µl RNase A was added in the above mixture and incubated for 1-2 h at 37°C.

4. The above mixture was divide into two. In one part 500µl buffer saturated phenol was added to the lysed cell suspension, mixed vigorously for 15 min, centrifuged at 8000 rpm at 20°C (cold centrifuge) for 10 min and the upper aqueous phase was carefully collected in a fresh tube.

5. Equal volume of phenol: chloroform (1:1) mix was added to the aqueous phase, invert mixed vigorously for 15 min and centrifuged at 8000 rpm for 10 min.

6. The upper aqueous phase was collected in a fresh tube and extraction was repeated with chloroform (200µl) invert-mixed vigorously for 15 min were separated by centrifugation as mentioned earlier.

7. Aqueous phase obtained was collected in a fresh tube and 3M Sodium acetate (1/10 volume) was added along with isopropanol (7/10 volume) and incubated at -20°C overnight.

8. The reaction mixture was centrifuged at 14000 rpm for 20 minutes at RT and washed with 500µl of 70% ethanol. DNA pellet obtained after decantation of ethanol was semi air

dried and resuspended in approximately 50 µl Tris EDTA buffer (TE solution (pH 8.0)) or autoclaved distilled water.

10. The quantity and quality of DNA was assessed by measuring the OD260/OD280 ratio. For long term storage, the DNA preparation was kept at -20°C for further use.

8.5. Copy Number analysis by Real-Time Quantitative PCR

The PIK3CA copy number was analysed by SYBR Green Real time PCR amplification assay on an QuantStudio^{TM}12K Flex Real-Time PCR System (Life Technologies).Each amplification reaction was checked for the absence of nonspecific PCR products by melting curve analysis. Type III collagen gene (COL8A1, 3q12-q13.1) was used as a control gene and is located on the same chromosomal arm as PIK3CA. The table shows the primer used in the qPCR; the qPCR reactions for each sample and each gene were performed in triplicate.

Primers	Sequences
PIK21E Forward	5'-ATCTTTTCTCAATGATGCTTGGCT3'
PIK 21E Reserve	5'-CTAGGGTCTTTCGAATGTATG-3'
COLA81Forward	5'-GGGCTAAGAAAGGCAAGAATGG-3'
COLA81Reverse	5'-GTGGGAAAGGTGCGGTTAGCT-3'

The primer for the PIK3CA gene was obtained from the exon region of 21 of the PIK3CA gene (PIK 21 E).The amplicon length of PIK3CA and COLA81 genes are 81 and 78 base pairs respectively. PCRs were carried out in a final volume of 20µl containing 20 ng of genomic DNA, 300 nM each primer (for both PIK3CAand COL8A1, in independent reactions) and 1X Power SYBR Green PCR Master Mix (Applied Biosystems, Foster City, CA). The PCR conditions were as follows:

Sr.No.	Steps	Temperature (°C)	Time sec)
1	Initial Denaturation	95	600

2	Denaturation	95	15
3	Annealing	52	60
4	Repeat steps 2 and 3	40 cycles	
5	Sybr Green dissociation step 1	95	15
6	Sybr Green dissociation	60	15
	step 2		
7	Sybr Green dissociation step 3	95	15

Samples were analyzed in triplicate. Each amplification reaction was checked for the absence of nonspecific PCR products by melting curve analysis. After validating that the efficiencies of PCR reactions of both PIK3CA and COLA81 were equal, the PIK3CA copy number calculation was carried out using comparative C_t method. PIK3CA gene copy number in normal ovarian cell line (IOSE) genomic DNA was set as 2 and copy number of more than 4 in cell lines was considered as increased.

Data analysis using the $2^{-\Delta\Delta Ct}$

The C_t values provided from the real time PCR instrumentation were imported into spread sheet programme such as Microsoft Excel. Real time PCR was performed from the corresponding genomic DNA from each cell line (IOSE, PA1 and A2780). The change in the expression of the PIK3CA target gene was normalised to the COLA81 gene. The data were analysed using the equation:

ΔΔCt = (Ct PIK3CA − Ct COLA81) Target – (Ct PIK3CA – Ct COLA81) IOSE

The fold change of the reference cell line is 1(since 2^0 =1). The fold change of more than one should be considered any change in the PIK3CA copy number. PIK3CA gene copy

number of IOSE 364 and A2780 was known and set as 2. A fold change of more than 2 would be considered as change in copy number.

8.6. ICPMS analysis

Inductively coupled plasma mass spectrometry (**ICP-MS**) is a type of mass spectrometry which is capable of detecting metals and several non-metals at concentrations as low as one part in 10^{15} (part per quadrillion, ppq) on non-interfered low background isotopes. This is achieved by ionizing the sample with inductively coupled plasma and then using a mass spectrometer to separate and quantify those ions. The detailed protocol is as follows:

Preparation of standards

Cisplatin (2000 ppm) standard was prepared by addition of 2 mg cisplatin in 200 µl DMSO and 200 µl concentrated HCl and 600 µl distilled water.

Preparation of samples for ICPMS analysis

To dissolve cell samples, 200 ul of conc. HCl is required. (Normally, the cells dissolve in concentrated HCl within 1h. If not completely solubilized, the samples should be heated in a water bath at90 for 10 – 15 minutes).200µl of DMSO was added to the sample to normalise the contribution of DMSO in standard. Once dissolved, volume was made up to
3 ml with D/W.

Procedure:

1. Approximately, 10x 10^6 cells were used to get sufficient Pt concentration that can be detected by ICP-MS for cisplatin treated samples.
2. Samples were prepared by the above mentioned procedure, and debris were removed by spinning down. (Note: ICP-MS requires clear solutions for analysis.)
3. Gold was used as an internal standard for ICP-MS analysis in the facility of BARC

(VGPQ2 plus, inductively coupled plasmon mass spectrometer (ICPMS) system), Mumbai, India.

8.7. DCFDA Assay

DCFDA assay is the most straightforward techniques that use cell permeable fluorescent and chemiluminescent probes. It is the cell permeant reagent 2', 7' –dichloro fluorescein diacetate (DCFDA), a fluorogenic dye that measures hydroxyl, peroxyl and other reactive oxygen species (ROS) activity within the cell. After diffusion in to the cell, DCFDA is deacetylated by cellular esterases to a non-fluorescent compound, which is later oxidized by ROS into 2', 7' –dichlorofluorescin (DCF). DCF is a highly fluorescent compound which can be detected by fluorescence spectroscopy with maximum excitation and emission spectra of 495nm and 529nm respectively.

Source of reagent

DCFDA dye was procured from ABCAM

Procedure

1. Equal amount of cells (75000 cells) were seeded.

2. Endogenous levels of ROS was calculated by collecting the cells (1,500 rpm, 4^0, 10min) and staining with DCFDA dye. Unstained cells were kept as controls. Three controls were used (only cells, cells + DCFDA, Cells + DCFDA+H_2O_2).

3. Samples are washed with 1X PBS and centrifuged (15,000 rpm, 4^0, 10min).

4. In each sample 300-400 µl 1X PBS was added.

5. 0.5 µM DCFDA (Stock, 5mM, made in DMSO) was added in the samples and placed in dark place for 20-30 min incubation at 37^0 C.

6. Samples were analysed directly in FACS-Caliber.

8.8 Bacterial Cell Culture

Reagent/chemicals	Source
LB broth	Hi media, India
LB agar	Hi media, India
Yeast extract	Hi media, India
Bactotryptone	Hi media, India
Kanamycin	Sigma, USA;
Ampicillin	Sigma, USA;
DMSO	Sigma, USA;

Luria-Bertani (LB) medium

A minimal growth medium used is used for culture and maintenance of different *E. coli* strain DH5α. This strain is further used for harbouring desired plasmids. Powdered Luria Broth (20 g) was dissolved in 800 ml deionized 'MilliQ' processed water (D/W) and the volume was adjusted to 1 litre (L) with D/W and sterilized by autoclaving. For making LB-agar plates, 35 g Luria agar powder was dissolved/ L sterilized by autoclaving and poured in 90 mm sterile plates. Specific antibiotic either ampicillin or kanamycin was added in the medium according to the plasmid antibiotic marker.

Preparation of ultra-competent cells

Composition of Transformation Buffer (TB)

The following components were added to 100 ml of distilled water; 10mM PIPES,15 mM CaCl2, 250 mM KCl, adjusted pH to 6.7 with 5N KOH, 55 mM MnCl2, filter sterilized through 0.2 μ membrane filter.

Composition of Super Optimal Broth (SOB)

Following components were mixed in the required volume of D/W; 2% Bactotryptone, 0.5%Yeast extract, 10 mM NaCl, 2.5 mM KCl, 10 mM MgCl2, 10 mM MgSO4;

P*rocedure*

1. E.coli strain DH5α strain glycerol stock was streaked on a fresh LB agar plates without antibiotics and incubated overnight at 37°C.

2. Single colony was inoculated in 250 ml SOB broth and incubated at 18°C /250 rpm till

O.D.600 reached ~0.4 (Approximately 3-4 days of incubation are required).

3. The cells were harvested by pelleting down at 4°C and resuspended in 80 ml of TB followed by incubation on ice for 10 min and centrifugation.

4. The cell pellet was resuspended in 18.6 ml TB. 1.4 ml (7%) DMSO was added to the cells and mixed completely.

5. 100µl aliquots of the cells were made in sterile microfuge tubes and snap frozen in liquid nitrogen followed by storage at -80°C.

Bacterial transformation

1. Competent cells (100 µl) were thawed on ice and mixed with 1-5ng of plasmid DNA or 20 µl of ligation mixture and incubated on ice for 30 min.
2. Heat shock was given to the mixture at 42°C for 60 sec and the sample was snap chilled on ice.
3. LB medium was added to the cells and incubated at 37°C for 60 minutes at 170 rpm.
4. The cells are then plated on an LB agar plate with the appropriate antibiotic.

Plasmid DNA mini-preparation:

The plasmid isolation was performed following the procedure described in the Qiagen mini prep kit. Briefly following steps were performed.

1. Overnight grown, 1-5 ml of bacterial cultures transformed with plasmids were spun in a micro-centrifuge tube at 3500rpm for 15-20 minutes at 4°C.

2. Bacterial pellet was resuspended in 250µl of Buffer P1 (Re-suspension buffer containing RNase (10mg/ml)).

3. The cells were incubated at room temperature (RT) for 5 min and 250µl Buffer P2 (lysis solution) was added followed by invert mixing.

4. The cells were incubated at RT for 5 min and 350µl of Buffer N3 (neutralizing solution) was added and incubated at RT for 5 min. after complete invert mixing.

5. The above mixture was then centrifuged at 12,000Xg for 10 min.

6. The supernatants from step 5 was applied to the QIAprep spin column by decanting or pipetting.

7. The column was centrifuged for 30–60 s and the flow-through was discarded.

8. QIAprep spin column was washed by adding 0.75 ml Buffer PE and centrifuging for 30–60 s.

9. The flow-through was discarded and centrifuged at full speed for an additional 1 min to remove residual wash buffer.

10. The QIAprep column was placed in a clean 1.5 ml micro centrifuge tube.DNA was eluted by addition of 50 µl Buffer EB (10 mM Tris Cl, pH 8.5) or water to the center of each QIAprep spin column for 1 min and centrifuged for 1 min.

8.9. Cloning

Polymerase Chain Reaction (PCR)

PCR is a method of an enzymatic amplification of the DNA *in vitro*. The reaction uses a pair of oligonucleotide primers that hybridizes on the opposite strands and flank the target sequence to be amplified. The elongation of DNA strands is carried out by a thermostable polymerase in a cell free system and repetitive cycles involving denaturation, annealing and elongation exponentially accumulates the amplified products of specific size and sequence.

The products are then separated on an appropriate gel and visualized under UV light in presence of intercalating dyes.

Source of reagent

A typical PCR reaction mixture contains the following components.

PCR Reaction Mix components	**Source**
DNA Polymerase and PCR buffer containing $MgCl_2$	Phusion® DNA Polymerase Kit(Finnzymes)
	Standard Taq Polymerase Kit (Fermentas; NEB)
dNTPs	Hi media, India
Primers	Sigma, USA

Following below contents were mixed in PCR tube and PCR was set in a thermal cycler (Bio-Rad, CA).

Components	**Final concentration**
PCR Buffer	1X
dNTPs (1mM)	0.1 mM
Forward Primer	5-10 pM
Reverse Primer	5-10 pM
Enzyme	1unit
Template DNA	10-100ng
Distilled water (D/W)	Total volume 25 µl

The cycling profile was standardized according the target DNA to be amplified.

Amplified product is visualised and analysed by agarose gel electrophoresis.

Agarose gel electrophoresis and Gel extraction:

Composition of the Tris Borate–EDTA buffer (TBE)

Tris Borate EDTA (TBE) buffer: 0.9 M Tris base, 0.9 M Boric acid, 0.02 M EDTA (10X buffer stock was made and diluted to 1X for use)

Other components: Agarose powder, 6X gel loading dye; Ethidium bromide (EtBr): 0.5 μg/ml; agarose, DNA markers: 100 bp, 1 Kb or Mass ruler.

Procedure

1. The agarose gel percentage varying from 0.7% – 2% (according to the size of the DNA to be resolved) was casted on the gel tray. EtBr was added while casting the gel as an intercalating agent.
2. Solidified gel was transferred to the electrophoresis tank that has electrode fitted to it at the two ends.
3. The required 1X TBE buffer is then poured into the tank over the gel. Before loading the PCR product into the wells, the PCR product is mixed with the loading dye containing glycerol and bromophenol blue which indicate the DNA migration front.
4. Standard DNA markers of known fragment sizes were run in parallel to the samples in order to have standard reference. The gel was run at a constant voltage.
5. EtBr stained DNA bands were visualized and documented on a Gel documentation system.

Gel extraction

The PCR amplified product was gel extracted and purified by using QIAGEN gel extraction kit. Briefly, the following procedure was followed:

1. The DNA fragment from the agarose gel was excised with a clean, sharp scalpel.
2. The gel slice was weighed in a micro centrifuge tube. 3 volumes Buffer QG was added to 1 volume gel (100 mg ~ 100 μl).

3. Reaction was incubated at 50°C for 10 min (or until the gel slice has completely dissolved). Vortex the tube every 2–3 min to help dissolve gel.

4. 1 gel volume of isopropanol was added to the sample and mixed. Thereafter, a QIAquick spin column were placed on a 2 ml collection tube and the above reaction mix was added in the column.

5. The tube was incubated for 1-2 minutes and centrifuged for 1 min at 13000 rpm.

6. The flow-through was discarded and further washed with 0.5ml of buffer QG by centrifugation for 1min at 13000rpm.

7. Buffer PE (0.75 ml) was added to QIAquick column and was incubated for 5 minutes before centrifuging for 1 min at 13000 rpm. The flow-through was discarded and was given another wash with buffer PE.

8. An additional dry spin was given to the column and the column was placed in a clean 1.5 ml micro centrifuge tube.

9. To elute DNA, 50 µl Buffer EB (10 mM Tris·Cl, pH 8.5) or water was added to the centre of the QIAquick membrane and centrifuged at 13000 rpm for 1 min.

Restriction Digestion

Source of RE enzymes

NheI, BglII, Bam HI, and EcoRI was used from NEB, UK.

One unit of restriction endonuclease (RE) activity is defined as the amount of enzyme required to completely digest 1µg of substrate DNA in a total reaction volume of 50µL in one hour using the buffer provided. Restriction digestion is a tool for many molecular applications like ligation, gene isolation, etc.

Both insert and vector were digested with two RE enzymes simultaneously. NEB buffer that results in maximum activity of both the enzymes was chosen using the enzyme activity chart.

Before beginning with digestion the recommended buffer was allowed to thaw completely on ice also the water bath was set at 37°C. A typical restriction digestion mix consists of following components: 10 X NEB buffer, DNA (insert/vector), Restriction enzyme and autoclaved distilled water. The reaction mixture was incubated at 37°C water bath, overnight.

Ligation

Ligation is performed by using DNA ligase is a special type of enzyme that catalyzes the formation of phosphodiester bond between juxtaposed 5'phosphate and 3'hydroxyl terminal in duplex DNA or RNA. This enzyme joins blunt and sticky ended termini as well as repair single stranded nicks in duplex DNA, RNA or DNA/RNA hybrids. The ligation reaction was set depending upon the concentration of the insert. Ideally the vector to insert ratio is (1:3) which is essential for carrying out successful ligation reaction.

Source of reagents

Quick ligase enzyme and its 10 X buffer was obtained from NEB, UK.

Ligation Reaction.

Reagents	**Test sample**	**Negative control**	**Positive control**
Insert	5µl (120ng)	--	--
Vector	1µL (40ng)	1 µl(40ng)	1 µl (10ng)
D/W	10µl	6µl	6µl
Buffer	2µl	2µl	2µl
Enzyme	1µl	1µl	1µl

1. The ligation reaction was carried out at room temperature and incubated for 10-15 minutes before performing bacterial transformation.

2. After transformation the LB agar plates were placed in the incubator for overnight. After 16-18 hrs of incubation, the plates were checked for colonies.

3. Colonies were cultured in LB broth and plasmid were isolated. Screening for the positive clone was performed by restriction digestion.

Positive clone obtained by cloning was further verified by DNA sequencing. The reaction mixture used for the sequencing reaction was as follows:

Component(s)	**Volume (µL)**
PIK3CA promoter Forward Primer (5pM)	**1**
PIK3CA promoter Reverse Primer (5pM)	1
Plasmid DNA (concentration < 300ng/ul)	1

Sequencing was performed using the ABI automated DNA sequencer present in the Genomics facility of ACTREC.

8.11. Total RNA Isolation, Visualisation and Quantification

Source of Reagents

Reagent/chemicals	**Source**
DEPEC	Sigma, USA
Total RNA isolation kit	BIOLINE
Formaldehyde	Sigma, USA
Formamide	Sigma, USA
Ethidium bromide	Sigma, USA
6X RNA loading	Sigma, USA
Agarose	INVITROGEN

Preparation of 10X MOPS buffer:

0.2M MOPS, 50mM sodium acetate, 10mM.

Preparation of Tank buffer:

30 ml 10X MOPS buffer+ 30ml formaldehyde and Volume was made upto 300ml.

Preparation of RNase Free MQ:

1ml of Diethyl Pyrocarbonate (DEPEC) was added to 1000ml of fresh MilliQ water and incubated overnight at 37°C. It was used after autoclaving.

Procedure:

Total RNA was isolated from different cell lines using total RNA isolation kit. Isolated RNA was further visualized on gel and quantified using Nano drop. Isolated RNA is further used to synthesize cDNA by reverse transcription PCR, synthesised cDNA is then used to check levels of different genes at transcript level using PCR.

Isolation of total cellular RNA:

1. Four million of cells were harvested and washed with 1X PBS for 5mins at 1200 rpm 4°C.

2. The supernatant was discarded.

3. The pellet was resuspended in Lysis buffer R (400µl) by pipetting and incubated for 3mins.

4. The lysed solution was transferred to Spin column R1 placed in a collection tube and it was spun at 10,000Xg for 2 minutes.

5. The filtrate was saved and the Spin column R1 was discarded.

6. Equal volume of 70% ethanol (400µl) was added in the filterate, mixed well and transferred to Spin column R2 placed in a fresh collection tube.

7. The column was spun at10,000 X g for 2 minutes. The filterate was discarded.

8. The Spin column R2 was placed in the fresh collection tube. 500µl of wash buffer AR was added in the column and spun at 10000Xg for 1min. The filterate was discarded.

9. Wash buffer BR (700µl) was added in the column and spun at 10000Xg for 1minute.

10. The filterate is again discarded and the column is placed in the collection tube. A dry spin of 10000 X g for 3 minutes was given to the Spin column R2.

11. The Spin column R2 was placed in the 1.5cm^3 elution tube and 30-80µl (50µl) of RNase free water to spin column R2.

12. The column was incubated for 5-10 mins and spun at 6000Xg for 1 minute to elute the

RNA. The eluted RNA was stored at -80°C. The RNA was quantified by using nanodrop.

Preparation of denaturing gel for visualisation of RNA (90ml):

Agarose(1.08g) + RNase free water: 76.5 ml was boiled to melt agarose completely. 10X MOPS buffer (9ml) and formaldehyde (4.5ml) and EtBr was added. The gel is poured in the gel casting tray with a comb and allowed to solidify.

Preparation of RNA sample for gel loading

Reagents	**Quantity(µl)**
Formaldehyde	1
Formamide	3
10X MOPS buffer	2
RNA sample	1-2

The following components are added to form a reaction mix:

The reaction mix is incubated for 5-10min a 65°C for denaturation. 6X RNA loading dye (1-2 µl) was added to load on a gel. The gel was visualised on UV trans-illuminator.

8.12. cDNA Synthesis from Total RNA, Semi-quantitative reverse transcriptase PCR and Real time quantitative (qPCR)

A good quality total RNA isolate has an O.D 260/280 ratio of 1.8-2 and O.D 260/230 ratio of 1.8 or more. The cDNA was synthesized from total RNA using a cDNA synthesis kit from NEB, UK, according to the manufacturer's protocol.

Procedure

1. cDNA synthesis reaction is set on ice as follows on ice:

   Nuclease free water: 9 µl

   Primer dT2sVN: 2 µl

   dNTP mix : 4 µl

   RNA (900ng/µl): 1 µl

   Total volume: 16 µl

2. The contents were mixed and kept at 70°C for 5 minutes on dry bath and later chilled on ice.
3. Following components were added to the 16 µl reaction mix

   10X RT buffer: 2 µl

   Murine RNase inhibitor: 0.1 µl

   Nuclease free water: 1 µl

   Reverse transcriptase enzyme: 0.5 µl

4. PCR tubes were kept in thermal cycler with following conditions

   42°C one hour for synthesis of cDNA from mRNA.

5. The reverse transcriptase enzyme was inactivated at 80°C for 5 minutes

6. The cDNA synthesized was checked for GAPDH a house keeping gene by reverse transcriptase PCR.

Semi-quantitative reverse transcriptase PCR reaction and quantitative RT-PCR (qRT-PCR) reactions.

A general principle and procedure of PCR is described in the section 8.9. In order to check gene expression semi-quantitative reverse transcriptase or quantitative real time PCR is used.

Procedure:

1. The semi quantitative PCRs were performed using 50ng cDNA per reaction and Taq DNA polymerase for amplification of the PCR product.
2. The qRT-PCRs were performed using 10ng cDNA per reaction and the ABI SYBR Green PCR Master mix as per the manufacturer's protocol.
3. Common semi quantitative RT-PCR and qRT-PCR primers were generated using the Oligo explorer software (Gene Link).
4. A few parameters were followed in making the real time primers:

a) Primers were designed between exon boundaries. b) The melting temperature (Tm) value of the primers were between 60ºC to 65ºC. c) The Tm difference between these primers was not be more than 5ºC. d) The self-annealing and loop formation within the primers were minimum or none. e) Primer dimer formation was minimum or none. f) Primers were designed in such a way that the PCR product size was not more than 200 bps and was normally kept between 80 to 150 bps. g) The primer length ranged between 19 to 25 bps. h) The Gibb's free energy (ΔG) value for primer dimer interactions or for primer looping should be preferably positive and should not be less than -5 kilo calories/moles. A negative value of ΔG indicates a thermodynamically favourable reaction, thus if primer dimer formation or primer looping or primer self-annealing has a negative ΔG, then the primers

will have a greater tendency to form dimers or loop or self-anneal than to bind to the template cDNA provided in the reaction mixture. This leads to failure of RT-PCR reactions. Thus, primers were selected such that the ΔG value for primer dimerization, looping and self-annealing was either 0 or +ve. The primers obtained with this criteria was verified using the BiSearch software to ensure that the PCR product obtained is specific for the mRNA and does not amplify any part of the chromosome and by Primer BLAST to ensure that the primers amplify only the specific target cDNA.

5. The primers were synthesized by Integrated DNA technologies (IDT) or Eurofins Scientific and delivered as High purity salt free (HPSF) oligonucleotides in a lyophilized form. The concentration of the primers were made up to 100pM by adding the required amount of water as mentioned by the manufacturer's protocol and stored for further use. A primer concentration of 10pM was required for semi quantitative RT-PCR while a primer concentration of 5pM was used for qRT-PCR.

8.13. Protein Estimation

Source of Reagents

Reagent/chemicals	Source
Passive Lysis buffer (5X)	Promega
Protease inhibitor cocktail (10X)	Sigma,USA
Bradford reagent	Sigma,USA

Preparation of lysates

1. Cells were harvested after trypsinisation by centrifugation at 1200 rpm for 5minutes at 4°C.

2. The cell pellet was washed with 1X PBS by centrifugation at 1200 rpm for 5 minutes.

3. Supernatant was discarded and approximately 50µl of 1X passive lysis buffer per one million cells was added.

4. Thereafter, 1µl of 10X protease inhibitor per 100µl of 1X passive lysis buffer was added in the cell lysate.

5. The reaction was thoroughly mixed by vortexing and incubated at RT for 10-15 minutes.

6. After incubation the reaction mixture was centrifuged at 13,000 rpm for 25 minutes at 4˚C.

7. The supernatant was collected and protein estimation was performed using Bradford reagent.

Bradford assay

Bradford is a colorimetric protein assay based on the absorbance shift of the dye Coomassie Brilliant Blue G-250 in which under acidic conditions the red/brown form of the dye is converted into its bluer form to bind to the protein being assayed. This colour change is estimated by using the formula obtained by plotting the absorbance of standards (1-5 µg/ml) in a linear regression analysis.

The procedure for the Bradford assay is as follows.

1. BSA standards were made by serially diluting 1mg/ml stock in 96 well flat bottom plates.

Concentration (µg)	**BSA(µL)**	**1X PBS (µL)**
1	1	4
2	2	3
3	3	2
4	4	1
5	5	0
Blank	0	5

2. Absorbance was measured at 595nm, values were subtracted against the blank and a standard curve was plotted by using the linear regression analysis. The formula derived from the standard curve was used for estimating protein concentration of the cell lysates.

3. Lysates were diluted 1:5 using 1X PBS.

4. 250µl of Bradford reagent was taken per well in a 96 well plate.

5. 5µl of protein sample per well was mixed thoroughly.

6. Colorimetric absorbance was taken at 595nm using a colorimeter.

7. Protein concentration was calculated using the formula derived from the standard curve.

8.14. Luciferase Reporter Assay

The luciferase reporter assay is commonly used as a tool to study gene expression at the transcriptional level. Luciferases make up a class of oxidative enzymes found in several species that enable the organisms that express them to 'bioluminesce' or emit light. The light emitted is a by-product of the oxidative reaction catalyzed by the luciferase enzyme. In a luciferase reporter system, a gene promoter (of interest) is fused with the cDNA encoding a luciferase enzyme (either firefly luciferase or renilla luciferase). Modifications in the promoter activity can be monitored by the measurement of luciferase enzyme activity which is directly proportional to the bioluminescence emitted.

Source of Reagents

Reagent/chemicals	**Source**
LAR II (Substrate for firefly luciferase *in vitro*)	Promega
Colenterazine (Substrate for renilla luciferase)	Biosynth
D-Luciferin (Substrate for firefly luciferase *in vivo*)	Biosynth
Dual Luciferase reporter assay system	Promega

Procedure for in vitro luciferase assay

1. 50µl of substrate was taken in the wells of 96-well plate
2. 10µl of lysate was added in each well
3. The combination was mixed properly with pipette tip.
4. Each of the luciferase reactions was measured in a Berthold luminometer for a period of 60 seconds.
5. The relative light unit per second (RLU/sec) obtained was normalised with protein estimated by Bradford method.

8.15. Western Blotting/ Immunoblotting

Immunoblotting is a technique used for analysis of individual proteins in a protein mixture (e.g. a cell lysate). The protein mixture is applied to a gel electrophoresis in a carrier matrix (SDS-PAGE, native PAGE, isoelectric focusing, 2D gel electrophoresis, etc.) to sort the proteins by size and charge in individual protein bands. The separated protein bands are then transferred to a carrier membrane (e.g. nitrocellulose membrane (NCM), nylon or PVDF). This process is called blotting. The proteins adhere to the membrane in the same pattern as they have been separated due to interactions of charges. The proteins on this immunoblot are then accessible for antibody binding for detection.

Source of reagents

Reagent/chemicals/ Equipment	**Source**
Acrylamide and Bisacrylamide	Sigma,USA
SDS	Sigma,USA
Ammonium Per sulphate (APS)	SRL Chemicals, India
N,N,N',N'-tetramethylethylenediamine TEMED	Sigma,USA
Glycine	Sigma,USA

Butanol	Qualigens
Pre-stained protein marker	Fermentas
Tris base	Sigma,USA
Nitrocellulose Membrane (NCM)	Mdi, India
Beta mercaptoethanol	Sigma,USA
Tween20	Sigma,USA
Sodium chloride	SRL Chemicals, India
Gel cast, run unit with power pack	BioRad

Composition of 30% Acrylamide

(30% acrylamide / 0.8% bisacrylamide) weight/volume in distilled water

Composition of Resolving Buffer

1.5mM Tris base, adjust the pH to 8.8 using 1N-HCl

Composition of Stacking Buffer

0.5mM Tris base, adjust the pH to 6.8 using 1N-HCl

Composition of Running Buffer

25mM Tris-Cl- 3.208g; 200mM Glycine-15.012g;0.1%w/v SDS-1g

Composition of Gel loading Dye

50mM Tris HCl, pH 6.8, 2% SDS, 20% Glycerol, 12.5mM EDTA, 0.02% Bromophenol blue.

Composition of Transfer buffer

25mM Tris base, 190mM Glycine, 0.04% SDS, 20% methanol

Composition of Tris Buffered Saline (TBS)

Tris base, 150mM NaCl, adjust the pH to 7.6 using 1N-HCL

Contents of resolving gel

Gel percent	Milli Q (ml)	30% acrylamide	1.5M Tris-Cl pH-8.8 (ml)	10% (w/v) SDS buffer (µl)
8	4.7	2.7	2.5	100
10	4.1	3.3	2.5	100
12	3.4	4	2.5	100
15	2.4	5	2.5	100

Degassing was carried out with pipette and 50µL of APS and 5µL TEMED was added followed by gentle mixing.

Contents of stacking gel

Gel percent	Milli Q (ml)	30% acrylamide (µl)	1.5M Tris-Cl pH-8.8 (ml)	10% (w/v) SDS buffer (µl)
4	1.26	260	500	10

10µL of APS and 2µL of TEMED was added to the mixture followed by swirling.

Preparation of sample

Appropriate volume of protein lysate for the desired concentration was taken and mixed with gel loading dye. The reaction mix was heated at 100°C on dry bath for 3 minutes and a short spin was given. The samples were kept on ice until they were loaded on the gel.

Composition of blocking buffer

1X TBS with 5% BSA

Composition of Wash buffer (TBSt)

1X TBS with 0.05% Tween 20

Composition of stripping buffer

20%SDS, 100µM β-mercaptoethanol and 50µM Tris, pH6.8

Procedure of Western blotting

1. Glass plates were cleaned thoroughly and were set up carefully in the casting stand.
2. According to the protein of interest, the required percentage of resolving gel was prepared.
3. Immediately the resolving gel solution was loaded between the glass plates using the pipette and the gel was overlaid with 200µL of water saturated butanol.
5. The gel was allowed to polymerize for 35-40 minutes.
6. After the resolving gel was solidified completely the butanol layer was washed thoroughly and the stacking gel was prepared.
7. The wells for loading the samples were formed by placing the 10-well comb. The gel was allowed to polymerize for 15-25 minutes.
8. The solidified gel was placed in the cassette and fitted with electrodes in the tank.
9. The tank was filled with 1X running buffer till $(1/4)^{th}$ of its volume. The comb was then gently removed and the wells were washed with the buffer to remove the traces of any acryl/bisacrylamide deposits.
10. The sample prepared was then loaded into respective wells and 4µL of pre-stained ladder was also loaded in one of the wells.

11. The gel was then allowed to run at 60V, 400mA. After the sample entered the resolving gel the voltage was gradually increased to 80V. The run was stopped as soon as the dye reached the bottom of the gel.

12. The gel, blotting paper and NCM were then soaked in 1X transfer buffer and incubated for 10 minutes.

13. Onto the base of the Trans blot system the two soaked blotting papers were placed one after another, the transfer buffer was poured on top of the membrane and the air bubbles were removed carefully. Then, the NCM was placed and the gel was placed over it properly.

14. The remaining two blotting papers were placed on the top of the gel and same as before the transfer buffer was poured, ensuring that the bubbles were removed. Then, the system was started and the transfer was set to 13V, 400mA for 1 hr.

15. After complete transfer the membrane was removed carefully and then incubated in 40 ml of 5% blocking buffer for 1 hr on a shaker.

16. After blocking, the membrane was probed with primary antibody(s) and incubated overnight at $4^{o}C$ with gentle shaking.

17. Next day, the membrane was washed thrice with the wash buffer (1X TBSt) and then incubated with the secondary antibody for 2 h.

19. After the secondary Ab incubation the membrane was again washed thrice with the wash buffer.

20. The proteins present on the membrane could be visualized by using the Enhanced Chemiluminescence (ECL) detection system.

Stripping and reprobing the membrane:

1. In order to reprobe the membrane with another primary antibody stripping protocol is used.

2. For stripping the membrane was incubated with the stripping buffer for 10 minutes at RT.

3. The membrane was then washed thrice with 1X TBSt, blocked with the blocking buffer for 1 hour, then incubated with primary antibody overnight at 4^{o}C with gentle shaking.

4. The next day, the membrane was again washed with 1X TBSt, incubated with secondary antibody for 1-2 h at RT with continuous shaking and then washed with wash buffer and developed in dark with the ECL detection system.

8.16. Immunofluorescence

Immunofluorescence is an antigen-antibody reaction where the antibodies are tagged (labelled) with a fluorescent dye and the antigen-antibody complex is visualized using ultra-violet (fluorescent) microscope. Immunofluorescence can be used to determine the localization, abundance and co-localization with another proteins.

Source of reagents/chemicals

Reagent/chemicals	Source
Paraformaldehyde	Sigma,USA
Bovine Serum Albumin	Sigma, USA
DAPI	Sigma, USA
VECTASHIELD (Mounting media)	Vector Labs, USA
Triton X 100	Sigma, USA
Anti-Mouse FITC	Sigma, USA
Anti-Rabbit FITC	Sigma, USA
Anti- Rabbit FITC	Sigma, USA
Anti-Mouse Dy Light 633	Sigma, USA

Preparation of 4% paraformaldehyde

Paraformaldehyde was weighed equal to 4% volume of the final solution (for 100 ml final volume, weigh 4 g of paraformaldehyde) and added in 1X PBS (volume equal to slightly less than 2/3 of the final desired volume). The mixture stirred at 60°C using a magnetic stirrer and after complete dilution of PFA the final volume was made up. The solution was filtered by Watman filter paper and was chilled on ice before use. Freshly prepared paraformaldehyde solution was usually preferred for the experiment.

Procedure

Different staining and fixation procedures were followed to stain the cells with different antibodies. The general procedure for immuno-fluorescence was as follows:

1. 80% confluent plate was trypsinized and 30,000 - 40,000 cells were seeded per cover slip in a 6 well plate. Two cover slips per sample: One for secondary antibody control (without primary antibody) and the other as a test sample for staining were seeded.
2. Cells were then incubated in 5% CO2 at 37°C for 24h.
3. After 24h, the spent medium was aspirated and cells were washed twice with 1X PBS.
4. Cells were fixed on coverslip with 2ml of 4% PFA and incubated at room temperature for 10min. PFA was then removed and cells were washed thrice with PBS.
5. Permeabilization is often required for nuclear staining. Coverslips containing cells were then incubated in Triton X 100 (0.025 to 0.3%) in 4% PFA. The permeabilization solution was removed and cells were washed thrice with PBS.
6. The cells were now incubated with 5% BSA for 60 min at room temperature (blocking).
7. Each cover slip (containing cells) was then incubated with 50µl of primary antibody (1:100 dilution in 1X PBS) on a clean glass slide. Cover slip was placed with cell surface facing downward.

8. Cells were incubated with the primary antibody overnight in a moist chamber at 4°C.
9. On the next day, cover slips were washed thrice with PBS. Each cover slip (containing cells) was then incubated with 50µl of secondary antibody (1:200 dilution in 1X PBS) on a clean glass slide. Cover slip was placed with cell surface facing downward.
10. Incubation was carried out for 2 hours at room temperature in dark after which cells were washed thrice with PBS.
11. Cells were counter stained with 50µl of DAPI (0.05%) for 30 seconds and after washing for three times with PBS, coverslips were mounted on clean glass slide (cell surface facing downward) using Vectashield mounting medium.
12. Cells were observed under confocal laser scanning microscope within 1hour. Argon, Helium/Neon and diode lasers were used to capture images on a Carl Zeiss LSM 510 Meta confocal microscope and the images were analysed using LSM Image Browser.

8.17. Clonogenic Assay/ Colony Formation Assay

Clonogenic assay or colony formation assay is an *in vitro* cell survival assay based on the ability of a single cell to grow into a colony. A single colony consists a minimum of 50 cells.

Source of reagents/chemicals

Reagents/Chemical	Source
Crystal violet	Sigma, USA
4% Paraformaldehyde	Sigma, USA
Methanol	Sigma, USA
6 well culture plates	Nunc, Thermoscientific, USA

Procedure

1. Single cell suspension from a confluent (70-80%) plate was prepared and equal numbers of viable cells (500 cells/well) were seeded in a 6-well plate after counting with trypan blue dye.
2. Cells were then incubated in 5% CO2 at 37°C overnight.
3. Next day, cells were washed twice with 1X PBS and different drugs (cisplatin and paclitaxel) in appropriate dilutions were added for 24h.
4. The drug-containing medium was removed, washed twice and the cells were allowed to grow for 7-15 days.
5. The plates were monitored for the colony formation.
6. Once the colonies in control wells started merging, the plates were removed from incubators, washed with 1X PBS, and the colonies were fixed by chilled methanol for 10 minutes.
7. Alternatively, the colonies can be fixed with chilled 4% paraformaldehyde for 10 minutes.
8. After two washes of 1X PBS, the plates were stained with 0.01% w/v crystal violet stain for 10 minutes.
9. The extra stain was washed out and the colonies were counted using inverted microscope.
10. The surviving fraction was calculated by using following formula:

The plating efficiency (PE) is the ratio of colonies to cells.

$$PE = \frac{number\ of\ colonies\ formed}{number\ of\ cells\ seeded} \times 100\%$$

The number of colonies that arise after treatment of cells is called surviving fraction (SF).

$$SF = \frac{number\ of\ colonies\ formed\ after\ treatment}{number\ of\ cells\ seeded\ X\ PE}$$

8.18. Site Directed Mutagenesis (SDM)

SDM is a molecular technique that deliberately changes sequences in gene or DNA locus with specific intentions. It is used to create point mutation (single base pair change), deletion, insertion or substitution of more than one base pair. SDM is often used in application like amino acid changes for protein structure and functional studies, promoter sequences changes to vary expression of the gene or to study binding affinity of transcription.

Guidelines for Primer Design

1. Both of the mutagenic primers must contain the desired mutation and anneal to the same sequence on opposite strands of the plasmid

2. Primers should be between 25 and 45 bases in length, with a melting temperature (*T*m) of ≥78°C.

3. The desired mutation (deletion, insertion or substitution) should be in the middle of the primer with ~10–15 bases of correct sequence on both sides.

4. The primers optimally should have a minimum GC content of 40% and should terminate in one or more C or G bases.

5. 125 ng of each oligonucleotide primer is used in the amplification reaction. To convert nanograms to picomoles of oligo, use the following equation:

$$\text{X picomoles of oligos} = \frac{125\text{ng of oligo}}{330 \times \text{number of bases of oligo}} \times 1000$$

Using SDM, site specific mutations can be generated in virtually any double-stranded plasmid using a four-step procedure. The steps are as follows:

Step I. Plasmid Preparation

Preparation of the plasmid (template DNA) for SDM by using miniprep plasmid isolation, bearing target DNA sequence for mutation. DNA is isolated from the *E.coli* strains that produce methylated DNA and are susceptible to *DpnI* digestion.

Step II. Temperature Cycling

1. Denaturation of the plasmid.

2. Annealing with the mutagenic primers (oligonucleotides primers containing desired mutation).

3. *Pfu turbo* DNA polymerase, that does not displace the newly synthesized strand and stops the extension, is used to extend and incorporate mutagenic primers resulting in the nicked circular DNA strands.

Step III. DpnI Digestion

The methylated and non-mutated template DNA is digested with *DpnI restriction* enzyme (overnight at 37°C).*DpnI* endonuclease (target sequence: 5´-Gm6ATC-3´) is specific for methylated and hemi-methylated DNA and is used to digest the parental DNA template and specifically select for mutation-containing synthesized DNA.

Step IV. Transformation

The circular nicked, ds DNA is transformed in DH5α-E.coli competent cells. After transformation the competent cells repairs the nicks in the mutated plasmids.

Colonies obtained from this procedure are cultured and the plasmid obtained are confirmed for desired mutation by sequencing.

8.19. *In Vivo* Bioluminescence Imaging In Living Mice

In vivo bioluminescence imaging (BLI) is sensitive tool that is based on detection of light emission from cells or tissues. BLI allows a non-invasive, and real-time analysis of biological processes at the molecular level in living organisms. In vivo imaging allows longitudinal monitoring of disease like tumor formation in the same animal and offers desirable alternative to analyse number of animals at many time points during the progression of tumor formation. The *in vivo* BLI in mice uses the following procedure.

Cell preparation

Luciferase (firefly luciferase or renilla luciferase) expressing ovarian cancer cell lines (A2780 and SKOV3)were established in the laboratory. These cells are highly tumorigenic and can be used in pre-clinical mouse models. The cells are cultured in standard growth conditions and amplified in amount required for implantation in specific number of mice. A 70-80% confluency flask is considered optimum for its use in implantation. An *in vitro* validation of the bioluminescence activity was performed earlier by luciferase assay.

Animal Injection

1. A 70-80% confluent flask cells were harvested by trypsinisation and counted using trypan blue.

2. Four-six million cells per mouse were used for implantation. Accordingly total number of cells required for all the mice were counted and collected in a microfuge tube. The final count of the cell number was dissolved in 100µl of 1X PBS and the cells were kept in ice. Care should be taken that the mice should be kept ready for implantation to avoid loss of viable cells and cells should be immediately implanted in mice.

3. Usually, in order to facilitate optimal formation of tumor athymic immunocompromised mice were preferred for implantation. Animal care and euthanasia were performed with the approval from Institutional Animal Ethics Committee of ACTREC. If SCID (Severe Combined Immuno-deficiency) mice were used, then the fur of the mice were removed by razor, to facilitate proper implantation and optical imaging. For nude mice no such pre-treatment is required.

4. Prior to implantation, animals were anesthetized by Xylazine (100 µl) -Ketamin (360 µl) combination.

5. Required amount of cells were loaded in a syringe with 26 gauge needle.

6. The skin of the mice was lifted to make a tent and the cells were injected at the base to get a subcutaneous injection.

7. The newly injected mice can be imaged immediately.

Animal imaging

1. For each imaging session, D-luciferin (100 µl of 30mg/ml per mouse) or coelenterazine (50µg/mouse) was given through either intraperitoneal or tail-vein injection respectively.

2. After substrate injection the animals were imaged with Berthold's NightOwl II LB 983 optical imaging system or IVIS-Spectrum optical imager.

3. In both the system, the bioluminescence signals from the animal were captured by a back-thinned charge coupled device camera cooled to -90°C.

4. For imaging through Berthold's NightOwl II LB 983 optical imaging system, region of interests (ROIs) were drawn over the tumors of mice and quantified by using the Winlight Optimas Live Image Software 32. Bioluminescence signal was recorded as maximum (photons/sec/cm2) with a fixed angle at 2*pi.

5. For imaging through IVIS 200 optical imager, ROIs were drawn over the tumors and quantified by using the Live Image (4.4) software. Bioluminescence signals were recorded as maximum (photons/s/cm^2/sr). Photon flux (bioluminescence signal) from the tumor is proportional to the number of live cells expressing luciferase so bioluminescence correlates directly with tumor size.

6. Field of view is selected for the number of animals being imaged. Upto 5 animals can be maintained in the instrument under the influence of anaesthetic agent.

7. In Living Image software, exposure time, aperture size (f-stop) and pixel binning can be optimized based on the expression level of the cell line. These settings can be changed at any time during an experiment without affecting the quantitative result. However, for the Winlight Optimas Live image software, the above parameters cannot be tampered after capturing the image.

In vivo cisplatin treatment

1. After 10- 20 days post implantation tumor were palpable, and the mice were divided in two groups- control and test group.
2. When the size of tumor in mice of test group was around 60 mm^3 the mice were given cisplatin treatment. Size of the tumor were estimated by caliper measurement. Test group was group was injected with either one or two cycles of cisplatin (8 mg/kg/week) diluted in 1X PBS. To avoid the toxicity the intraperitoneal dose of cisplatin was divided into three parts.
3. The control group of mice were given treatment of 1X PBS (as vehicle control).
4. After each round of treatment BLI was performed.

Publications..

OPEN ACCESS Freely available online

PLOS ONE

Non-Invasive Imaging of Phosphoinositide-3-Kinase-Catalytic-Subunit-Alpha (PIK3CA) Promoter Modulation in Small Animal Models

Snehal M. Gaikwad[1], Lata Gunjal[1], Anitha R. Junutula[2], Arezoo Astanehe[3], Sanjiv Sam Gambhir[2], Pritha Ray[1]*

1 Advanced Centre for Treatment, Research and Education in Cancer (ACTREC), Tata Memorial Centre, Navi Mumbai, Maharashtra, India, **2** Molecular Imaging Program at Stanford (MIPS), Departments of Radiology and Bioengineering, Department of Materials Science and Engineering, Bio-X Program, School of Medicine, Stanford University, Palo Alto, California, **3** Department of Obstetrics and Gynecology, University of British Columbia, Vancouver, British Columbia, Canada

Abstract

Activation of the PI3K/Akt pathway, a critical step for survival in cancer cells is often associated with decreased sensitivity to several chemotherapeutic drugs. *PIK3CA* gene amplification is observed in 16–24% of epithelial ovarian cancer (EOC) patients in conjunction with p53 mutations. A 900 bp long *PIK3CA* promoter is shown to be negatively regulated by p53 in ovarian surface epithelial cells but the consequence of chemotherapeutic drug treatments on this promoter in ovarian cancer cells is largely unknown. We aim to study the modulation of this promoter by cisplatin using an improved fusion reporter in ovarian cancer cells and tumor xenografts by non-invasive imaging approach. A *PIK3CA* sensor was developed using a bi-fusion reporter from a newly constructed library of bi- and tri-fusion vectors comprising of two mutant far red fluorescent proteins (mcherry/mch and tdTomato/tdt), a mutant firefly luciferase (*fluc2*), and a PET reporter protein (*ttk*). *In vivo* imaging of mice implanted with 293T cells transiently expressing these bi- and tri-fusion reporters along with respective controls revealed comparable activity of each reporter in the fusion background and *fluc2-tdt* as the most sensitive one. Repression of the *PIK3CA* sensor by drugs was inversely proportional to cellular p53 level in a germline (PA1) and in an EOC (A2780) cell line but not in a p53 deficient EOC (SKOV3) cell line. Bioluminescence imaging of tumor xenografts stably expressing the *PIK3CA* sensor in PA1 and A2780 cells exhibited attenuating activity without any change in SKOV3 tumors expressing the *PIK3CA* sensor after cisplatin treatment. Sequential mutation at p53 binding sites showed gradual increase in promoter activity and decreased effects of the drugs. These newly developed *PIK3CA-fluc2-tdt* and the mutant reporter sensors thus would be extremely useful for screening new drugs and for functional assessment of *PIK3CA* expression from intact cells to living subjects.

Citation: Gaikwad SM, Gunjal L, Junutula AR, Astanehe A, Gambhir SS, et al. (2013) Non-Invasive Imaging of Phosphoinositide-3-Kinase-Catalytic-Subunit-Alpha (PIK3CA) Promoter Modulation in Small Animal Models. PLoS ONE 8(2): e55971. doi:10.1371/journal.pone.0055971

Editor: Russell O. Pieper, University of California San Francisco, United States of America

Received July 30, 2012; **Accepted** January 4, 2013; **Published** February 5, 2013

Funding: This work is supported by ACTREC start up fund, IRG-2698 and CSIR 27(232)/10 (PR), NIH In Vivo Cellular and Molecular Imaging Centre grant (ICMIC grant P50CA114747) (SSG). SMG acknowledges fellowship funding from Council of Scientific and Industrial Research (India). The funders had no role in study design, data collection and analysis, decision to publish, or preparation of the manuscript.

Competing Interests: Co-author Dr. Sanjiv Sam Gambhir is a PLOS ONE editorial board member. This does not alter the authors' adherence to all the PLOS ONE policies on sharing data and materials.

* E-mail: pray@actrec.gov.in

Introduction

The class 1 phosphatidylinositol-3-kinase (PI3K) family of lipid kinases phosphorylate the phosphatidylinositol 4,5 bisphosphate (PIP2) at the 3 position of the inositol ring that act as second cellular messenger for cell growth, survival, proliferation and morphology [1]. p110α, the catalytic subunit of the class I PI3K encoded by *PIK3CA* gene is de-regulated in many neoplasia by differential gene expression, amplification and mutation [2,3,4,5]. In comparison to breast and hepatocellular carcinomas, amplification rather than mutation in *PIK3CA* is a common event in ovarian carcinomas and is frequently associated with *TP53* mutations [6,7,8]. About 16–24% of ovarian carcinomas harbour *PIK3CA* amplification irrespective of a histological subtype and is negatively associated with platinum sensitivity and PTEN over expression [7,9]. While p110α mutations are extensively studied for targeted therapy with PI3K inhibitors, consequence of *PIK3CA* amplification for therapeutic intervention is yet to be fully investigated. Studies on ovarian cancer cell lines revealed that activation of the PI3K/AKT pathway may also lead to resistance to chemotherapy [10,11].

Recent characterization of a 900bp long *PIK3CA* promoter fragment isolated from normal human ovarian surface epithelium (OSE) exhibited four p53 binding response elements and p53 mediated attenuation [12]. The same promoter isolated from Human Bacterial chromosome showed to bear NF-kβ, hypoxia inducible factor, heat shock protein and activator protein 1(AP1) binding sites [13]. Inhibition of nuclear translocation of NF-kβ or incubation with TNF-α resulted in down or up regulation of *PIK3CA* promoter activity [13]. Thus *PIK3CA* expression encounters complex regulation by several factors. However, the effect of the common therapeutic drugs (cisplatin and paclitaxel) on this *PIK3CA* promoter in ovarian cancer cells still remains to be investigated.

Non-invasive molecular imaging of living animals with reporter genes has opened up new avenues to understand fundamental molecular pathways in modern biomedicine [14,15]. A variety of reporter genes have been developed for Optical, Magnetic Resonance and Radionuclide imaging techniques to study specific biological processes and monitor disease progression and therapy [16,17,18]. Modality specific reporter genes when used in combination add extra advantage of generating superior information with higher sensitivity, resolution and tomography. Multimodality imaging vectors generated by 'fusion gene' approach are most suitable for visualizing molecular events from both live cells and living organisms. Our previous multimodality fusion reporters (a combination of bioluminescent, fluorescent and PET reporters) [19,20,21], though accomplished significant achievements in non-invasive imaging of gene expression in living subjects [22,23,24] were limited for *in vivo* fluorescence imaging. The monomeric red fluorescent (mRFP1) protein used in these vectors is limited by lower quantum yield. The developments of fluorescent proteins as molecular tags have revolutionized the understanding of biological systems in live cells [25,26,27]. While the green fluorescent proteins and its mutants are suitable for imaging molecular events at cellular level, its red counterparts are optimal for small animal imaging. Some of these red fluorescent proteins (such as tdtomato, mTangarine, mStrawberry, mCherry etc.) have emission spectra near or slightly above 600 nm, a wavelength which experiences lesser attenuation and absorption in biological tissues. Further, constant molecular modification for functional improvement in bioluminescence reporters enhances the possibilities to construct improved and highly sensitive fusion reporters for non-invasive imaging.

To understand and monitor the *PIK3CA* promoter modulation by drugs, we generated a *PIK3CA* sensor with a newly constructed fusion reporter competent for both *in vitro* and *in vivo* imaging studies. Continuing improvement of our existing vectors [19,21,28] we first created several bi-fusion and tri-fusion reporters with higher *in vivo* optical imaging ability using two mutant red fluorescent proteins with better photon efficiency (tandem dimer Tomato or *tdt*) and or longer emission wavelength (mCherry or *mch*) and a codon optimized highly sensitive bioluminescence reporter (firefly luciferase2 or *fluc2*). Comparison of our newly constructed vectors with the existing ones carrying a mutated thermostable firefly luciferase (*mtfl*), monomeric red flourescence protein (*mrfp1*) and truncated sr39thymidine kinase (*ttk*) showed the utility of these improved vectors for *in vivo* multimodality imaging as a proof of principle. We then evaluated the ability of *fluc2-tdt*, the most optimized vector to monitor the modulation of (*PIK3CA*) promoter in response to chemotherapeutic drugs in ovarian cancer cells and in tumor xenografts. Sequential mutations at the p53 binding sites gradually augmented the *PIK3CA* promoter activity and abolished the effects of drugs indicating a p53 mediated tight regulation of PIK3CA signalling in cellular homeostasis.

Materials and Methods

Chemicals

[8-^{3}H] Pencyclovir was obtained from Moravek Biochemicals (Brea, CA). ^{18}F-labeled 9-(4-[^{18}F] Fluoro-3-hydroxymethylbutyl) guanine (FHBG) was synthesized at Stanford. The *tdtomato* and *mcherry* red fluorescent proteins were kind gift of Dr. R. Tsien (UCSD, CA). The *fluc2*, phRL–TK, Luciferase assay systems were purchased from Promega. D-luciferin and Coelenterazine were procured from Biosynth International (Switzerland). Cisplatin (cis-Diammineplatinum-(II)-dichloride), Paclitaxel, Adriamycin, β-actin antibody, secondary antibodies (i.e., anti-mouse and anti-rabbit) were obtained from Sigma while anti-p110α and anti-p53 antibodies purchased from Cell Signaling Technologies (Danvers, MA, USA).

Construction of *mtfl/fluc2-tdt/mcherry-ttk* Fusion genes and *PIK3CA-fluc2-tdt* Vector

PCR amplification and standard cloning techniques were used to generate the *CMV-mtfl/fluc2-tdt/mch-ttk* tri-fusion and *CMV-mtfl/fluc2-tdt/mch bifusion* plasmids in pCDNA3.1(+) backbone using the existing triple fusion reporter vector CMV-*mfl-mrfp1-ttk* [28]. The *PIK3CA* promoter [12] was PCR amplified using primers (5′GTAAGATCTACTGCTCCTACGCTTTTC) and (3′ GCAGCTAGCTCGTGTAAACAAACAACG) and cloned in *CMV-fluc2-tdt* bifusion plasmid by replacing the CMV promoter. Positive clones were confirmed by PCR amplification, restriction digestion and sequencing.

Site Directed Mutagenesis

PIK3CA promoter bearing four p53 binding sites was sequentially mutated using the mutagenic primers (Table 1) which consist of the substitutions at the core sequence of p53 binding sites by site directed mutagenesis. The colonies obtained were screened and verified by sequencing for desired mutations.

Cell Lines, Transient Transfection, and Stable Cell Generation

293T (human embryonic kidney cells), A2780 (undifferentiated EOC cell) were obtained from ATCC (Manassas, VA, USA) and PA1 (germline ovarian cancer cells) was obtained from NCCS (Pune, India). The 293T cells were grown in MEM, while PA1 and A2780 cells were cultured in DMEM supplemented with 10% FBS and 1% penicillin/streptomycin solution [28]. The SKOV3 cells were cultured in McCoy's medium supplemented with 10% FBS and 1% penicillin/streptomycin solution. All transient and stable transfections were carried out using the Superfect transfection reagent (Qiagen, Valencia, CA) and clonal selections were done by G418 selection. All the cell lines were tested for Mycoplasma contamination using EZdetectTM Hoechst Stain kit (#CCK008) (HiMedia Lab, Mumbai, India) and found to be negative. There is no dedicated cell line testing service provider in India.

TK, RL, FL and β-GAL Activity

Thymidine kinase and β- Galactosidase enzyme activity assays were performed as previously described [28]. Renilla and Firefly luciferase assays were performed using Dual–Luciferase Reporter Assay System from Promega. Each of the luciferase reactions was measured in a Berthold luminometer for period of 1 sec. All transfection and drug treatment experiments were done in triplicates and repeated at least twice.

Western Blotting

PA1 and A2780 cells stably expressing the *PIK3CA-fluc2-tdt* vector were treated with drugs for 2 and 24 hrs, lysed in passive lysis buffer. Equal amounts of protein from control and treated cells were resolved in SDS PAGE gel and probed with various primary and respective secondary antibodies.

FACS Analysis and Immunofluorescence

293T cells transfected with various bi-fusiosn reporters for 24 hrs were trypsinized, washed in PBS and analyzed for tdTomato expression on the FL3 channel using a FACS Caliber (BD Biosciences, CA, USA). Analysis was performed using FlowJo Sofwatre (Tree Star).

Table 1. The p53 binding sites in the PIK3CA promoter with core sequence (underlined) and the mutagenic primers.

p^{53} binding sites	Mutagenic primers
Site 1 CACCAAGACA	5′ GGTACGCAGCACTGTGACACTACCTTG 3′ F 5′ CAAGGTAGTGTTACAGTGCTGCGTACC 3′ R
Site 2 TGGCATTACG CACCACGTCT	5′ CGCGAAAAATCCCCAGAATCTTCTGAATAG 3′ F 5′ CTATTCAGAAGATTCTGGGGATTTTTCGCG 3′ R
Site 3 ACGCTGGTTA CGGTTAGCCA	5′ TCCATAACCACGAGAATTAGCCACTGAC 3′ F 5′ GTCAGTGGCTAATTCTCGTGGTTATGGA 3′ R
Site 4 AAGCAAGACG GCACATATTG	5′ TCGGGCGGAAAAGTGTGACGCAGGCG 3′ F 5′ CGCCTGCGTTACACTTTTCCGCCCGA 3′ R

doi:10.1371/journal.pone.0055971.t001

To analyze the localization of p53, treated (cisplatin and paclitaxel) and control PA1 and A2780 cells were grown on cover slips, fixed in 4% paraformaldehyde, washed and blocked in 5% BSA followed by overnight incubation with primary antibody (1:200). Cover slips were then washed, incubated with secondary antibody (2 hrs), counterstained briefly with DAPI and were observed under a Zeiss LSM 510 Meta confocal microscope. At least five representative fields were studied for p53 and DAPI staining.

Fluorescence Imaging in Living Mice

Animal care and euthanasia were performed with the approval of the Administrative Panels on Laboratory Animal Care (A-PLAC) of Stanford University and Institutional Animal Ethics Committee (IAEC) of ACTREC. All images were acquired using a Maestro^{TM} (Cambridge Research and Instrumentation, Woburn, MA) or Xenogen IVIS^{TM} -200 (Xenogen Corp., Alameda, CA) optical imaging system. The mice were anesthetized, injected with 10×10^6 cells transiently expressing the *fluc2-tdt-ttk* and *fluc2-tdt, mtfl-tdt-ttk, mtfl–tdt* fusion genes, and placed inside the imaging system [20]. For Maestro^{TM} *in vivo* imaging system, the MSI data sets (cubes) were acquired with images spaced every 10 nm spectral interval in the 550 nm to 700 nm spectral range (Excitation filter 503–550 nm and Emission filter 580–700 nm). All the images were corrected for background auto-fluorescence. Region of interests were drawn on the site of interests and mean fluorescence intensity (MFI) were recorded. While using the Xenogen IVIS^{TM} -200 system for imaging, the whole body image was acquired for 1 second with an excitation filter at 500–550 nm and an emission filter 575–600 nm. ROIs were drawn over implanted cell area and quantified by using Living IMAGE Software version 2.5. Fluorescence signal was recorded as maximum (photons/sec/cm^2/sr).

Bioluminescence Imaging in Living Mice

For *in vivo* bioluminescence imaging with Xenogen IVIS^{TM}-200 optical imaging system, mice implanted with 293T cells transfected with various single, bi and triple fusion reporter genes were anesthetized and placed in a light tight chamber and whole body images were obtained for 1 min after intra peritoneal injection of 100 µl D-luciferin (30 mg/ml) diluted in phosphate-buffered saline (pH 7) [20]. ROIs were drawn over the implanted cell area(s) and quantified by using the Living Image Software version 2.5. Bioluminescence signal was recorded as maximum (photons/sec/cm^2/sr). For imaging with Berthold's NightOwl II LB 983 optical imaging system, A2780 and PA1 cells stably expressing the *PIK3CA-fluc2-tdt* reporter were implanted in mice and imaged for bioluminescence when the tumors reached 5–8 mm size. The mice were then divided in two groups and one group was injected with cisplatin (8 mg/kg). ROIs were drawn over the tumors of control and cisplatin treated mice and quantified by using the Winlight Optimas Live Image Software 32. Bioluminescence signal was recorded as maximum (photons/sec/cm^2) with a fixed angle at 2*pi.

Small Animal PET Imaging in Living Mice

Mice were anesthetized, injected with 10×10^6 293T cells transiently expressing *fluc2-tdt-ttk, tdt, and fluc2* and *ttk* vectors. After fluorescence and bioluminescence imaging, mice were scanned using a microPET (P4, Simens) for 18F-FHBG uptake as described earlier [20]. Briefly, each mouse injected with 200 µCi of 18F-FHBG intravenously and scanned for 10 min after 1 hr of uptake. The microPET images were reconstructed with the ordered-subsets expectation maximization algorithm and analyzed using a Medical Imaging Data Examiner. Volumetric regions of interest were drawn over the tumors and the mean activities were recorded from the entire ROI. The percent injected dose (%ID/g) was calculated by dividing the ROI counts by the injected dose (decay corrected).

Results

Multimodality Imaging of a Newly Developed Optimized Triple Fusion (fluc2-tdt-ttk) Reporter in Living Mice

We aim to construct new triple and bi-fusion vectors by modifying the existing fusion reporters (CMV-*mtfl-mrfp1-ttk*) to achieve high enough sensitivity, useful for imaging different molecular pathways *in vivo*. To improve the lower fluorescence quantum yield, extinction coefficient and photostability of mRFP1, Shaner *et al* (2008) [29] performed a rigorous mutagenesis screen focusing on selected amino acids. Of all those mutants, we chose to work with *tdtomato* and *mCherry* protein due to their higher quantum yield, brightness, and longer emission wavelength. To improve the sensitivity of the bioluminescence component of the fusion vectors, a mutant of firefly luciferase (*fluc2*) having 5–10 fold higher light output than original *fluc* was used. Amongst all the newly constructed triple fusion reporters, *fluc2-tdt-ttk* showed highest fluorescence and bioluminescence but moderate TK activity as measured by FACS, FL and TK assays from 293T cells transiently expressing the new generation triple fusion vectors with appropriate controls (data not shown).

To test the efficiency of our most sensitive vector *fluc2-tdt-ttk in vivo*, we implanted 5×10^6 293T cells transiently expressing *fluc2-tdt-ttk* (site A), *fluc2* (site C), *tdt* (site D) and *ttk* (site B) reporter genes at four different sites in nude mice (n = 3) and imaged by fluorescence, bioluminescence and microPET scanner after 24 hrs. The *in vivo* fluorescence and bioluminescence imaging noticeably showed very high levels of fluorescence and biolumi-

nescence signals from cells expressing *fluc2-tdt-ttk* compared to cells expressing *tdt* or *fluc2* reporters (Figure 1a1 & 1a2). microPET imaging with 18F-FHBG showed low but distinct accumulation of the tracer at the implanted sites of cells expressing the triple fusion reporter and *ttk* reporter alone (Figure 1a3 & 1a4). A graphical analysis of the quantified signals of all the modalities showed that the fluorescence, bioluminescence and microPET signals of triple fusions are lower than the signals of *tdt* or *fluc2* or *ttk* vector alone which met significance only for bioluminescence signal (Figure 1b1, 1b2 & 1b3).

The Fluorescence and Bioluminescence Imaging of the Most Sensitive Fusion Reporter (fluc2-tdt)

We next sought to compare the reporter activities of bi (*fluc2-tdt* & *mtfl-tdt*) and triple fusions (*fluc2-tdt-ttk* & *mtfl-tdt-ttk*) by FACS and *in vivo* fluorescence and bioluminescence imaging. When comparisons were made between the triple fusion and bi-fusion vectors in transiently transfected 293T cells, *fluc2-tdt* exhibited very high fluorescence activity (even higher than cells expressing *tdt* alone) (Figure 1c). We tried to compare different cell numbers (10,000 to 5 million) transiently transfected with all the four vectors and implanted in mice. As shown in Figure 1d & 1e, very bright fluorescence and bioluminescence signals were visible from the site of cells (50,000) expressing the *fluc2-tdt* fusion reporter. The expression of *fluc2-tdt* could also be visible from much lower number of cells (10,000) (data not shown).

Monitoring Drug Induced Modulation of PIK3CA Promoter with a Unique Sensor (PIK3CA-fluc2-tdt)

Astanehe *et al* (2009) [12] demonstrated that binding of p53 suppresses the *PIK3CA* promoter activity in normal OSE. Both cisplatin and paclitaxel, the standard chemotherapeutic drugs for ovarian cancer are known to induce p53 mediated cell death [30,31]. To study the modulation of *PIK3CA* promoter by chemotherapy drugs in ovarian cancer cells, we cloned the *fluc2-tdt*, under the *PIK3CA* promoter [12]. A dose dependent treatment of cisplatin and paclitaxel for 2 hrs indicated that a 5 μg/ml concentration of both drugs were able to decrease the promoter activity in PA1 cells (data not shown). Treatments with three drugs [cisplatin, paclitaxel and adriamycin (1 μM/ml)], significantly decreased the *PIK3CA* promoter activity (Figure S1a) but not the co-transfected TK promoter activity (*pTK-hrl*) (Figure S1b) in PA1 cells. Similar results were observed in A2780 cells transiently transfected with *PIK3CA-fluc2-tdt & pTK-rluc* and treated with cisplatin, paclitaxel & adriamycin (data not shown).

Cisplatin and Paclitaxel Treatments in PA1 and A2780 Cells Stably Expressing PIK3CA-Fluc2-tdt Exhibit PIK3CA Promoter Modulation and p53 Activation

Treatments with cisplatin and paclitaxel showed attenuated luciferase activity in PA1-*PIK3CA-fluc2-tdt* (PPF) and A2780-*PIK3CA-fluc2-tdt* (APFT) cells following the same trend observed in transient expression study (Figure 2a–2d). Interestingly same concentration of drug (5 μg/ml) (either cisplatin or Paclitaxel) exerted different levels of promoter attenuation to A2780 (less sensitive) and PA1 (highly sensitive) cells. Western blot analysis of the same lysates did not show any change in the endogenous p110α level but the p53 level significantly increased after 24 hrs of drug treatments as compared to 2 hrs (Figure 2e, 2f & 2g, 2 h). In APFT cells, the level of p53 activation by cisplatin seemed to be higher than the level induced by paclitaxel (8.1 fold vs. 4.4 fold) (Figure 2 h). Immunofluorescence study clearly demonstrated nuclear localisation of p53 protein in cisplatin treated PPF and APFT cells (Figure 2i & 2j).

To investigate the effect of chemotherapeutic drugs on *PIK3CA* promoter in absence of endogenous p53 protein, stable clones of SKOV3 (a p53 deficient cell line) cells expressing the *PIK3CA* sensor was developed (SPFT). The mutant background was verified by western blotting (Figure 2 m). The *PIK3CA* promoter activity in these SPFT cells did not show any attenuation when treated with increasing concentrations of cisplatin and paclitaxel for 2 hrs (Figure 2k & 2l).

Imaging of Cisplatin Induced Modulation in PIK3CA Promoter Activity in Tumors of Living Mice

Non-invasive optical imaging is a great approach to track molecular events in living animals and correlate the findings with *in vitro* results. To explore the kinetics of *PIK3CA* promoter modulation by cisplatin *in vivo*, we used two different tumor xenograft models (PA1-*PIK3CA-fluc2-tdt* and A2780-*PIK3CA-fluc2-tdt*) with differential growth pattern. For each model, six million cells were subcutaneously implanted in nude mice and tumor growth was monitored by bioluminescence imaging (Figure 3a & 3b). Once the tumors were palpable, either one or two cycles of cisplatin (8 mg/kg/week) [32] was injected intraperitoneally in three nude mice for three days a week. To avoid toxicity, we chose to divide each dose in three parts. Since ovarian germline tumors are more sensitive to cisplatin in comparison to epithelial ovarian tumors and PA1 cells in our study showed higher promoter attenuation mediated by cisplatin (Figure 2a & 2e), we decided to treat the PA1 tumor bearing mice (n = 6) with one cycle and A2780 tumor bearing mice (n = 7) with two cycles of cisplatin. Attenuation in luciferase activities for PA1 model ($4.4\times10^8\pm2.2\times10^8$ p/sec/cm^2 to $3\times10^8\pm1.9\times10^8$ p/sec/cm^2) (~0.7 fold) were detected at 14th day of completion of treatment which further decreased ($0.82\times10^8\pm5.7\times10^7$ p/sec/cm^2) (~0.2 fold) with time (22nd day). The control mice, however, had increased luminescence and tumor growth with time ($5.8\times10^8\pm4.1\times10^8$ p/sec/cm^2 to $8.7\times10^8\pm4.5\times10^8$ p/sec/cm^2 to $1.3\times10^9\pm7.4\times10^8$ p/sec/cm^2) (Figure 3a1 & 3a2). In the A2780 tumor model (n = 4), which exhibited a faster growth kinetics, the bioluminescence signal did not decrease after first treatment ($6.93\times10^9\pm1\times10^9$ p/sec/cm^2 to $6.1\times10^9\pm1\times10^9$p/sec/cm^2) (0.9 fold) at 11 days but decreased rapidly ($1.9\times10^9\pm3\times10^8$ p/sec/cm^2) (~0.27 fold) after the completion of two treatments at 15 days. The control mice (n = 3) showed increased bioluminescence and tumor growth ($1.2\times10^9\pm3\times10^8$ p/sec/cm^2 to $4\times10^9\pm7.6\times10^8$ p/sec/cm^2 to $7.4\times10^9\pm2\times10^9$ p/sec/cm^2) over time (Figure 3b1 & 3b2). The bioluminescence signals in the cisplatin treated mice at day 15 post-treatment showed a significant decrease (p = 0.025) as compared to the control mice (Figure 3b1).

In contrast to the PPF and APFT tumor models, the bioluminescence signals of SKOV3 tumor xenografts (n = 5) did not decrease rather exhibited an increase after first treatment ($3.9\times10^7\pm2.7\times10^7$ p/sec/cm^2 to $9.6\times10^7\pm3.8\times10^7$ sec/cm^2) (2.4 fold) of cisplatin at 7th day, which further increased to $1.2\times10^8\pm8\times10^7$ p/sec/cm^2 (3.1 fold) after completion of two treatments at 24 days. The control mice (n = 5) also showed increased bioluminescence and tumor growth ($4.4\times10^7\pm2.9\times10^7$ p/sec/cm^2 to $1.1\times10^8\pm4.5\times10^7$ p/sec/cm^2 at day 7 to $1.3\times10^8\pm5.9\times10^7$ p/sec/cm^2) (~3 fold) over time (Figure 4a1 & 4a2). The representative images of the bioluminescence signals of pre- and post- treatment in PA1, A2780 and SKOV3 tumor models are shown in the Figure 3a3, 3b3 and 4a3.

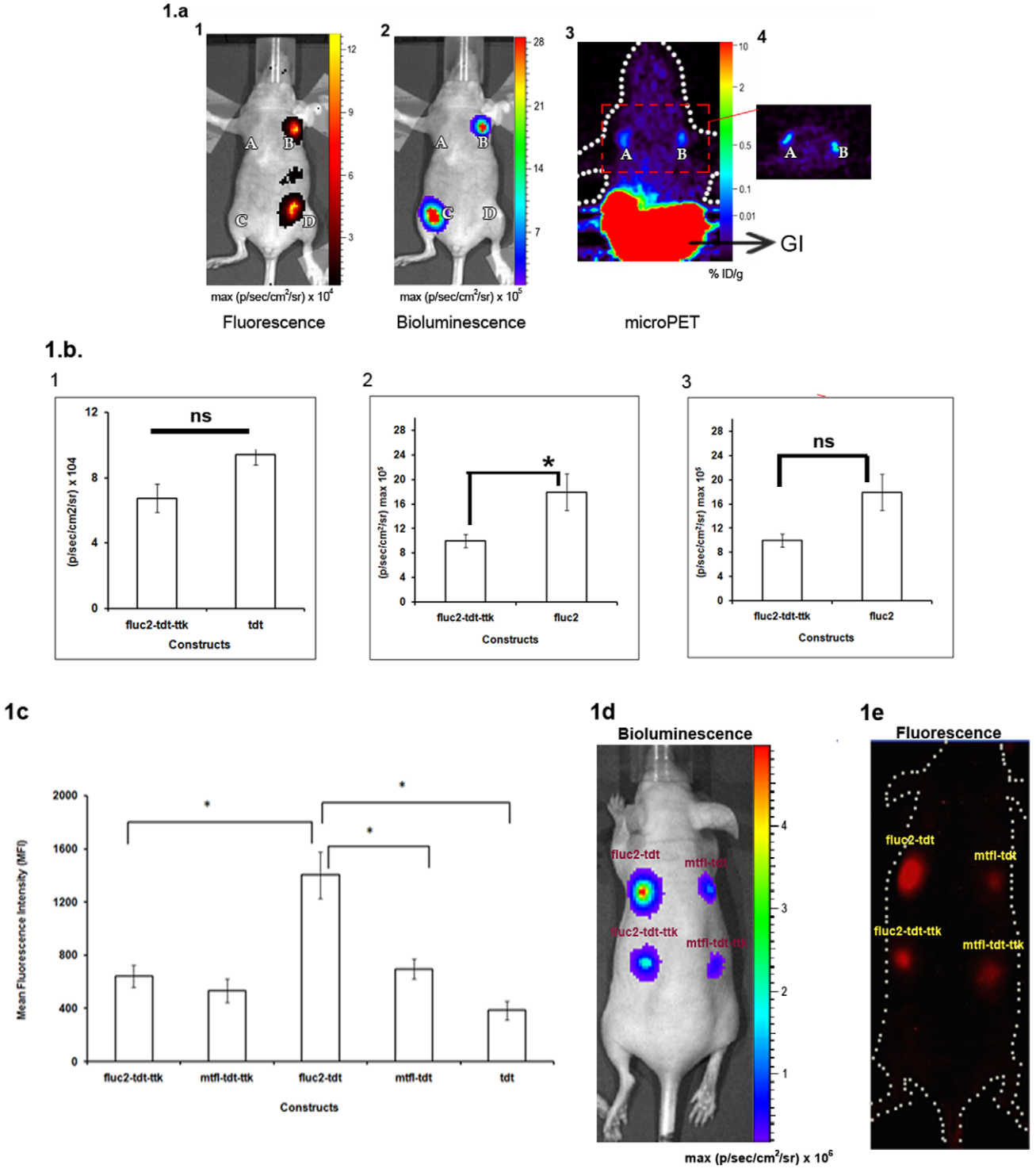

Figure 1. Multimodality imaging of the new generation bi- and tri-fusion vectors in living mice. 1a1 and 1a2. Fluorescence and Bioluminescence imaging. 10×10^6 of 293T cells transfected with *CMV-ttk (A), CMV-fluc2-tdt-ttk (B), CMV-fluc2(C),* and *CMV-tdt (D)* plasmids were implanted subcutaneously in living mice (n = 3) and were imaged first for fluorescence and then for bioluminescence after injection of D- luciferin using IVIS imaging system. Signals were seen only from the cells expressing *CMV-tdt* and *CMV-fluc2-tdt-ttk* vector (for fluorescence) and from cells expressing *CMV- fluc2* and *CMV-fluc2-tdt-ttk* reporter for bioluminescence. Signals were recorded as max (pixel/sec/cm^2/steradian). 1a3. microPET imaging. Mice described in 1a1 were injected with 200 μCi of 18F-FHBG and microPET imaging was performed after 1 hr for 10 minutes. Specific uptake of 18F-FHBG was seen in cells expressing the *CMV-ttk* and *CMV-fluc2-tdt-ttk* vectors. High nonspecific accumulation of 18F-FHBG was seen in the gastro-intestinal tract (GI). 1a4. Coronal section of the same microPET image described in 1a3. 1b. Graphical representation of the quantified fluorescence (1b1), bioluminescence (1b2) and microPET (1b3) signals. 1b1 and 1b2. Fluorescence (B and D) and bioluminescence (B and C) signals were calculated for the respective ROIs drawn over the sites of implanted cells. The SEM represents 3 experiments (ns.- statistically non-significant and *indicates $p<0.05$). 1b3. Percent injected dose (%ID/G) of 18F-FHBG uptakes were calculated for the respective ROIs drawn over the implanted cell (A and B) which showed similar uptake (ns). 1c. Comparative analysis of the fluorescence activity of the new bi and trifusion vectors in cell culture:

293T cells were transiently transfected with *CMV-fluc2-tdt-ttk*, *CMV-mtfl-tdt-ttk*, *CMV-mtfl-tdt* and *CMV-fluc2-tdt* plasmids and FACS analysis was done from equal number of cells after 24 hrs. All the experiments were performed in triplicate (*indicates $p<0.05$). 1d & 1e. Fluorescence and bioluminescence imaging of the new bi and triple fusion vector. 10×10^6 of 293T cells transfected with *CMV-fluc2-tdt-ttk*, *CMV-mtfl-tdt-ttk*, *CMV-mtfl-tdt* and *CMV-fluc2-tdt* plasmids were implanted on the dorsal side of a nude mouse and imaged for fluorescence (1d) using Maestro system and bioluminescence (1e) as described above. Cells expressing *CMV-fluc2-tdt* clearly exhibited highest fluorescence and bioluminescence signals among all group of cells.

doi:10.1371/journal.pone.0055971.g001

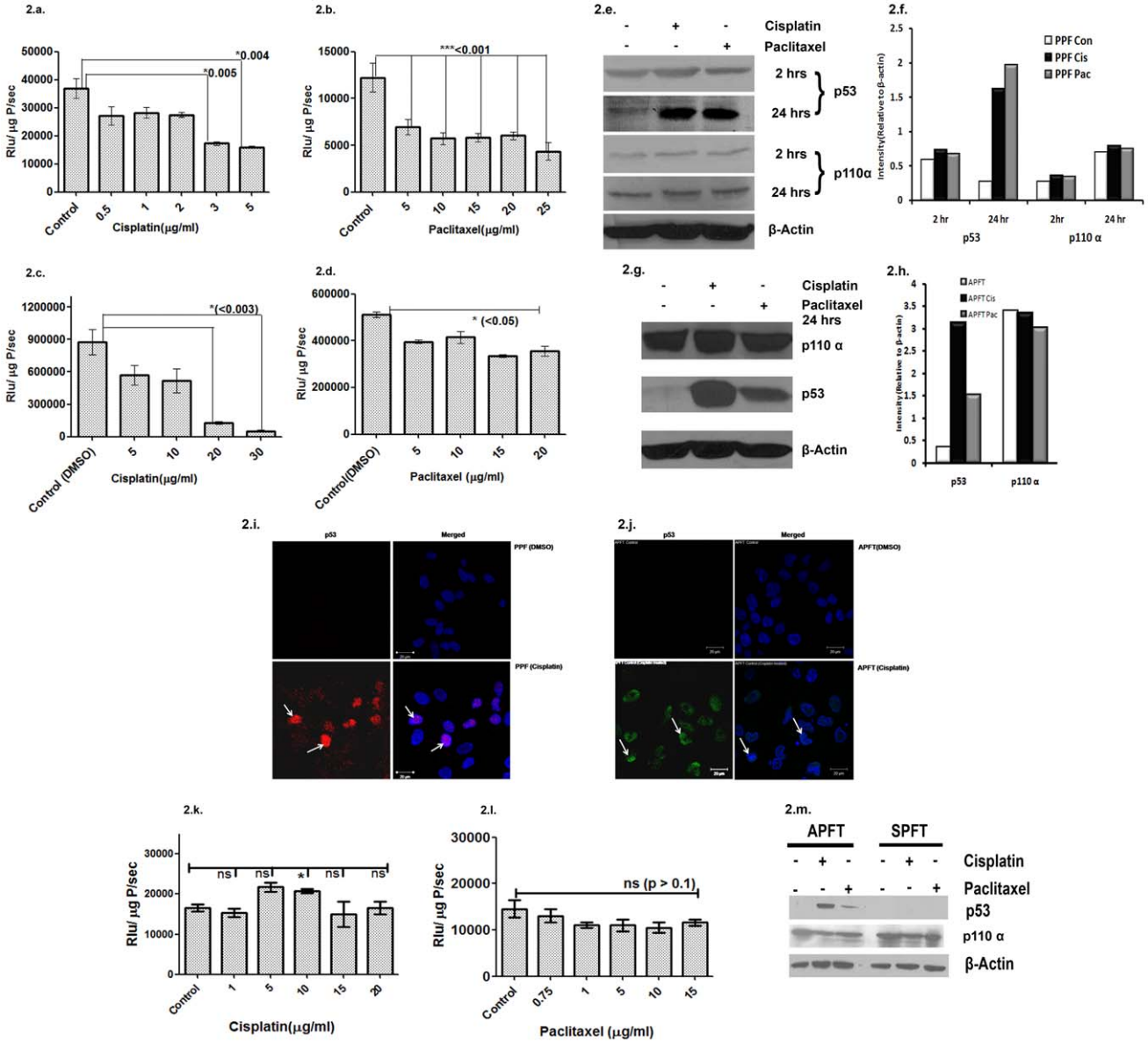

Figure 2. In vitro studies on effect of Cisplatin and paclitaxel on PIK3CA promoter and p53. 2a-d and 2k -2l. *PIK3CA* promoter activity in drug treated PA1-*PIK3CA-fluc2-tdt* (PPF), A2780-*PIK3CA-fluc2-tdt* (APFT) and SKOV3-*PIK3CA-fluc2-tdt* (SPFT) (2k and l) cells. A dose dependent decrease in luciferase activity (*PIK3CA* promoter activity) was observed on increasing concentrations of cisplatin treatments in PPF cells (at 3 & 5 µg/ml cisplatin, $p<0.03$) (2a) and in APFT cells at 20 and 30 µg/ml cisplatin ($p<0.003$) (2c). Similar dose dependent decrease in luciferase activity was obtained on increasing concentration of paclitaxel treatment in PPF up to 25 µg/ml, $p<0.001$) (2b) and in APFT cells upto 20 µg/ml paclitaxel, $p<0.05$ (2d) No such dose dependent change was observed on treatments with increasing concentration of cisplatin and paclitaxel (2k and 2l) in SPFT cells. 2e-2 h. Endogenous expression of p110α and p53 proteins after drug treatments. Western blot analysis of p53 protein from lysates of cisplatin and paclitaxel treated PPF and APFT cells showed induction in p53 level after 24hrs; however no change was observed after 2hrs. The p110α levels did not show any change after drug treatment (2e & 2g). The densitometric analysis representing the same is shown in 2d & 2h. The p53 mutant status in SPFT cells was verified by western blotting (2 m). 2i & 2j. Nuclear localization of p53 after treatment in cisplatin treated cells. p53 protein (red in 3g and green in 3h) showed nuclear localization upon treatment with cisplatin for 2hrs as compared to the vehicle treatment in PPF and APFT cells. DAPI (blue) indicated the nuclear staining.

doi:10.1371/journal.pone.0055971.g002

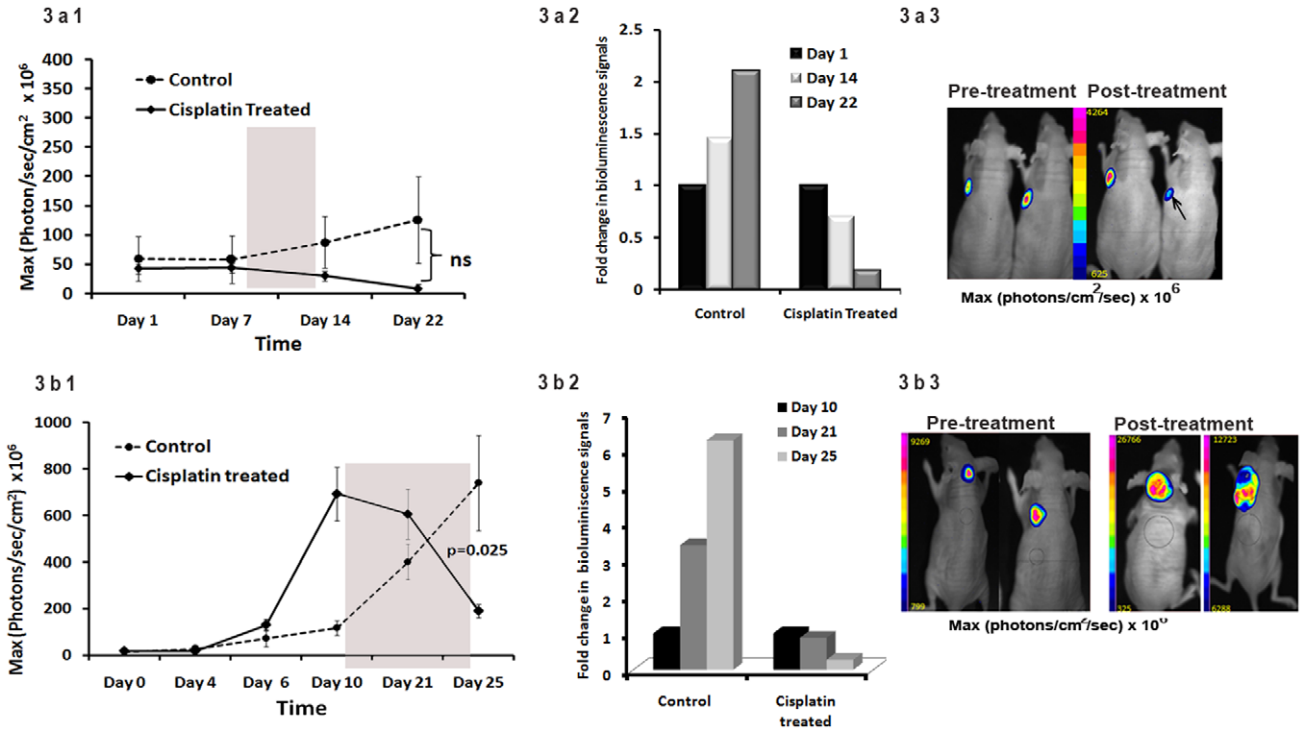

Figure 3. Non-invasive imaging of PIK3CA promoter modulation in tumor xenografts of living mice after cisplatin treatment. 3a. Bioluminescence signal of PIK3CA promoter in PPF tumors. 3a1. Graphical representation of the kinetics of *PIK3CA* promoter modulation. The luciferase activity in the control group of mice (n = 3) increased with time while that of the treated group (n = 3) attenuated from the fourteenth day of treatment till the 22nd day (end point) after one treatment (8 mg/kg) (shaded area represented the days of treatment). At 22nd day, measurable attenuation in the bioluminescence signal between the control and treated mice was evident however it did not reach statistical significance. (Day 1 represents the day prior to treatment). 3a2. Graphical representation of fold-changes in the bioluminescence signals. The temporal fold change in bioluminescence signal (post treatment signal/pre treatment signal) demonstrated augmented bioluminescence in the control group and attenuation in the treated group. 3a3. Representative bioluminescent images of the mice bearing PPF tumors. Mouse from the control and treated group exhibited specific and similar intensity signals which decreased after treatment (arrowhead). 3b. Bioluminescence signal of PIK3CA promoter in APFT tumors after cisplatin treatment. 3b1. Graphical representation of the kinetics of *PIK3CA* promoter modulation. The bioluminescence signal in the control mice (n = 3) increased with time while that of the treated group (n = 4) showed a slight decrease at 11th day after first treatment and significant attenuation at 15th day after second treatment ($p<0.025$). 3b2. Graphical representation of fold-changes in the bioluminescence signals. The temporal fold change in bioluminescence signals (post treatment signal/pre treatment signal) demonstrated augmented bioluminescence in the control group and but attenuation in the treated (Day 10 represented signal prior to treatment). 3b3. Representative bioluminescent images of the mice bearing APFT tumors. Mouse from control and treated group exhibited specific signals which decreased only in treated mouse as shown by an arrow.

doi:10.1371/journal.pone.0055971.g003

Mutations at p53 Binding Sites Augment *PIK3CA* Promoter Activity

Mutation in one of the four p53 binding sites (site 4) in PIK3CA promoter showed 50% less attenuation in presence of conditionally activated p53 protein [12]. We performed a series of site directed mutagenesis to sequentially abolish the binding of p53 in the promoter (Figure 5a) and measured luciferase activities from transiently transfected A2780 cells with wild and the four mutant *PIK3CA-fluc2-tdt* reporters along with *pTK-hrl* gene after cisplatin treatment. Mutation at site 3 alone (MPFT-1), sites 3&4 (MPFT-2), sites 3,4&2 (MPFT-3) and sites 3,4,2&1 (MPFT-4) did not exhibit any signal attenuation by cisplatin in comparison to the 20% reduction showed by the wild type promoter (Figure 5b). Intriguingly, three of these mutant promoters (MPFT-1, 2, 3) showed gradual augmentation of *PIK3CA* expression in comparison to the wild type promoter with MPFT-3 showing the maximal increase (2.5-fold). The MPFT-4 promoter showed overall decrease in *PIK3CA* expression in comparison to the wild type and other mutants. This attenuated activity of MPFT-4 was unexpected however after careful analysis of the *PIK3CA* promoter two important transcription factor binding (NF-kβ & HIF-1 ancillary sequence) sites were found to overlap at site 2 (Table 2). Our preliminary result suggested that TNF-α induced up regulation of wild type *PIK3CA* promoter was lost in MPFT-4 construct (data not shown) and further experiments are ongoing. Finally to assess the modulation of mutant *PIK3CA* promoter *in vivo*, stable clone of A2780 cells expressing the MPFT-3 construct was generated and treated with cisplatin and paclitaxel. In corroboration with the transient transfection result, the stable clones (APFT vs. A2780-MPFT3) showed an increase in luciferase activity (1.4 fold). However, no significant change in the promoter activity of A2780-MPFT3 cells was observed with increasing concentration of cisplatin and paclitaxel (Figure 5c & 5d) except for the high concentration (15 μg/ml) of cisplatin. The APFT cells did exhibit attenuated promoter activity with all concentrations of cisplatin and paclitaxel. Further to observe the effect of cisplatin on MPFT-3 promoter *in vivo*, six million A2780-MPFT3 cells were implanted and tumors were allowed to grow in nude mice (n = 3). As expected, the bioluminescence signals in treated mice did not decrease rather exhibited an increase after first treatment ($4\times10^8\pm1.4\times10^8$ p/sec/cm^2 to $7.5\times10^8\pm2.3\times10^8$ sec/cm^2) (2.4 fold) at 7th day, which remained constant to $7.5\times10^8\pm2.5\times10^8$ p/

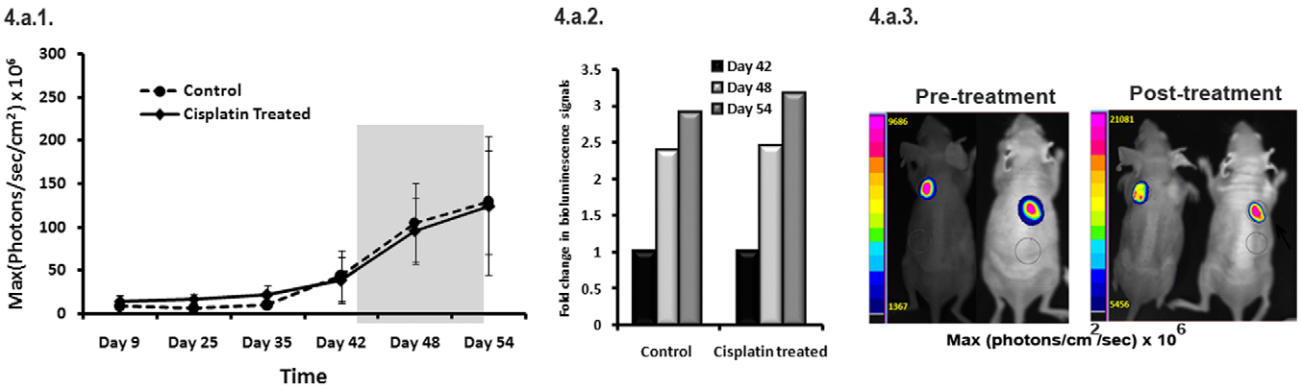

Figure 4. PIK3CA promoter activity in SKOV3 (p53 deficient) tumor xenograft model after cisplatin treatment. 4a1. Graphical representation of the kinetics of *PIK3CA* promoter modulation in the control and cisplatin treated mice. The bioluminescence signal in both control and treated mice increased with time even after two rounds of cisplatin treatment (n = 5). 4a2. Graphical representation of fold-changes in the bioluminescence signals of the control and treated mice. The temporal fold change in bioluminescence signals calculated ratiometrically (post treatment signal/pre treatment signal) demonstrated augmented bioluminescence in both the control and treated group (Day 42 of 4c1 is represents Day1 i.e. signal prior to treatment). 4a3. Representative bioluminescent images of the mice bearing tumors of SPFT cells before and after treatment. Mouse from control and treated group exhibited specific [Fig. 4a3 (pre-treatment)] signals which did not decrease even after two treatments of cisplatin [Fig. 4a3 (post-treatment)].
doi:10.1371/journal.pone.0055971.g004

sec/cm^2 after completion of two treatments at 24 days. The control mice (n = 3) also showed increased bioluminescence and tumor growth ($2.3\times10^8\pm2\times10^8$ p/sec/cm^2 to $4.4\times10^8\pm2.2\times10^8$ p/sec/cm^2 at day 7 to $9.2\times10^8\pm4.5\times10^8$ p/sec/cm^2) (~4 fold) over time (Figure 5e1 & 5e2). The representative images of the bioluminescence signal in mice pre- and post- treatment in A2780-MPFT3 tumor models are shown in the Figure 5e3.

Discussion

The standard therapeutic regimen for treating ovarian cancer is a combinatorial treatment of platinum (cisplatin or carboplatin) and taxol (paclitaxel) based drugs often followed by de-bulking surgery [33]. Both these drugs induce apoptotic pathways either by forming DNA adducts or by inducing cell cycle arrest and subsequent cell death [30]. Activation of p53 is a central molecular event that guides the cells to follow either a survival or an apoptotic route after the genotoxic insult. Activation of p53 might down-regulate the PIK3CA/Akt signalling as indirectly evidenced by association of *PIK3CA* gene amplification with p53 mutations in ovarian carcinoma [7,9].

p110α, the catalytic subunit of class I PI3K and encoded by *PIK3CA* gene is tightly regulated in normal cells. PI3KCA activation either by mutation or gene amplification initiates a signal transduction pathway that promotes growth, metabolism, and survival in cancer cells [5,8,9]. The putative ~900 bp *PIK3CA* promoter carries several important binding sites for p53, NF-κβ, HIF, and AP1 transcription factors [12,13]. While direct binding of p53 attenuates the *PIK3CA* promoter activity, inhibition of NF-kβ degradation or treatment with TNF-α results in moderate induction. However, none of these studies have attempted to find the effect of a chemotherapeutic drug on this promoter.

Non-invasive imaging of molecular events in small animals has become a standard practice to evaluate new drugs. Reporter genes or combination of reporter genes which can be used with multiple imaging devices add the advantage of collecting multiple signals from deep inside the body, with higher sensitivity and specificity over reporter genes suitable for only a single imaging modality [20,34]. Thus fusion reporter genes have gained popularity in preclinical imaging. Over the years we have built a small library of fusion reporter vectors and have been applying to monitor tumor metastasis, cell/stem cell trafficking, stem cell therapy, and other areas [22,23,24]. These fusion vectors comprise of a bioluminescent (either *fluc* or *hrluc* and their mutants), a fluorescent (either *gfp* or red fluorescent proteins and their mutants) and a PET reporter (*sr39* mutant thymidine kinase or wild type thymidine kinase) gene joined by small peptide linkers [20,21]. Our previous fusion reporters using a monomeric red fluorescent protein1 emitting light at 608 nm wavelength have suffered at sensitivity due to poor quantum yield and low photostability of the protein. Recently Tsien's group at UCSD developed several mutant red fluorescent proteins of which tdTomato is the most optimal for *in vivo* imaging. Even a low number of breast cancer cells expressing tdTomato can be imaged noninvasively from living mice including metastasis to lymph nodes [35]. The mCherry protein though having lower quantum yield has excitation spectra at 613 nm, a far red region optimal for *in vivo* imaging. When both these RFP mutants (tdTomato and mCherry) were tried as triple fusion partners, only tdTomato fusions could retain significantly higher fluorescence activity [29]. Among the bi-fusions and triple fusions carrying tdTomato, the bi-fusions are the brightest.

In parallel to improvement of fluorescent proteins, the luciferase genes were also attempted for enhancement of light output by mutagenesis, deletion of cryptic transcription factor binding sites and codon optimization for improved mammalian expression. The optimized version of *fluc (fluc2)* from Promega is able to generate 10-fold higher signals than *fluc* gene and this *fluc2* was used to generate the third generation fusion reporters by replacing the mutated thermostable *fluc* (*mtfl*). Interestingly, the newly developed *fluc2* containing fusion reporter (*fluc2-tdt*) show higher fluorescence along with higher luciferase activity than the previous fusions. This apparent increase in overall fluorescent activity after introduction of *fluc2* protein maybe due to the change in the quaternary structure resulting in better exposure of the flurophores present in the fluorescent proteins.

To understand the regulation of *PIK3CA* promoter in ovarian cancer cells, we utilized this optimized *fluc2-tdt* fusion reporter to monitor the effects of cisplatin and paclitaxel from intact cells to living animals. To our best of knowledge this is the first report of understanding the kinetics of drug induced *PIK3CA* promoter

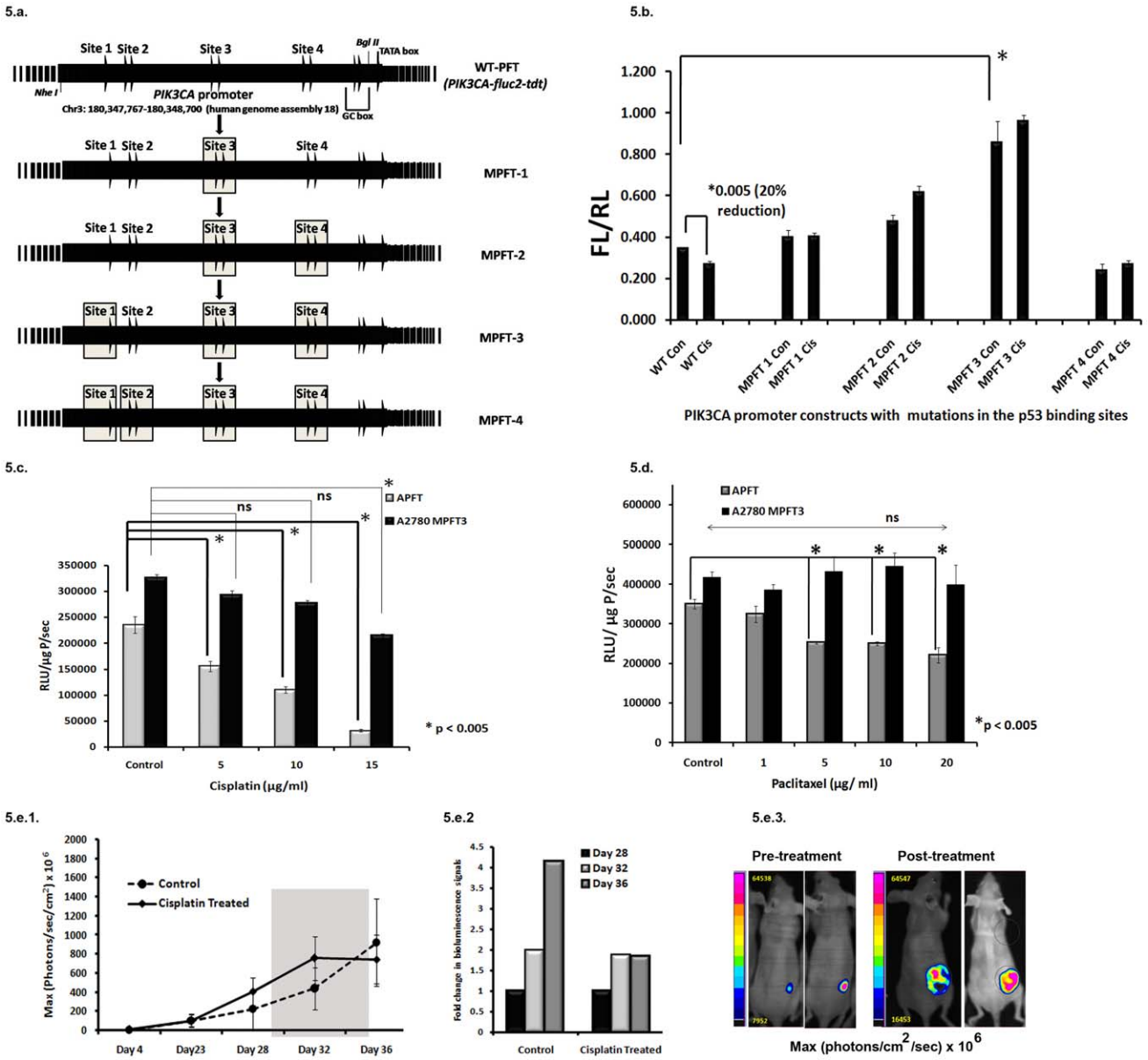

Figure 5. Mutations at p53 binding sites augment PIK3CA promoter activity. 5a. Substitutions in core sequence of p53 binding sites of *PIK3CA* promoter by sequential site directed mutagenesis to obtain four mutant *PIK3CA-fluc2-tdt* reporters (MPFT-1, MPFT-2, MPFT-3 and MPFT-4). 5b. Sequential mutation augments *PIK3CA* promoter activity. Ratiometric analysis of wild type and mutant *PIK3CA-fluc2-tdt* reporters with *pTK-hRL* from transiently transfected A2780 cells with and without cisplatin treatment (2 hrs) were graphically represented. Twenty percent reduction in WT-PFT activity ($p<0.005$) without any attenuation in the mutant promoters (MPFT-1, MPFT-2 and MPFT-3) were observed post cisplatin treatment. These mutant promoters showed a gradual augment of PIK3CA expression compared to WT-PFT with MPFT 3 showing a maximum of 2.5-fold increase (*Fig. 5b). The MPFT-4 promoter showed an overall decrease in *PIK3CA* expression in comparison to WT-PFT. The SEM represents triplicate experiments. 5c and 5d. Effect of cisplatin and paclitaxel in A2780-MPFT3 cells. Treatment with increasing concentrations of cisplatin (5 and 10 µg/ml) and paclitaxel (1–20 µg/ml) exhibited attenuated luciferase activity in APFT cells but not in A2780-MPFT3 cells except at very high dose of cisplatin (15 µg/ml). The SEM represents triplicate experiments. 5e. Non invasive imaging of cisplatin treated A2780-MPFT3 tumor xenografts. 5e1. Graphical representation of the kinetics of *PIK3CA* promoter modulation. The bioluminescence signal in both control and treated mice increased with time even after two rounds of cisplatin treatment (n = 3). 5e2. Graphical representation of fold-changes in the bioluminescence signals. The temporal fold change in bioluminescence signals calculated ratiometrically (post treatment signal/pre treatment signal) demonstrated augmented bioluminescence in both the control and treated group (Day 28 of 5e1 is represents Day1 i.e. signal prior to treatment). 5e3. Representative bioluminescent images of the mice bearing tumors of A2780-MPFT3 cells. Mouse from control and treated group exhibited specific [Fig. 5e3 (pre-treatment)] signals which did not decrease even after two treatments of cisplatin [Fig. 5e3 (post-treatment)].
doi:10.1371/journal.pone.0055971.g005

modulation. Our newly constructed *PIK3CA (PIK3CA-fluc2-tdt)* sensor exhibited significant attenuation after treatment with three chemotherapeutic drugs (cisplatin, paclitaxel and adriamycin) commonly used for ovarian cancer patients in two different cancer cells. The similar treatments did not affect the *TK* (Thymidine kinase) promoter in PA1 and A2780 cells. The level of attenuation varied between the cell lines with PA1 cells being more sensitive (2.3 fold reduction in promoter activity) than A2780 cells (1.3 fold)

Table 2. Transcription factor binding sites in PIK3CA promoter*.

Sequence	Transcription Factors	Position (bp)
TTACAACAAAAGACCAGTAGGGGGA	SOX/SRY-sex/testis determining and related HMG box factors	24–48
CACCAAGACA	Half p53 binding element (**site 1**)	142–151
TGGCATTACG CCCCACGTCT	p53 binding site **(Site 2)**	201–210 220–229
CGCGAAAAATCCCCC	NF kβ (overlap at **site 2**)	209–223
AAGTGAGTCAAAG	AP1	320–332
ACGCTGGTTA CGGTTAGCCA	p53 binding site (**Site 3**)	457–466 481–490
TAGAAACAAATATACTA	Fork head domain factors	608–624
CACGTACGCTGT	HIF-1	624–636
GATGACACAACA	AP1	642–653
AAGCAAGACG GCACATATTG	p53 binding site (**Site 4**)	732–741 753–762

Note: *As analysed by the Genomatix software and using references from Astanehe et al, 2008 and Yang et al, 2009.
doi:10.1371/journal.pone.0055971.t002

at same concentrations of cisplatin or paclitaxel (5 μg/ml) reflecting their respective clinical behaviour. All these drugs are known to induce cell death directly or indirectly via p53 mediated apoptotic pathways [31,32,36]. Reduction in promoter activity but no detectable variation in the endogenous p110α level after cisplatin or paclitaxel treatments indicates the strength of *fluc2-tdt* fusion reporter and reporter assay technique in measuring subtle changes of *PIK3CA* at molecular level. The endogenous p53 protein level, however, was significantly induced by the drugs. Activation of p53 by these drugs thereby leads to increased binding of p53 to the *PIK3CA* promoter and its suppression. This drug mediated attenuation of *PIK3CA* activity due to increased binding of activated p53 was not detected in a p53 deficient EOC (SKOV3) cell line. Both cisplatin and paclitaxel with increasing concentrations were not able to attenuate the *PIK3CA* promoter in these cells. The *in vivo* imaging kinetics showed a decrease in bioluminescence signal in both PA1 and A2780 tumors (expressing *PIK3CA-fluc2-tdt*) after cisplatin treatment. While a single treatment of cisplatin caused measurable reduction in luminescence activity in PA1 tumors at 14^{th} day, it did not effectively reduce the PIK3CA promoter activity in A2780 tumors. Two successive treatments were required to achieve significant reduction in luminescence activity in A2780 tumors. This differential effect of cisplatin on two different tumor types correlates well with their origin as ovarian germline tumors are known to be more sensitive to cisplatin in comparison to epithelial ovarian tumors. In corroboration with the *in vitro* results, cisplatin treatment *in vivo* also did not reduce the bioluminescence signals of SKOV3 tumor xenografts stably expressing the PIK3CA sensor indicating that presence of p53 protein is essential for *PIK3CA* regulation in ovarian cancer.

Surprisingly, sequential deletion of the p53 binding sites exhibited a gradual increase in the normal promoter activity indicating a temporary relief of p53 mediated suppression. Cisplatin induced attenuation of these mutant promoters were abolished. Inability to down regulate the mutant *PIK3CA* promoter by cisplatin was also reflected through non-invasive imaging of tumor xenografts stably expressing MPFT3, the promoter carrying three mutated p53 binding sites. Surprisingly, MPFT4 carrying mutations at all the four p53 binding sites showed an overall attenuation which might occur due to destabilization of co-operative bindings of other transcription factors required for PIK3CA expression. Indeed after careful analysis of *PIK3CA* promoter, site 2 was found to contain overlapping binding sites for NF-kβ and Hypoxia Inducible Factor ancillary sequence (Table 2). We are currently analyzing the role of these two factors in regulation of this MPFT-4 promoter. The PIK3CA pathway is one of the most crucial cellular defence mechanisms and therefore requires tight regulation at transcriptional and translational level. These newly developed *PIK3CA-fluc2-tdt* and the mutant reporter sensors could act as screening tools for potential new drugs. The power of these vectors from translating such information from single cells to the organism level will facilitate wide application in functional assessment of PIK3CA pathway for future therapeutic evaluation.

Supporting Information

Figure S1 Drug treatment modulates PIK3CA promoter but not TK promoter as revealed by luciferase activity. 1a. A unique *PIK3CA* sensor (*PIK3CA* promoter driven *fluc2-tdt*) shows attenuation in promoter activity (luciferase activity) on treatment with cisplatin and adriamycin of transiently transfected PA1 cells ($p<0.05$). Treatment with paclitaxel showed decreasing trend in *PIK3CA* activity, but did not meet significance ($p>0.05$). 1b. Humanized renilla luciferase driven by the TK promoter (*pTK-hrl*) co-transfected in PA1 cells does not show any change in luciferase activity after drug treatment ($p = ns$).
(TIF)

Author Contributions

Conceived and designed the experiments: PR SSG. Performed the experiments: SMG LG ARJ. Analyzed the data: SMG PR SSG. Contributed reagents/materials/analysis tools: AA. Wrote the paper: SMG PR.

References

1. Bunney TD, Katan M (2010) Phosphoinositide signalling in cancer: beyond PI3K and PTEN. Nat Rev Cancer 10: 342–352.
2. Vivanco I, Sawyers CL (2002) The phosphatidylinositol 3-Kinase AKT pathway in human cancer. Nat Rev Cancer 2: 489–501.
3. Yuan TL, Cantley LC (2008) PI3K pathway alterations in cancer: variations on a theme. Oncogene 27: 5497–5510.
4. Bader AG, Kang S, Zhao L, Vogt PK (2005) Oncogenic PI3K deregulates transcription and translation. Nat Rev Cancer 5: 921–929.
5. Gaikwad SM, Ray P (2012) Non-invasive Imaging of PI3K/Akt/mTOR signalling in Cancer. American Journal of Nuclear Medicine and Molecular Imaging. 2(4): 418–431.
6. Lee JW, Soung YH, Kim SY, Lee HW, Park WS, et al. (2005) PIK3CA gene is frequently mutated in breast carcinomas and hepatocellular carcinomas. Oncogene 24: 1477–1480.
7. Kolasa IK, Rembiszewska A, Felisiak A, Ziolkowska-Seta I, Murawska M, et al. (2009) PIK3CA amplification associates with resistance to chemotherapy in ovarian cancer patients. Cancer Biol Ther 8: 21–26.
8. Campbell IG, Russell SE, Choong DY, Montgomery KG, Ciavarella ML, et al. (2004) Mutation of the PIK3CA gene in ovarian and breast cancer. Cancer Res 64: 7678–7681.
9. Network TCGA (2011) Integrated genomic analyses of ovarian carcinoma. Nature 474: 609–615.
10. Abedini MR, Muller EJ, Bergeron R, Gray DA, Tsang BK (2009) Akt promotes chemoresistance in human ovarian cancer cells by modulating cisplatin-induced, p53-dependent ubiquitination of FLICE-like inhibitory protein. Oncogene. 11–25.
11. Fraser M, Leung B, Jahani-Asl A, Yan X, Thompson WE, et al. (2003) Chemoresistance in human ovarian cancer: the role of apoptotic regulators. Reprod Biol Endocrinol 1: 66.
12. Astanehe A, Arenillas D, Wasserman WW, Leung PC, Dunn SE, et al. (2008) Mechanisms underlying p53 regulation of PIK3CA transcription in ovarian surface epithelium and in ovarian cancer. J Cell Sci 121: 664–674.
13. Yang N, Huang J, Greshock J, Liang S, Barchetti A, et al. (2008) Transcriptional regulation of PIK3CA oncogene by NF-kappaB in ovarian cancer microenvironment. PLoS One 3: e1758.
14. Massoud TF, Gambhir SS (2003) Molecular imaging in living subjects: seeing fundamental biological processes in a new light. Genes Dev 17: 545–580.
15. Min JJ, Ahn Y, Moon S, Kim YS, Park JE, et al. (2006) In vivo bioluminescence imaging of cord blood derived mesenchymal stem cell transplantation into rat myocardium. Ann Nucl Med 20: 165–170.
16. Ray P, Bauer E, Iyer M, Barrio JR, Satyamurthy N, et al. (2001) Monitoring gene therapy with reporter gene imaging. Semin Nucl Med 31: 312–320.
17. Doubrovin M, Serganova I, Mayer-Kuckuk P, Ponomarev V, Blasberg RG (2004) Multimodality in vivo molecular-genetic imaging. Bioconjug Chem 15: 1376–1388.
18. Mayer-Kuckuk P, Menon LG, Blasberg RG, Bertino JR, Banerjee D (2004) Role of reporter gene imaging in molecular and cellular biology. Biol Chem 385: 353–361.
19. Ray P, De A, Patel M, Gambhir SS (2008) Monitoring caspase-3 activation with a multimodality imaging sensor in living subjects. Clin Cancer Res 14: 5801–5809.
20. Ray P, Tsien R, Gambhir SS (2007) Construction and validation of improved triple fusion reporter gene vectors for molecular imaging of living subjects. Cancer Res 67: 3085–3093.
21. Ray P, Wu AM, Gambhir SS (2003) Optical bioluminescence and positron emission tomography imaging of a novel fusion reporter gene in tumor xenografts of living mice. Cancer Res 63: 1160–1165.
22. Cao F, Lin S, Xie X, Ray P, Patel M, et al. (2006) In vivo visualization of embryonic stem cell survival, proliferation, and migration after cardiac delivery. Circulation 113: 1005–1014.
23. Shu CJ, Guo S, Kim YJ, Shelly SM, Nijagal A, et al. (2005) Visualization of a primary anti-tumor immune response by positron emission tomography. Witte ONProc Natl Acad Sci U S A 102(48): 17412–17417.
24. Yaghoubi SS, Creusot RJ, Ray P, Fathman CG, Gambhir SS (2007) Multimodality imaging of T-cell hybridoma trafficking in collagen-induced arthritic mice: image-based estimation of the number of cells accumulating in mouse paws. J Biomed Opt 12: 064025.
25. Chudakov DM, Matz MV, Lukyanov S, Lukyanov KA (2010) Fluorescent proteins and their applications in imaging living cells and tissues. Physiol Rev 90: 1103–1163.
26. DeBlasio SL, Sylvester AW, Jackson D (2010) Illuminating plant biology: using fluorescent proteins for high-throughput analysis of protein localization and function in plants. Brief Funct Genomics 9: 129–138.
27. Lippincott-Schwartz J, Patterson GH (2003) Development and use of fluorescent protein markers in living cells. Science 300: 87–91.
28. Ray P, De A, Min JJ, Tsien RY, Gambhir SS (2004) Imaging tri-fusion multimodality reporter gene expression in living subjects. Cancer Res 64: 1323–1330.
29. Shaner NC, Lin MZ, McKeown MR, Steinbach PA, Hazelwood KL, et al. (2008) Improving the photostability of bright monomeric orange and red fluorescent proteins. Nat Methods 5: 545–551.
30. Siddik ZH (2003) Cisplatin: mode of cytotoxic action and molecular basis of resistance. Oncogene 22: 7265–7279.
31. Rakovitch E, Mellado W, Hall EJ, Pandita TK, Sawant S, et al. (1999) Paclitaxel sensitivity correlates with p53 status and DNA fragmentation, but not G2/M accumulation. Int J Radiat Oncol Biol Phys 44: 1119–1124.
32. Prasad SB, Rosangkima G, Khyynriam D (2006) Cisplatin -induced Toxicological Effects in Relation to the Endogenous Tissue Glutathione Level in Tumor-Bearing Mice. Asian J Exp Sci, Vol 20: 55–68.
33. Agarwal R, Kaye SB (2003) Ovarian cancer: strategies for overcoming resistance to chemotherapy. Nat Rev Cancer 3: 502–516.
34. Massoud TF, Paulmurugan R, De A, Ray P, Gambhir SS (2007) Reporter gene imaging of protein-protein interactions in living subjects. Curr Opin Biotechnol 18: 31–37.
35. Winnard PT Jr, Kluth JB, Raman V (2006) Noninvasive optical tracking of red fluorescent protein-expressing cancer cells in a model of metastatic breast cancer. Neoplasia 8: 796–806.
36. Giannakakou P, Robey R, Fojo T, Blagosklonny MV (2001) Low concentrations of paclitaxel induce cell type-dependent p53, p21 and G1/G2 arrest instead of mitotic arrest: molecular determinants of paclitaxel-induced cytotoxicity. Oncogene 20: 3806–3813.

The International Journal of Biochemistry & Cell Biology 61 (2015) 90–102

Contents lists available at ScienceDirect

The International Journal of Biochemistry & Cell Biology

journal homepage: www.elsevier.com/locate/biocel

Differential activation of NF-κB signaling is associated with platinum and taxane resistance in MyD88 deficient epithelial ovarian cancer cells

Snehal M. Gaikwad [1], Bhushan Thakur [1], Asmita Sakpal, Ram K. Singh, Pritha Ray *

Advanced Centre for Treatment, Research and Education in Cancer (ACTREC), Tata Memorial Centre, Navi Mumbai, Maharashtra, 410210, India

ARTICLE INFO

Article history:
Received 23 July 2014
Received in revised form 23 January 2015
Accepted 3 February 2015
Available online 11 February 2015

Keywords:
Chemoresistance
Ovarian cancer
NF-κB signaling
Dual bioluminescence imaging
MyD88

ABSTRACT

Development of chemoresistance is a major impediment to successful treatment of patients suffering from epithelial ovarian carcinoma (EOC). Among various molecular factors, presence of MyD88, a component of TLR-4/MyD88 mediated NF-κB signaling in EOC tumors is reported to cause intrinsic paclitaxel resistance and poor survival. However, 50–60% of EOC patients do not express MyD88 and one-third of these patients finally relapses and dies due to disease burden. The status and role of NF-κB signaling in this chemoresistant MyD88^{negative} population has not been investigated so far. Using isogenic cellular matrices of cisplatin, paclitaxel and platinum-taxol resistant MyD88^{negative} A2780 ovarian cancer cells expressing a NF-κB reporter sensor, we showed that enhanced NF-κB activity was required for cisplatin but not for paclitaxel resistance. Immunofluorescence and gel mobility shift assay demonstrated enhanced nuclear localization of NF-κB and subsequent binding to NF-κB response element in cisplatin resistant cells. The enhanced NF-κB activity was measurable from *in vivo* tumor xenografts by dual bioluminescence imaging. In contrast, paclitaxel and the platinum-taxol resistant cells showed down regulation in NF-κB activity. Intriguingly, silencing of MyD88 in cisplatin resistant and MyD88^{positive} TOV21G and SKOV3 cells showed enhanced NF-κB activity after cisplatin but not after paclitaxel or platinum-taxol treatments. Our data thus suggest that NF-κB signaling is important for maintenance of cisplatin resistance but not for taxol or platinum-taxol resistance in absence of an active TLR-4/MyD88 receptor mediated cell survival pathway in epithelial ovarian carcinoma.

1. Introduction

Ovarian cancer primarily the epithelial ovarian cancer (EOC) has the highest mortality rate of all gynaecologic malignancies in women. In spite of improved treatment modalities in recent years, about 60% patients succumb to the disease within 5 years due to recurrence and acquired drug resistance (Armstrong et al., 2006; Rocconi et al., 2006). Patients with relapsed disease either show intrinsic resistance or develop resistance through repetitive exposures to drugs. Among various factors contributing to chemoresistance, genes involved in cell death and cell survival pathways play major role in acquirement and sustainment of resistance phenotype (Chaudhury et al., 2014; Gaikwad and Ray, 2012; Gottesman, 2002; Kartalou and Essigmann, 2001; Kim et al., 2005; Siddik, 2002; Singh et al., 2014). Altered expression of anti-apoptotic proteins such as members of Bcl-2 family proteins and components of mitogen-activated proteins kinase (MAPK) pathway, PI3K/AKT/mTOR pathway and NF-κB signaling are shown to be involved in resistance and recurrence (Beale et al., 2000; Brozovic et al., 2004; Karin, 2009; Koti et al., 2013; Mabuchi et al., 2004a; Nehra et al., 2010; Tang et al., 2001). The NF-κB family of transcription factors are induced by a broad range of stimulators and can initiate dynamic modulations in gene expressions of immune surveillances, differentiation, proliferation, apoptosis, angiogenesis, cell cycle progression and drug resistance (Hayden and Ghosh, 2012).

The Toll-like receptor (TLR) family plays a central role in commencement of innate immunity through activation of NF-κB (Blasius and Beutler, 2010). The activation of TLR signaling pathways originates from the cytoplasmic TIR domains and TIR domain containing adapter protein, myeloid differentiation factor88 or MyD88. Among all the TLRs, TLR-4 and TLR-3 induce NF-κB activation either through MyD88 (MyD88 dependent) or

* Corresponding author. Tel.: +91 02227405119.
E-mail address: pray@actrec.gov.in (P. Ray).
[1] These authors have equally contributed to the work.

http://dx.doi.org/10.1016/j.biocel.2015.02.001
1357-2725/

via another adapter protein called TICAM-1 (MyD88 independent) (Akira, 2003; Kawai and Akira, 2006, 2007). Both MyD88 and TICAM-1 activate IκB kinases (IKKα/IKKβ or IKKε/IKKι) via activation of either IRAK/TRAF-6 or IRF-3/TBK1 which are responsible for phosphorylation and degradation of inhibitory κB (IκB) proteins, nuclear localization of NF-κB and initiation of the cascade of gene expression.

Interestingly, active TLR-4/MyD88 signaling is also found on epithelial ovarian cancer cells and presence of MyD88 but not TLR-4 significantly influences the drug response (Kelly et al., 2006; Muccioli et al., 2012; Silasi et al., 2006; Szajnik et al., 2009). Following paclitaxel treatment, MyD88 positive EOC cells show increased proliferation and tumor growth, activated NF-κB and AKT signaling and overexpression of antiapoptotic proteins. However, MyD88 negative EOC cells do not show proliferation rather induce caspase dependent apoptosis after paclitaxel treatment (Szajnik et al., 2009). Patients devoid of MyD88 expression show a significantly higher disease free progression interval compared to the patients whose tumors express MyD88 (Kim et al., 2012). Thus MyD88 has been proposed as a potential biomarker for determining chemo-response to paclitaxel in ovarian cancer (Kelly et al., 2006). Recently, the relationships between the expression of TLR-4, MyD88 and NF-κB were examined in a large cohort of 123 cases of epithelial ovarian cancer patients using immunohistochemistry (Kim et al., 2012). While this study indicated that MyD88 expression was associated with poor survival in patients, it also revealed that a significant percentage of EOC patients (~60%) were MyD88^{negative} and around 40% (32/78) of them exhibited disease recurrence. The status and role of NF-κB signaling in these chemoresistant MyD88^{negative} populations is unclear and certainly requires further investigation for devising new therapeutic strategies.

In this study, using isogenic cellular matrices of cisplatin, paclitaxel and platinum-taxol resistant MyD88^{negative} ovarian cancer cells (A2780) expressing a NF-κB reporter sensor, we showed that enhanced NF-κB activity was only required for cisplatin resistance but not for paclitaxel or platinum-taxol resistance. This enhanced NF-κB activity was evident from higher nuclear expression and could be imaged from cisplatin resistant tumor xenografts in real time. Increased expression associated with cisplatin resistance indicated Bcl-2 as a possible molecular player for sustained resistance. In contrast, paclitaxel and platinum-taxol resistant cells were not associated with NF-κB activation. Cisplatin, paclitaxel and platinum taxol treatment did not exhibit any change in NF-κB activity in MyD88^{positive} and naturally occurring cisplatin resistant TOV21G cells. However, when MyD88 expression was suppressed using sh-RNA mediated silencing; only cisplatin treatment exhibited enhanced NF-κB activity. Similar result was observed in SKOV3, another MyD88^{positive} and naturally occurring cisplatin resistant cell line. Taken together, these data show the complexity of the NF-κB signaling pathway involved in acquired drug resistance and dispensability of MyD88 during development of cisplatin resistance in epithelial ovarian cancer.

2. Material and methods

2.1. Reagents and antibodies

Cisplatin (cis-Diammineplatinum (II) dichloride), Paclitaxel, G418 disulfate salt, puromycin, Lipopolysaccharide (LPS), polybrene, primary antibodies (β-actin and α-tubulin), and HRP conjugated secondary antibodies (anti-mouse and anti-rabbit) were purchased from Sigma–Aldrich (USA). Luciferase assay system was procured from Promega. D-luciferin and coelenterazine were procured from Biosynth International (Switzerland). NF-κB (p65), Lamin-A, MyD88, TLR-4 and Bcl-2 antibodies were procured from ABCAM (Cambridge, USA) and Cell Signaling Technologies (Danvers, MA, USA) respectively.

2.2. Construction of NF-κB sensor

The 160 bp sequence consisting of NF-κB response element (composed of four tandem copies of the NF-κB consensus binding sequence) followed by a minimal TA promoter was PCR amplified from pNF-κB-Met-Luc-2 plasmid (Clontech, USA). The amplified product was cloned in place of CMV promoter of pcDNA-3.1(+)-puro vector carrying the hRL-eGFP or hRL-mRFP bi-fusion reporter (Ray et al., 2003). Positive clones of pNF-κB-hRL-eGFP/mRFP-pcDNA3.1 (+)-puro were confirmed by PCR amplification, restriction digestion and sequencing.

2.3. Cell line, culture conditions and transfection

A2780 cells (undifferentiated EOC cell), SKOV3 (high grade serous), OAW42 (high grade serous) and TOV21G (clear cell) cells obtained from ATCC (Manassas, VA, USA) were cultured in DMEM, RPMI, and MEM medium (GIBCO, Carlsbad, CA) respectively supplemented with 10% fetal bovine serum (HiMedia) and 1% penicillin-streptomycin (GIBCO). For NF-κB activity, cells were transiently transfected with pNF-κB-hRL-eGFP/mRFP and CMV-fl2-tdt (9:1 ratio) and ratiometrically measured by Renilla luciferase/ Firefly luciferase (RL/FL) activity. A2780 cells stably expressing PIK3CA promoter driving firefly luciferase were engineered for stably expressing the NF-κB sensor (Gaikwad et al., 2013). All the transient and stable transfections with NF-κB sensor were carried out using Superfect transfection reagent (Qiagen, Valencia, CA) and stable cells were selected using puromycin. For all the drug treatments, cells were incubated for 24 h with cisplatin (10 μg/ml) or carboplatin (0.5–1.25 μg/ml) or paclitaxel (5 μg/ml) diluted in DMSO or water. Combinatorial treatments were given with both cisplatin (1 μg/ml) and paclitaxel (500 ng/ml) for 24 h. All transfection and drug treatment experiments were performed in triplicates and repeated at least twice.

2.4. MyD88 silencing by lentiviral mediated sh-RNA constructs

Lentivirus mediated RNA interference was used to silence the expression of MyD88 gene. First the pLL3.7 lentiviral vector was used to clone the target (5′ GACCCAATGTACCAGTATT, adapted from Yang et al., 2013) and scramble sequence (5′ ATAATCGCCGTGAATTCC) between Hpa1 and Xho1 sites. Positive clones were verified by restriction digestion and sequencing. Later 2×10^6 293FT cells were seeded in 100 mm culture dish followed by cotransfection of vector plasmid carrying the desired shRNA construct along with the packaging plasmids (pδ 8·9, VSVG) using lipofectamine 2000 (Invitrogen). After 16 h of transfection, supernatant was removed and supplemented with 10 ml fresh medium. Viruses were harvested post 48 h and filtered through 0.45 μm filter and stored at −80 °C.

2.5. FACs sorting of MyD88 stable knockdowns cells

TOV21G and SKOV3 cells transiently or stably expressing pNF-κB hRL-mRFP reporter were seeded at 60% confluency in 100 mm culture dish. Transduction with lentivirus particles was performed by adding 2 ml of viral particles and 4 ml of complete media in presence of polybrene (4 μg/ml). Stable clones were isolated by FACS sorting using the eGFP reporter present in the lentiviral vector.

2.6. Establishment of cisplatin, paclitaxel and combinatorial resistance in A2780 cells

To develop cisplatin, paclitaxel and platinum-taxol resistant models, 1×10^6 A2780 cells were treated with incremental doses for a period of 6 months with each dose repeated for three cycles. Based upon percent viability, cells were categorized as A2780-Cis^{LR} (cells resistant to cisplatin), A2780-Pac^{LR} (resistant to paclitaxel) and A2780-Cis-Pac^{LR} (resistant to both cisplatin and paclitaxel). Both TOV21G and SKOV3 cells are known to show resistance towards different concentration of cisplatin (Dier et al., 2014; Koh et al., 2012; Yuan et al., 2011).

2.7. Luciferase reporter assay

Renilla and Firefly luciferase activities were measured using luciferase assay system (Promega) and coelenterazine in a Berthold luminometer as described previously (Gaikwad et al., 2013).

2.8. MTT assays

Cell viability was assessed using the standard thiazolyl blue tetrazolium bromide (MTT) method and percent viability was counted using the formula $\{[\text{Absorbance}^{(\text{Test})} \div \text{Absorbance}^{(\text{Control})}] \times 100\}$. Drugs were added at different concentrations and the inhibitory concentrations were calculated for the sensitive and resistant cells. All experiments were performed at least three times. Resistance index (RI) for each model was calculated using the formula (IC_{50} of resistant cells/IC_{50} of sensitive cells). For calculating doubling time, 5×10^2 cells/well were plated in 96 well plates and cell viability was assessed by MTT in quadruplicate every 24 h interval for 6 days. The data were subjected to linear regression analysis and doubling time (Td) was calculated using online calculator of doubling time (Roth, 2006).

2.9. Clonogenic assay

Single-cell suspensions were plated in six well dishes at a density of 500 cells/well. Once adhered, cells were treated with increasing concentrations of drugs for 24 h. The plates were further incubated for 7 days and colonies were stained with 0.05% crystal violet and counted under inverted microscope. Colonies consisting more than 50 cells were counted. Plating efficiencies (PE) and survival fractions (SF) were calculated using the formula: PE = Number of colonies/Number of cells seeded; SF = Number of colonies/Number of cells seeded × PE and plotted graphically to obtain survival curves.

2.10. Immunofluorescence

Immunofluorescence studies were performed as described earlier (Gaikwad et al., 2013) Briefly, cells plated on coverslips were fixed with 4% paraformaldehyde, permeabilized with 0.025% Triton-X and probed with NF-κB or TLR-4 antibody for overnight at 4 °C. Next day, after 2 h of incubation with secondary antibody, cells were counterstained with DAPI and images were observed under Carl Zeiss, LSM 710 microscope. At least five representative fields were studied.

2.11. Preparation of nuclear and cytosolic proteins and Western blotting

1×10^7 cells were lysed with 400 μl (five times the cells pellet volume) of Cytoplasmic Extract (CE) buffer [(10 mM KCl, 0.1 mM EDTA, 10 mM HEPES and 0.3% NP-40 with proteinase inhibitor cocktail (Sigma))] at 4 °C for 10 min. The lysate was centrifuged for 15 min at 6000 rpm at 4 °C and supernatants were collected as cytosolic extract. The resulting pellet was re-suspended in CE buffer and washed for 2–3 times for 15 min at same conditions. Further, the pellet was resuspended in 50 μl of ice-cold 20 mM HEPES (pH 7.9), 420 mM NaCl, 20% (v/v) glycerol, 1 mM EDTA and proteinase inhibitor cocktail. After 5 min incubation at 4 °C, the lysate was centrifuged for 10 min at 14,000 rpm at 4 °C, and the supernatant was collected as nuclear extract. The concentrations of cytosolic and nuclear extracts were determined using Bradford Reagent (Sigma). Western blot analysis was done as described earlier (Gaikwad et al., 2013).

2.12. Quantitative and semi-quantitative RT-PCR

2 μg of total RNA extracted from cells using RNeasy kit (Qiagen, Netherland) was reverse transcribed using cDNA synthesis kit (Invitrogen, Carlsbad, CA). Quantitative-PCR (q-PCR) was performed using SYBR Green method (Invitrogen). GAPDH was used as an internal control. Primer sequences used were as follows: GAPDH (forward TGCACCACCAACTGCTTAGC, reverse GGCATGGACTGTGGTCATGAG); MyD88 (forward CGCCGGATGGTGGTGGTTGT, reverse TGTAGTCGCAGACAGTGATGAACC); Cyclin D1 (forward TATTGCGCTGCTACCGTTGA, reverse CCAATAGCAGCAAACAATGTGAAA); XIAP (forward GATGATGTGAGTTCTGATAGG and reverse CTTAATGTCCTTGAAACTGAAC). The relative expression levels of mRNAs were calculated by the $2^{-\Delta Ct}$ and fold change measurement by $2^{-\Delta\Delta Ct}$ method. Semi-quantitative RT-PCR was done as mentioned earlier (Gaikwad et al., 2013).

2.13. Electrophoretic mobility shift assay (EMSA)

NF-κB DNA binding activity was assessed by EMSA using biotin labeled oligo probes. Briefly, oligomers containing NF-κB consensus sequences were labeled using Biotin 3′ End DNA labeling kit (Thermo Scientific). 10 μg of respective nuclear lysates were equilibrated in binding buffer containing 10 mM Tris, 50 mM KCl, 1 mM DTT, 5 mM $MgCl_2$, 2.5% glycerol, 0.05% NP40, 20 ng/μl sheared salmon sperm DNA and 0.1% BSA for 5 min at room temperature. For binding reaction, 250 fmol of labeled oligo were added in each reaction and incubated for 30 min at room temperature. Competition assay was performed using 100 fold excess unlabeled oligo added during equilibration step prior to addition of labeled oligo. DNA-protein complexes were separated using 5% polyacrylamide gel and transferred to nylon membrane. DNA-protein complexes and free oligo were detected using chemiluminescent nucleic acid detection kit (Thermo scientific, USA).

2.14. Bioluminescence imaging of tumor xenografts

Animal care and euthanasia were performed with the approval from Institutional Animal Ethics Committee of ACTREC. Mice were implanted with 6×10^6 cells stably expressing either single or dual luciferases and tumors were allowed to grow till 5–8 mm. Mice were divided into two groups and one (treated) group was injected with cisplatin (8 mg/kg). Whole body images of anaesthetized mice using IVIS Spectrum optical imaging system were obtained after 100 μl intra-peritoneal injection of D-luciferin (3 mg/mouse) or tail-vein injection of coelenterazine (50 μg/mouse) diluted in phosphate-buffered saline. Region of Interests (ROIs) were drawn over the tumors and quantified by using the Live Image (4.4) software. Bioluminescence signals were recorded as maximum (photons/s/cm^2/sr). Bioluminescence imaging of the same mouse was acquired in sequence (first NF-κB-renilla luciferase followed by firefly luciferase).

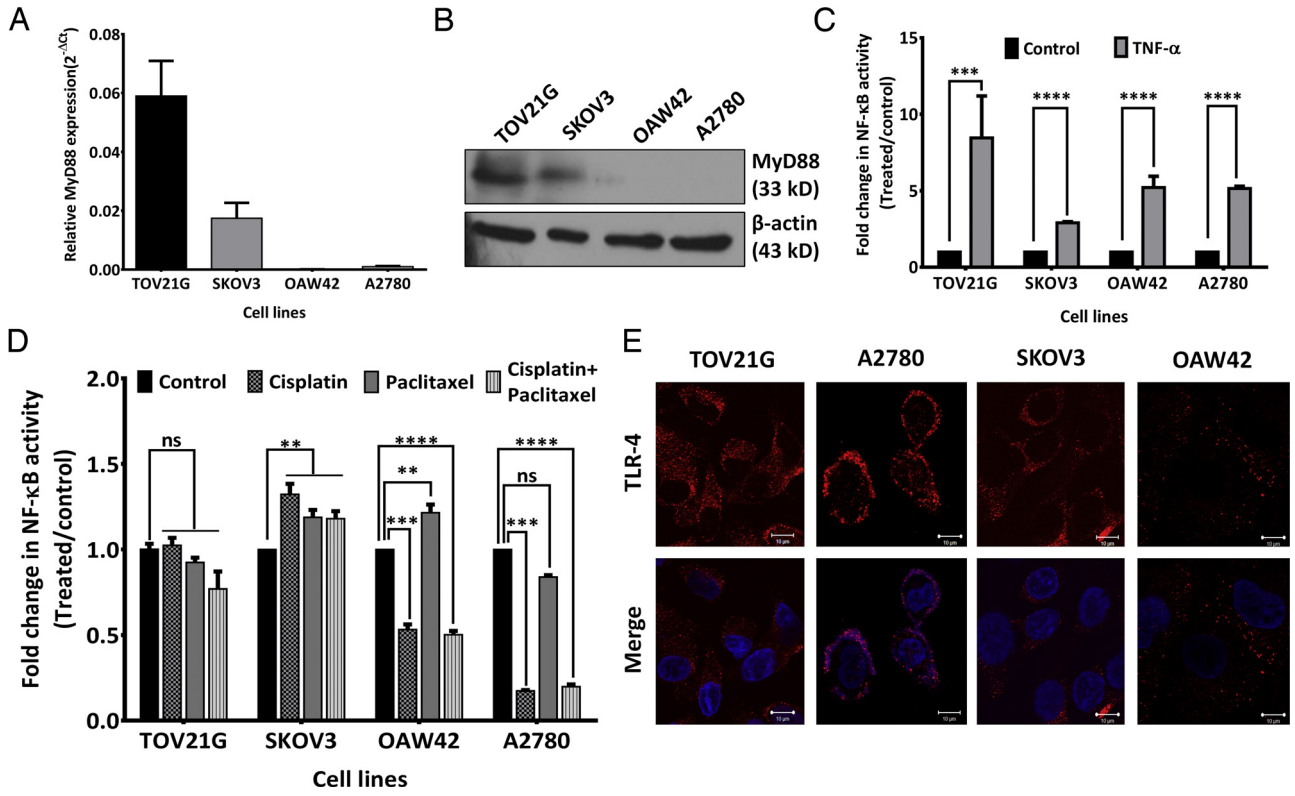

Fig. 1. Characterization of cell lines for TLR-4/MyD88/NF-κB pathway: A–B. MyD88 expression analysis. Quantitative-PCR (qPCR) and Western blot analysis showed positive expression for MyD88 in TOV21G and SKOV3 cells while A2780 and OAW42 were found to be negative for MyD88 expression, GAPDH and β-actin were used as internal control respectively. C–D. Transient transfection study for NF-κB activity TOV21G, SKOV3, OAW42 and A2780 cells were transiently transfected with pNF-κB-RE-driven-renilla luciferase and CMV driven-firefly luciferase constructs followed by TNF-α (200 ng/ml), cisplatin (10 μg/ml), paclitaxel (5 μg/ml) and cisplatin-paclitaxel (1 μg/ml; 500 ng/ml) treatment for 24 h. Relative NF-κB activity were calculated ratiometrically as RL/FL activity which showed significant increase by TNF-α treatment (C) (***$p < 0.001$), however reduced luciferase activity was observed with cisplatin and cisplatin-paclitaxel treatment (****$p < 0.0001$) and no change after paclitaxel treatment (D). E. Immunofluorescence study. Membrane localization of TLR-4 was observed in all the cells where upper panel represents the staining pattern of the TLR-4 and lower panel showing merged images with nuclear stain (DAPI).

3. Results

3.1. Differential activation of NF-κB was associated with differential drug treatments in MyD88^{negative} but not in MyD88^{positive} cells

Though absence of MyD88 expression is thought to associate with effective paclitaxel treatment and longer survival in epithelial ovarian cancer patients, a significant number of them exhibit disease recurrence (Kim et al., 2012). In order to understand the status of NF-κB activation in MyD88^{positive} and MyD88^{negative} cells by various chemotherapeutics, a panel of cell lines (TOV21G, SKOV3, OAW42 and A2780) were analyzed for the level of MyD88 expression by real time PCR and Western blot. As shown in Fig. 1A and B, while OAW42 and A2780 cells were devoid of MyD88 expression, TOV21G exhibited 3-fold higher expression than SKOV3. All these cells were then transiently transfected with NF-κB sensor and normalization plasmid and treated with various drugs and inducers. While 2 h of TNF-α treatment induced 5 fold increase, cisplatin and cisplatin + paclitaxel treatments resulted in 50–80% decrease in NF-κB-renilla luciferase activity in MyD88^{negative} OAW42 and A2780 cells. No significant change in luciferase activity was observed after paclitaxel treatment (Fig. 1C and D). In contrary both the MyD88^{positive} cells (TOV21G and SKOV3) did not exhibit any significant change in NF-κB activity after cisplatin, paclitaxel and cisplatin + paclitaxel treatments though a trend in enhanced activation was observed in SKOV3 cells (Fig. 1D). Two hours of TNF-α treatment induced ~8 fold and 3 fold increase in NF-κB activity in these cells (Fig. 1C). All these cells showed prominent TLR-4 expression and membrane localization except for OAW42 cells where only low cytoplasmic expression was observed (Fig. 1E).

Since the transient expression of any reporter gene is often influenced by the heterogeneity of the experimental procedure, two A2780 cell clones stably expressing the NF-κB sensor were generated. TNF-α showed increased (6–7 fold) NF-κB activity while LPS, a paclitaxel analogue did not induce NF-κB activation (Fig. 2A). These stable clones also displayed no change in NF-κB reporter activity after paclitaxel treatment but significant attenuation after cisplatin and combinatorial treatments (Fig. 2B).

In accordance with luciferase activity, changes in NF-κB expression in nuclear extracts were found after paclitaxel, cisplatin and dual treatments by Western blotting (Fig. 2C). Nuclear localization of NF-κB, a key event for NF-κB transcriptional action was differentially altered by various drug treatments. Minimal nuclear localization of NF-κB was found after cisplatin and dual treatments while enhanced localization was observed after paclitaxel treatment. An overall increase in NF-κB expression was evident in paclitaxel treated cells (Fig. 2D) by immunoflorescence.

3.2. Cisplatin and paclitaxel resistant cells with enhanced AKT phosphorylation exhibited slower proliferation and lower clonogenicity than the dual resistant cells

To understand the drug resistant characteristics of MyD88^{negative} cells, three isogenic cellular models of resistance (cisplatin, paclitaxel and cisplatin-paclitaxel) were developed

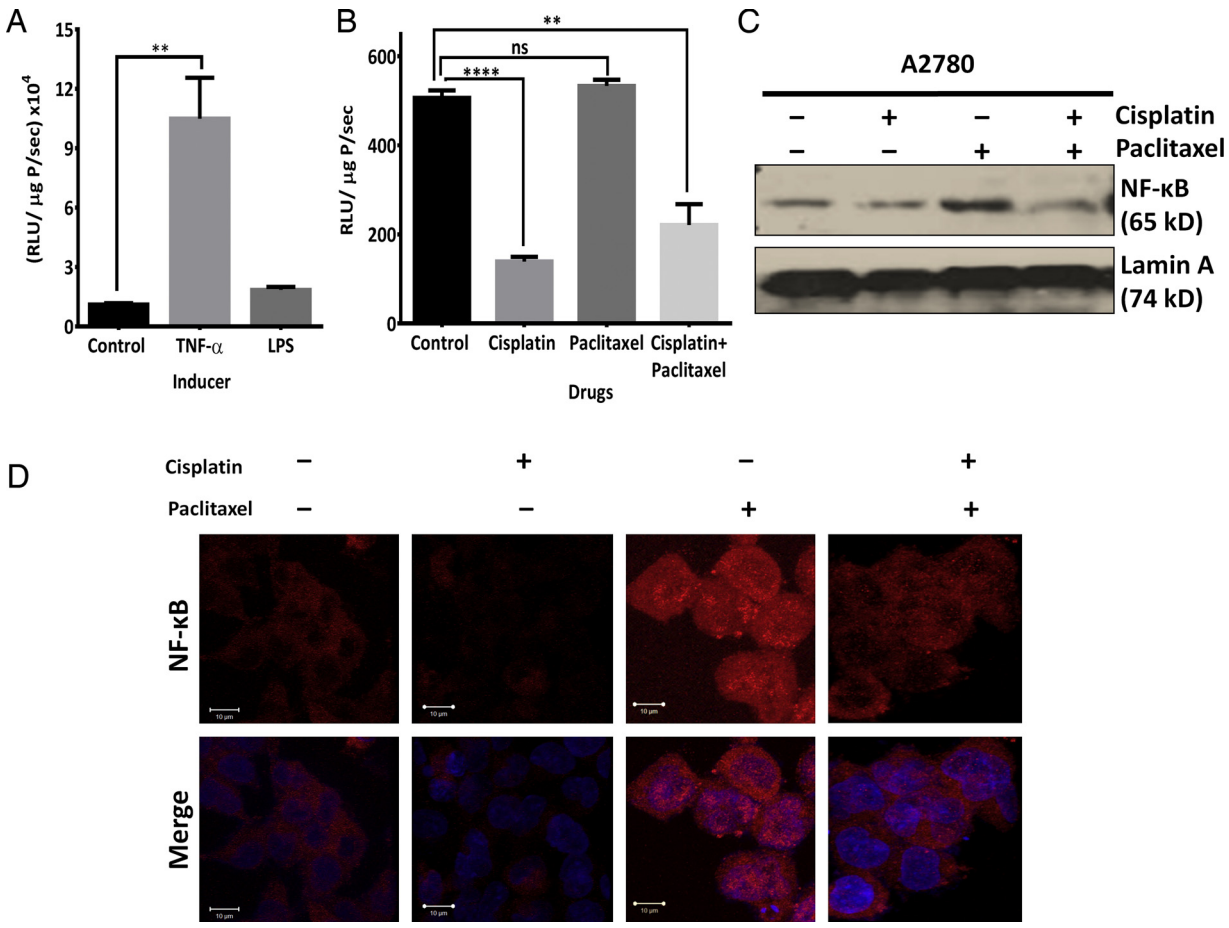

Fig. 2. Different chemotherapeutics showed differential expression of NF-κB upon treatments in MyD88 negative EOC cells: A–B. Stable expression study. An increased NF-κB luciferase activity was observed with TNF-α (**$p < 0.01$) but not with Lipopolysaccharide (LPS) treatment (A). A2780 cells stably expressing NF-κB sensor showed significant decrease in luciferase activity after cisplatin (****$p < 0.0001$) and combinational treatment of cisplatin and paclitaxel (**$p < 0.01$) while no changes were observed after paclitaxel treatment (B). C. Immunoblotting study. Increased NF-κB levels were observed after paclitaxel treatment but not after cisplatin and dual drug treatment in nuclear lysates of the drug treated A2780 cells. Lamin A was used as loading control. D. Immunofluorescence study. Increased nuclear localization of NF-κB was observed in A2780 cells after paclitaxel treatment, however, such localization were absent in cisplatin and platinum-taxol treated cells. Upper panel showed the staining pattern of the NF-κB and lower panel showed merged images with DAPI.

using A2780 cells with sequential treatment of increasing doses of drugs. The MyD88 deficient status of A2780 cells and their resistant counterparts was confirmed again (Fig. 3B). The late resistant cells demonstrated 92% viability for A2780-Cis^{LR}, 68% viability for A2780-Pac^{LR} and 96% viability for A2780-Cis-Pac^{LR} cells at IC_{50} concentration of respective drugs. The resistance indices (RI) for A2780-Cis^{LR}, A2780-Pac^{LR} and A2780-Cis-Pac^{LR} cells were found to be 7.5, 5 and 10 fold higher than the sensitive counterparts respectively (Fig. 3A). The A2780-Cis^{LR} cells also demonstrated resistance to carboplatin, another platinum drug often used in clinics (Suppl. Fig. 1). Interestingly, proliferation rate for the dual resistant model was found to be comparable to sensitive cells (Doubling time: 27.70 ± 1.15 h vs. 25.30 ± 1.22 h) while both the single drug resistant cells showed much slower proliferation (Cis^{LR}: 33.44 ± 1.35 h and Pac^{LR}: 37.55 ± 1.86 h) (Fig. 3D). Similarly, the A2780-Cis-Pac^{LR} cells demonstrated a much higher rate of colony formation (1,000 fold) at an elevated drug concentration than A2780-Cis^{LR} and A2780-Pac^{LR} cells (~10 fold) when compared to the sensitive cells (Fig. 3E–G and supplementary Fig. 1). All the three cellular models showed gradual activation of AKT with acquirement of resistance without any significant change in total AKT level. The activation of AKT seemed to occur at much earlier stages for cisplatin and dual resistance than paclitaxel resistance (Fig. 3C).

3.3. The A2780 cisplatin resistant cells retained the resistant characteristics in vivo

One of the caveats of establishment of *in vitro* drug resistant cells is frequent reversal of the resistant phenotype and they often require to be maintained under drug selection. To test whether our cellular models could retain their resistant properties without any selection and in *in vivo* situation, A2780-Cis^{LR} cells were grown as tumors in nude mice and treated with cisplatin (8 mg/kg) and change in cellular viability was measured by bioluminescence imaging (all these cellular models stably express a PIK3CA promoter driven firefly luciferase reporter) (Gaikwad et al., 2013). In corroboration with the proliferation data, the tumors of resistant cells had slower growth than their sensitive counter parts (data not shown). The bioluminescence activity of these cisplatin resistant tumors ($n = 3$) did not decrease after treatment rather slightly increased ($3.72 \times 10^8 \pm 1.99 \times 10^8$ p/s/cm^2/sr to $1.19 \times 10^9 \pm 4.31 \times 10^8$ p/s/cm^2/sr) due to tumor growth. This increase was consistent even after another dose of cisplatin treatment ($3.36 \times 10^9 \pm 1.26 \times 10^9$ p/s/cm^2/sr). The untreated resistant tumors ($n = 3$) exhibited increased bioluminescence ($2.46 \times 10^8 \pm 4.81 \times 10^7$ p/s/cm^2/sr to $9.89 \times 10^8 \pm 2.78 \times 10^8$ p/s/cm^2/sr to $5.59 \times 10^9 \pm 1.03 \times 10^9$ p/s/cm^2/sr) over time (Fig. 4A and C). Tumor volume of the treated A2780-Cis^{LR} tumors

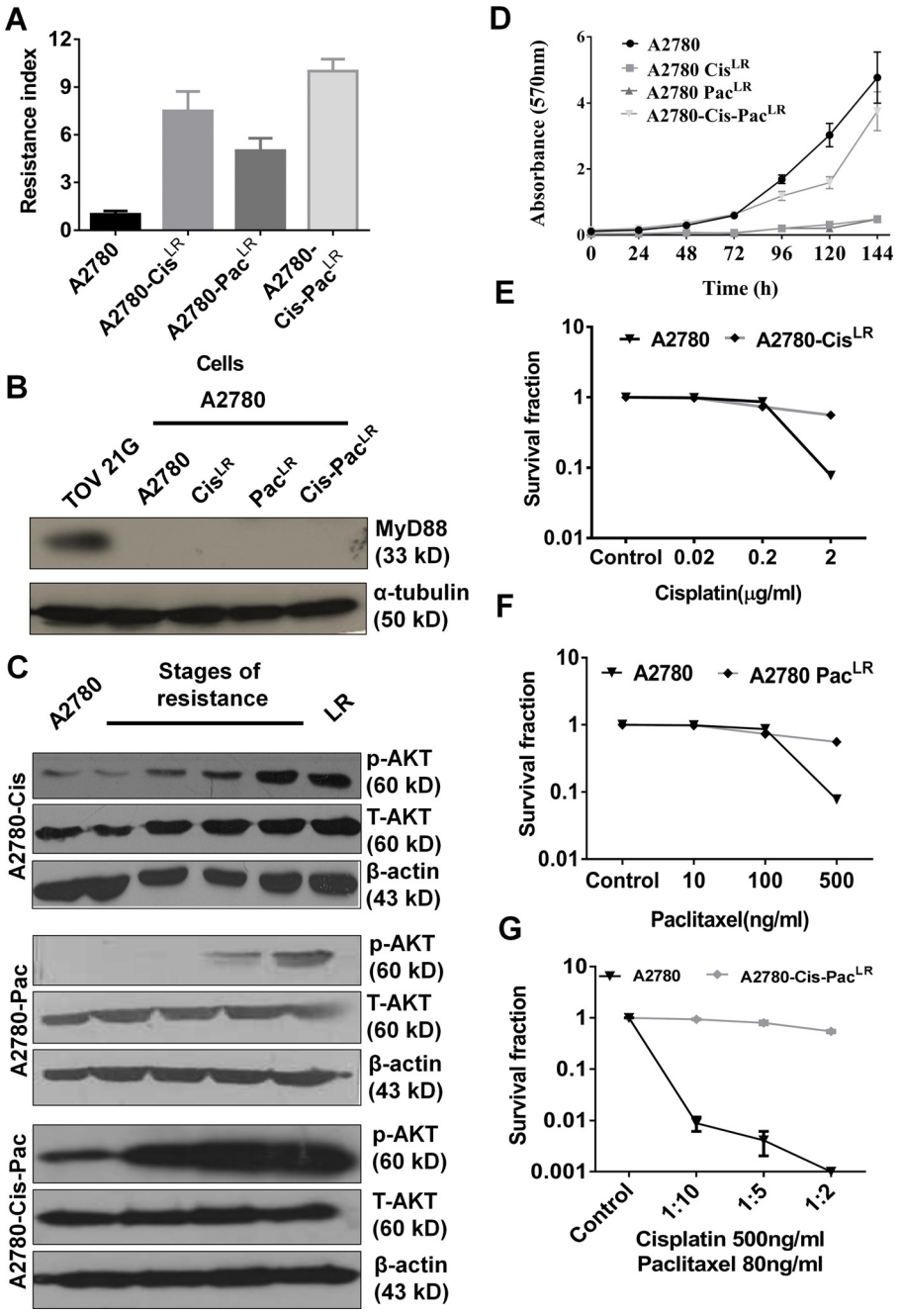

Fig. 3. Characterization of the isogenic resistant variants of A2780 cells: A. Resistance index. Resistance index of A2780 cells, A2780-Cis^{LR}, A2780-Pac^{LR} and A2780-Cis-Pac^{LR} were calculated using IC_{50} doses of cisplatin, paclitaxel and platinum-taxol for A2780 and the resistant variants as described in methods. The three resistant variants of A2780 cells, A2780-Cis^{LR}, A2780-Pac^{LR} and A2780-Cis-Pac^{LR} demonstrated 8, 5 and 10 fold higher resistance than control respectively. B. MyD88 status. Western blot analysis showed absence of MyD88 protein in A2780 and its resistant variants. TOV21G cells were used as positive control and α-tubulin as a loading control. C. Immunoblotting study. High expression of phosphorylated AKT was observed in late stages of all resistant cells, however, no change was observed with total AKT. β-actin was used as loading control. D. Proliferative rate of the resistant cells. MTT assay of A2780 and its isogenic resistant variants to estimate growth rate showed a much slower proliferative capacity for A2780-Cis^{LR}, A2780-Pac^{LR} than A2780 cells. Interestingly, A2780-Cis-Pac^{LR} cells demonstrated a proliferation rate comparable to A2780 cells. E–G. Clonogenic assay. A2780 cells and all the isogenic resistant variants showed higher clonogenic potential ($^{***}p < 0.001$) with increasing concentration of drugs.

remained stable whereas the control tumors exhibited gradual increase (Fig. 4B).

3.4. Acquirement of cisplatin resistance augmented NF-κB activity

Activated AKT is a critical regulator of NF-κB signaling which phosphorylates and activates inhibitory κB kinase (IKK) leading to phosphorylation and degradation of IKBα. Since all our resistant models exhibited gradual increase in AKT phosphorylation, we sought to monitor the changes in NF-κB signaling by stably expressing the NF-κB sensor in these resistant (A2780-Cis^{LR}, A2780-Pac^{LR} and A2780-Cis-Pac^{LR}) cells. Interestingly, A2780-Cis^{LR} cells stably expressing the NF-κB sensor exhibited a significant increase in luciferase activity (~10 fold) after cisplatin treatment (Fig. 5A). This increase was not clone specific and observed independently in two other clones (data not shown). NF-κB also showed distinct nuclear localization in A2780-Cis^{LR} cells with or without cisplatin

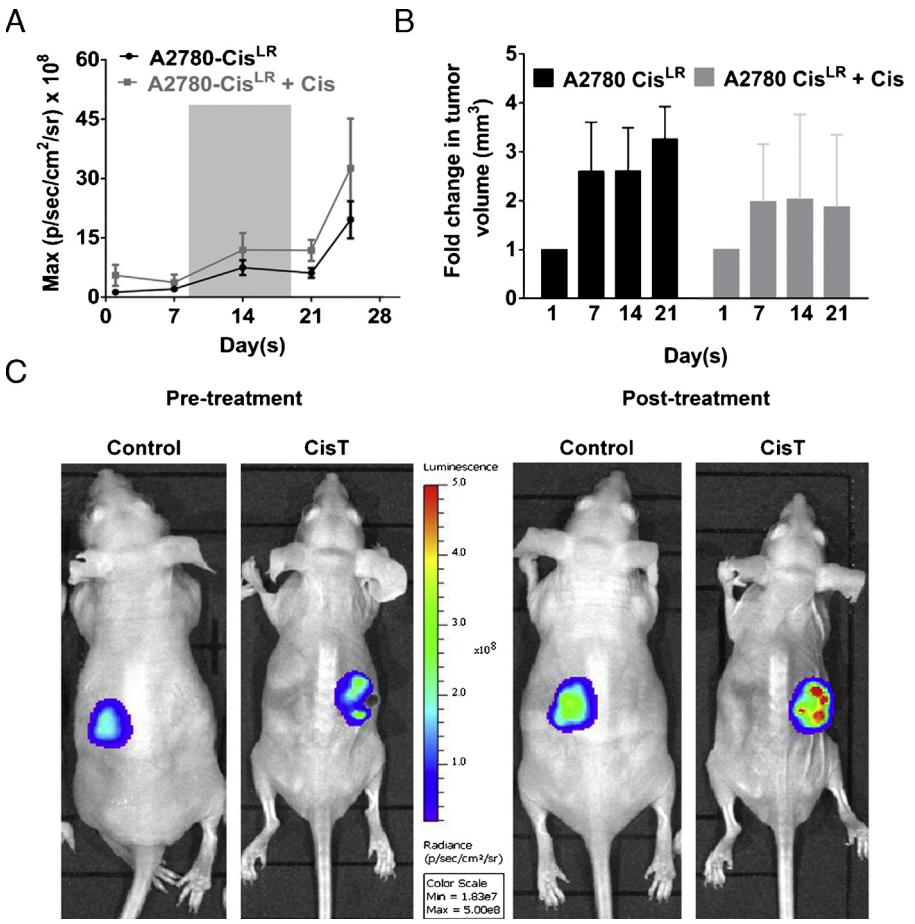

Fig. 4. Non-invasive imaging of A2780-Cis^{LR} tumor xenografts demonstrated resistant characteristics after cisplatin treatment: A. Bioluminescence signal analysis. Graphical representation of the bioluminescent signals of pre and post-treated A2780-Cis^{LR} tumor xenografts showed increased luminescence with time after two rounds of cisplatin treatment in both control ($n = 3$) and treated mice ($n = 3$). Shaded area displays the day/s of cisplatin treatment. B. Tumor volume assessment. Measurement of fold change in tumor volume (mm^3) of cisplatin treated mice showed similar trend of tumor growth in both control and treated mice. C. Bioluminescence imaging. Representative bioluminescent images of A2780-Cis^{LR} tumor xenografts bearing mice before and after treatment did not exhibit attenuated luciferase activity after two treatments of cisplatin (post-treatment). The control group was injected with normal saline and exhibited increased luciferase activity.

treatment (Fig. 5D). Immunoblotting of nuclear lysates did not show any change in NF-κB level after cisplatin treatment to the A2780-Cis^{LR} cells (Fig. 5G).

On contrary, A2780-Pac^{LR} cells demonstrated a significant decrease in NF-κB activity after paclitaxel treatment (Fig. 5B). In contrast to the sensitive cells, where paclitaxel could induce nuclear localization, the A2780 Pac^{LR} cells did not exhibit nuclear localization of NF-κB in pre and post treatment (Fig. 5G). Western blot analysis showed decreased nuclear NF-κB after treatment (Fig. 5D). Interestingly, about 1.5 fold induction in NF-κB activity was observed when A2780-Pac^{LR} cells were challenged with cisplatin (Fig. 5E). However, similar cross treatment of paclitaxel to A2780-Cis^{LR} cells resulted in reduction (~1.5 fold) in NF-κB activity (Fig. 5F).

Surprisingly, A2780-Cis-Pac^{LR} cells stably expressing the NF-κB sensor showed decreased NF-κB activity after combinatorial drug treatment (Fig. 5C). This decrease was found to be associated with reduced expression and localization of NF-κB in nucleus (Fig. 5D and G).

3.5. Cisplatin resistant cells showed enhanced NF-κB DNA binding activity

To evaluate the DNA binding capacity of NF-κB in sensitive and resistant cells, a biotinylated NF-κB response sequence was used for gel shift assay. Paclitaxel and combinatorial drug treatments in sensitive cells slightly reduced the intensity of the DNA-protein complex; however, cisplatin treatment resulted in complete abolishment of the complex. A 100 fold excess cold probe could compete and abolish the complex while a scrambled oligonucleotide did not exhibit such competition indicating the specificity of the observed high molecular weight DNA-protein complex (Fig. 6A). In cisplatin resistant cells, cisplatin treatment did not abolish and rather slightly increased the intensity of the DNA-protein complex. In paclitaxel treated A2780 and cisplatin-paclitaxel treated A2780-Cis-Pac^{LR} cells slight decrease in the DNA-protein complex formation was observed after treatments (Fig. 6B). A graphical representation of semi-quantitative comparison between the untreated and treated DNA-protein complex is shown in Fig. 6C.

3.6. Differential expression of Bcl-2 was associated with differential resistance

Activated NF-κB controls cell proliferation and apoptosis by directly regulating various molecular players like Cyclin-D1, Bcl-2, and XIAP. While Cyclin-D1 expression did not show significant alteration in A2780-Cis^{LR} and A2780-Pac^{LR} cells, A2780-Cis-Pac^{LR} cells exhibited two-fold increase in Cyclin-D1 expression (Fig. 7A).

Among the two important antiapoptotic proteins controlled by NF-κB, Bcl-2 expression was enhanced in cisplatin resistant cells but was down-regulated in paclitaxel and platinum-taxol cells (Fig. 7C). In contrary, anti-apoptotic protein XIAP transcripts

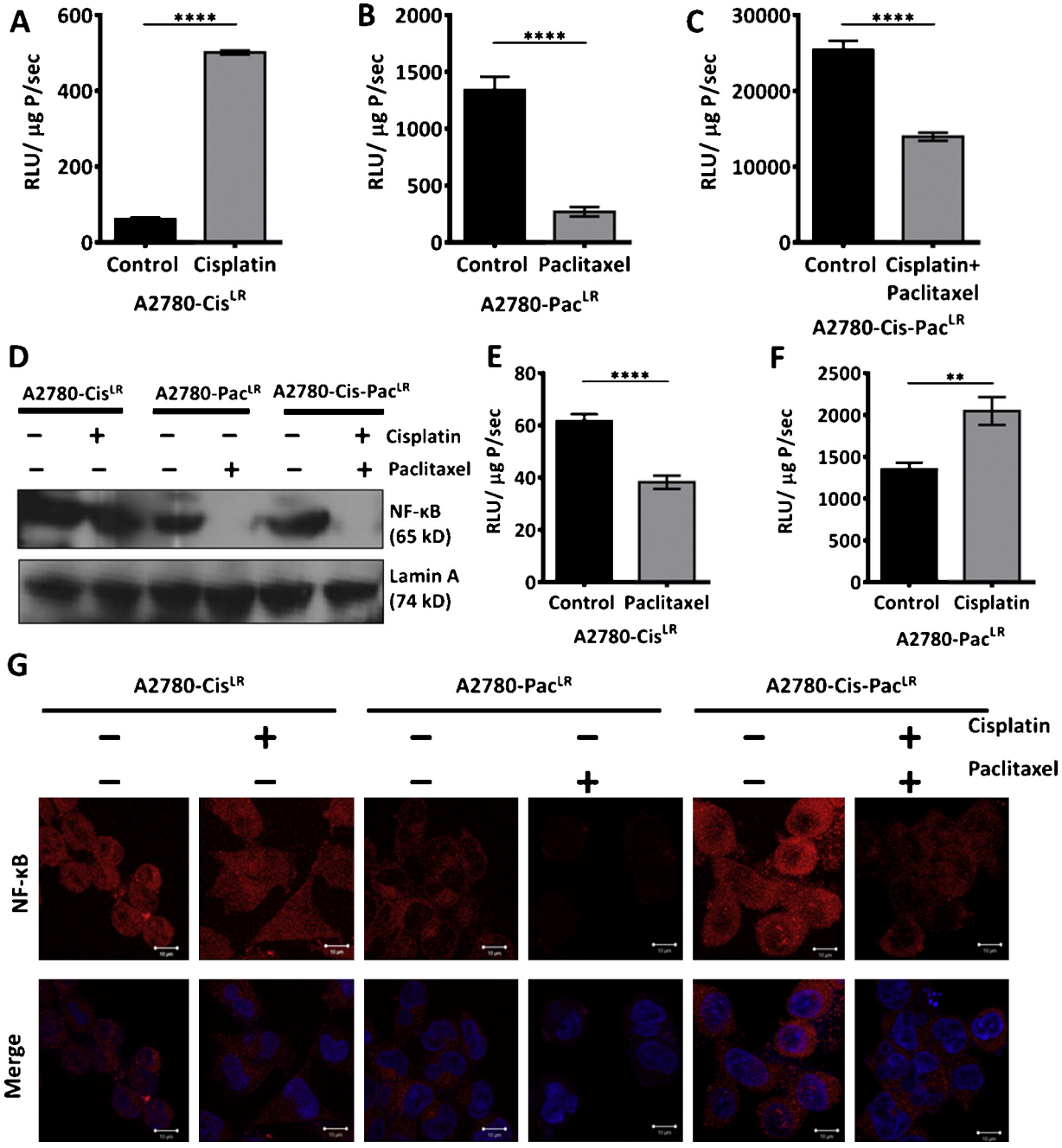

Fig. 5. Upregulated NF-κB activity was associated with cisplatin resistant cells but not with paclitaxel and dual resistant cells: A–C. Luciferase assay study A2780-Cis^{LR} cells stably expressing NF-κB sensor showed significant increase (****$p < 0.0001$) in luciferase activity after cisplatin treatment (A). A2780-Pac^{LR} and A2780-Cis-Pac^{LR} with stably expressing NF-κB sensor showed significant decrease (****$p < 0.0001$) in luciferase activity after paclitaxel and platinum-taxol treatment respectively (B and C). D. Immunoblotting study. Decreased NF-κB levels were evident in nuclear cell lysates of drug treated of A2780-Pac^{LR} and A2780-Cis-Pac^{LR} cells. However, no obvious change was observed after cisplatin treatment in A2780-Cis^{LR}. Lamin A was used as loading control. E–F. NF activity after cross treatment A2780-Cis^{LR} cells showed significant decrease (****$p < 0.0001$) in luciferase activity after paclitaxel treatment (E) whereas A2780-Pac^{LR} showed significant increase (**$p < 0.01$) in luciferase activity after cisplatin treatment (F). G. Immunofluorescence study. No apparent change was observed in the nuclear staining of NF-κB in A2780-Cis^{LR} after cisplatin treatment. However, decreased in NF-κB staining was evident in A2780-Pac^{LR} and A2780-Cis-Pac^{LR} (upper panel) cells after treatment. Lower panels showed the merged images with DAPI.

though decreased after cisplatin treatment showed slight change after drug treatments to A2780-Cis^{LR}, A2780-Pac^{LR}, and A2780-Cis-Pac^{LR} cells (Fig. 7B).

3.7. Cisplatin treatment to the A2780-Cis^{LR} cells augmented NF-κB activity in vivo

To non-invasively monitor NF-κB activation, subcutaneous tumor xenografts of A2780-Cis^{LR} cells stably expressing the NF-κB sensor were developed in nude mice ($n = 7$) and sequential bioluminescence imaging for firefly and renilla luciferase were performed. As expected firefly luciferase activity of A2780-Cis^{LR} tumor xenografts ($n = 4$) showed no change after cisplatin treatment ($6.2 \times 10^6 \pm 1.6 \times 10^5$ p/s/cm^2/sr to $7.1 \times 10^6 \pm 2.1 \times 10^5$ p/s/cm^2/sr) in comparison to control tumor xenografts ($8.7 \times 10^6 \pm 1.3 \times 10^5$ to $6.8 \times 10^6 \pm 1.7 \times 10^5$ p/s/cm^2/sr) ($n = 3$). However, a 14 fold increase in NF-κB-RL activity was found after cisplatin treatment ($n = 4$) ($5.43 \times 10^5 \pm 8.4 \times 10^3$ p/s/cm^2/sr to $4.31 \times 10^6 \pm 1.4 \times 10^4$ p/s/cm^2/sr) as compared to the control tumor xenografts ($n = 3$) ($3.8 \times 10^5 \pm 1.3 \times 10^4$ to $3.8 \times 10^5 \pm 1.2 \times 10^4$)

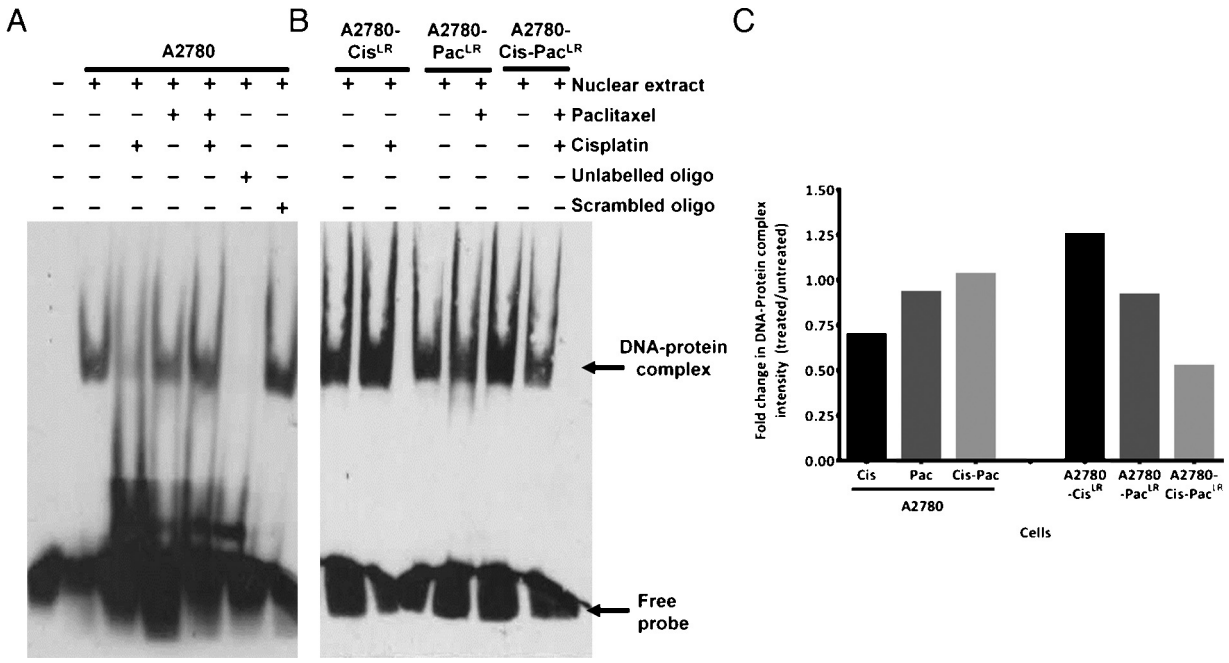

Fig. 6. Cisplatin resistant cells showed enhanced NF-κB DNA binding activity: A. NF-κB DNA binding activity in control cells. Electrophoretic mobility shift assay was performed to analyze the binding of NF-κB to respective response elements using nuclear extracts of A2780 cells treated with cisplatin, paclitaxel and both the drugs and a biotin labeled 22 bp long NF-κB response element. In comparison to paclitaxel and dual drug treatments, cisplatin treatment resulted in significant decrease in the DNA-protein complex. Disappearance of the DNA-protein complex after challenging with an unlabeled oligo confirmed the specificity of NF-κB binding. A scrambled oligo could not compete and abolish the complex. B. NF-κB DNA binding activity in drug resistant cells. The A2780-Cis^{LR} cells showed high NF-κB binding after cisplatin treatment while both A2780-Pac^{LR} and A2780-Cis-Pac^{LR} cells showed decrease in the DNA-protein complex. C. Densitometric analysis. A graphical representation of the ratiometric analysis of the intensity of the DNA-protein complexes represented the fold changes in NF-κB binding of pre and post treatments.

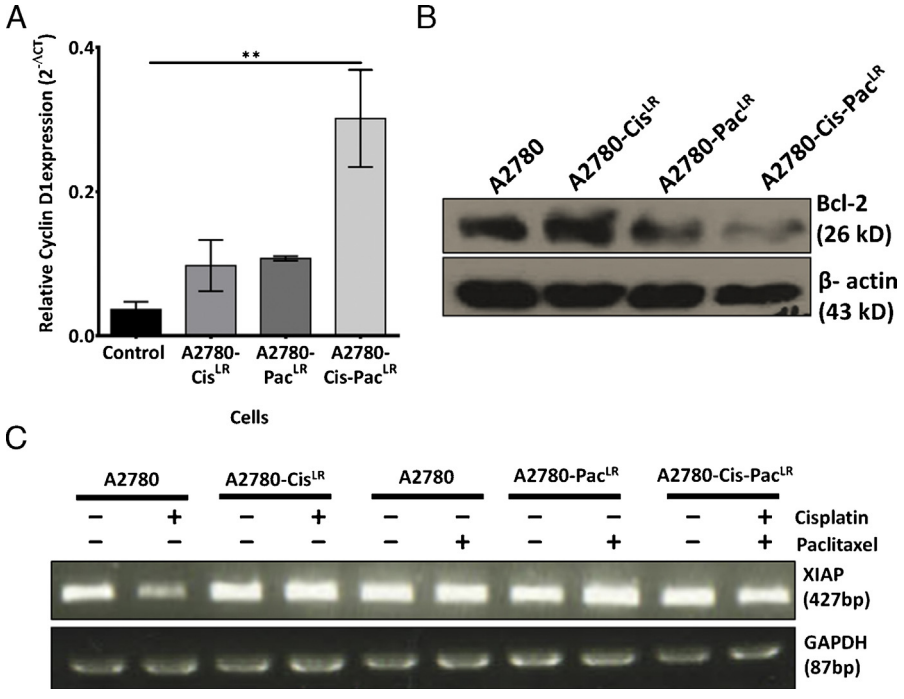

Fig. 7. Differential expression of downstream target genes of NF-κB: A–B. Expression analysis. qPCR of Cyclin D1 expression in A2780 and its isogenic resistant variants showed maximum expression in Cis-Pac^{LR} dual resistant cells (**$p < 0.01$) (A). Semi-quantitative analysis of XIAP expression in the same cells showed no change in expression level (B) C. Immunoblotting study. Endogenous Bcl-2 expression was highest in A2780-Cis^{LR} in comparison to A2780 and paclitaxel and dual resistant cells.

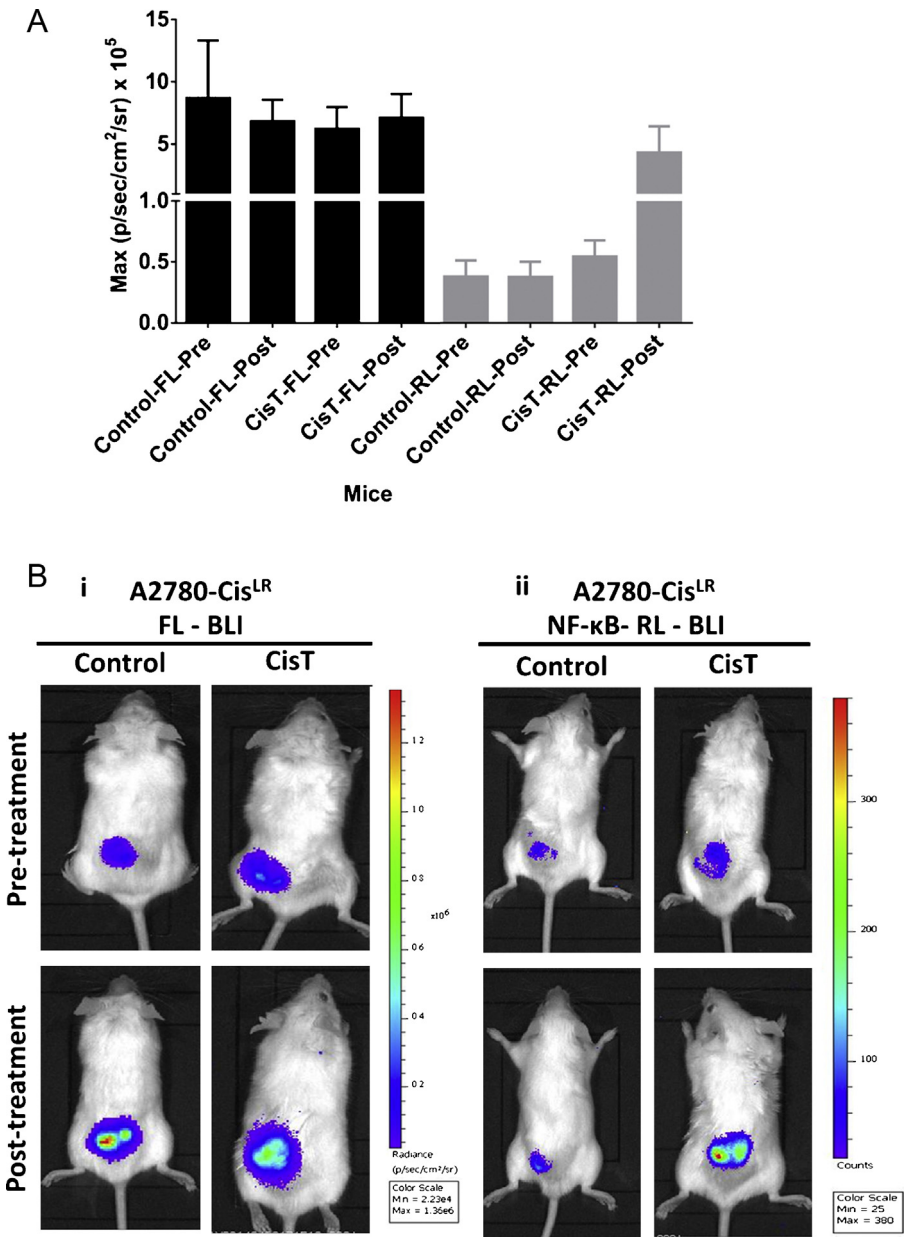

Fig. 8. Non-invasive imaging of NF-κB activity in A2780-Cis^{LR} tumor xenografts after cisplatin treatment: A. Graphical representation of bioluminescence signals. Bioluminescence signals for both firefly luciferase and NF-κB-renilla luciferase were calculated for the respective ROIs drawn over tumors of control and cisplatin treated mice. No change was observed for firefly luminescence (before and after treatment), however, a 14 fold increased luminescence was observed for NF-κB-renilla luciferase after cisplatin treatment. B. Bioluminescence imaging. Representative bioluminescent images of the same mouse bearing A2780-Cis^{LR} tumors are shown for pre- and post- cisplatin treatment. The left panel (7Bi) showed the mouse imaged for firefly luciferase signal and the right panel showed the same mouse imaged sequentially for the renilla luciferase signal (7Bii). The upper panel depicts images before treatment and lower panel depicts images after treatment.

(Fig. 8A). Representative images of same mouse scanned for firefly and renilla luciferase pre and post cisplatin treatment phases were shown in Fig. 8B.

3.8. Silencing of MyD88 did not affect cisplatin mediated NF-κB activation in cisplatin resistant TOV21G and SKOV3 cells

To ascertain that acquirement and maintenance of cisplatin resistance depends on TLR-4/MyD88 independent NF-κB activation in EOC cells, we suppressed MyD88 expression using lentiviral mediated MyD88 specific sh-RNA construct in naturally occurring cisplatin resistant TOV21G and SKOV3 cells and then evaluated the effect of the therapeutics. In MyD88 knock down TOV21G cells, transient transfection of NF-κB sensor showed 50% reduction in luciferase activity compared to cells transduced with a scrambled sh-RNA construct. After paclitaxel and cisplatin + paclitaxel treatments, NF-κB activity reduced to 40% and 50% respectively, however cisplatin treatment retained 80% of NF-κB activity (compared to similar treatments to cells transduced with the scrambled sh-RNA). A comparison between MyD88 knockdown control and MyD88 knockdown cisplatin treated cells showed 1.5 fold induction in NF-κB activity (Fig. 9A). Western blot analysis confirmed the reduction in MyD88 expression level after transduction of MyD88 specific sh-RNA construct (Fig. 9C).

To monitor the effect cisplatin on stable expression of NF-κB sensor in another cisplatin resistant EOC cell line, we first generated clones of SKOV3 cells stably expressing NF-κB promoter driving a renilla luciferase-monomeric red fluorescent fusion reporter (hRL-mRFP) by puromycin selection. Since our strategy to isolate cells stably expressing the sh-RNA constructs depended on the eGFP

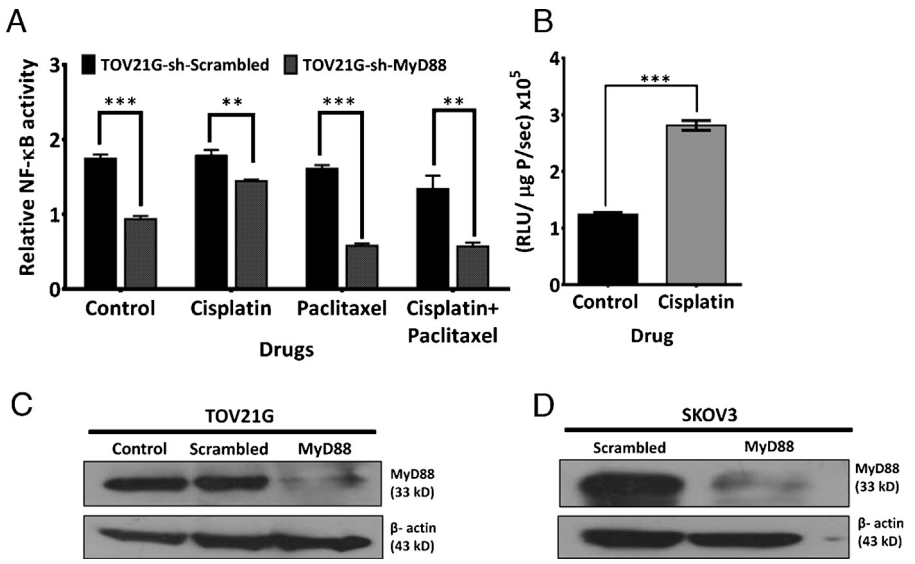

Fig. 9. Effect of MyD88 knockdown on NF-κB activity: A–B. NF-κB activity. Transient transfection of NF-κB driven-renilla luciferase-mRFP reporter in TOV21G stably expressing either sh-MyD88 or sh-scrambled constructs after cisplatin (10 μg/ml), paclitaxel (5 μg/ml) and cisplatin-paclitaxel (1 μg/ml; 500 ng/ml) treatment for 24 h resulted in significant decrease in NF-κB activity (A). Increased luciferase activity was observed after cisplatin treatment in SKOV3 cells stably expressing the NF-κB-renilla luciferase-mRFP reporter and sh-MyD88 construct (B). C–D. Validation of MyD88 knockdown cells. Western blot analysis for MyD88 protein showed significant level of knockdown in TOV21G (C) and SKOV3 (D) cells.

based FACS sorting (after lentiviral transduction), we had to use the pNF-κB–hRL-mRFP fusion reporter instead of pNF-κB–hRL-eGFP reporter which was used for other experiments. This stable clone was then transduced with MyD88 sh-RNA and then further treated with cisplatin. As expected a 2.8 fold higher NF-κB activity was observed with cisplatin treatment (Fig. 9B). The level of MyD88 suppression in these cells was analyzed as well (Fig. 9D).

4. Discussion

Despite significant improvements in clinical outcome, platinum resistance is still a major obstacle for effective treatment of epithelial ovarian carcinoma. Recent reports identified various candidate genes responsible for underlying molecular mechanisms of resistance (Chaudhury et al., 2014). MyD88, an essential adapter protein in TLR-4 mediated NF-κB signaling pathway has shown to influence the response of EOC cells to paclitaxel treatment. Though MyD88^{negative} population (~40% of total EOC patients) show better prognosis and longer survival, a significant proportion of them (~40%) acquire resistance over time (Kim et al., 2012). Moreover, NF-κB signaling shows a delayed kinetics in MyD88-independent pathway and induces IFN-β and IFN-responsible genes (Kawai and Akira, 2006). In this study we investigated the state of NF-κB signaling in MyD88 deficient EOC cell lines after making them resistant towards paclitaxel, cisplatin and combinatorial treatments. Our results indicated that cisplatin down-regulated NF-κB activity in sensitive cells as shown by luciferase assay, Western blot and EMSA. Such down-regulation was also found with cisplatin-paclitaxel treatment but not with paclitaxel. Interestingly we found that while NF-κB was down-regulated in paclitaxel and platinum-taxol resistance, acquirement of cisplatin resistance showed increased activation of NF-κB. In contrary, no difference in NF-κB activity was found in MyD88 positive and cisplatin resistant TOV21G and SKOV3 cells after all the drug treatments. Silencing of MyD88 resulted in induction in NF-κB activity only after cisplatin treatment but not after paclitaxel or combinatorial treatment in these cells. This activation can be imaged noninvasively from *in vivo* tumor xenografts of cisplatin resistant and MyD88 deficient A2780 cells. Bcl-2, but not XIAP, a downstream target of NF-κB showed differential expression in cisplatin and paclitaxel/platinum-taxol resistant cells. Thus our data indicates that an active NF-κB signaling and over expression of Bcl-2 is an essential phenomenon for acquirement of cisplatin resistance but not for paclitaxel or platinum-taxol resistance in MyD88^{negative} epithelial ovarian cancer cells.

The standard therapeutic regimen for management of EOCs is a combinatorial treatment of platinum (cisplatin or carboplatin) and taxane (paclitaxel) drugs. However, their clinical utility is often limited by development of drug resistance, partly owing to our poor understanding of the underlying mechanism of resistance (Chaudhury et al., 2014; Gaikwad and Ray, 2012). Several mechanisms like alterations in drug transport and drug targets, detoxification of drug, changes in DNA repair mechanisms, activation/down regulation of genes involved in survival and cell death pathways are shown as contributory factors to poor chemoresponse of ovarian cancer (Chaudhury et al., 2014; El-Deiry, 1997). Among various survival pathways, activated PI3K/AKT/mTOR and NF-κB signaling play important roles in development and maintenance of platinum and paclitaxel resistance (Agarwal and Kaye, 2003; Alvero, 2010; Annunziata et al., 2010; Peng et al., 2010). These two pathways are often found to be mutually dependent on each other for maximal activation. Via phosphorylation of IκB kinase (IKK) that phosphorylates and directs degradation of IκB, AKT activates NF-κB, which depending upon cellular context induces cell survival or cell death (Mabuchi et al., 2004a). Thus presence of high level of phosphorylated AKT in our cisplatin, paclitaxel and platinum-taxol resistant cells indicated a possible involvement of NF-κB signaling for maintenance of resistant characteristics. However, the differential activation of NF-κB by the three different treatments in these resistant cells indicates an additional layer of regulation.

The IKK family of proteins is also known be induced by various compounds through the Toll-like Receptors (TLRs) present on myeloid and non-myeloid cells (Akira et al., 2001). After stimulated by LPS, TLR-4, a member of TLR family activates IL-1R-associated kinase (IRAK)/TRAF-6 via recruitment of an adaptor protein (myeloid differentiation factor 88). Activated IRAK/TRAF-6 further phosphorylates IKKα/IKKβ and mediates NF-κB activation through degradation of IκB proteins. In absence of MyD88, TLR-4 induces late activation and delayed response of NF-κB possibly

through association of TIRAP (Toll-IL-Receptor Adaptor Protein) via activation of IKKε/IKKι kinases and degradation of IκB proteins (Kawai and Akira, 2006).

TLR-4 driven signaling cascade which primarily triggers inflammatory and immune response is found in ovarian cancer cells and is shown to influence the drug response towards paclitaxel, a TLR-4 ligand and analogue of lipopolysaccharide. Earlier reports showed that in MyD88^{positive} EOC cells, treatment with LPS and paclitaxel showed enhanced cell proliferation, activation of NF-κB, constitutive secretion of pro-inflammatory cytokines promoting tumor growth and thus rendering paclitaxel resistance. In contrast, MyD88^{negative} cells undergo apoptosis and do not secrete cytokines/chemokines in response to paclitaxel treatment. Induction of MyD88 expression in MyD88^{negative} EOC cells contributed to paclitaxel resistance (Kelly et al., 2006; Szajnik et al., 2009). MyD88 deficient A2780 cells exhibited decreased NF-κB activity after 6 h of cisplatin treatment (Mabuchi et al., 2004b). In this study, we found NF-κB activity did not alter significantly after cisplatin, paclitaxel or cisplatin + paclitaxel treatment in MyD88^{positive} EOC cells though there was a trend in increased NF-κB activation in SKOV3 cells. However, in MyD88^{negative} A2780 cells, reduced nuclear localization (by Western blotting and immunofluorescence assay) and decreased NF-κB activity (by reporter assay) were observed after 24 h of cisplatin treatment. Interestingly, treatment with cisplatin and paclitaxel together exhibited the similar pattern. Both these treatments resulted in complete or partial abolishment of NF-κB binding to the respective response elements. In contrast, no significant decrease in NF-κB activity and increased nuclear localization of NF-κB protein were found in paclitaxel treated cells with a slight reduction in the DNA-protein complex formation. The discrepancy found in NF-κB nuclear localization pattern after paclitaxel treatment between Szajnik et al. (2009) and us could be due to differential exposure time of the drug. Altogether our results like others indicate that MyD88 deficiency could influence the effect of different drugs upon NF-κB activation.

Previously, two subsequent studies had suggested MyD88 as a potential biomarker for measuring clinical response to paclitaxel in epithelial ovarian cancer (Kelly et al., 2006; Silasi et al., 2006). However the patient cohort in these studies was relatively small (12 in Kelly et al.'s study and 20 in Silasi et al.) and even in such small cohorts, around 50% epithelial ovarian tumors were found to be MyD88 negative. In a recent study by Kim et al. (2012), association of TLR-4/MyD88/NF-κB with survival and disease recurrence was investigated in 123 patients. Though higher disease recurrence was found in MyD88 positive tumors (~36%), around 40% of the MyD88 negative patients (60% of total population) showed relapse and 65% of these patients were turned to be NF-κB positive. Therefore expression of MyD88 seems to create a delicate balance between *Intrinsic* and *Acquired* drug resistance in EOC where both the situations involve NF-κB activation. To understand the status of NF-κB in acquirement of cisplatin, paclitaxel and combinatorial treatment resistance in absence of MyD88 adapter protein, we generated isogenic cellular matrices of acquired drug resistant cells using a well-known MyD88^{negative} cell line. To understand the effect of different drugs in single or in combination upon various pathways in resistant milieu, we challenged these cells with high dose of drugs for longer time period. Intriguingly, we found cisplatin treatment augmented NF-κB in cisplatin resistant cells while paclitaxel and combinatorial treatments down regulated NF-κB activity in paclitaxel and platinum-taxol resistant cells. This contrary effect was evident from luciferase, Western and immunofluorescence data. The DNA binding activity of NF-κB was increased in cisplatin treated A2780-Cis^{LR} cells while the same was reduced after paclitaxel or dual drug treatments in A2780-Pac^{LR} or A2780-Cis-Pac^{LR} cells. Cross treatments of cisplatin and paclitaxel to A2780-Pac^{LR} or A2780-Cis^{LR} cells also showed the same induction phenotype indicating role of NF-κB signaling evading cisplatin mediated cellular toxicity in drug resistant cells. Intriguingly, when MyD88 expression was silenced in MyD88^{positive} and cisplatin resistant cells, only cisplatin but not paclitaxel or combinatorial treatments could enhance NF-κB activity. Enhanced expressions of anti-apoptotic genes have been found to sustain the resistance properties of cancer cells (Cepeda et al., 2007). Enhanced Bcl-2 expression observed in A2780-Cis^{LR} cells is probably involved in maintenance of cisplatin resistance in our model. In contrast, decreased expression of Bcl-2 in paclitaxel and platinum-taxol resistant cells might have resulted from down-regulated NF-κB activity. Thus our data indicate that MyD88 expression is dispensable for acquirement of resistance towards cisplatin in epithelial ovarian cancer. The underlying molecular mechanism is not known and is currently under investigation.

Non-invasive imaging of molecular events in small animals has become an ideal practice to understand molecular mechanism at organ level and to evaluate therapeutic molecules (Chan et al., 2009; Chen et al., 2012). Reporter genes single or in combination, fused with gene of interest or driven by promoter of interest are frequently used with multiple imaging devices with appropriate probe/substrate. Using bioluminescence imaging modality, we first demonstrated that the cisplatin resistant tumors could effectively retained their resistant phenotype and did not exhibit attenuation in luciferase signal or tumor regression after cisplatin treatment. When these resistant cells were further engineered to stably express the NF-κB sensor, a 14 fold increase in NF-κB activity was observed after cisplatin treatment. Real time monitoring of NF-κB activity in animal models using various luciferases (renilla luciferase or gaussia luciferase) have already been demonstrated using TNF alpha as an inducer (Badr et al., 2009; Roth et al., 2006). However, to the best of our knowledge this is the first report in which NF-κB reporter activity was studied non-invasively in effect of cisplatin treatment. This unique model would be useful in screening therapeutic molecules against NF-κB or Bcl-2 for platinum resistant ovarian cancer cells particularly in a MyD88 compromised background.

5. Conclusion

MyD88, an adapter protein in TLR-4/MyD88 driven NF-κB signaling, imparts crucial influence on intrinsic taxol resistance in epithelial ovarian carcinoma. Since, about 50–60% EOC are MyD88 deficient, it is critical to understand how drug resistance is acquired in absence of MyD88. Our results demonstrated that paclitaxel, a TLR-4 ligand did not induce NF-κB in sensitive or in taxol/platinum resistant cells without MyD88 indicating an absolute dependency. In contrary, NF-κB upregulation by cisplatin and high Bcl-2 expression in MyD88 deficient cisplatin resistant cells indicated dispensability of MyD88 in acquired cisplatin resistance. In fact that silencing of MyD88 in MyD88^{positive} cisplatin resistant cells led to NF-κB activation by cisplatin strengthens our hypothesis. Thus our data has provided a new insight into the molecular complexity associated with chemoresistance which may be exploited for developing better therapeutic strategy for ovarian cancer in future.

Acknowledgments

This work is supported by funding from ACTREC-IRG no 71, CSIR grant 27(232)/10-EMRII and DBT grant BT/PR4141/Med/30/680/2011 to PR, UGC fellowship to RK and CSIR fellowship to SMG and BT. We also acknowledge support from the Molecular Imaging Facility at ACTREC.

Appendix A. Supplementary data

Supplementary data associated with this article can be found, in the online version, at http://dx.doi.org/10.1016/j.biocel.2015.02.001.

References

Agarwal R, Kaye SB. Ovarian cancer: strategies for overcoming resistance to chemotherapy. Nat Rev Cancer 2003;3:502–16.

Akira S. Toll-like receptor signaling. J Biol Chem 2003;278:38105–8.

Akira S, Takeda K, Kaisho T. Toll-like receptors: critical proteins linking innate and acquired immunity. Nat Immunol 2001;2:675–80.

Alvero AB. Recent insights into the role of NF-kappaB in ovarian carcinogenesis. Genome Med 2010;2:56.

Annunziata CM, Stavnes HT, Kleinberg L, Berner A, Hernandez LF, Birrer MJ, et al. Nuclear factor kappaB transcription factors are coexpressed and convey a poor outcome in ovarian cancer. Cancer 2010;116:3276–84.

Armstrong DK, Bundy B, Wenzel L, Huang HQ, Baergen R, Lele S, et al. Intraperitoneal cisplatin and paclitaxel in ovarian cancer. N Engl J Med 2006;354:34–43.

Badr CE, Niers JM, Tjon-Kon-Fat LA, Noske DP, Wurdinger T, Tannous BA. Real-time monitoring of nuclear factor kappaB activity in cultured cells and in animal models. Mol Imaging 2009;8:278–90.

Beale PJ, Rogers P, Boxall F, Sharp SY, Kelland LR. BCL-2 family protein expression and platinum drug resistance in ovarian carcinoma. Br J Cancer 2000;82:436–40.

Blasius AL, Beutler B. Intracellular toll-like receptors. Immunity 2010;32:305–15.

Brozovic A, Fritz G, Christmann M, Zisowsky J, Jaehde U, Osmak M, et al. Long-term activation of SAPK/JNK, p38 kinase and fas-L expression by cisplatin is attenuated in human carcinoma cells that acquired drug resistance. Int J Cancer 2004;112:974–85.

Cepeda V, Fuertes MA, Castilla J, Alonso C, Quevedo C, Perez JM. Biochemical mechanisms of cisplatin cytotoxicity. Anticancer Agents Med Chem 2007;7:3–18.

Chan CT, Paulmurugan R, Reeves RE, Solow-Cordero D, Gambhir SS. Molecular imaging of phosphorylation events for drug development. Mol Imaging Biol 2009;11:144–58.

Chaudhury S, Maheshwari A, Ray P. Ovarian cancer an ever challenging malady. Biomed Res J 2014;1:34–55.

Chen HH, Yuan H, Josephson L, Sosnovik DE. Theranostic imaging of the kinases and proteases that modulate cell death and survival. Theranostics 2012;2:148–55.

Dier U, Shin DH, Hemachandra LP, Uusitalo LM, Hempel N. Bioenergetic analysis of ovarian cancer cell lines: profiling of histological subtypes and identification of a mitochondria-defective cell line. PloS One 2014;9:e98479.

El-Deiry WS. Role of oncogenes in resistance and killing by cancer therapeutic agents. Curr Opin Oncol 1997;9:79–87.

Gaikwad SM, Gunjal L, Junutula AR, Astanehe A, Gambhir SS, Ray P. Non-invasive imaging of phosphoinositide-3-kinase-catalytic-subunit-alpha (PIK3CA) promoter modulation in small animal models. PloS One 2013;8:e55971.

Gaikwad SM, Ray P. Non-invasive imaging of PI3K/Akt/mTOR signalling in cancer. Am J Nucl Med Mol Imaging 2012;2:418–31.

Gottesman MM. Mechanisms of cancer drug resistance. Annu Rev Med 2002;53:615–27.

Hayden MS, Ghosh S. NF-kappaB, the first quarter-century: remarkable progress and outstanding questions. Genes Dev 2012;26:203–34.

Karin M. NF-kappaB as a critical link between inflammation and cancer. Cold Spring Harb Perspect Biol 2009;1:a000141.

Kartalou M, Essigmann JM. Mechanisms of resistance to cisplatin. Mutat Res 2001;478:23–43.

Kawai T, Akira S. TLR signaling. Cell Death Differ 2006;13:816–25.

Kawai T, Akira S. Signaling to NF-kappaB by Toll-like receptors. Trends Mol Med 2007;13:460–9.

Kelly MG, Alvero AB, Chen R, Silasi DA, Abrahams VM, Chan S, et al. TLR-4 signaling promotes tumor growth and paclitaxel chemoresistance in ovarian cancer. Cancer Res 2006;66:3859–68.

Kim D, Dan HC, Park S, Yang L, Liu Q, Kaneko S, et al. AKT/PKB signaling mechanisms in cancer and chemoresistance. Front Biosci 2005;10:975–87.

Kim KH, Jo MS, Suh DS, Yoon MS, Shin DH, Lee JH, et al. Expression and significance of the TLR4/MyD88 signaling pathway in ovarian epithelial cancers. World J Surg Oncol 2012;10:193.

Koh J, Lee SB, Park H, Lee HJ, Cho NH, Kim J. Susceptibility of CD24(+) ovarian cancer cells to anti-cancer drugs and natural killer cells. Biochem Biophys Res Commun 2012;427:373–8.

Koti M, Gooding RJ, Nuin P, Haslehurst A, Crane C, Weberpals J, et al. Identification of the IGF1/PI3K/NF kappaB/ERK gene signalling networks associated with chemotherapy resistance and treatment response in high-grade serous epithelial ovarian cancer. BMC Cancer 2013;13:549.

Mabuchi S, Ohmichi M, Nishio Y, Hayasaka T, Kimura A, Ohta T, et al. Inhibition of inhibitor of nuclear factor-kappaB phosphorylation increases the efficacy of paclitaxel in in vitro and in vivo ovarian cancer models. Clin Cancer Res 2004a;10:7645–54.

Mabuchi S, Ohmichi M, Nishio Y, Hayasaka T, Kimura A, Ohta T, et al. Inhibition of NFkappaB increases the efficacy of cisplatin in in vitro and in vivo ovarian cancer models. J Biol Chem 2004b;279:23477–85.

Muccioli M, Sprague L, Nandigam H, Pate M, Benencia F. Toll-like receptors as novel therapeutic targets for ovarian cancer. ISRN Oncol 2012;2012:642141.

Nehra R, Riggins RB, Shajahan AN, Zwart A, Crawford AC, Clarke R. BCL2 and CASP8 regulation by NF-kappaB differentially affect mitochondrial function and cell fate in antiestrogen-sensitive and -resistant breast cancer cells. FASEB J 2010;24:2040–55.

Peng DJ, Wang J, Zhou JY, Wu GS. Role of the Akt/mTOR survival pathway in cisplatin resistance in ovarian cancer cells. Biochem Biophys Res Commun 2010;394:600–5.

Ray P, Wu AM, Gambhir SS. Optical bioluminescence and positron emission tomography imaging of a novel fusion reporter gene in tumor xenografts of living mice. Cancer Res 2003;63:1160–5.

Rocconi RP, Case AS, Straughn JM Jr, Estes JM, Partridge EE. Role of chemotherapy for patients with recurrent platinum-resistant advanced epithelial ovarian cancer: a cost-effectiveness analysis. Cancer 2006;107:536–43.

Roth DJ, Jansen ED, Powers AC, Wang TG. A novel method of monitoring response to islet transplantation: bioluminescent imaging of an NF-kB transgenic mouse model. Transplantation 2006;81:1185–90.

Roth V. Doubling time calculator; 2006.

Siddik ZH. Biochemical and molecular mechanisms of cisplatin resistance. Cancer Treat Res 2002;112:263–84.

Silasi DA, Alvero AB, Illuzzi J, Kelly M, Chen R, Fu HH, et al. MyD88 predicts chemoresistance to paclitaxel in epithelial ovarian cancer. Yale J Biol Med 2006;79:153–63.

Singh RK, Gaikwad SM, Jinager A, Chaudhury S, Maheshwari A, Ray P. IGF-1R inhibition potentiates cytotoxic effects of chemotherapeutic agents in early stages of chemoresistant ovarian cancer cells. Cancer Lett 2014;354:254–62.

Szajnik M, Szczepanski MJ, Czystowska M, Elishaev E, Mandapathil M, Nowak-Markwitz E, et al. TLR4 signaling induced by lipopolysaccharide or paclitaxel regulates tumor survival and chemoresistance in ovarian cancer. Oncogene 2009;28:4353–63.

Tang G, Minemoto Y, Dibling B, Purcell NH, Li Z, Karin M, et al. Inhibition of JNK activation through NF-kappaB target genes. Nature 2001;414:313–7.

Yang G, Zhou Y, Liu X, Xu L, Cao Y, Manning RJ, et al. A mutation in MYD88 (L265P) supports the survival of lymphoplasmacytic cells by activation of Bruton tyrosine kinase in Waldenstrom macroglobulinemia. Blood 2013;122:1222–32.

Yuan Z, Cao K, Lin C, Li L, Liu HY, Zhao XY, et al. The p53 upregulated modulator of apoptosis (PUMA) chemosensitizes intrinsically resistant ovarian cancer cells to cisplatin by lowering the threshold set by Bcl-x(L) and Mcl-1. Mol Med 2011;17:1262–74.